Nonthermal X-ray Emission with SRG/eROSITA
A Biased View towards Pulsars

Martin Mayer – Remeis Observatory Bamberg (FAU)

Nonthermal Astrophysics in Southern Africa – 29.07.2024

In collaboration with

Manami Sasaki (FAU), Werner Becker (MPE), Peter Predehl (MPE)

FAU

ecap

eROSITA

Walter Benjamin-Programm

DFG Deutsche Forschungsgemeinschaft

Outline

- The SRG/eROSITA telescope: Mission design and data products
- eROSITA as a survey machine: Searching for new rotation-powered pulsars
- eROSITA for single objects: Investigating the extended Vela X pulsar wind nebula
- Summary

The SRG/eROSITA Telescope

Introduction: SRG/eROSITA

- eROSITA: Soft X-ray telescope on German-Russian SRG satellite
  - ➢ Original mission goal: 4-year all-sky X-ray survey, ~ 25 times deeper than precursor ROSAT
  - ➢ 2.2 years achieved until mission interruption

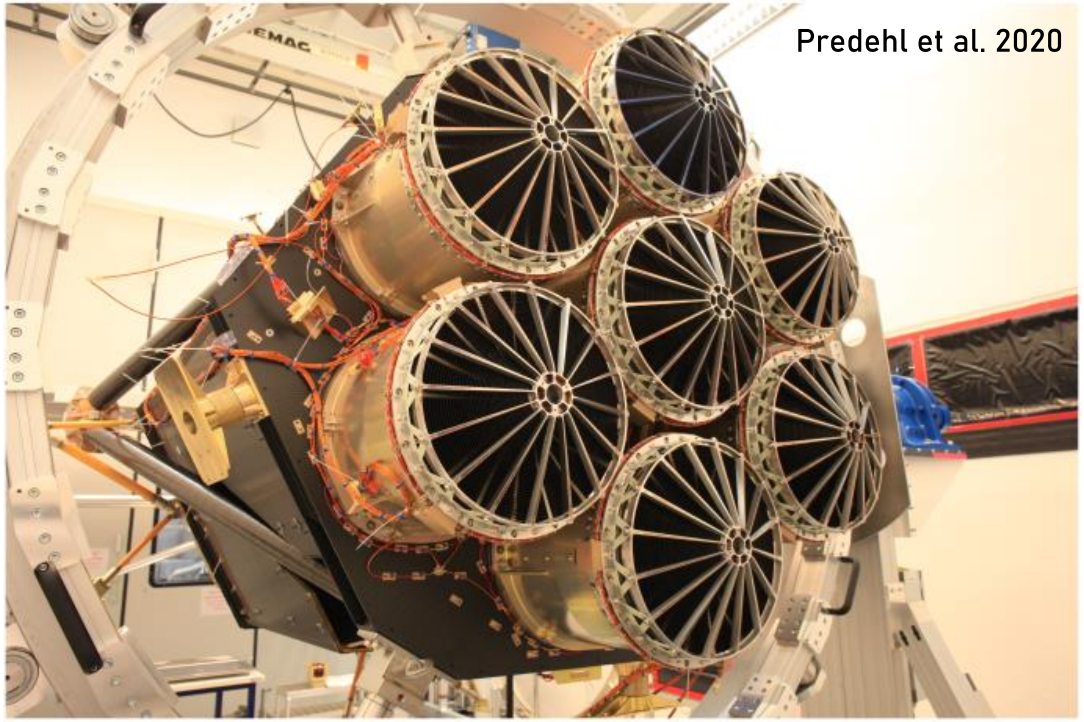

Predehl et al. 2020

Introduction: SRG/eROSITA

- eROSITA: Soft X-ray telescope on German-Russian SRG satellite
  - ➢ Original mission goal: 4-year all-sky X-ray survey, ~ 25 times deeper than precursor ROSAT
  - ➢ 2.2 years achieved until mission interruption

- Telescope specifics:
  - 7 identical telescope modules (TMs) with single-chip CCD detectors

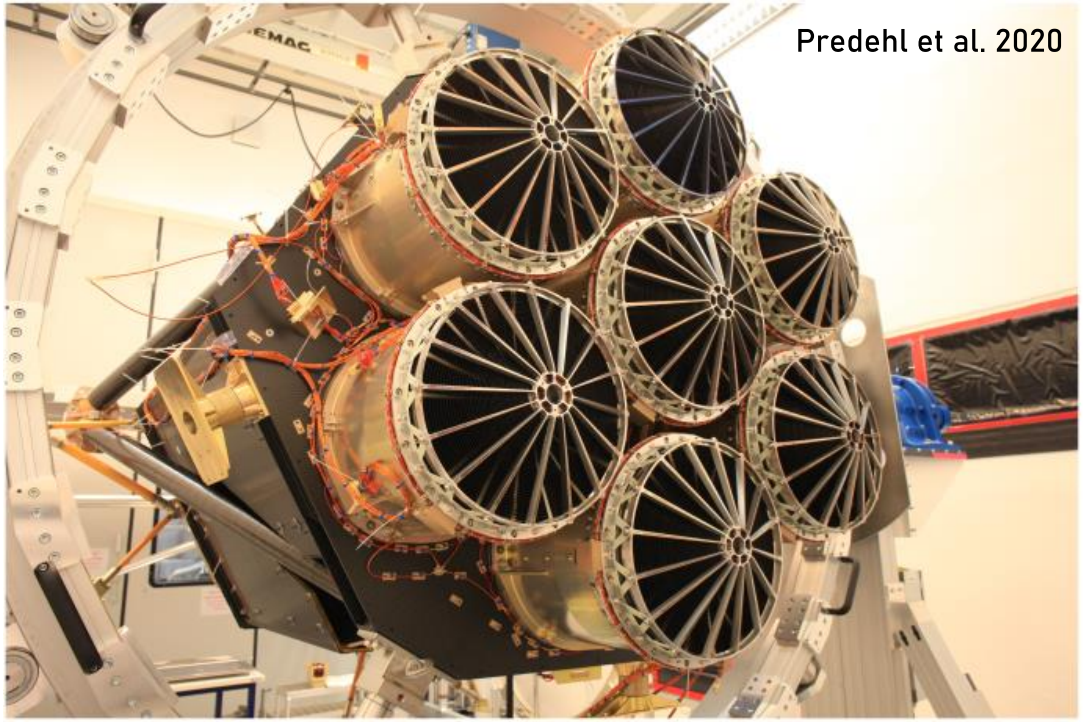
Predehl et al. 2020

Introduction: SRG/eROSITA

- eROSITA: Soft X-ray telescope on German-Russian SRG satellite
  - ➢ Original mission goal: 4-year all-sky X-ray survey, ~ 25 times deeper than precursor ROSAT
  - ➢ 2.2 years achieved until mission interruption

- Telescope specifics:
  - ▪ 7 identical telescope modules (TMs) with single-chip CCD detectors
  - ▪ Energy range 0.2 – 10 keV
  - ▪ Large combined effective area
  - ▪ Field of view ~ 1 degree

Predehl et al. 2020

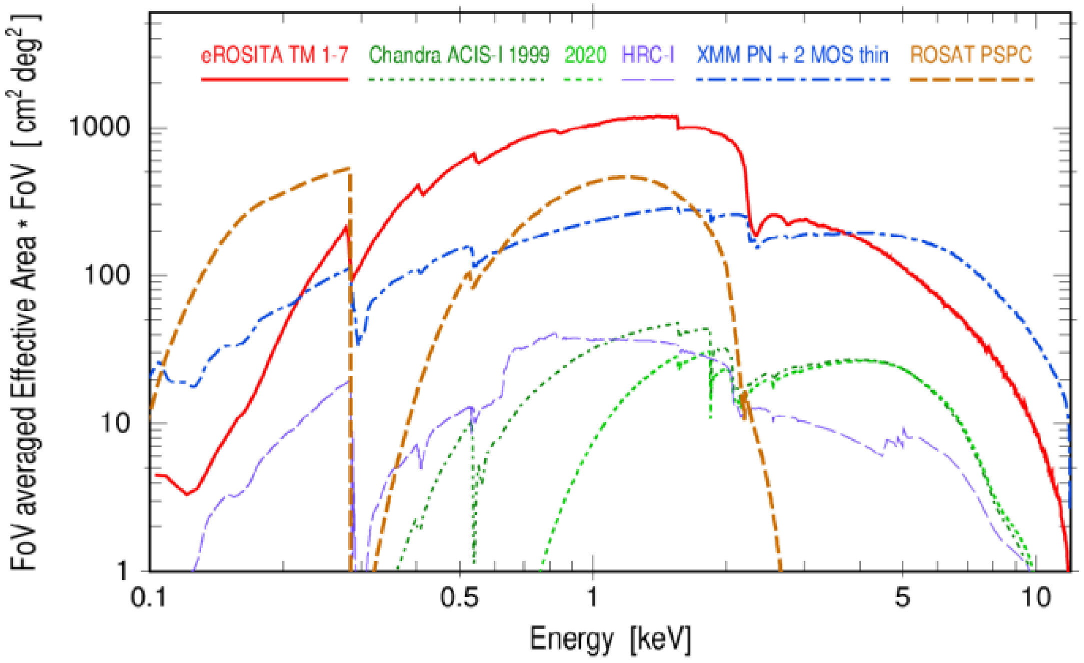

Introduction: SRG/eROSITA

- eROSITA: Soft X-ray telescope on German-Russian SRG satellite
  - ➢ Original mission goal: 4-year all-sky X-ray survey, ~ 25 times deeper than precursor ROSAT
  - ➢ 2.2 years achieved until mission interruption

- Telescope specifics:
  - 7 identical telescope modules (TMs) with single-chip CCD detectors
  - Energy range 0.2 – 10 keV
  - Large combined effective area
  - Field of view ~ 1 degree
  - Good spectral resolution (cf. XMM EPIC-pn)

eROSITA first-light press release
C. Maitra, F. Haberl (MPE)

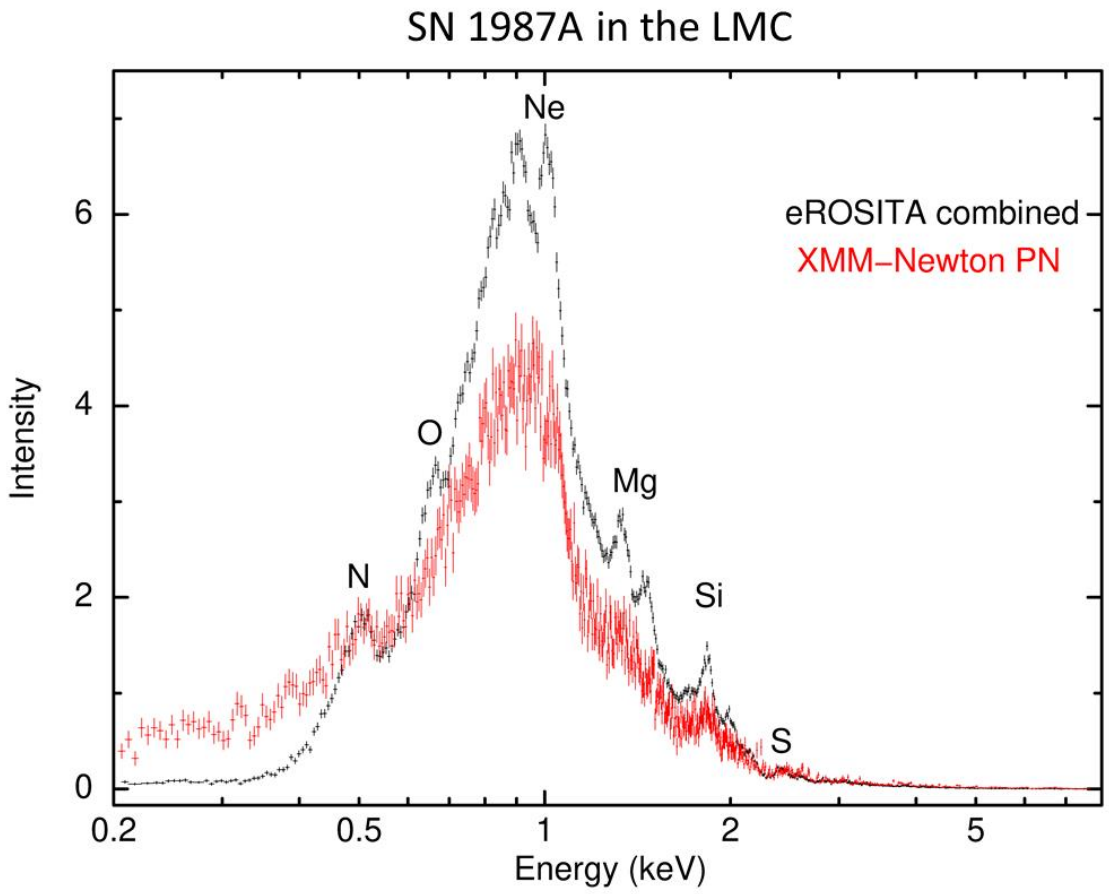

Introduction: SRG/eROSITA

eRASS1 all-sky image
Credit: MPE/IKI

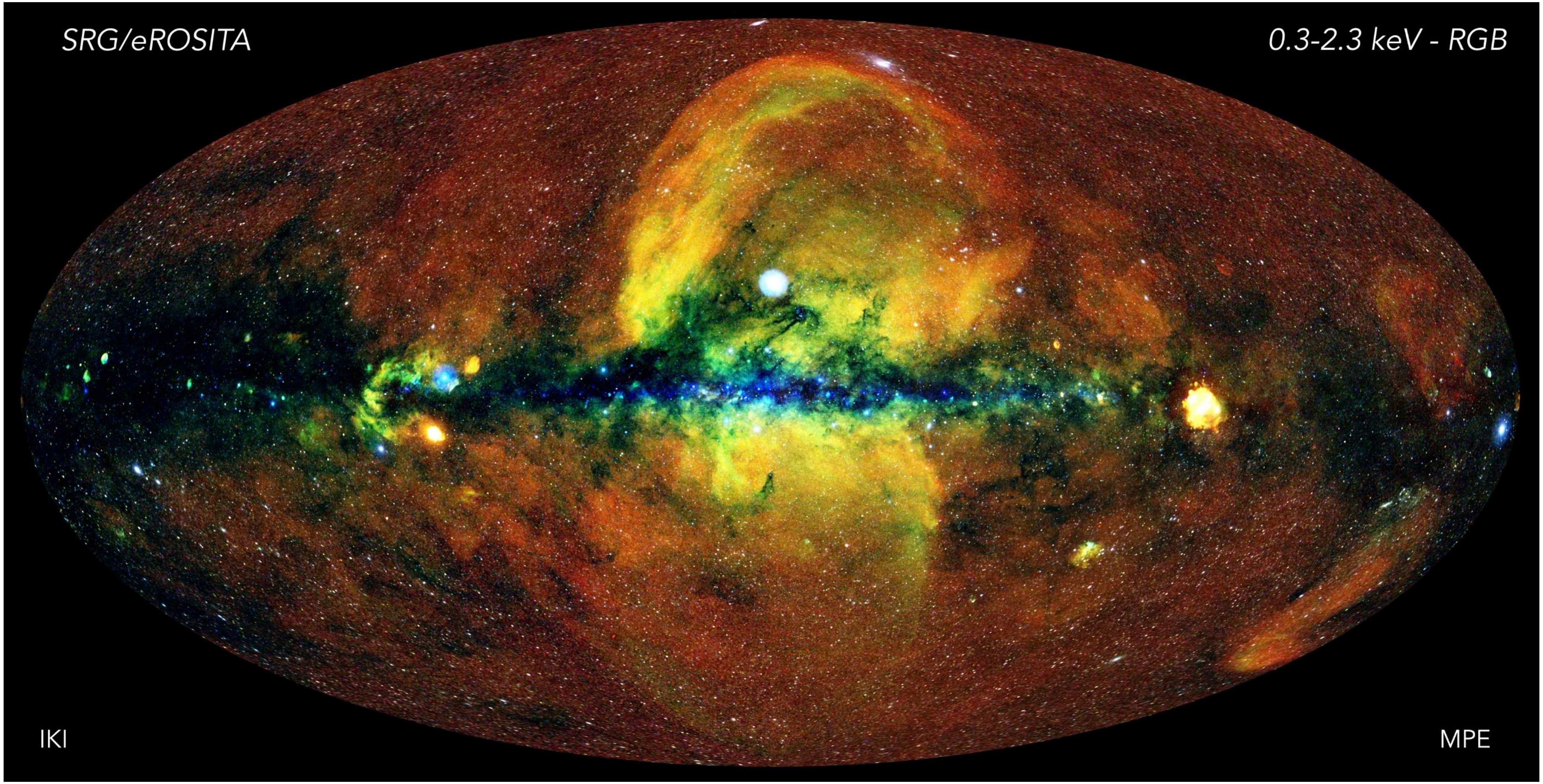

Introduction: SRG/eROSITA

eRASS1 all-sky image
Credit: MPE/IKI

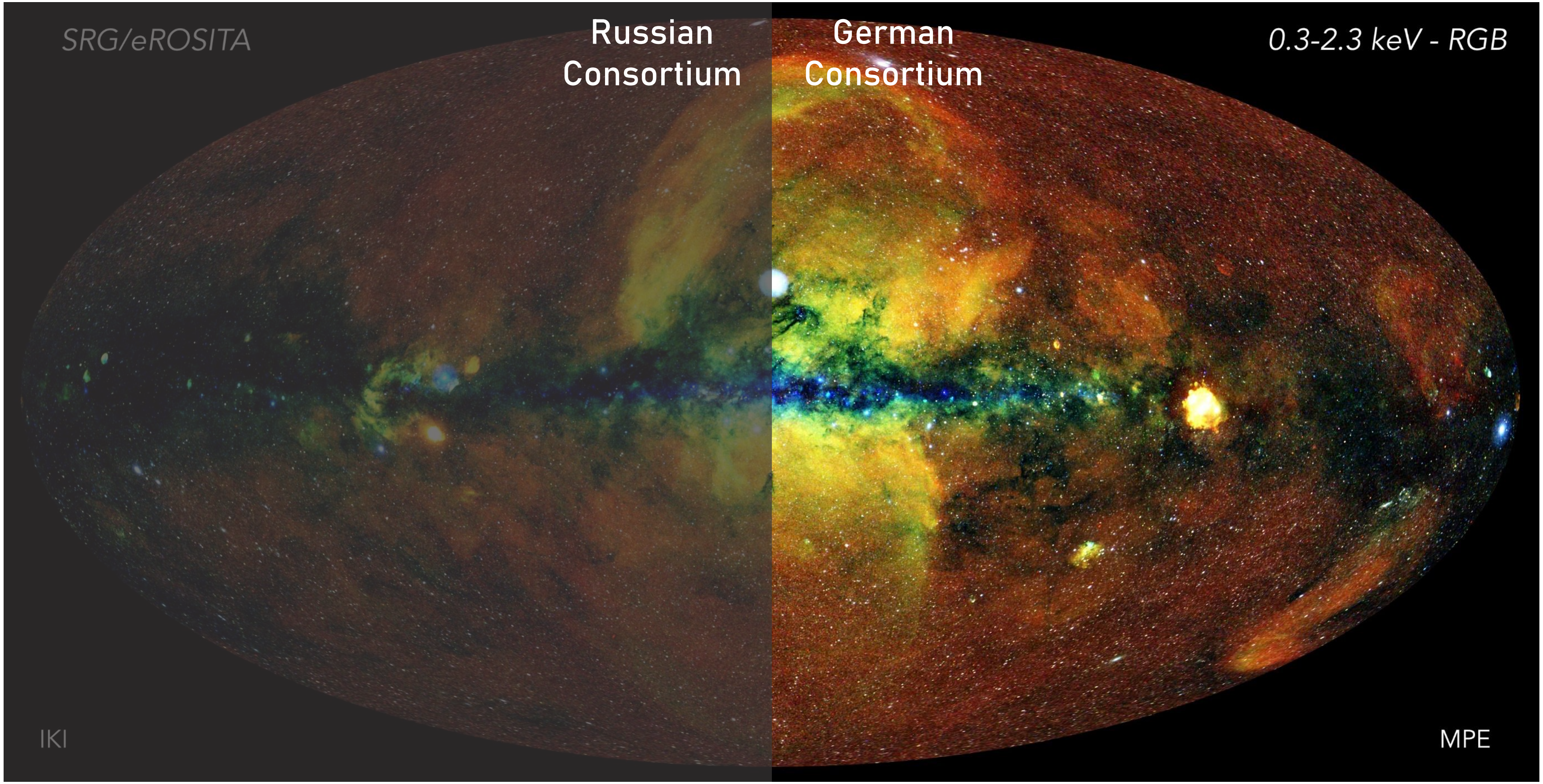

eROSITA DR1: The First All-Sky Survey (eRASS1)

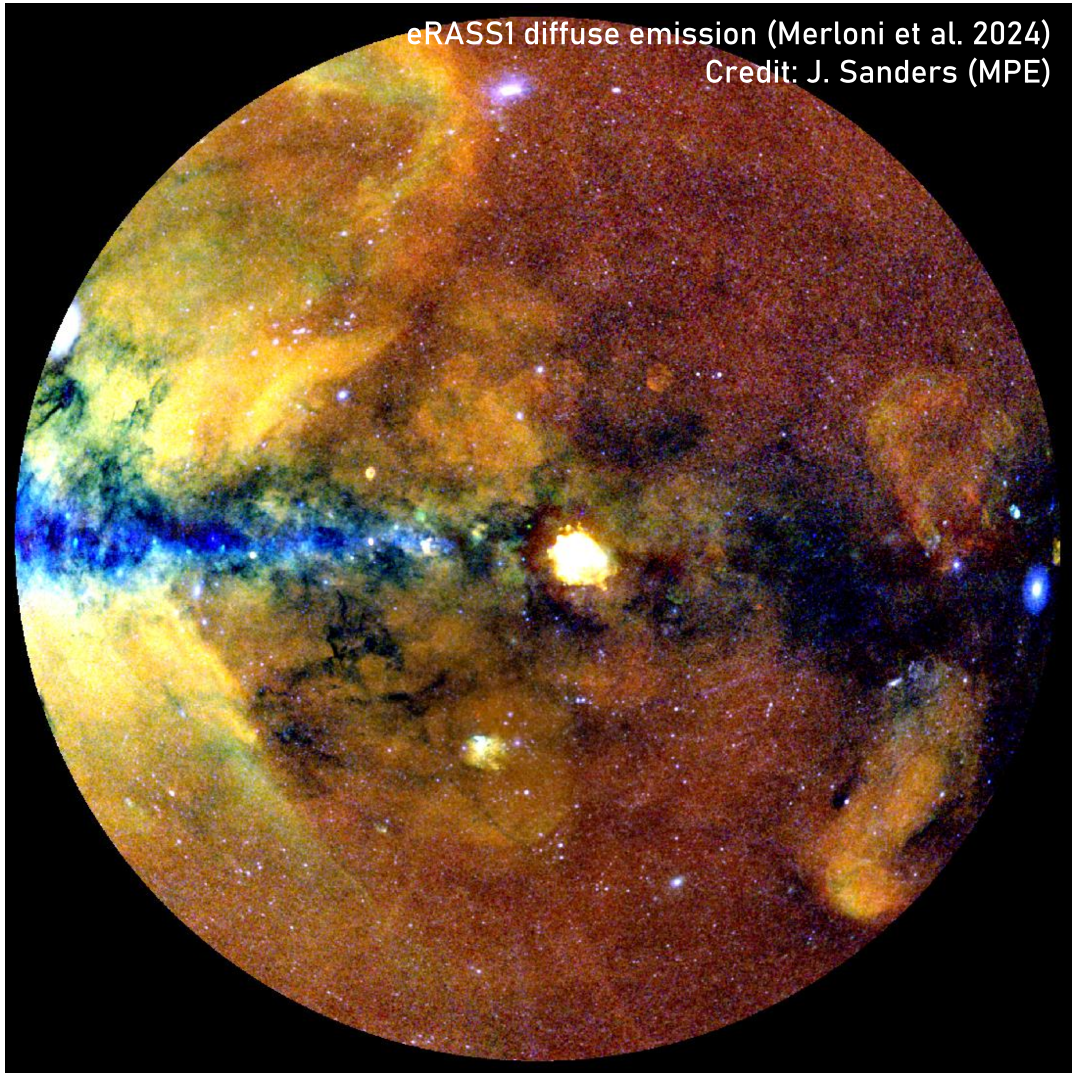

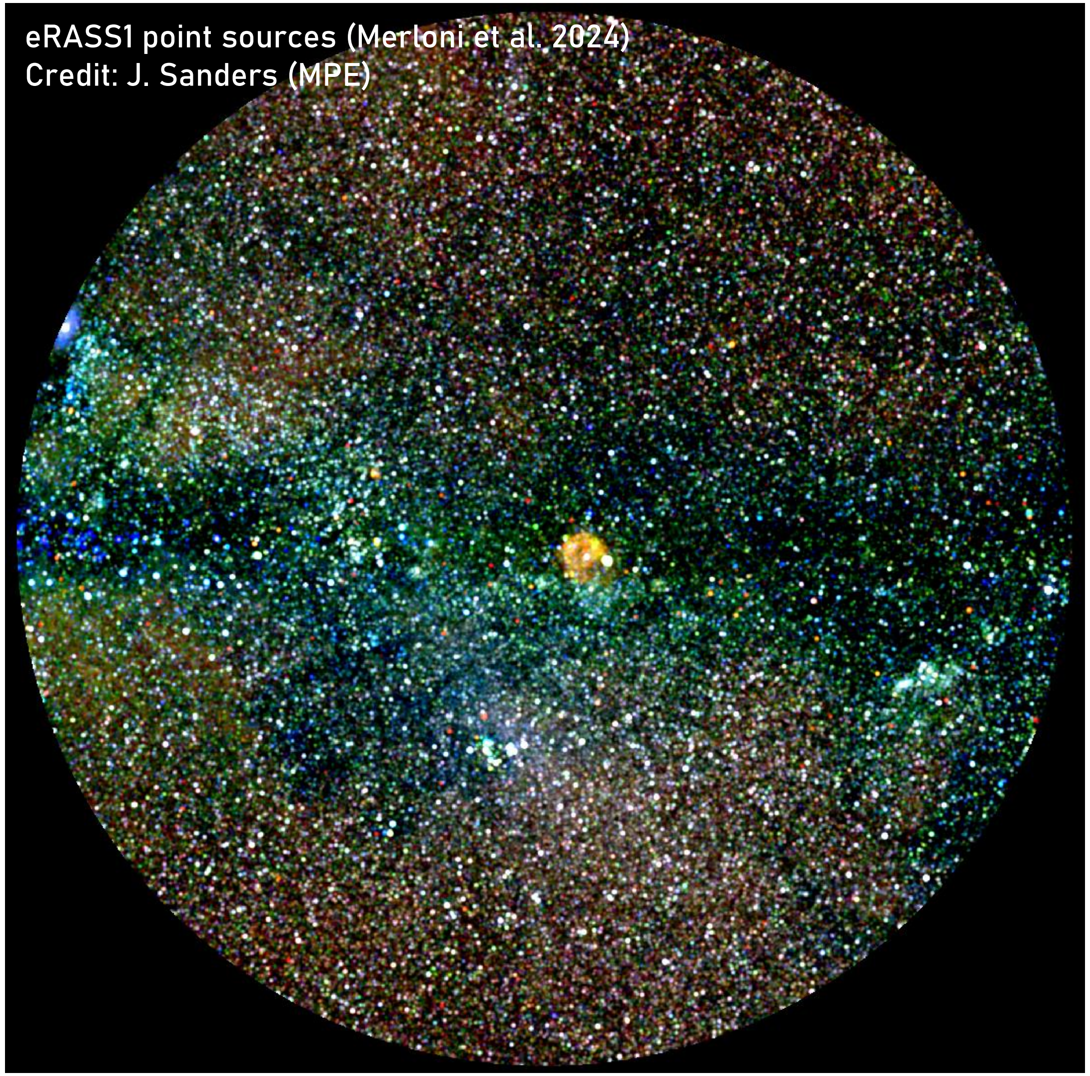

eROSITA DR1: The First All-Sky Survey (eRASS1)

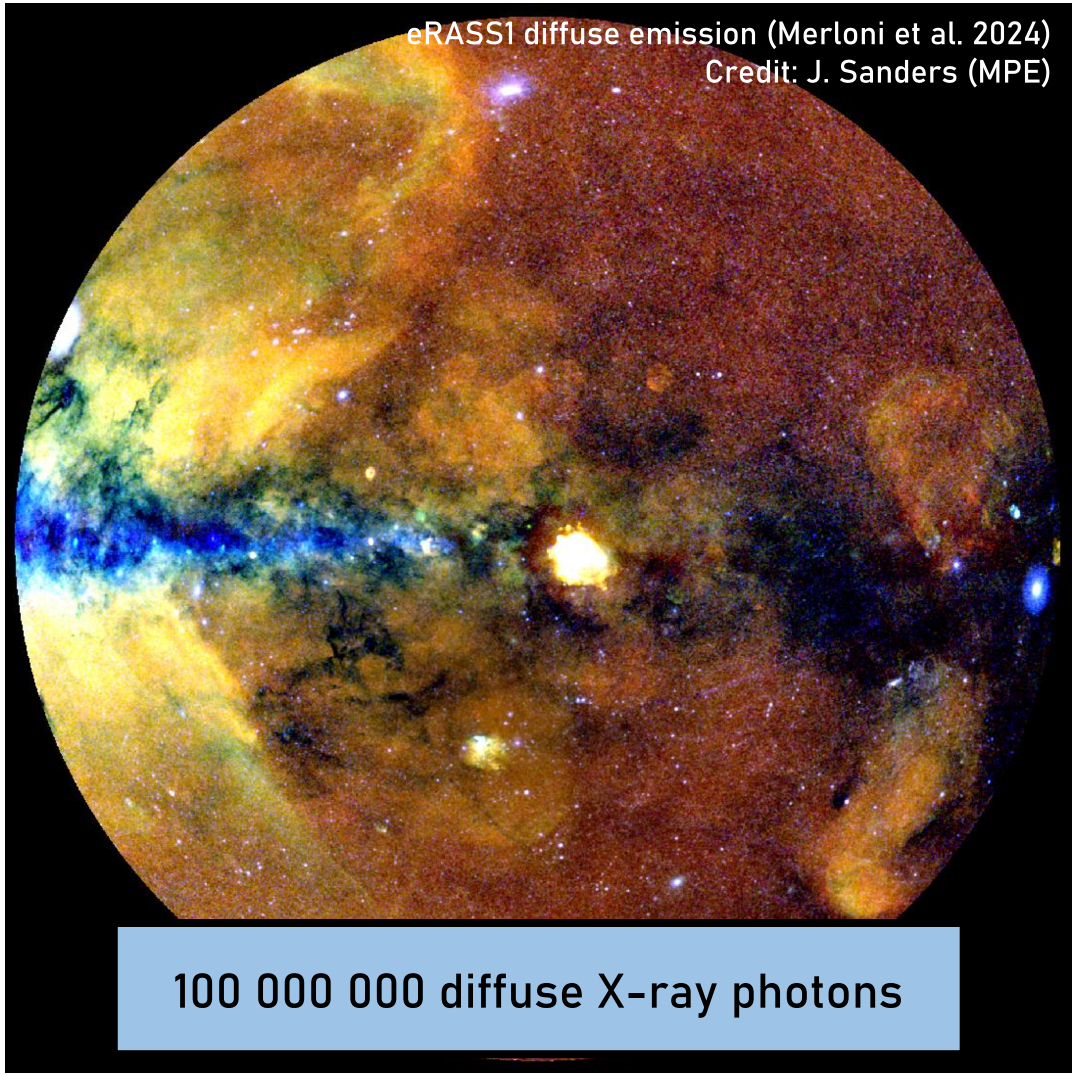

100 000 000 diffuse X-ray photons

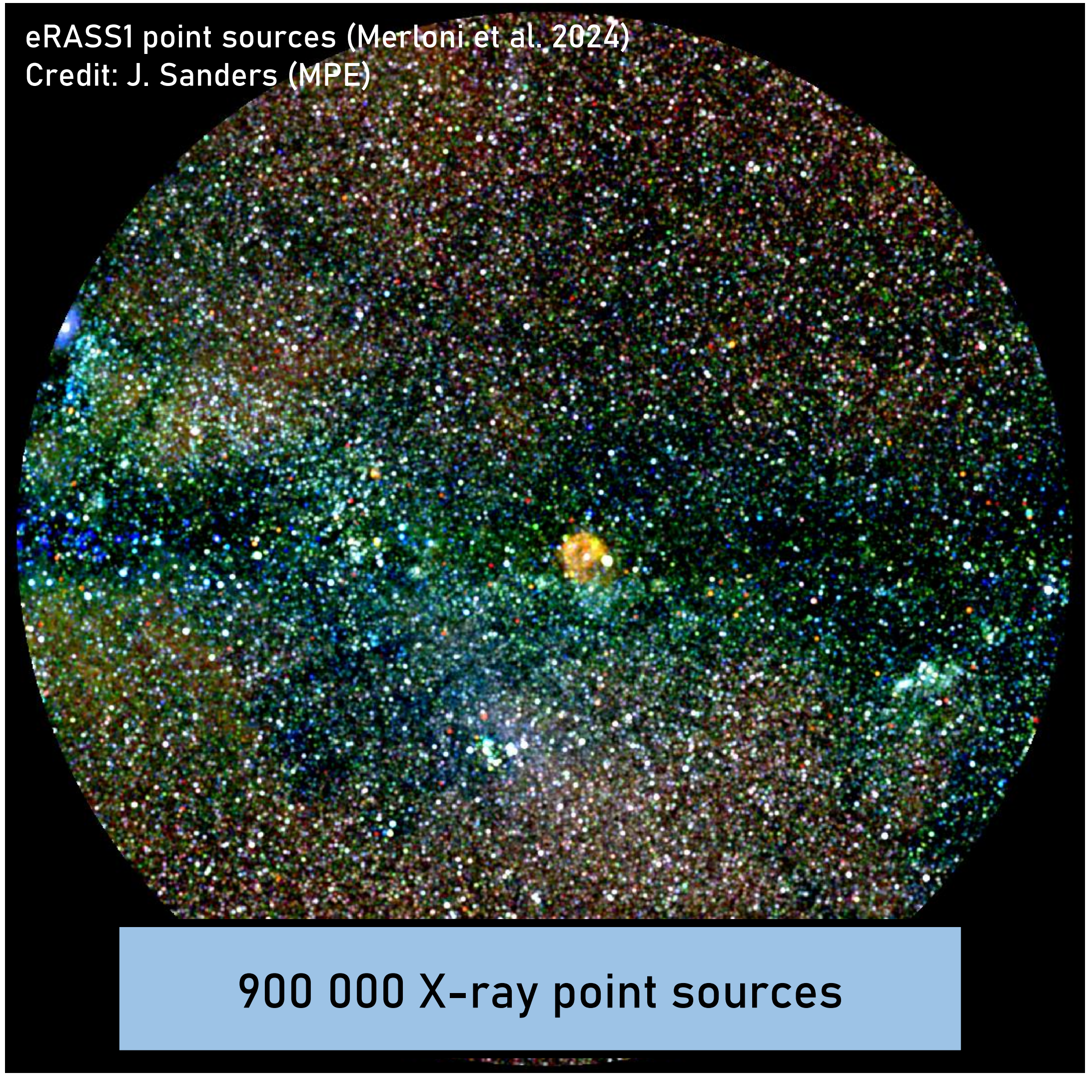

900 000 X-ray point sources


Searching for Rotation-Powered Pulsars
with Fermi-LAT & SRG/eROSITA


Searching for Rotation-Powered Pulsars
with Fermi-LAT & SRG/eROSITA
& Multiwavelength Followup

Motivation: The Fermi-LAT Source Catalog

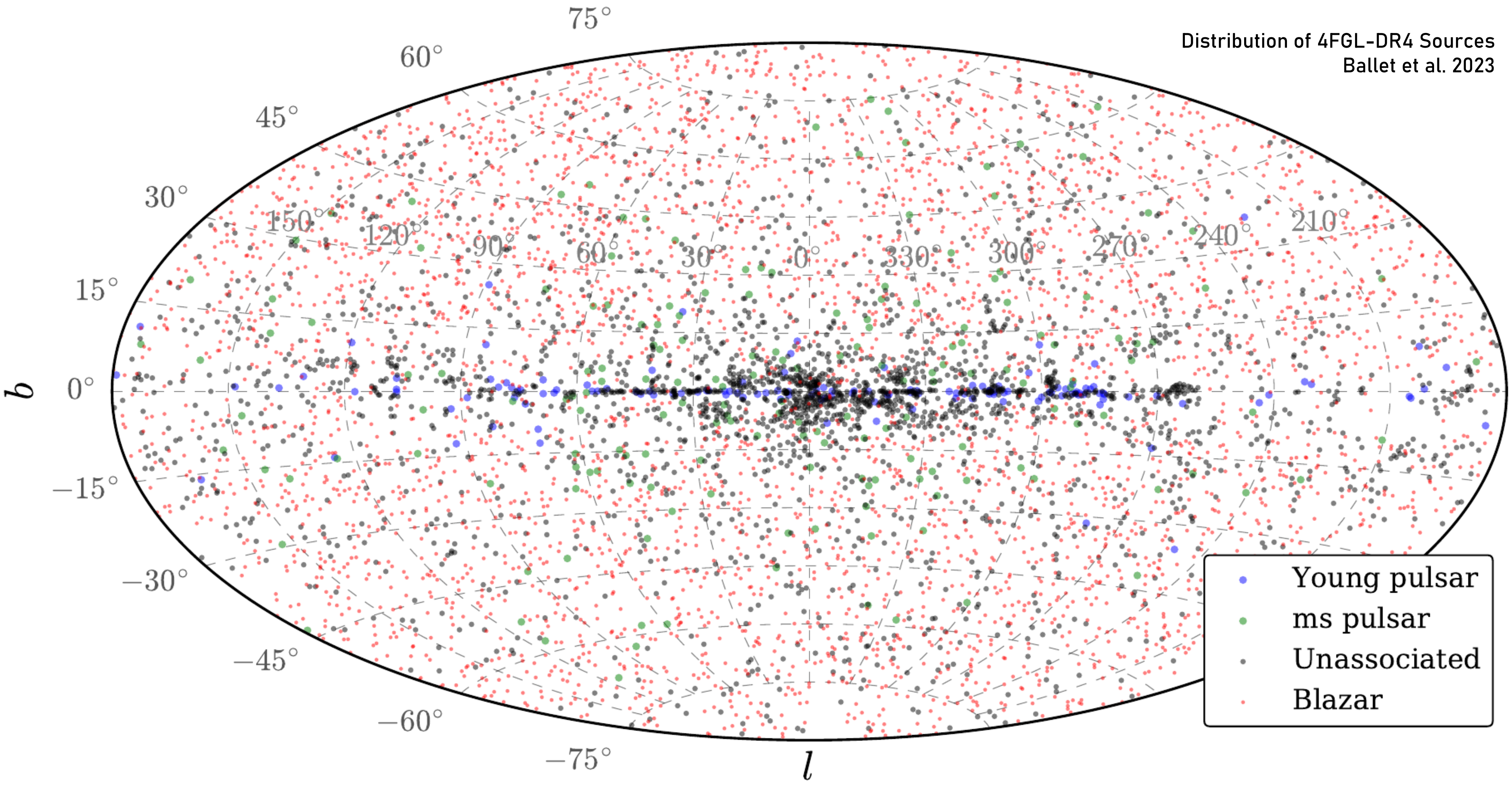

Motivation: Identifying Unassociated 4FGL Sources

- Goal: Identify unassociated sources (of pulsar-type) based on their X-ray counterparts
  - ➢ Precise positions allow for radio/optical confirmation

- Cross-match with eROSITA All-Sky Survey (eRASS:4) Catalog (see Merloni et al. 2024)

Example eRASS:4 image of 4FGL error ellipse

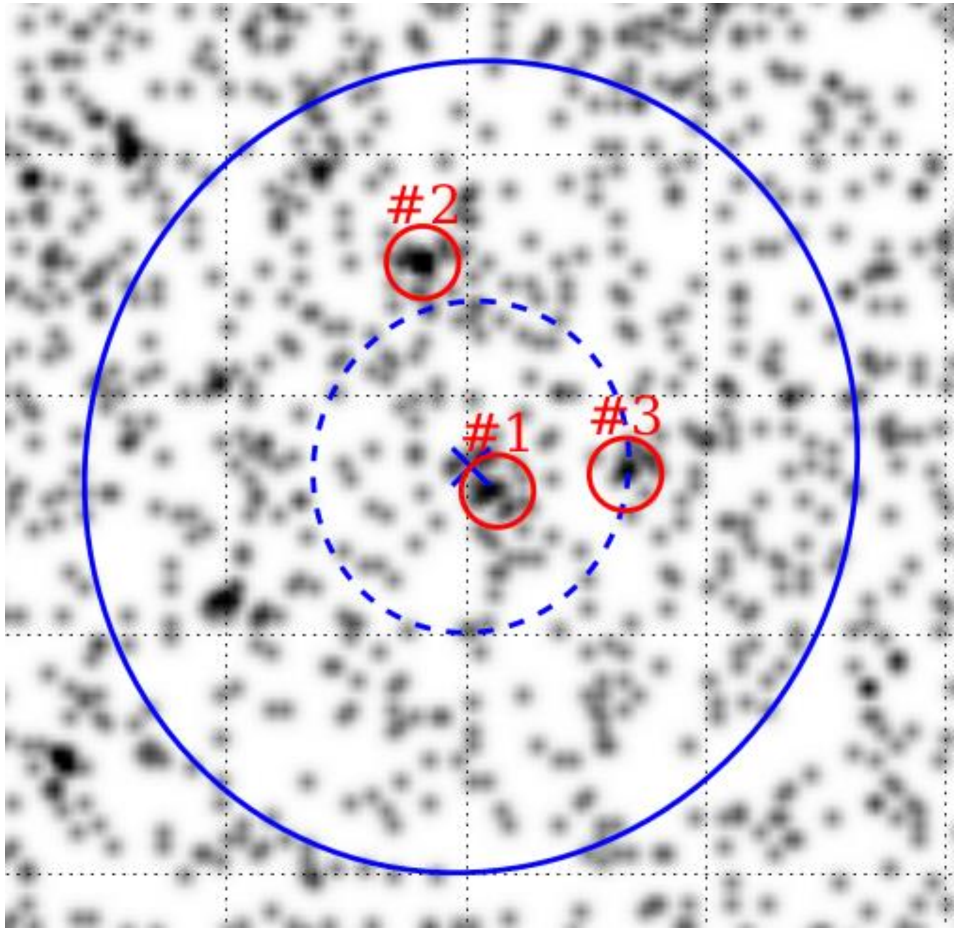

Motivation: Identifying Unassociated 4FGL Sources

- Goal: Identify unassociated sources (of pulsar-type) based on their X-ray counterparts
  - ➢ Precise positions allow for radio/optical confirmation

- Cross-match with eROSITA All-Sky Survey (eRASS:4) Catalog (see Merloni et al. 2024)

➢ Challenges:
  - Large gamma-ray error ellipses (~ 5 arcmin)
  - X-ray pulsar counterparts typically faint (~ 10 counts)

Example eRASS:4 image of 4FGL error ellipse

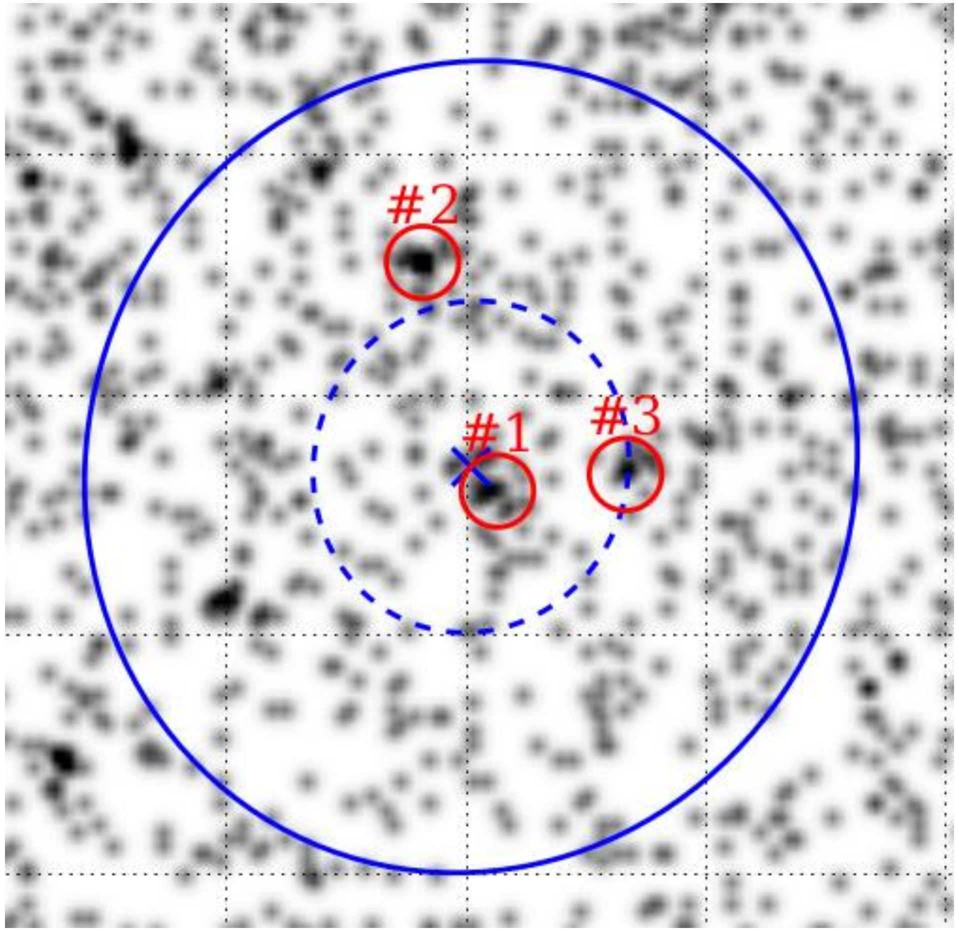

Search Strategy: Prior Classification

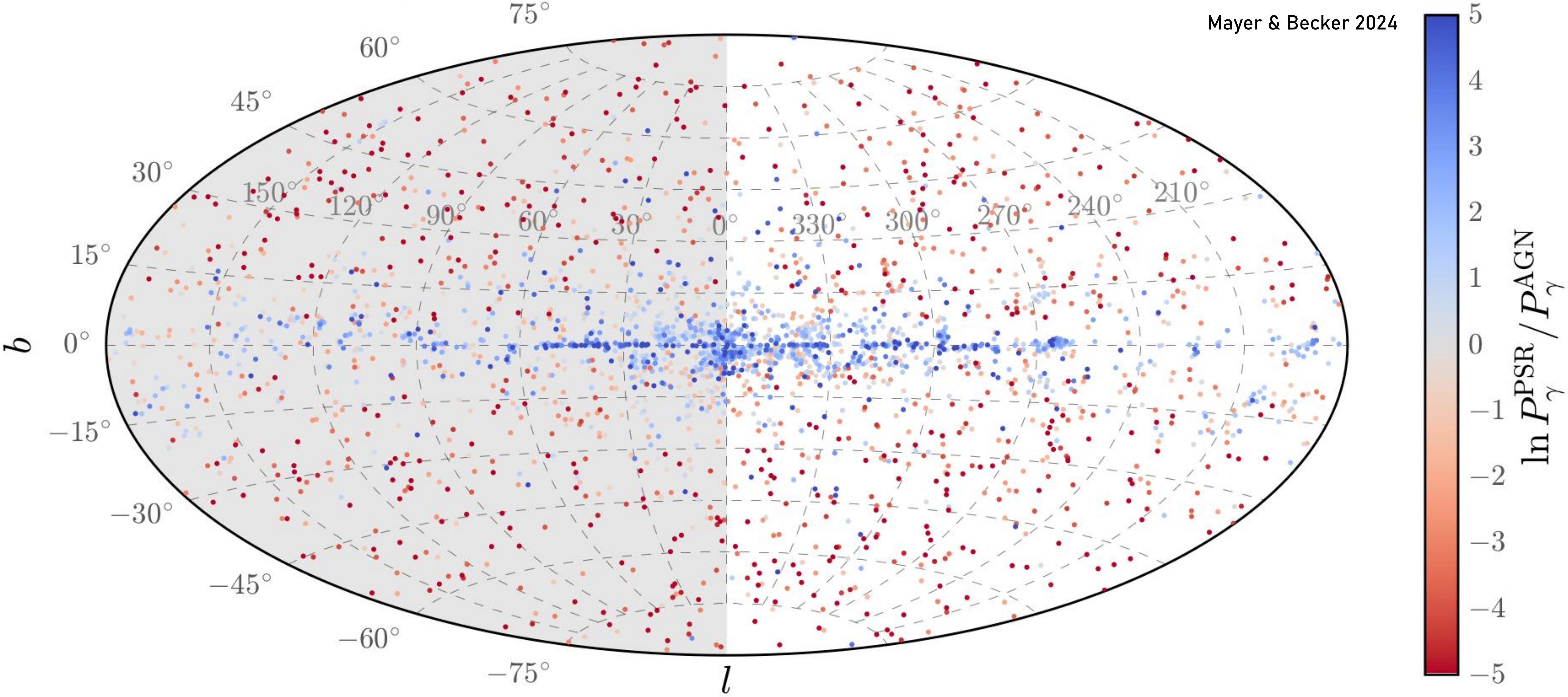

Results: Catalog of Pulsar Candidates

- Final cleaned catalog of candidate X-ray pulsar counterparts to Fermi-LAT sources
  - Around 160 candidates with $P_{PSR} > 0.1$
  - Predict ~ 25 new pulsars in top 100 candidate matches
  - Expect similar numbers of young (squares) and millisecond (triangle) pulsars

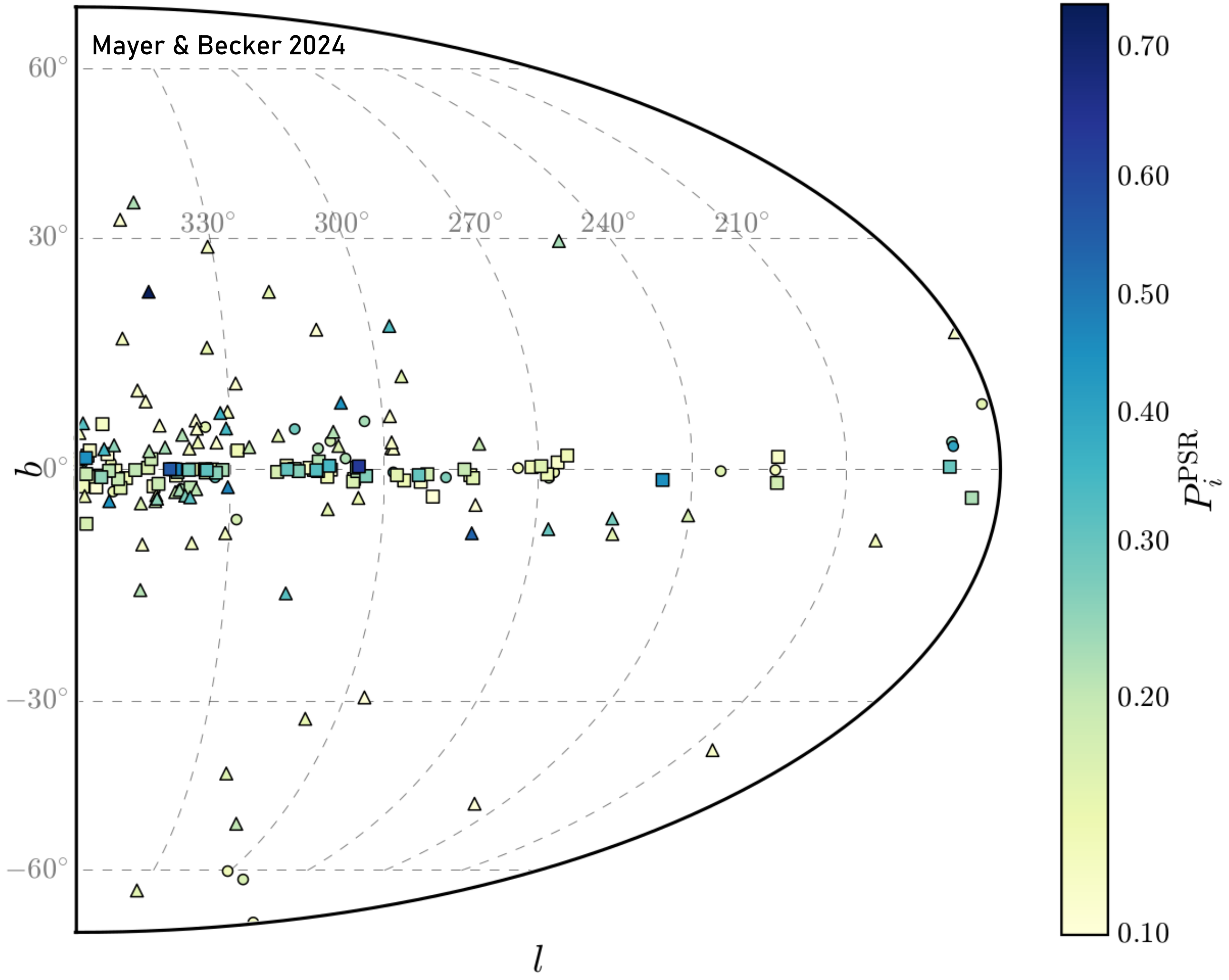

Followup example: Multiwavelength view of PSR J1803–6707

Clark et al. 2023

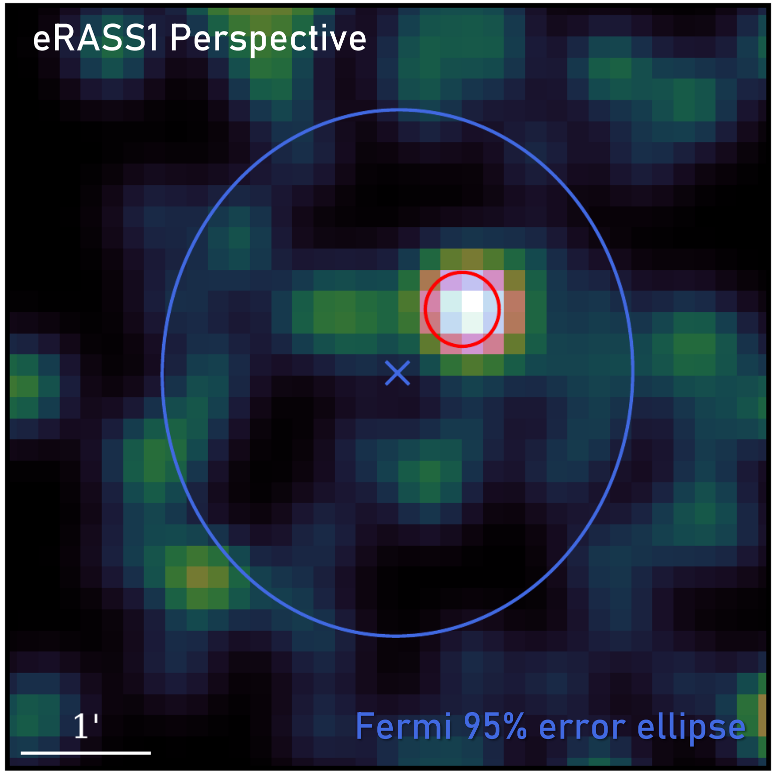

Followup example: Multiwavelength view of PSR J1803–6707

Clark et al. 2023

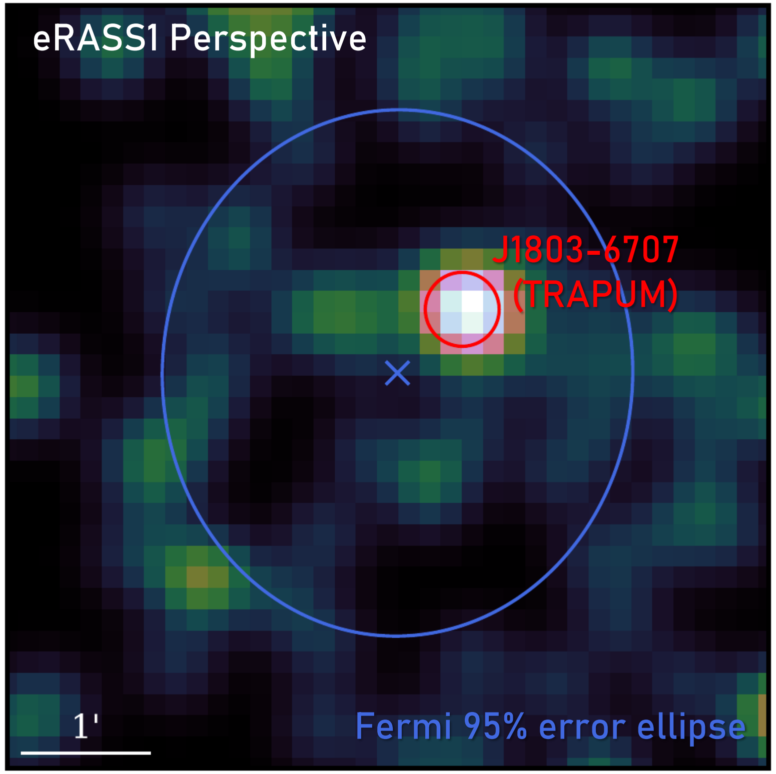

Followup example: Multiwavelength view of PSR J1803–6707

Clark et al. 2023

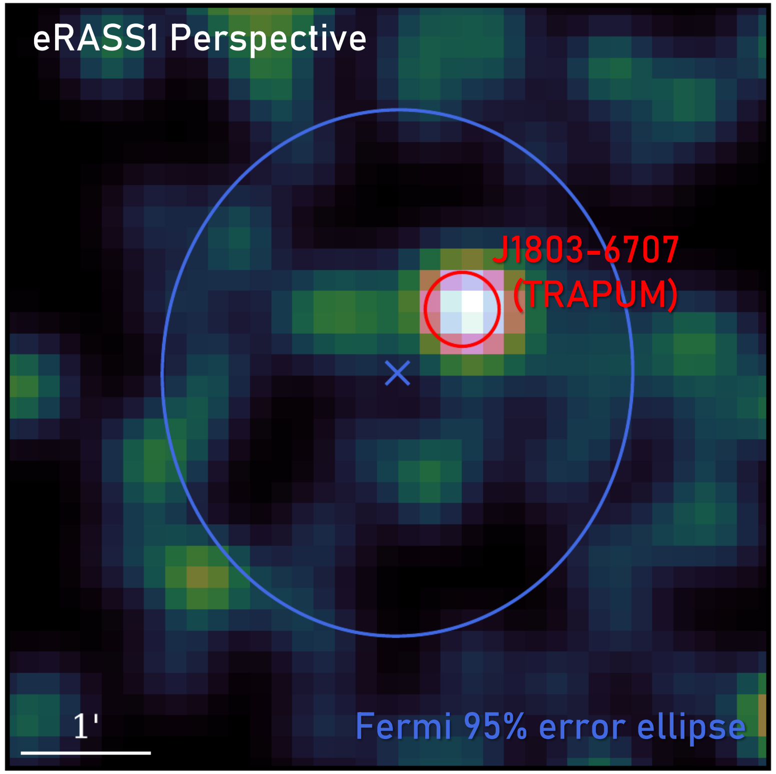

Radio pulsations

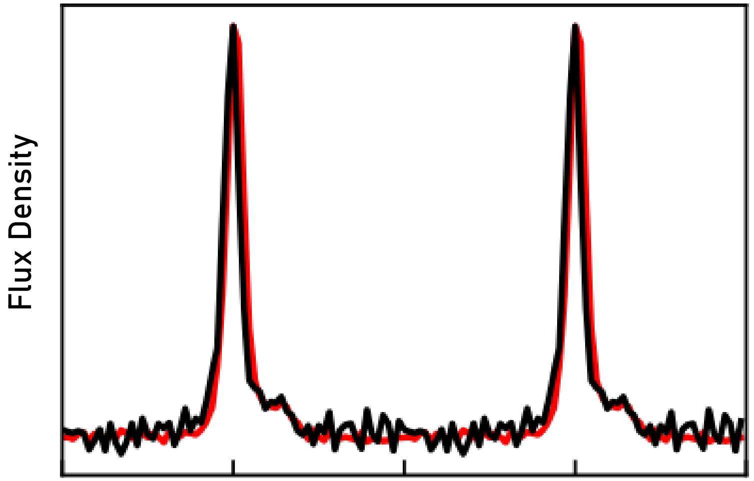

Followup example: Multiwavelength view of PSR J1803–6707

Clark et al. 2023

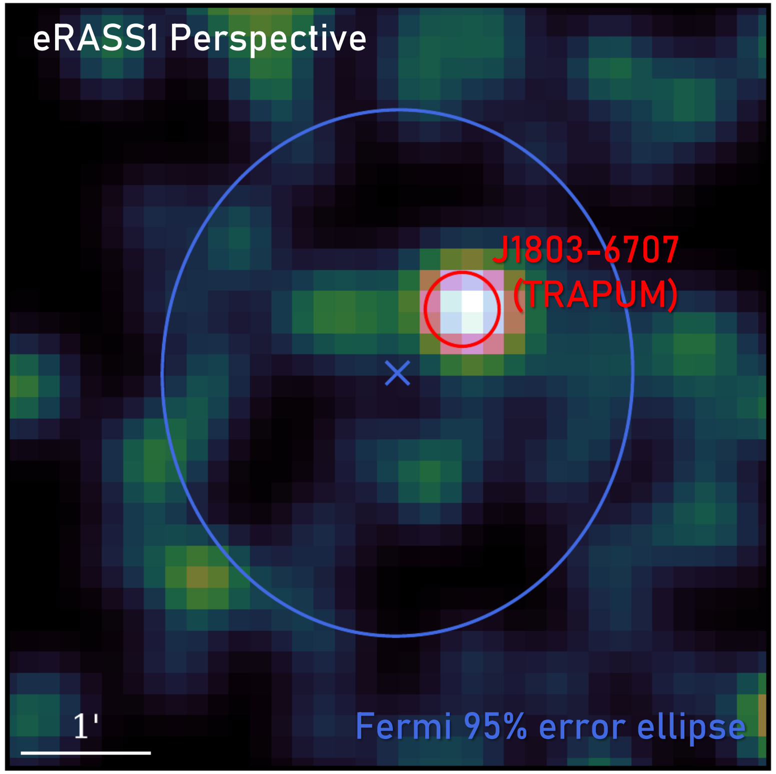

γ-ray pulsations
(Clark et al. 2023)

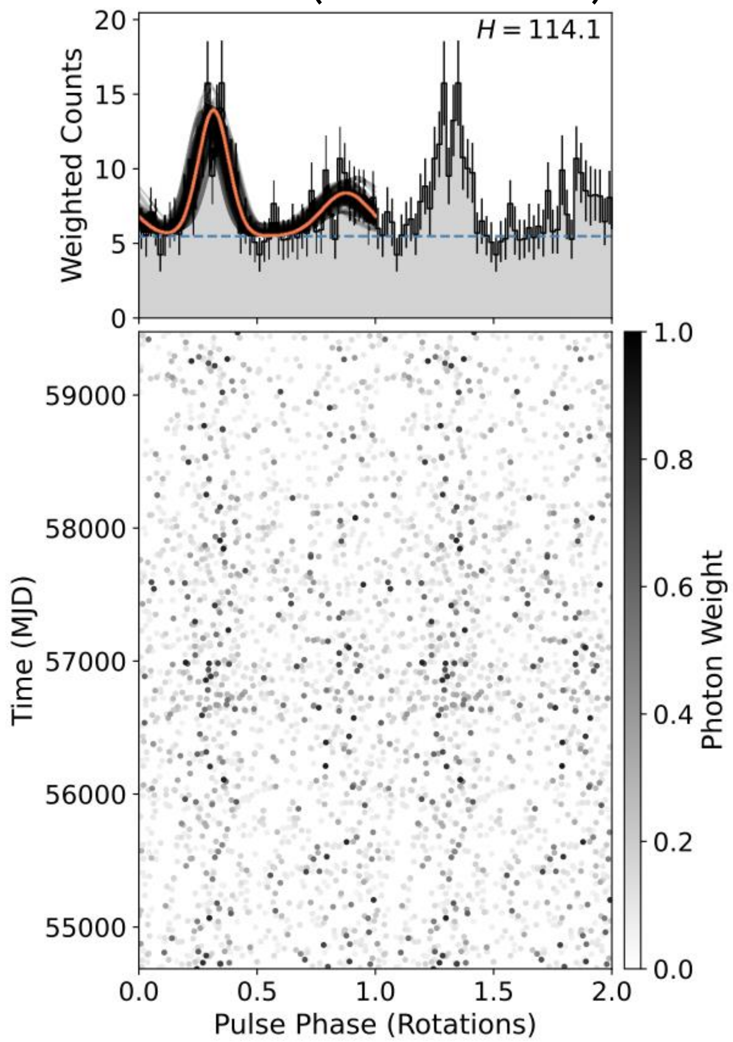

Radio pulsations

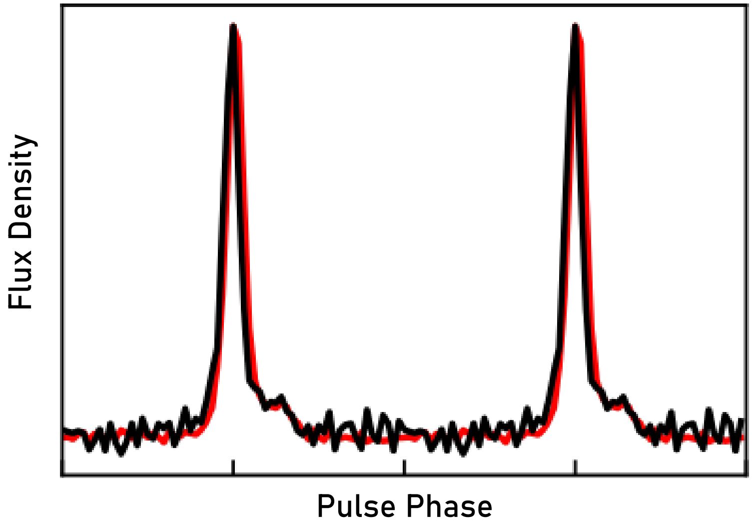

Followup example: Multiwavelength view of PSR J1803–6707

Clark et al. 2023

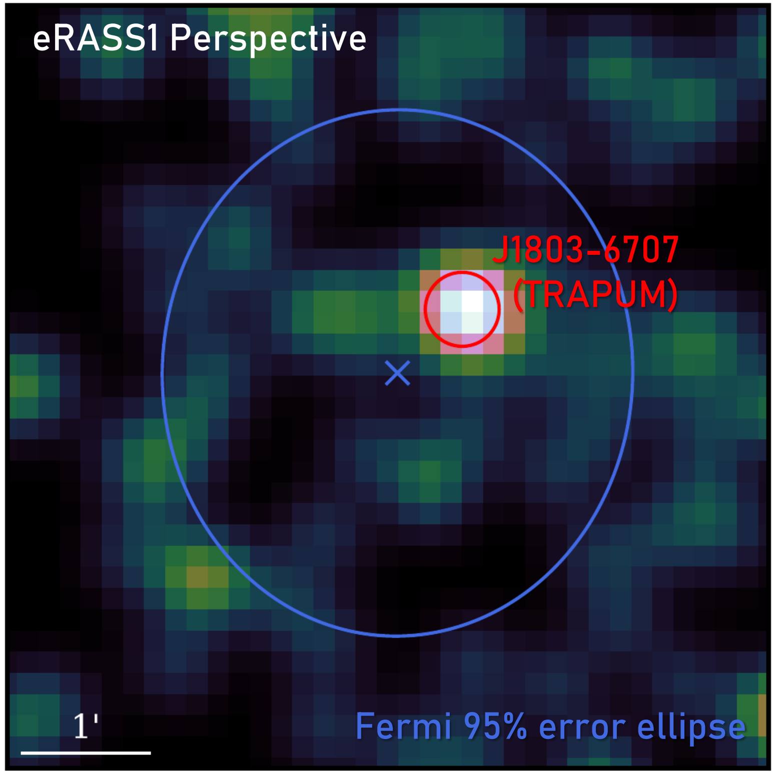

γ-ray pulsations
(Clark et al. 2023)

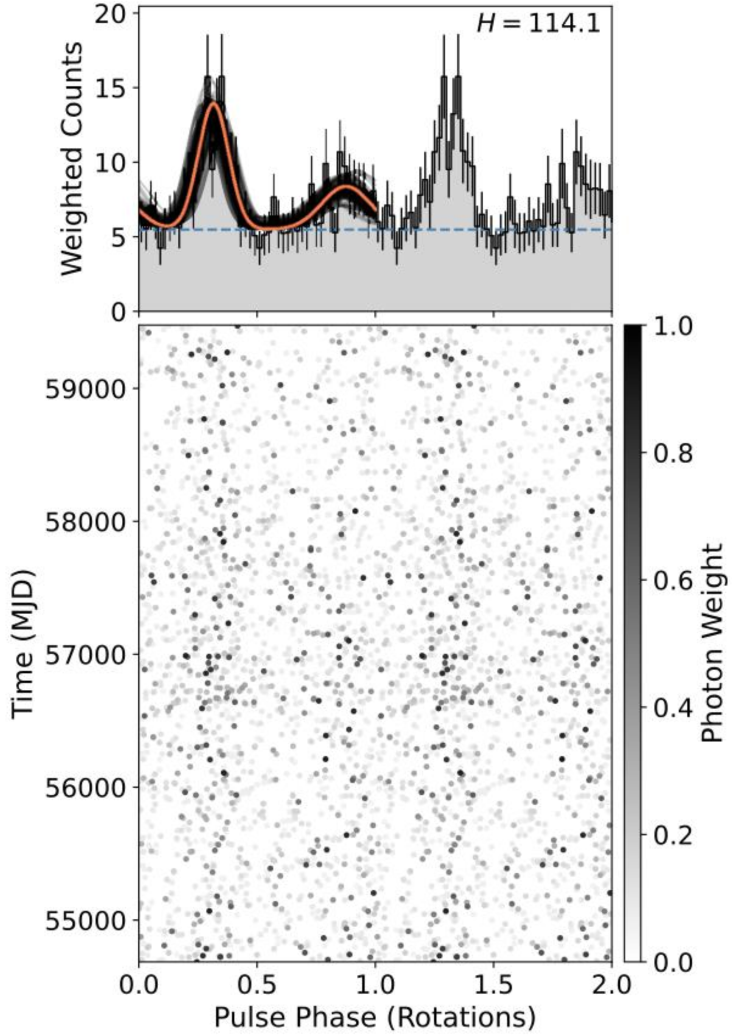

Radio pulsations

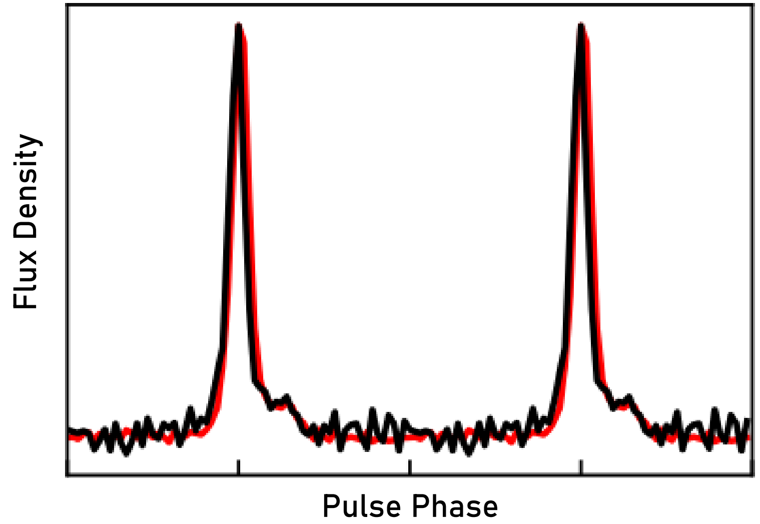

Optical modulation

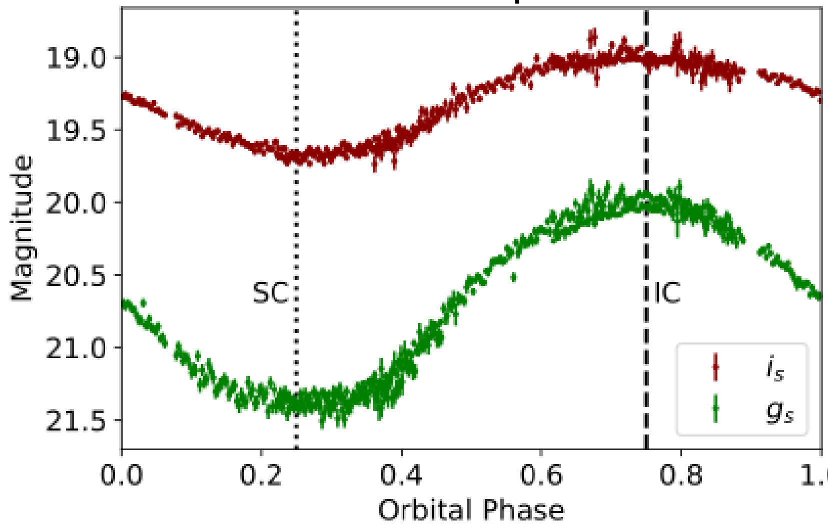

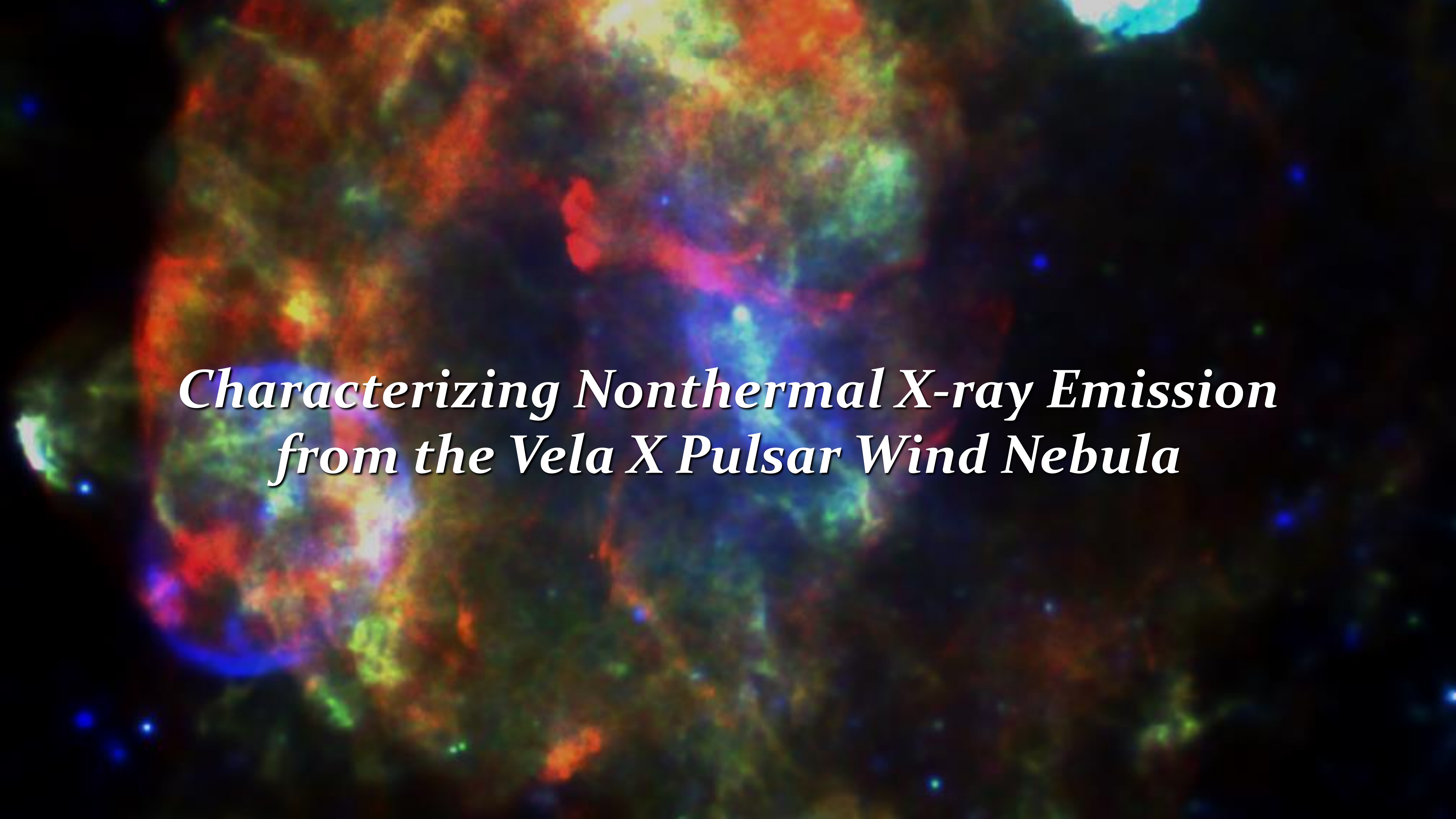

Characterizing Nonthermal X-ray Emission from the Vela X Pulsar Wind Nebula

Vela X & The Vela Supernova Remnant

- Vela X: Pulsar wind nebula (PWN) of energetic PSR B0833-45
  - Embedded in very extended Vela SNR
  - Nearby (~ 290 pc; Dodson+03)
  - Age ~ 11 – 30 kyr (Aschenbach+95, Lyne+96, Espinoza+17)

- eRASS:4 data allow for disentangling thermal & nonthermal X-rays
  - ➢ First view of X-ray synchrotron emitting electrons on large scales

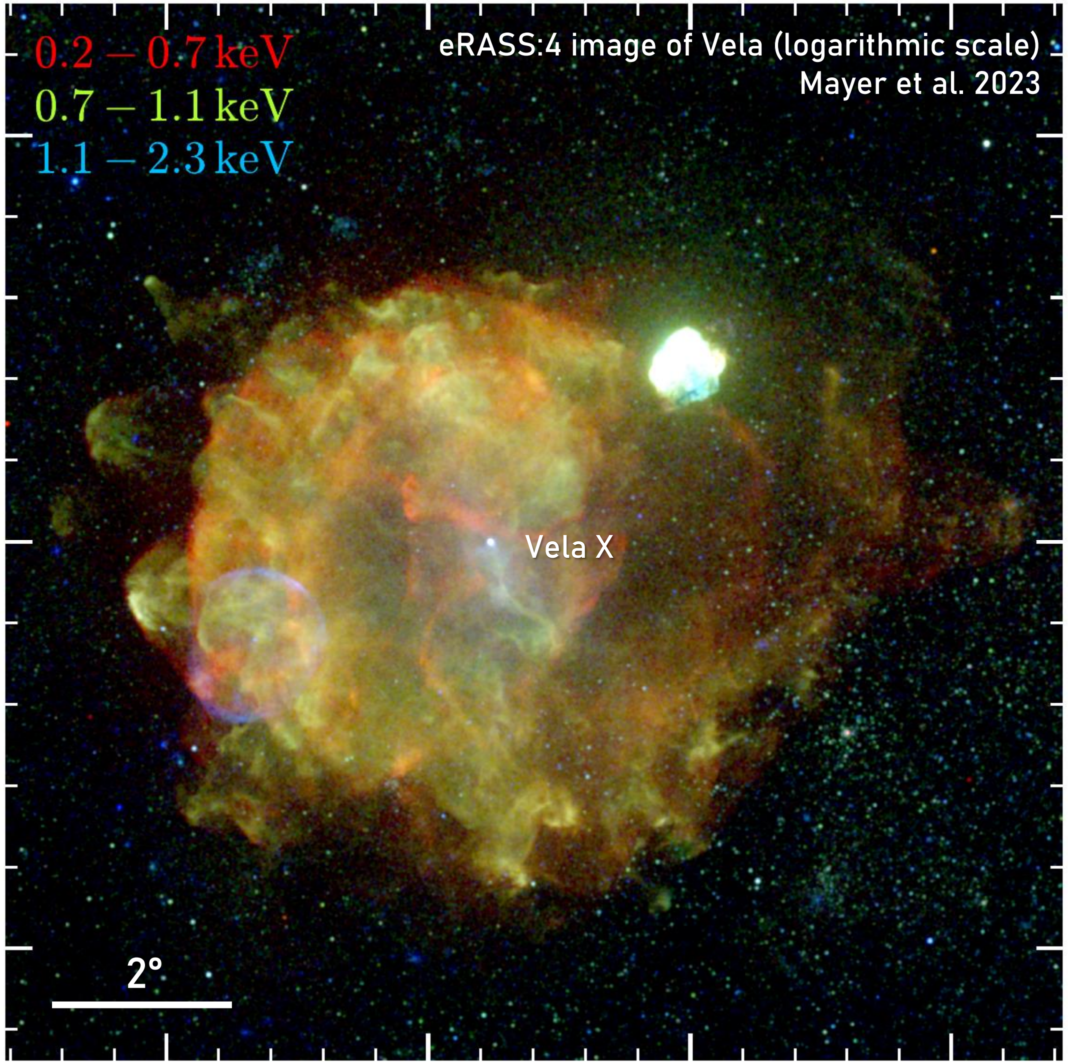

Vela X & The Vela Supernova Remnant

- Vela X: Pulsar wind nebula (PWN) of energetic PSR B0833-45
  - Embedded in very extended Vela SNR
  - Nearby (~ 290 pc; Dodson+03)
  - Age ~ 11 – 30 kyr (Aschenbach+95, Lyne+96, Espinoza+17)

- eRASS:4 data allow for disentangling thermal & nonthermal X-rays
  - ➢ First view of X-ray synchrotron emitting electrons on large scales

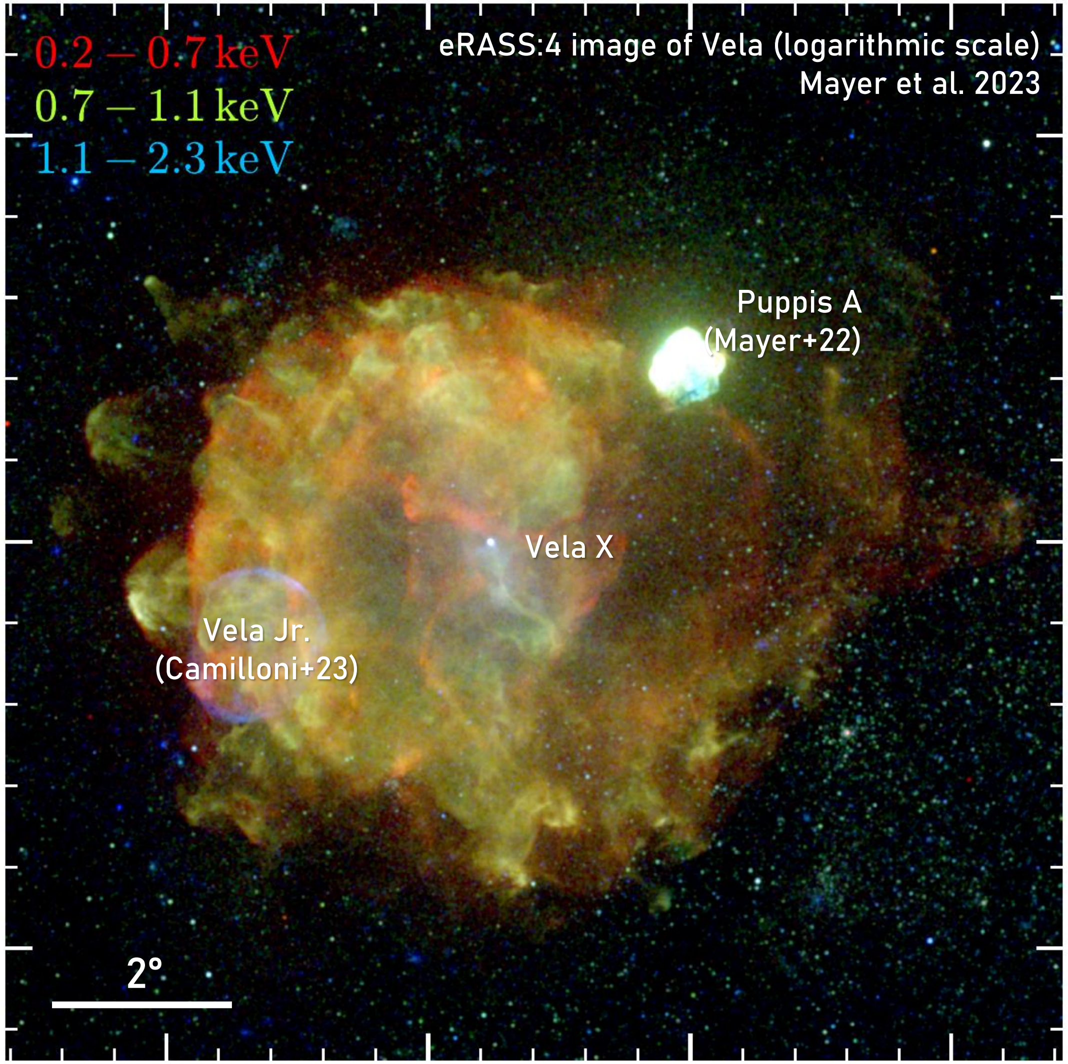

Vela X & The Vela Supernova Remnant

- Vela X: Pulsar wind nebula (PWN) of energetic PSR B0833-45
  - Embedded in very extended Vela SNR
  - Nearby (~ 290 pc; Dodson+03)
  - Age ~ 11 – 30 kyr (Aschenbach+95, Lyne+96, Espinoza+17)

- eRASS:4 data allow for disentangling thermal & nonthermal X-rays
  - ➢ First view of X-ray synchrotron emitting electrons on large scales

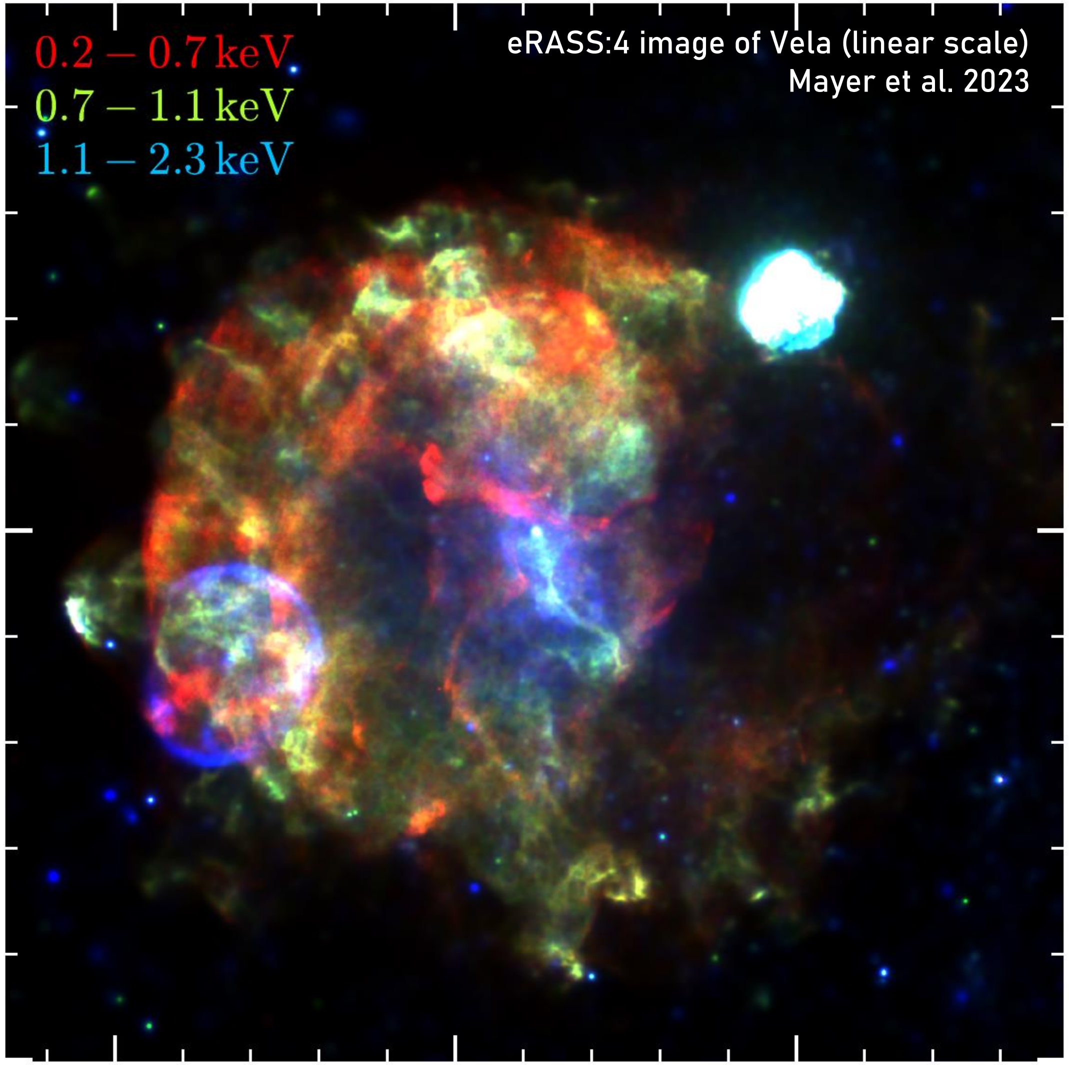

Analysis: X-ray Spectroscopy

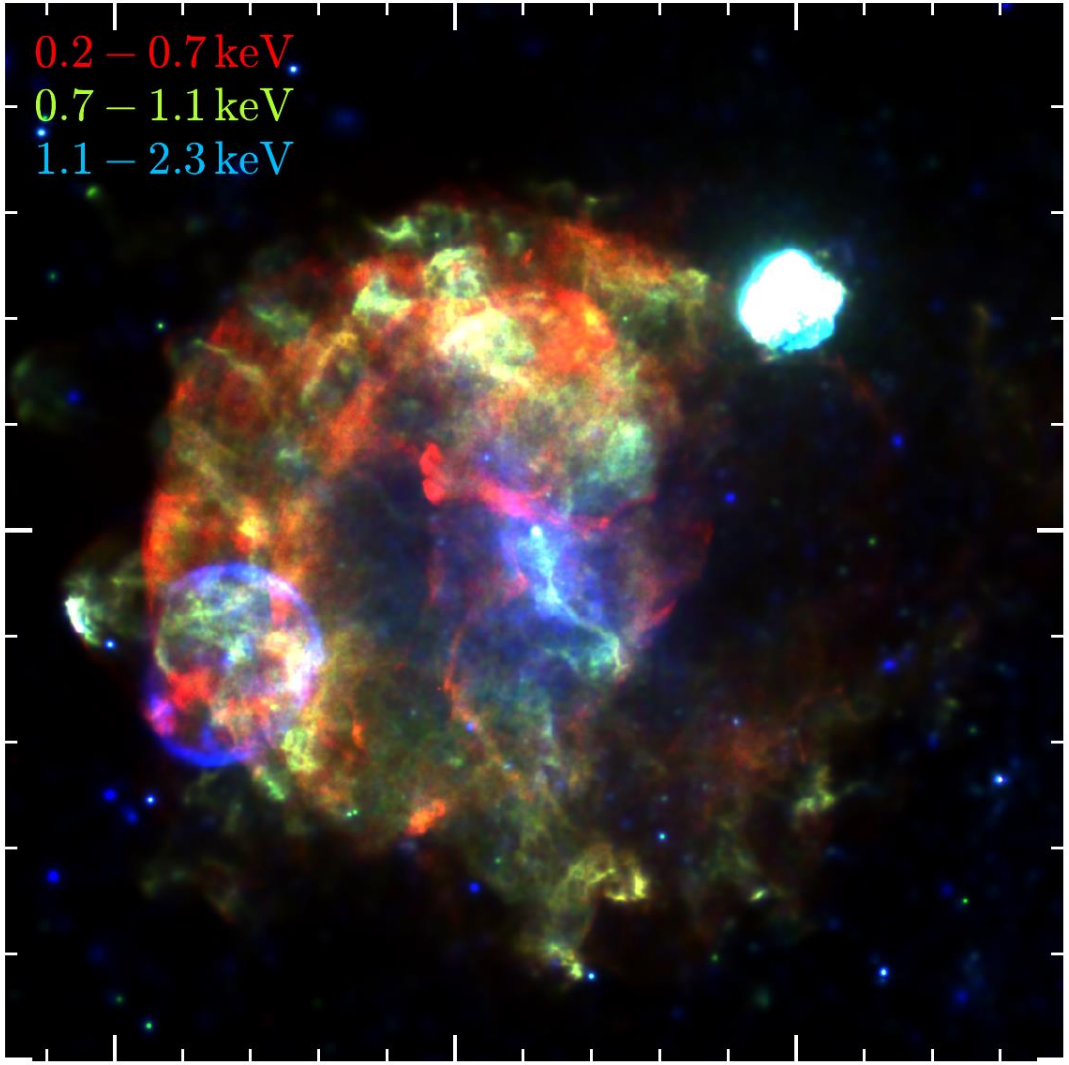

Analysis: X-ray Spectroscopy

- Adaptive Voronoi binning (Cappellari+03)
  - Around 500 spectra with uniform statistics (~ 10^4 X-ray photons)

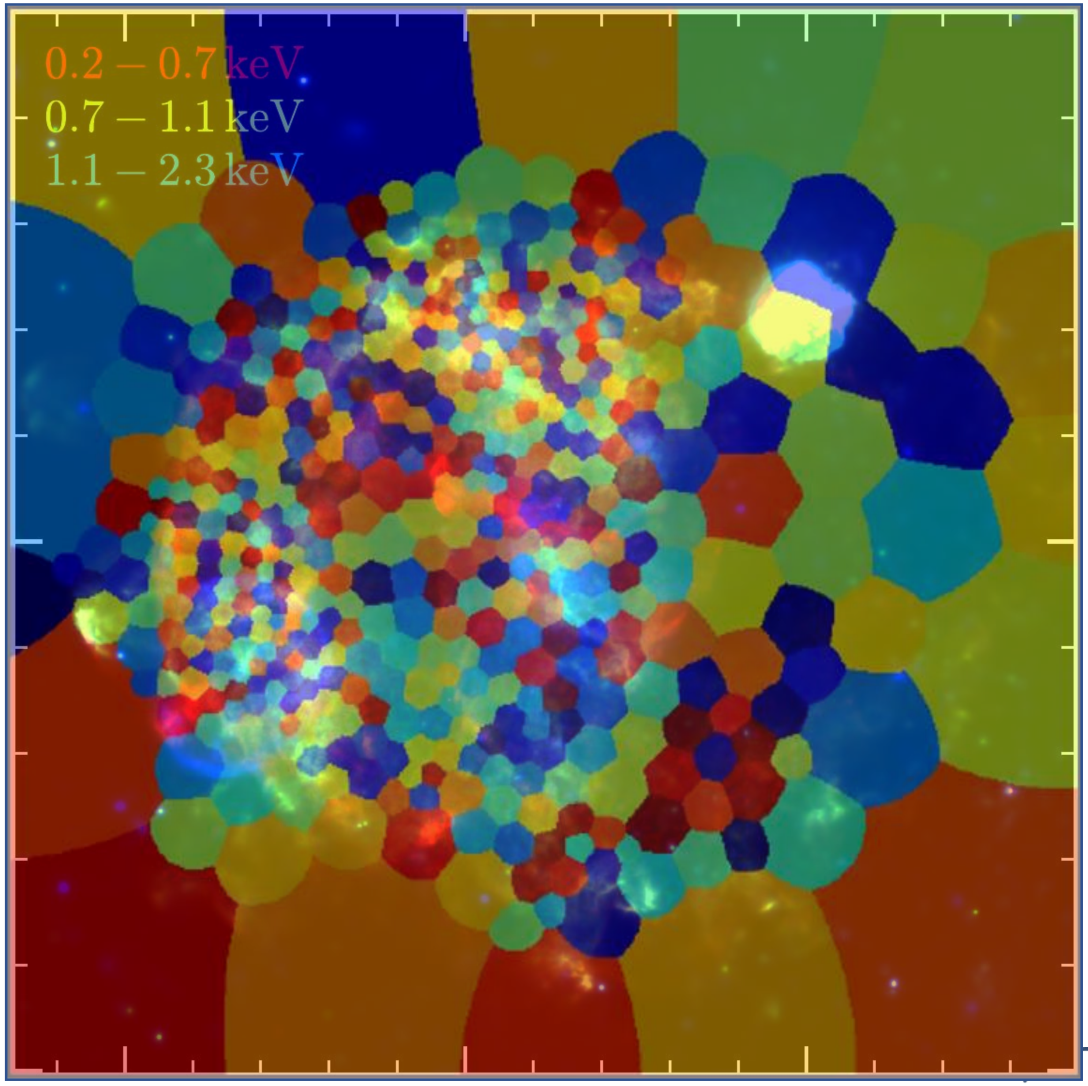

Analysis: X-ray Spectroscopy

- Adaptive Voronoi binning (Cappellari+03)
  - ➢ Around 500 spectra with uniform statistics (~ 10^4 X-ray photons)

- Characterize thermal & nonthermal components via spectral modelling
  - ➢ Nonthermal flux & photon index, (absorption, plasma temperature, abundances, ...)

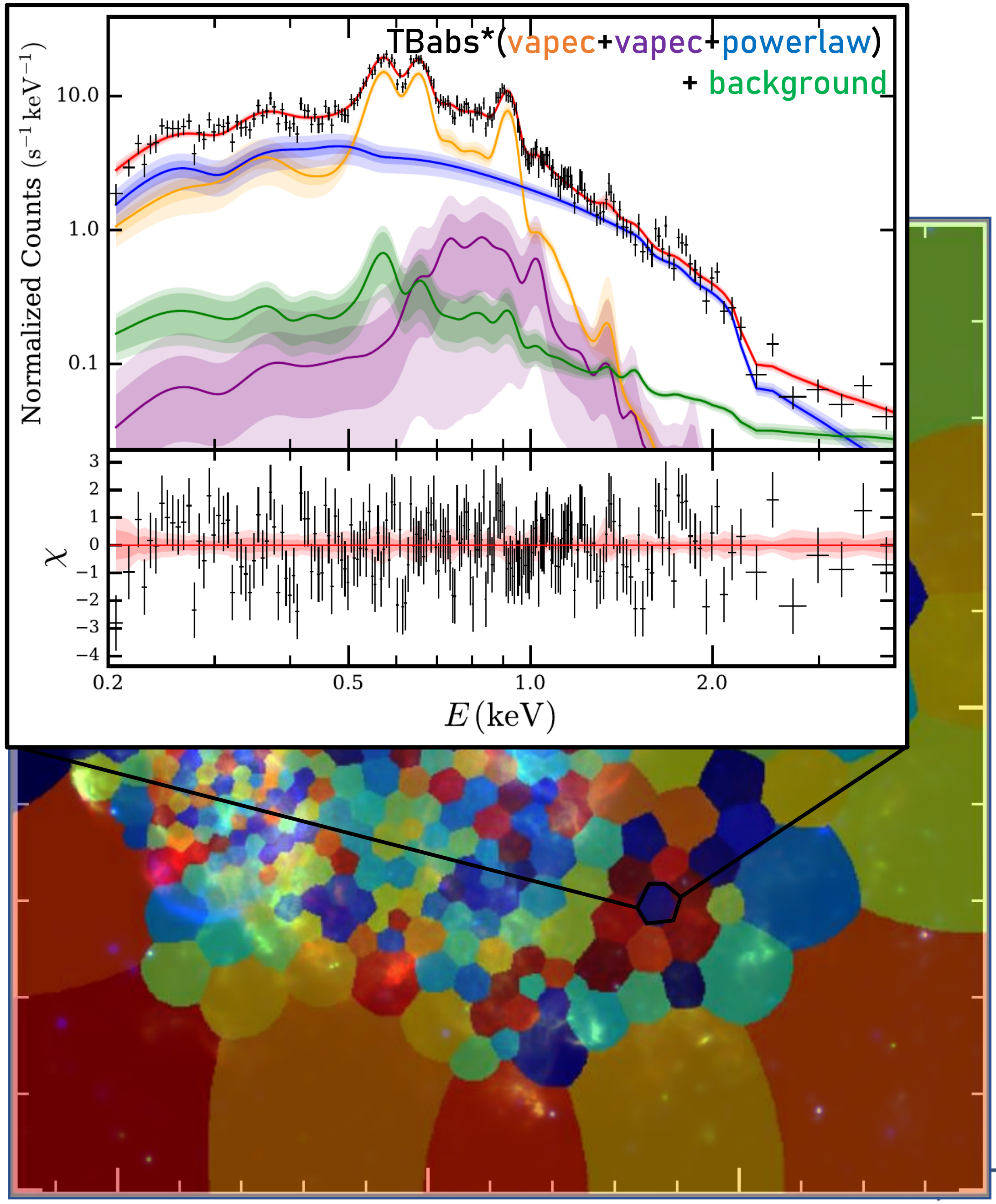

Results: Nonthermal Emission

- Vela X in X-rays:
  - Compact PWN core with „jet“ and equatorial torus (e.g., Helfand+2001)
  - X-ray synchrotron emission in „Cocoon“ visible with ROSAT & XMM (e.g. Markwardt+1995, Slane+2018)

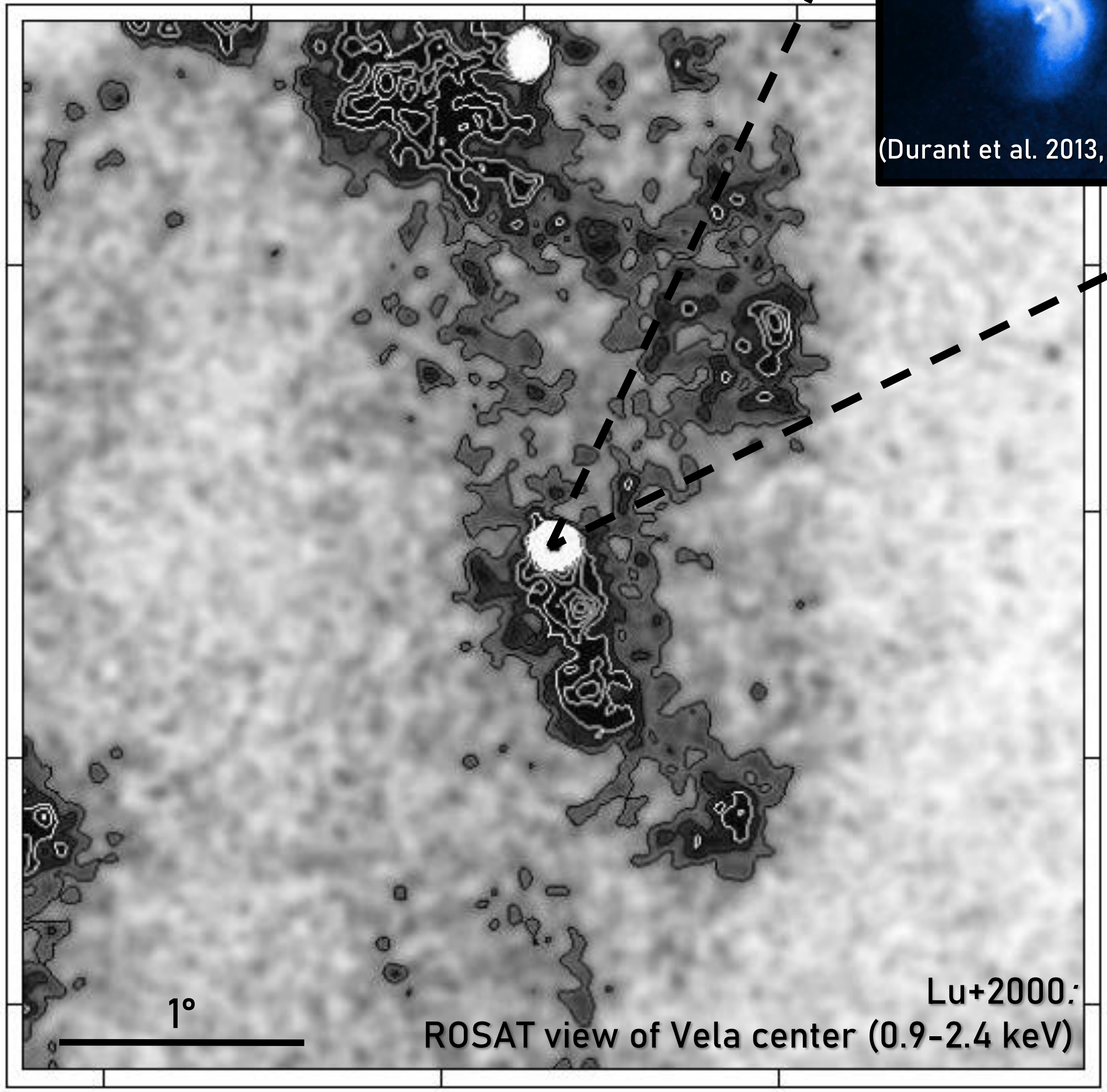

Results: Nonthermal Emission

- Vela X in X-rays:
  - Compact PWN core with „jet“ and equatorial torus (e.g., Helfand+2001)
  - X-ray synchrotron emission in „Cocoon“ visible with ROSAT & XMM (e.g. Markwardt+1995, Slane+2018)

➢Now: Observe much larger size of diffuse synchrotron emission of PWN; radial extent of 2° - 3°

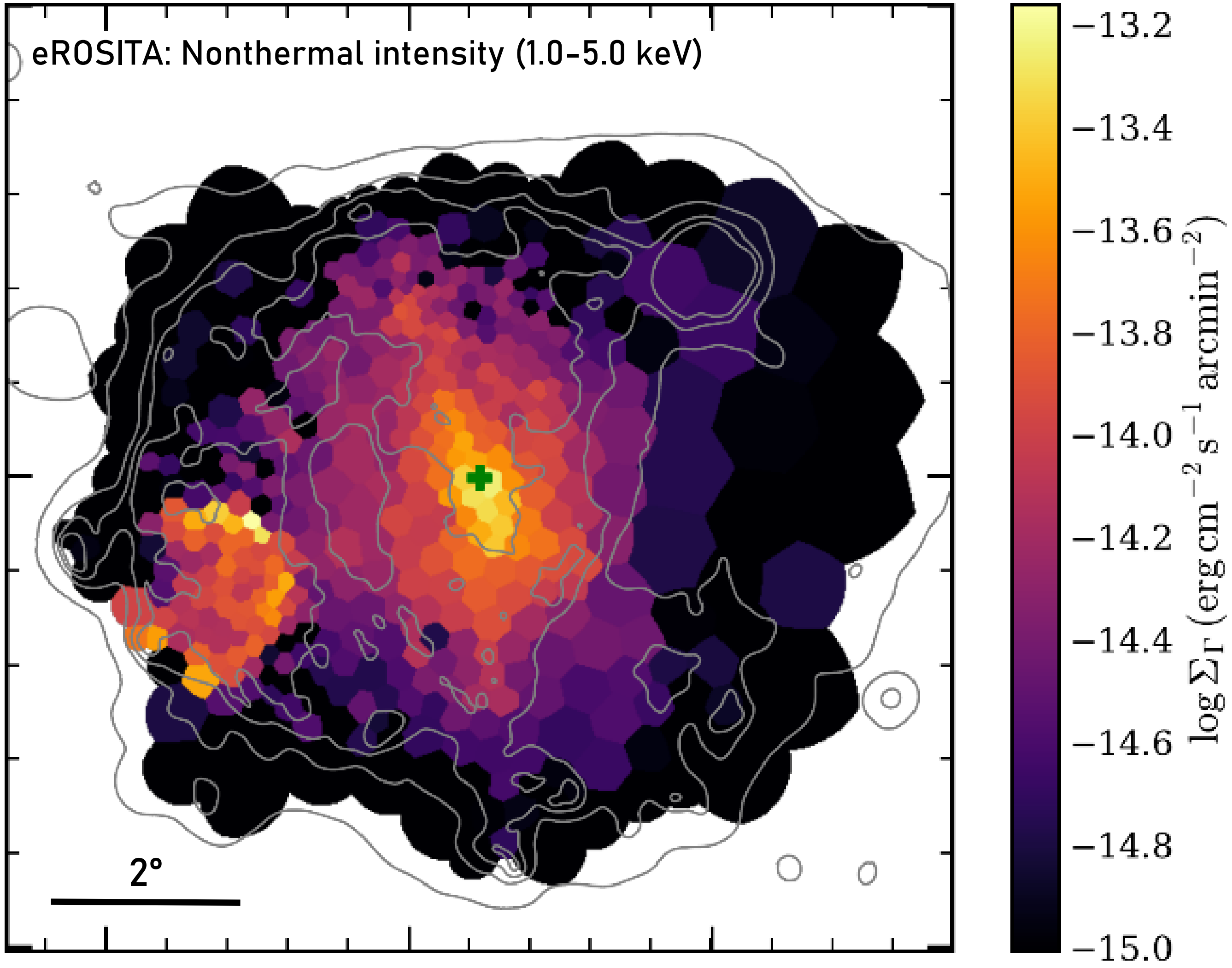

Results: Nonthermal Emission

- Vela X in X-rays:
  - Compact PWN core with „jet“ and equatorial torus (e.g., Helfand+2001)
  - X-ray synchrotron emission in „Cocoon“ visible with ROSAT & XMM (e.g. Markwardt+1995, Slane+2018)

➢ Now: Observe much larger size of diffuse synchrotron emission of PWN; radial extent of 2° - 3°

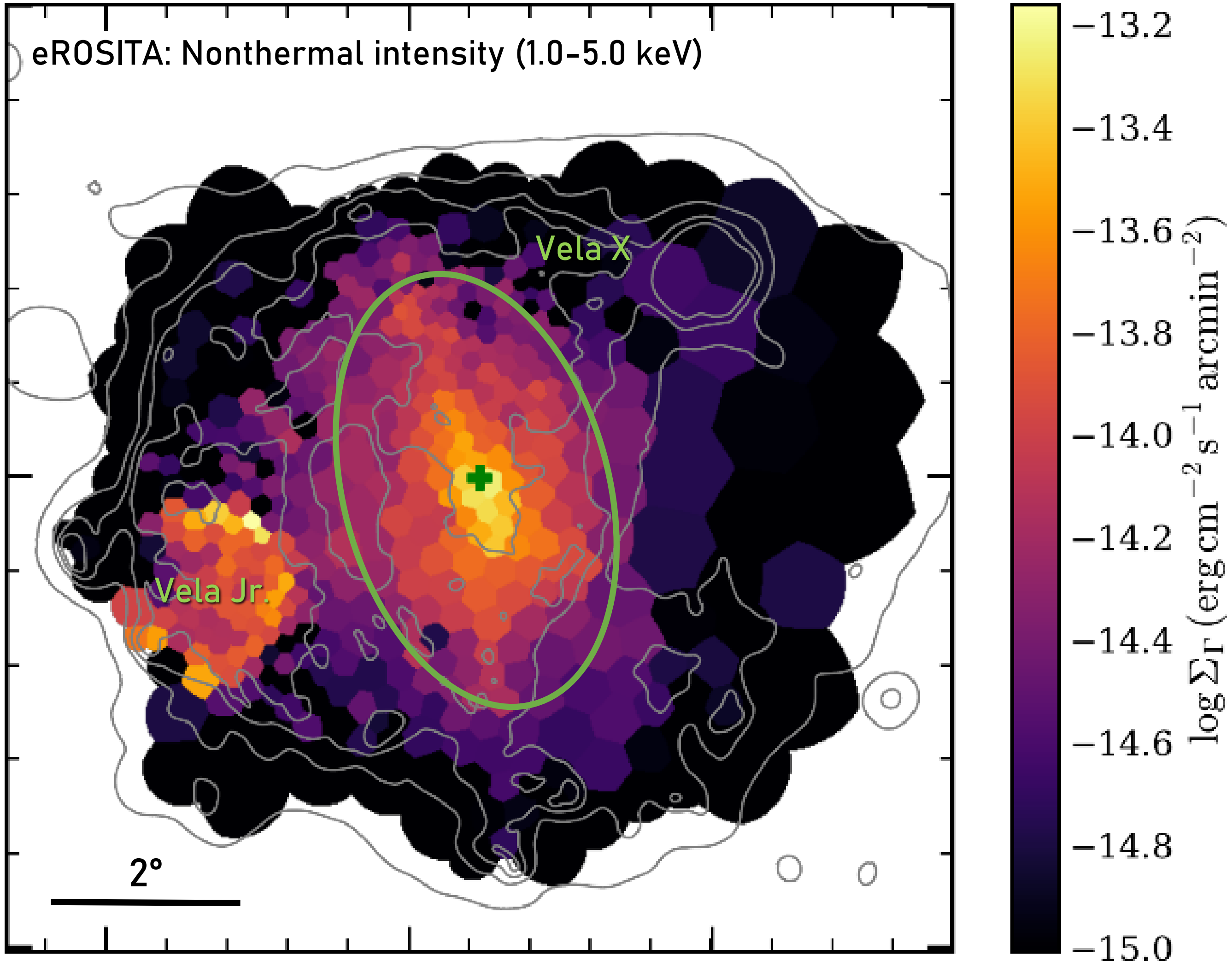

Results: Particle Diffusion in Vela X

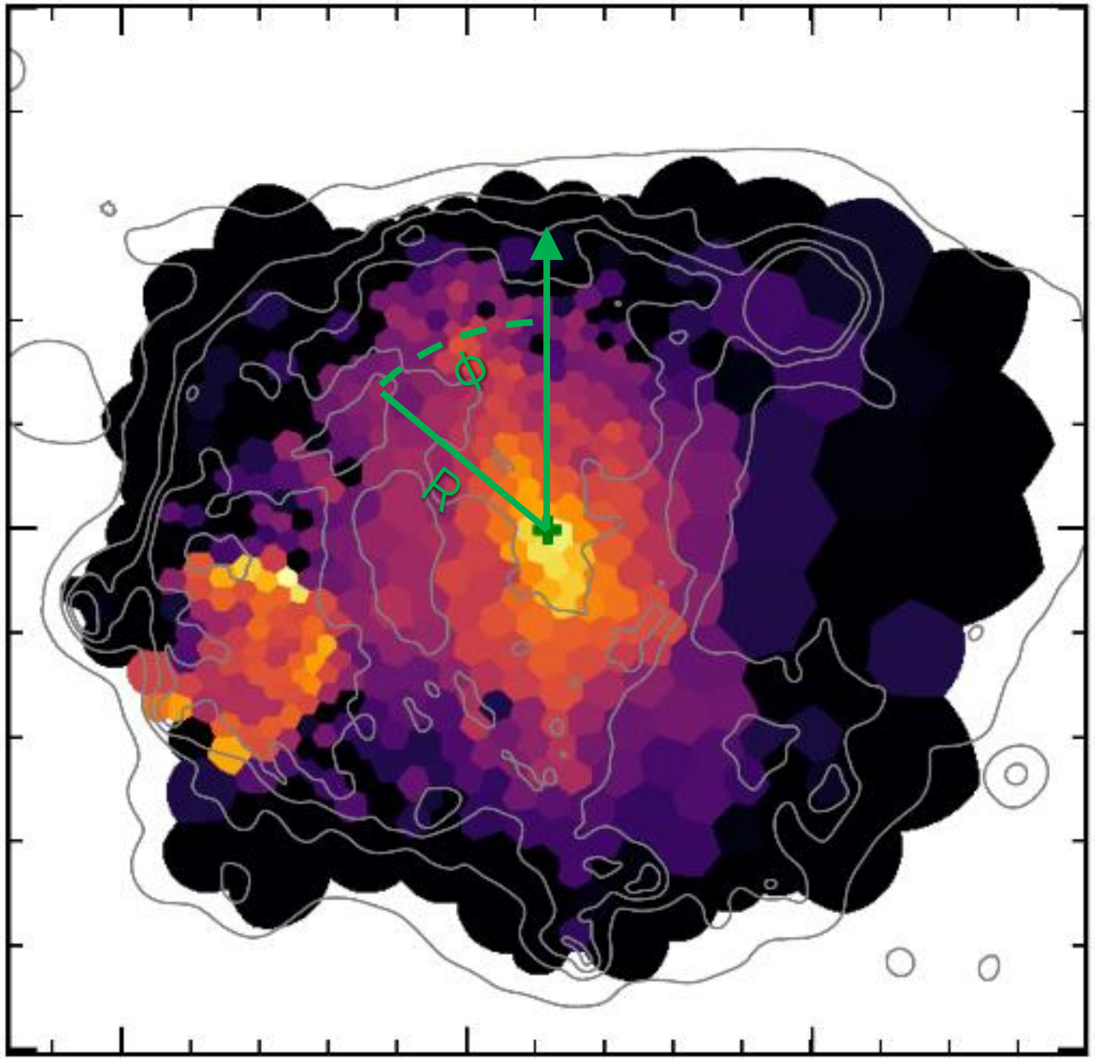

Results: Particle Diffusion in Vela X

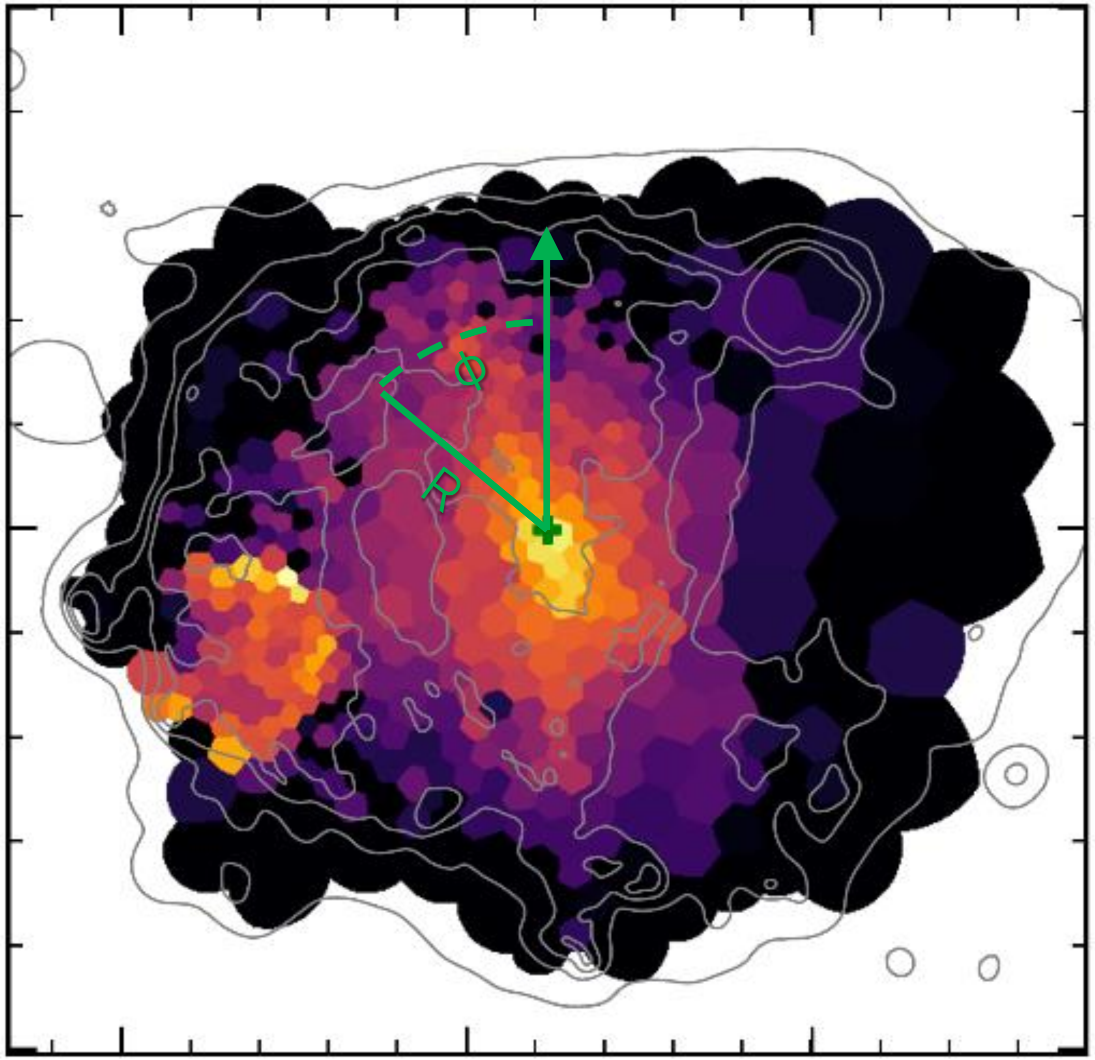

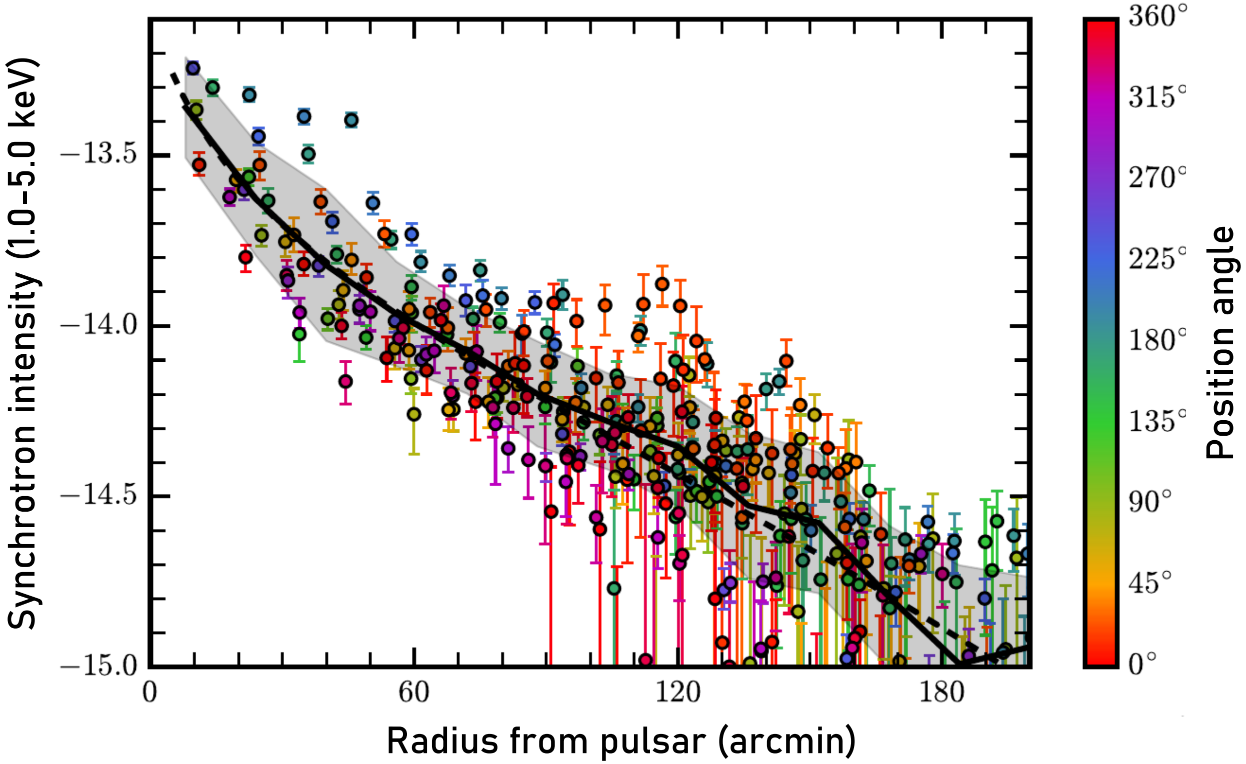

Results: Particle Diffusion in Vela X

- Synchrotron emission from relativistic electrons diffusing through ambient medium

$$dE/dt \propto -\left(U_B + U_\gamma\right) E^2$$

Synchrotron   Inverse Compton

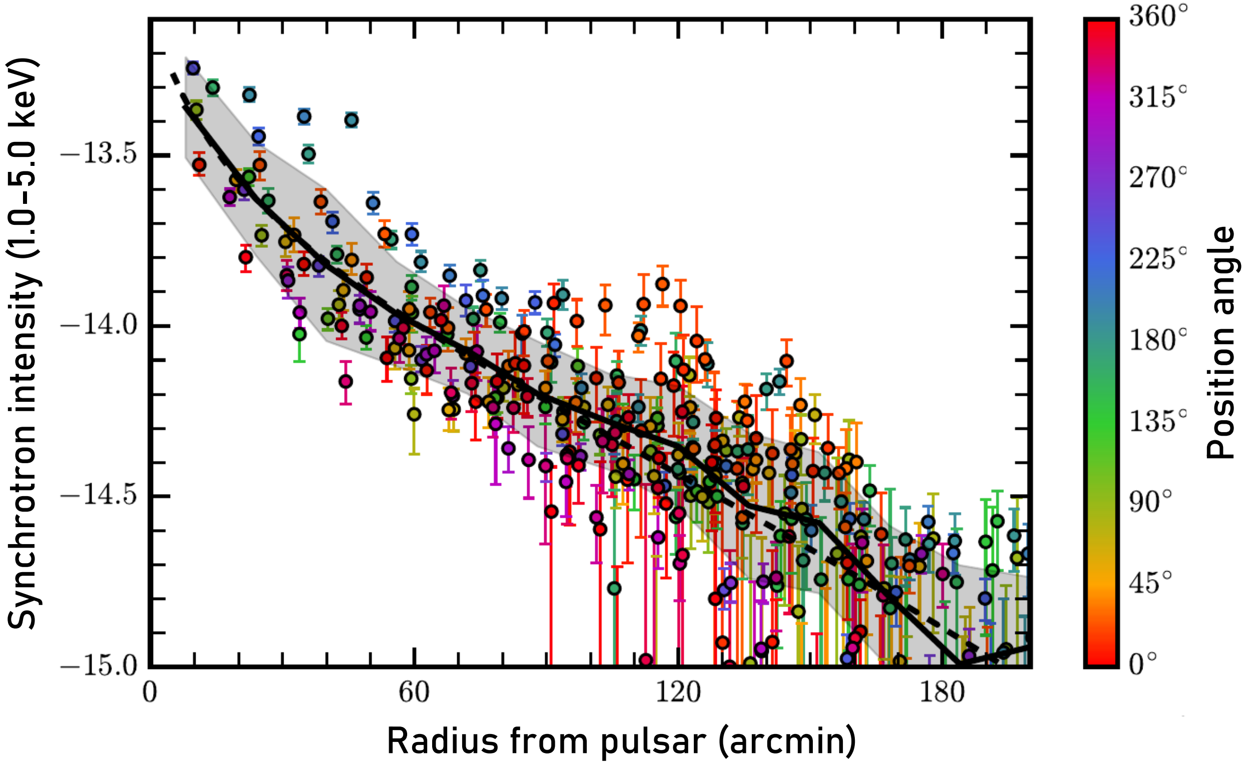

Results: Particle Diffusion in Vela X

- Synchrotron emission from relativistic electrons diffusing through ambient medium

$$dE/dt \propto -\left(U_B + U_\gamma\right) E^2$$

Synchrotron   Inverse Compton

➢Characteristic physical extent (Abeysekara+17) limited by energy loss

$$r_D = (4D\tau)^{1/2}$$

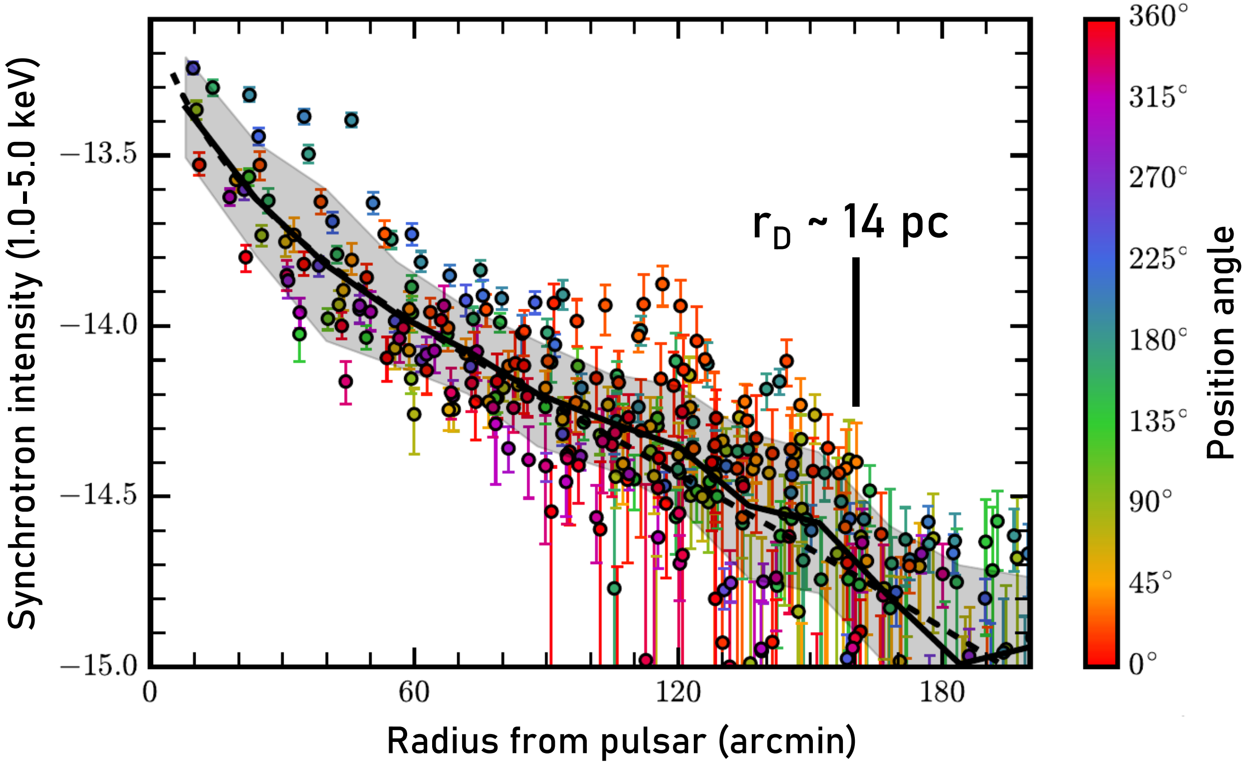

Results: Particle Diffusion in Vela X

- Synchrotron emission from relativistic electrons diffusing through ambient medium

$$dE/dt \propto -\left(U_B + U_\gamma\right) E^2$$

Synchrotron   Inverse Compton

➢ Characteristic physical extent (Abeysekara+17) limited by energy loss

$$r_D = (4D\tau)^{1/2}$$

➢ Spectral softening consistent with radiative energy losses (Tang+12)

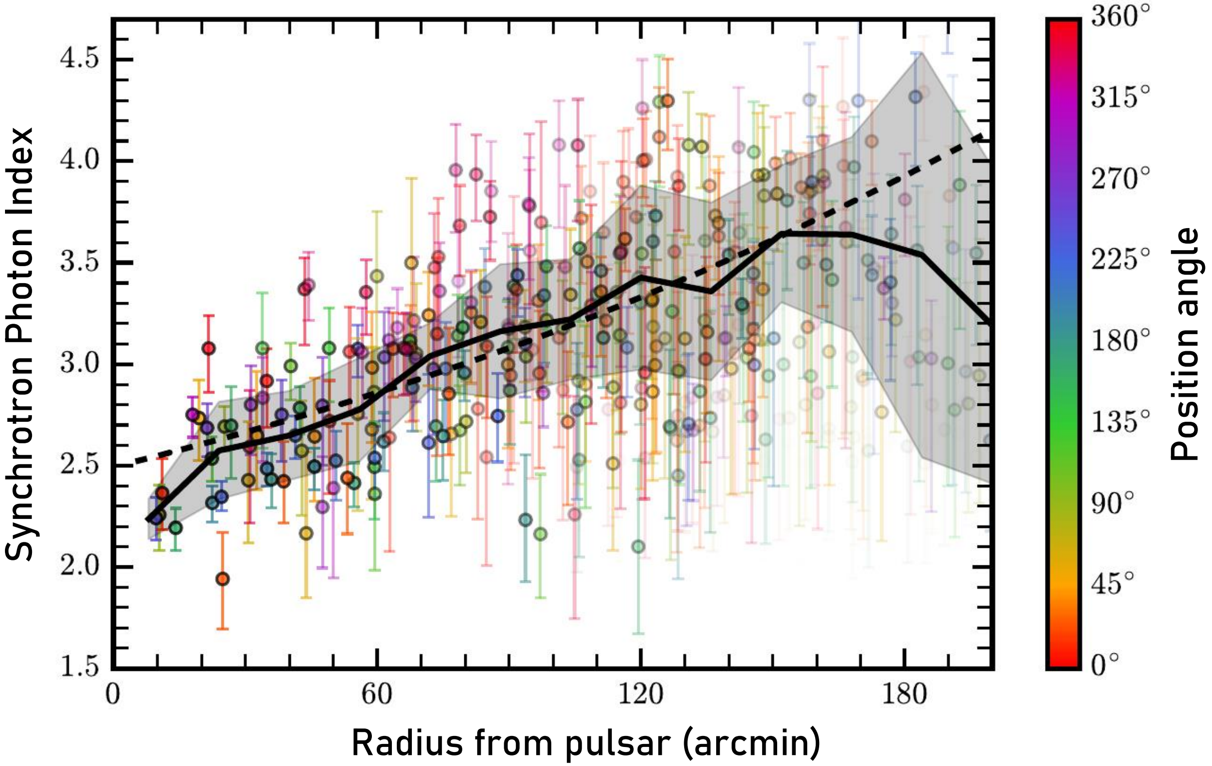

Results: Particle Diffusion in Vela X

- Synchrotron emission from relativistic electrons diffusing through ambient medium

$$dE/dt \propto -\left(U_B + U_\gamma\right) E^2$$

Synchrotron — Inverse Compton

➢ Characteristic physical extent (Abeysekara+17) limited by energy loss

$$r_D = (4D\tau)^{1/2}$$

➢ Spectral softening consistent with radiative energy losses (Tang+12)

➢ Assuming ISM B-field:

$$D = 3.6^{+0.6}_{-0.5} \times 10^{27}\ \mathrm{cm^2\ s^{-1}}$$

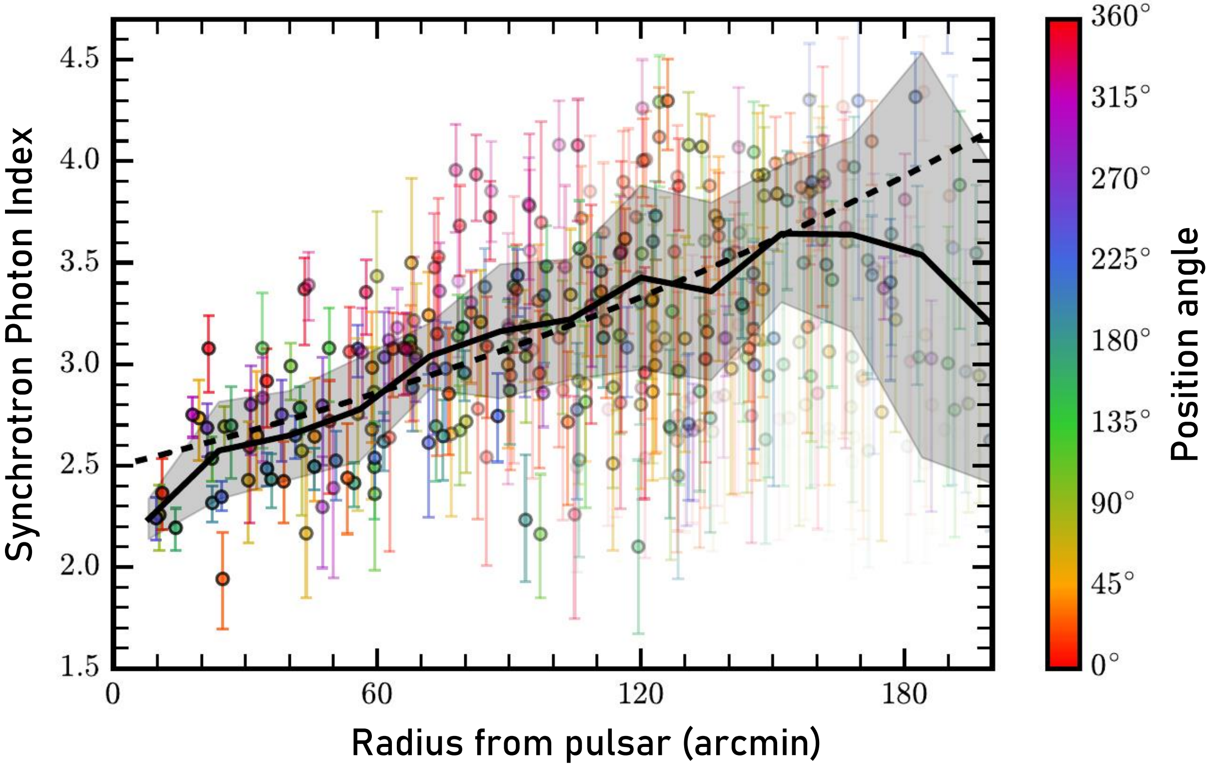

Results: Multiwavelength View of Vela X

X-ray synchrotron emission originates from TeV-energy electron population

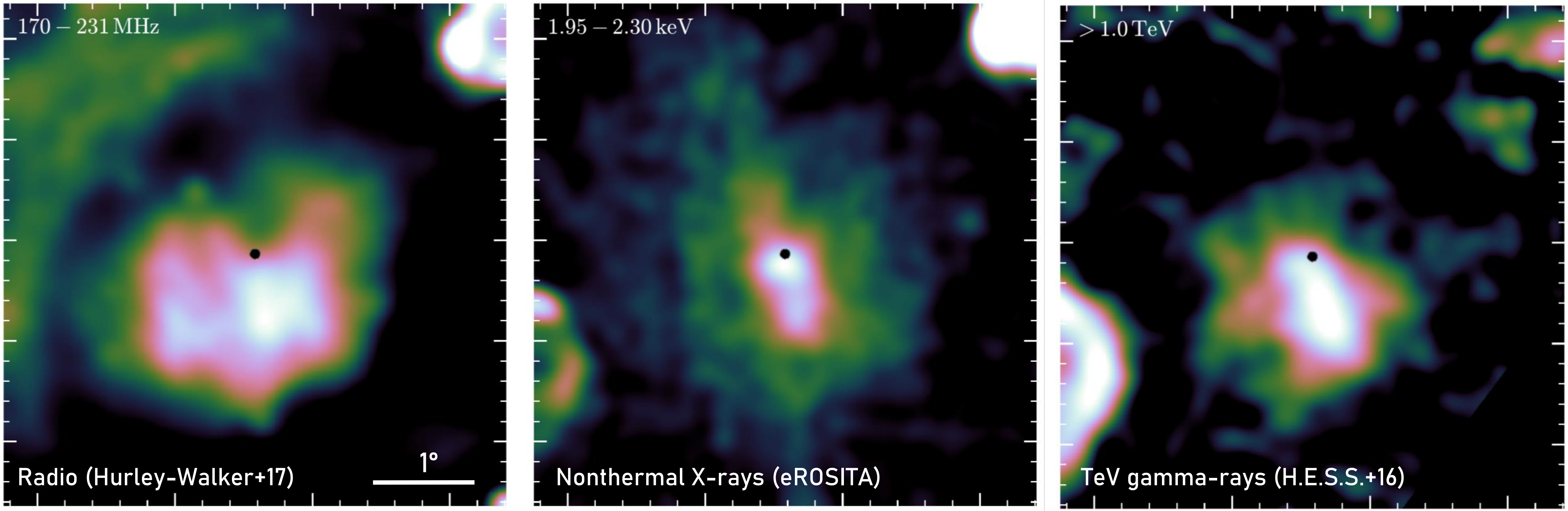

Results: Multiwavelength View of Vela X

X-ray synchrotron emission originates from TeV-energy electron population

- ➢No apparent counterpart in the north in TeV & radio bands
- ➢TeV emission would be crucial for constraining magnetic field & particle population

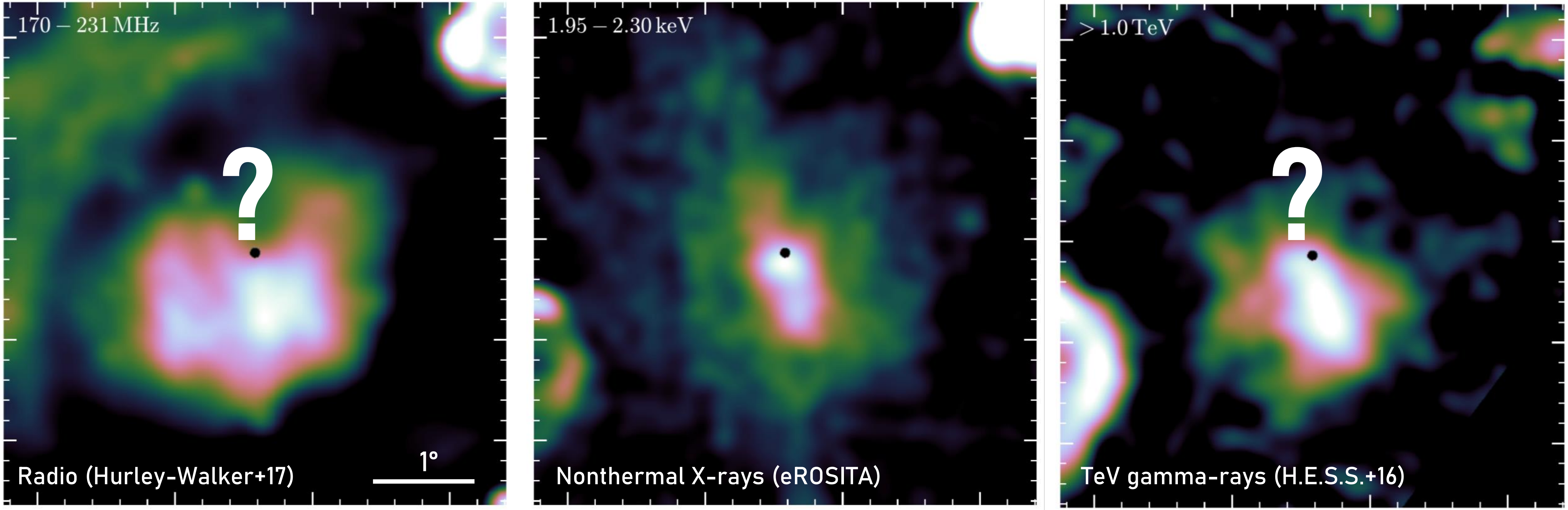

Summary

eROSITA all-sky survey data sensitive to nonthermal X-ray emission at E < 2 keV

- Systematic search for new pulsar candidates via Fermi-LAT - eROSITA crossmatch
  - ➢Candidate catalogue designed for optical/radio followup
- Discovery of very extended component in Vela X PWN
  - ➢Physical picture unclear without multiwavelength analysis

➢Mayer et al. (2023), A&A, 676, A68
Mayer & Becker (2024), A&A, 684, A208

Extra Slides Fermi Pulsars

Introduction: Neutron Star Zoo

- Rotation-powered pulsars: Energy for emission supplied by spin-down
  - Young energetic pulsars (e.g. Crab, Vela)
  - Millisecond („recycled“) pulsars: Small periods due to accretion-induced spin-up
  - ➢ Around 3000 known, mostly observed through radio pulsations
  - ➢ Magnetospheric emission at X-ray & gamma-ray energies

- „Exotic“ types: Magnetars, central compact objects, isolated neutrons stars, ...
- Accretion-powered X-ray binaries

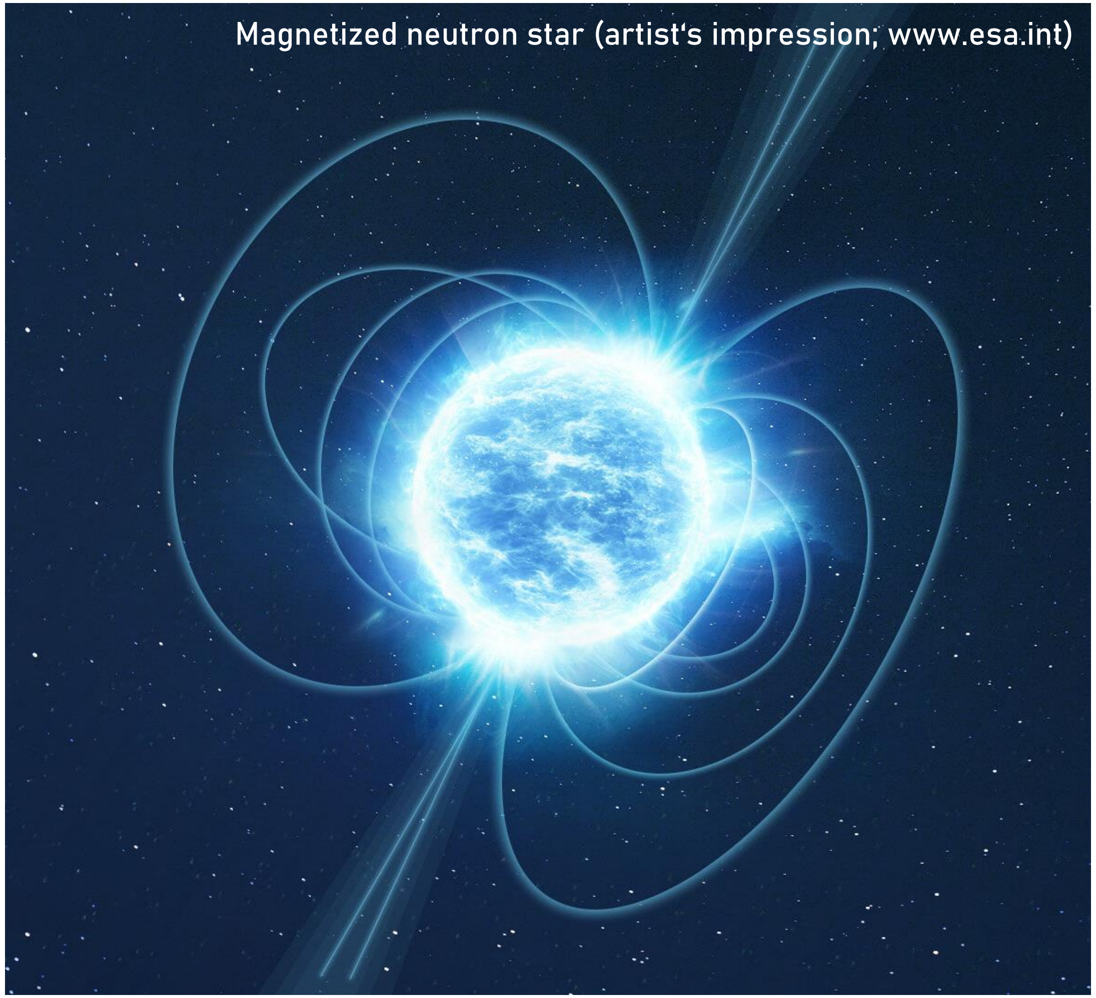

Introduction: Neutron Star Zoo

- Rotation-powered pulsars: Energy for emission supplied by spin-down
  - o Young energetic pulsars (e.g. Crab, Vela)
  - o Millisecond („recycled“) pulsars: Small periods due to accretion-induced spin-up
  - ➢ Around 3000 known, mostly observed through radio pulsations
  - ➢ Magnetospheric emission at X-ray & gamma-ray energies

- „Exotic“ types: Magnetars, central compact objects, isolated neutrons stars, ...
- Accretion-powered X-ray binaries

Zoo of non-accreting neutron stars
(Credit: ATNF pulsar database, Manchester et al. 2005)

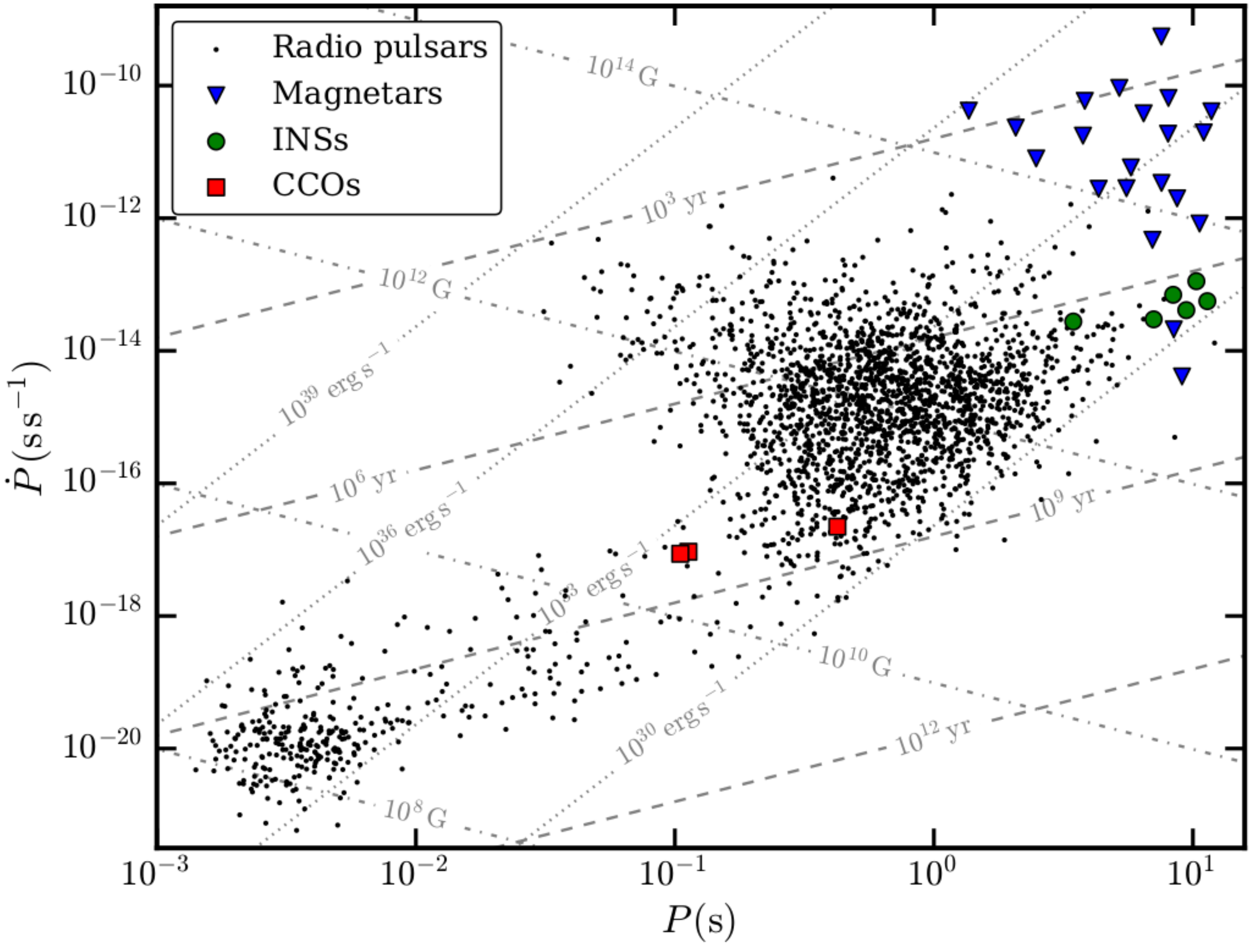

Introduction: Neutron Star Zoo

- Rotation-powered pulsars: Energy for emission supplied by spin-down
  - o Young energetic pulsars (e.g. Crab, Vela)
  - o Millisecond („recycled") pulsars: Small periods due to accretion-induced spin-up
  - ➢ Around 3000 known, mostly observed through radio pulsations
  - ➢ Magnetospheric emission at X-ray & gamma-ray energies

- „Exotic" types: Magnetars, central compact objects, isolated neutrons stars, ...
- Accretion-powered X-ray binaries

Zoo of non-accreting neutron stars
(Credit: ATNF pulsar database, Manchester et al. 2005)

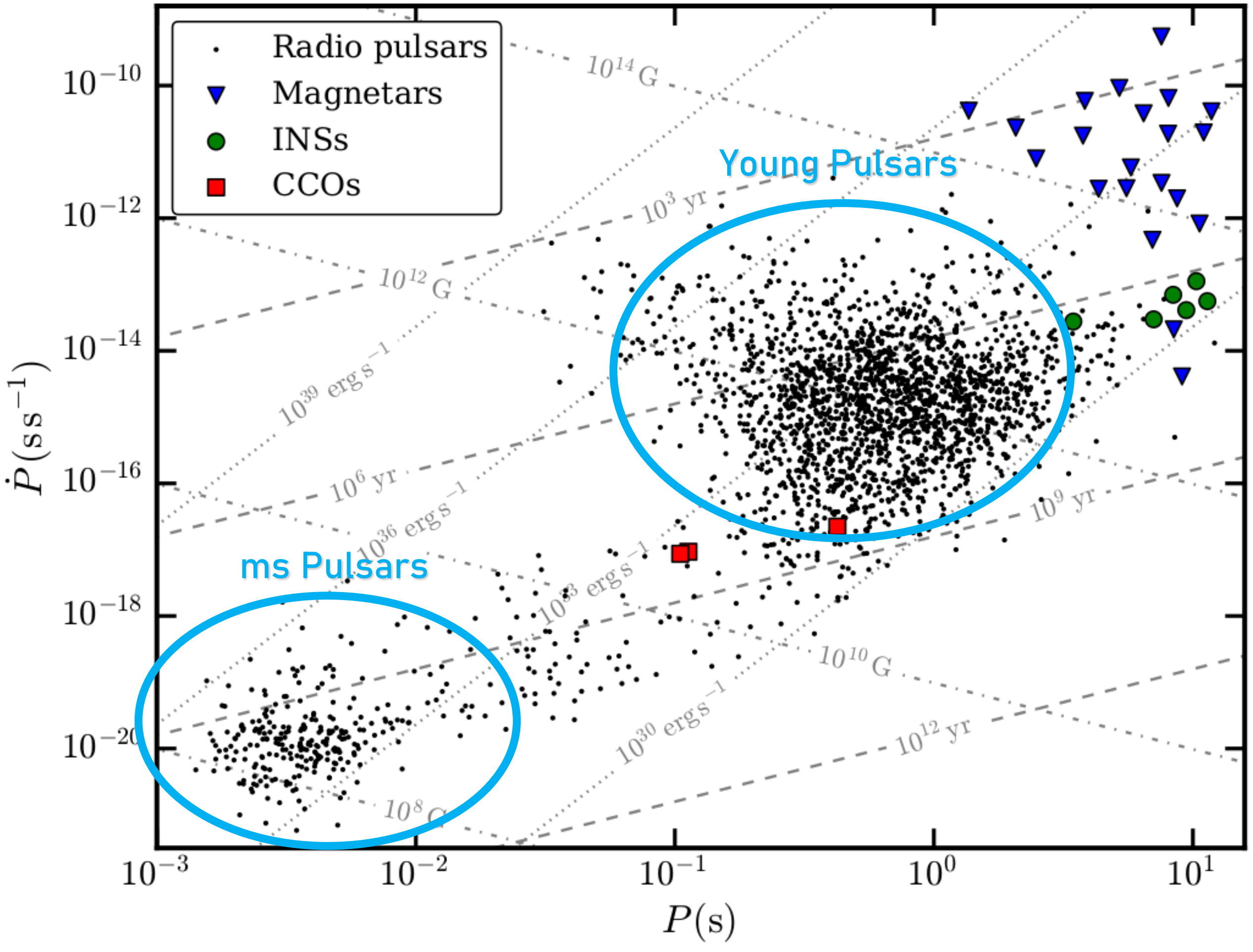

Motivation: High-Energy Pulsars

- Launch of Fermi satellite (2008) greatly increased sensitivity in GeV band
  - Present-day: 340 pulsars detected by Fermi-LAT (Smith et al. 2023)
  - Around 50% young pulsars – 50% millisecond pulsars
    - ➢ Spider binaries (redbacks, black widows): ms pulsars „consuming“ their companions

➢ Gamma-ray-based selection provides a unique view on pulsar population

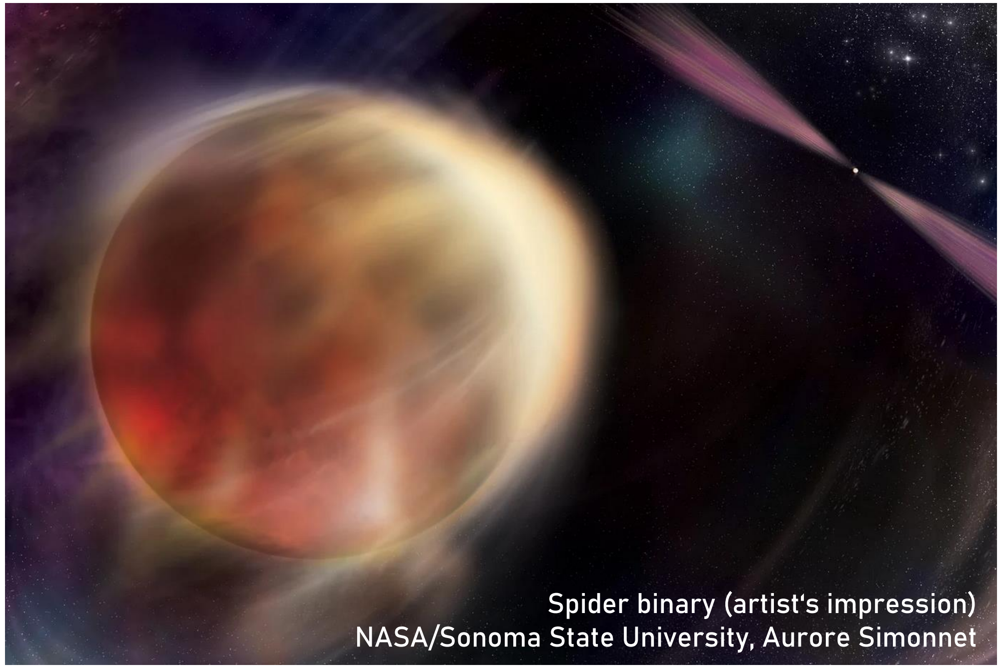

Spider binary (artist's impression)
NASA/Sonoma State University, Aurore Simonnet

Introduction: Pulsar Wind Nebulae

- PWN: Nebula of electrons (& positrons) accelerated in pulsar magnetosphere
  - ➢ GeV to TeV (PeV?) energies

- Ambient Magnetic field ~ $10^{-5} – 10^{-4}$ G
  - ➢ Synchrotron emission from radio to X-rays

- Ambient radiation field
  - ➢ Inverse Compton radiation powers GeV to TeV gamma-rays

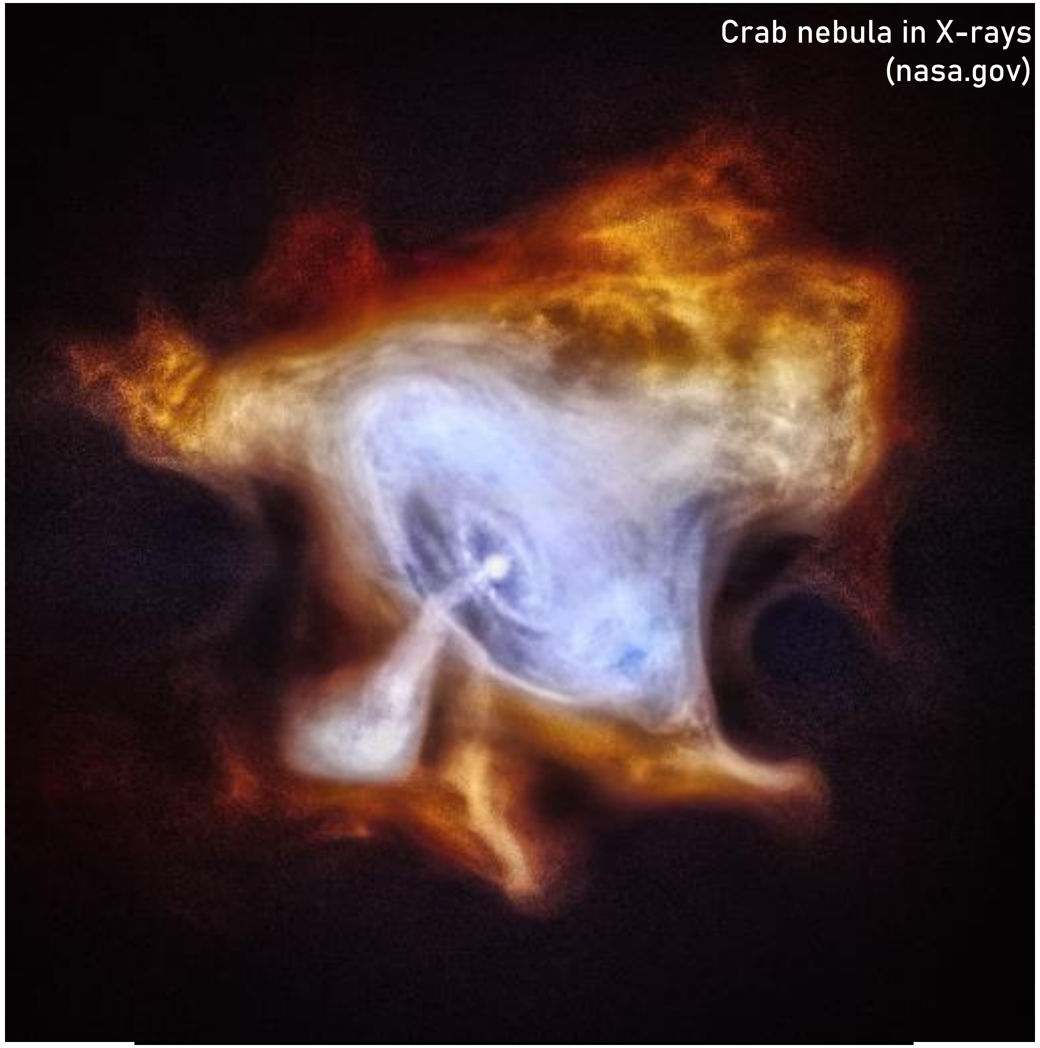

Crab nebula in X-rays (nasa.gov)

Introduction: Pulsar Wind Nebulae

- PWN: Nebula of electrons (& positrons) accelerated in pulsar magnetosphere
  - ➢ GeV to TeV (PeV?) energies
- Ambient Magnetic field ~ $10^{-5} – 10^{-4}$ G
  - ➢ Synchrotron emission from radio to X-rays
- Ambient radiation field
  - ➢ Inverse Compton radiation powers GeV to TeV gamma-rays

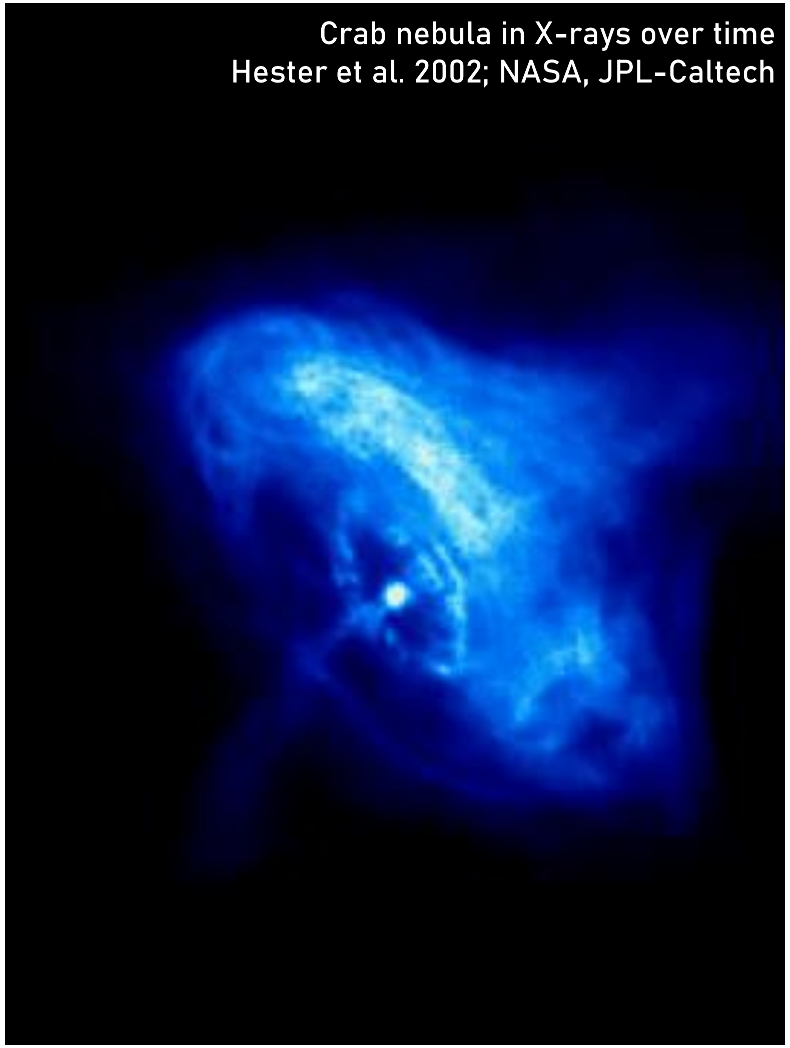

Crab nebula in X-rays over time
Hester et al. 2002; NASA, JPL-Caltech

Motivation: eROSITA Two-Year Catalog (eRASS:4)

- Cross-match with eROSITA All-Sky Survey (eRASS) Catalog (see Merloni et al. 2024)
  - Use four-survey catalog (eRASS:4) for maximum sensitivity
  - Around three million sources on western Galactic hemisphere (~ 140 sources deg^{-2})
  - Down to F ~ 2×10^{-14} erg s^{-1} cm^{-2} in 0.2 – 2.3 keV

Example eRASS:4 image of 4FGL error ellipse

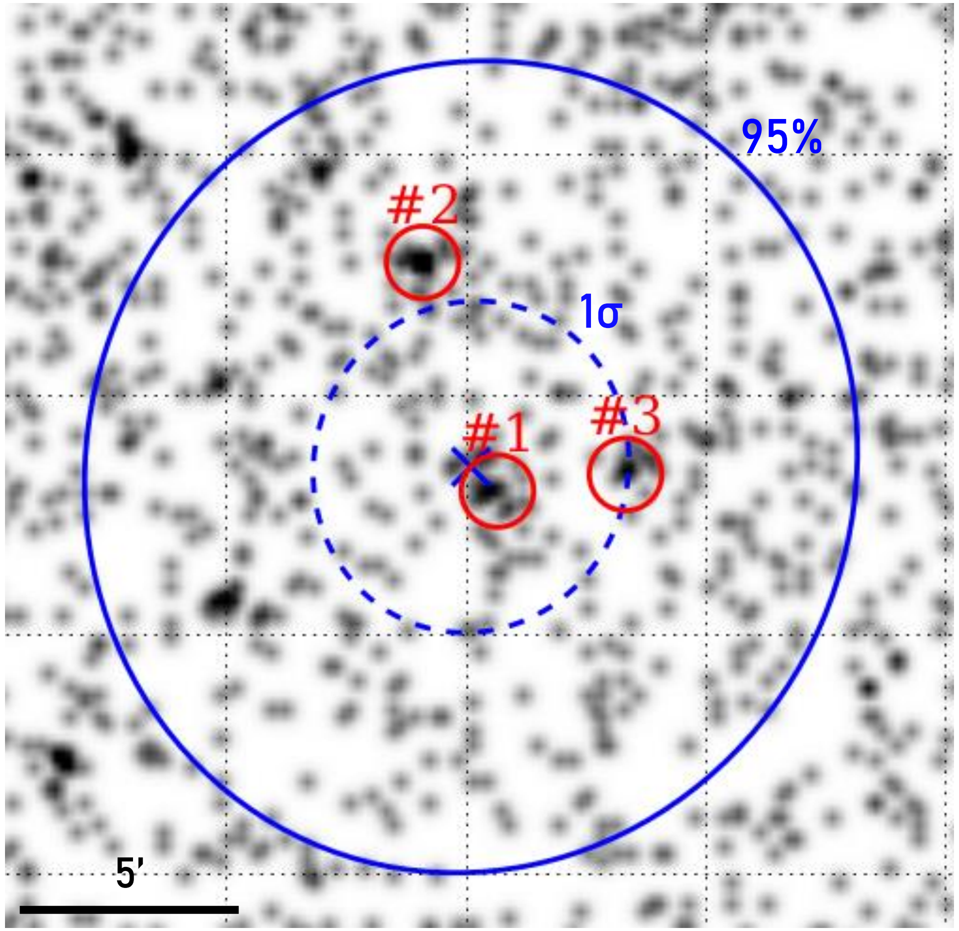

Motivation: eROSITA Two-Year Catalog (eRASS:4)

- Cross-match with eROSITA All-Sky Survey (eRASS) Catalog (see Merloni et al. 2024)
  - Use four-survey catalog (eRASS:4) for maximum sensitivity
  - Around three million sources on western Galactic hemisphere (~ 140 sources deg^{-2})
  - Down to F ~ 2×10^{-14} erg s^{-1} cm^{-2} in 0.2 – 2.3 keV

- Challenges:
  - Large gamma-ray error ellipses (~ 5 arcmin)
  - X-ray pulsar counterparts typically faint (~ 10 counts)

➢ Multiwavelength source properties & probabilistic approach crucial (Salvato et al. 2018)

Example eRASS:4 image of 4FGL error ellipse

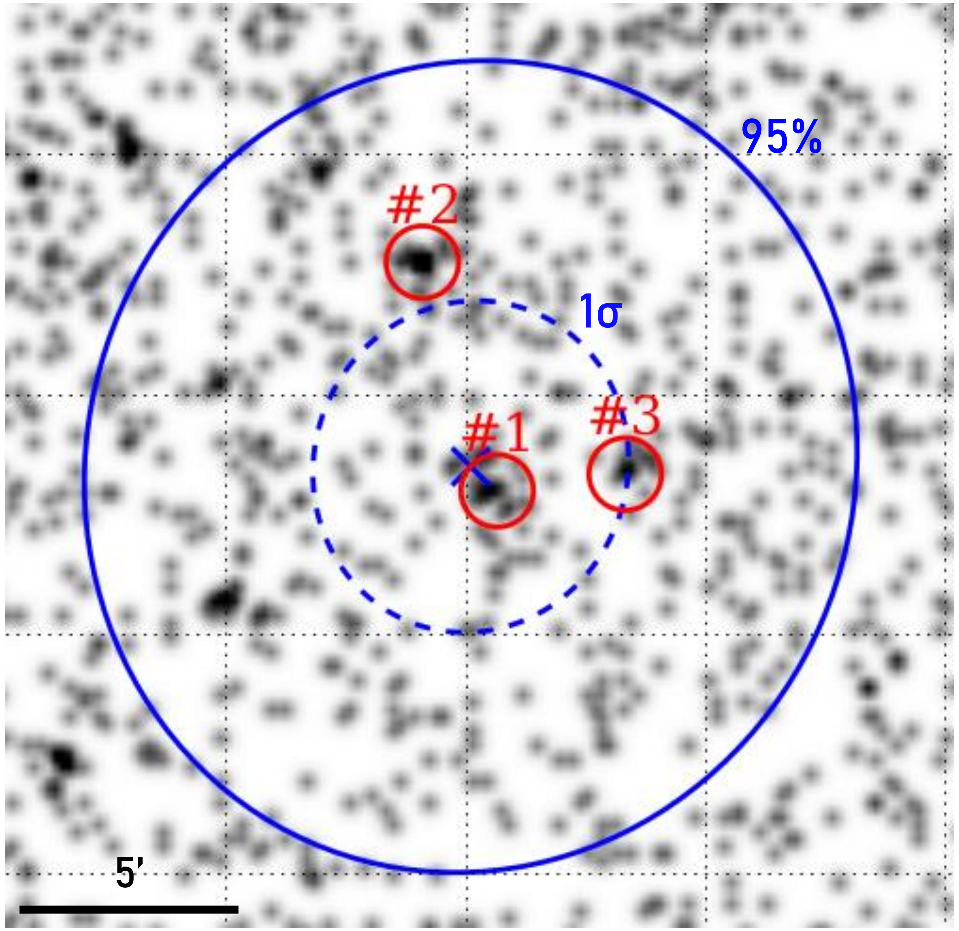

Search Strategy: Prior Classification

- Improve on pure positional cross-match using basic X-ray & gamma-ray source properties:
  - Use random forest classification on 4FGL source properties to predict probability of PSR/AGN class (e.g. Saz Parkinson et al. 2016)

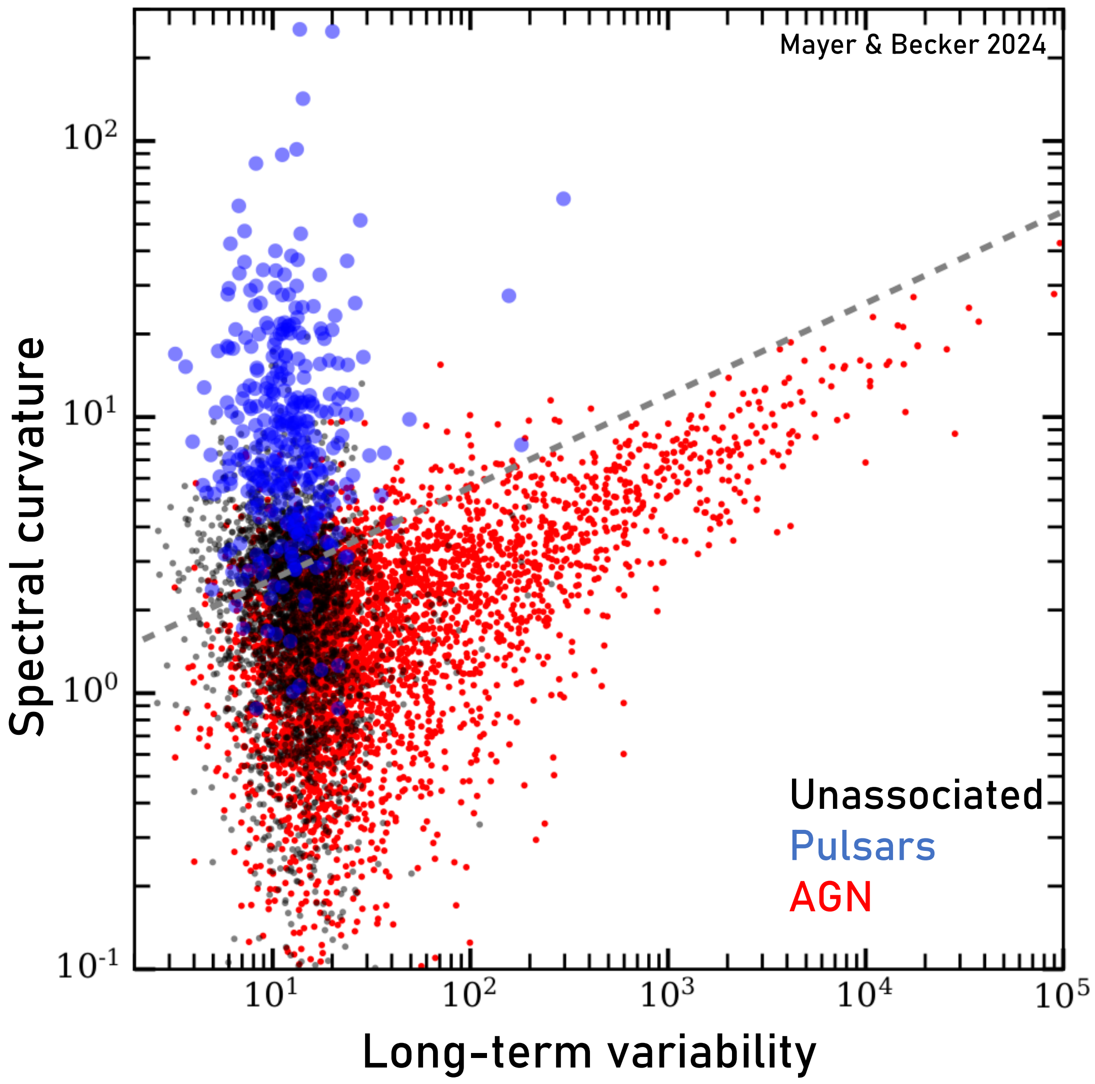

Search Strategy: Prior Classification

- Improve on pure positional cross-match using basic X-ray & gamma-ray source properties:

  - Use random forest classification on 4FGL source properties to predict probability of PSR/AGN class (e.g. Saz Parkinson et al. 2016)

  ➢ Efficiently separates PSR/AGN candidates

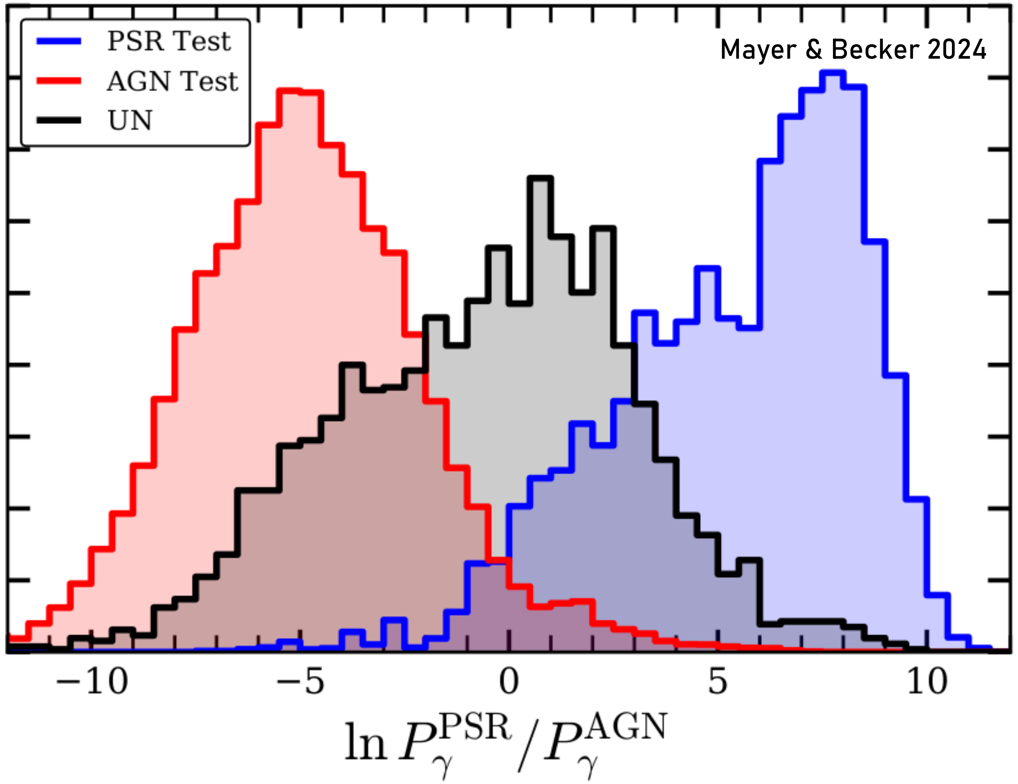

Precision-Recall Curve

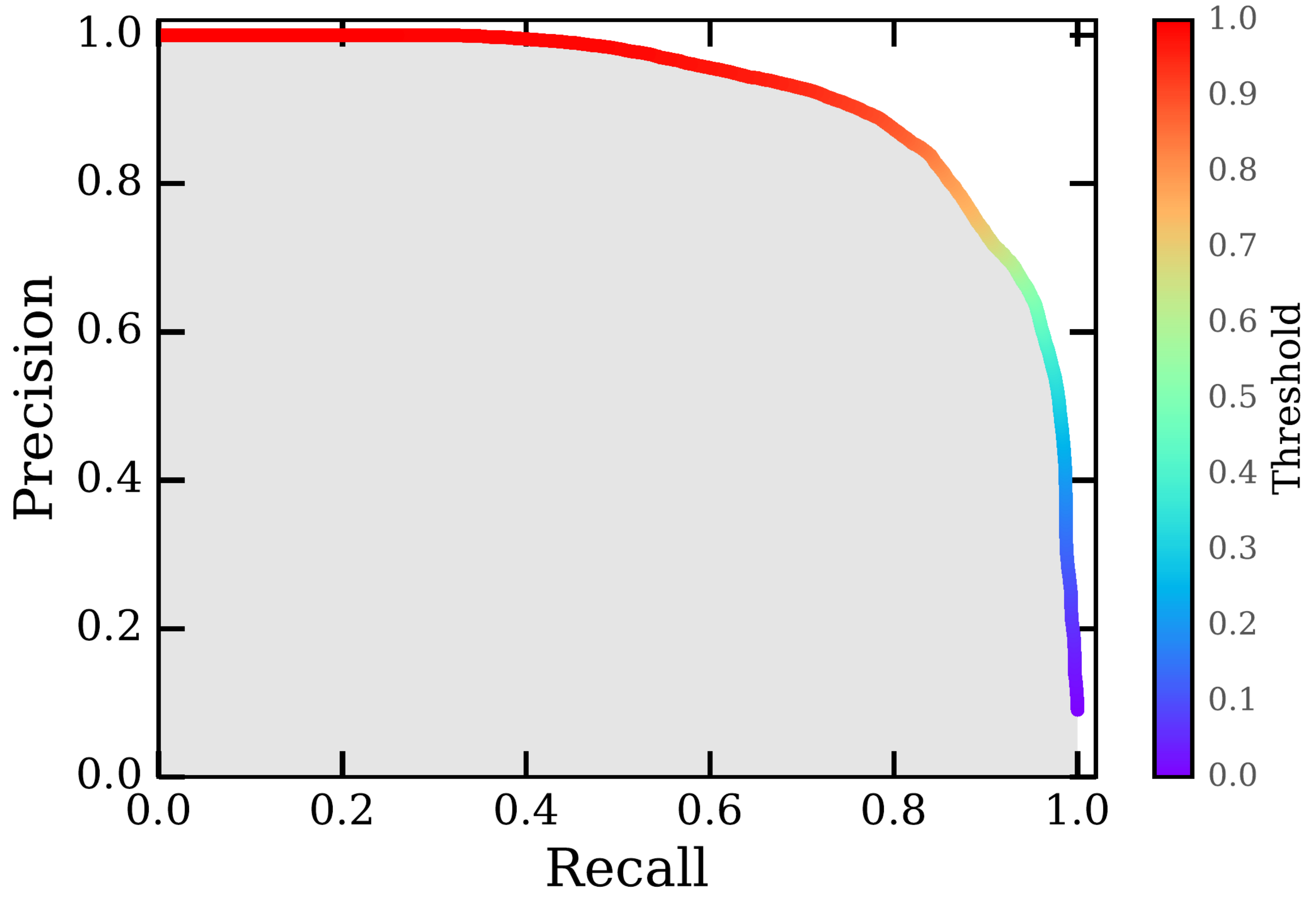

Feature Elimination

Feature	Importance	Description
SigCombined	0.276	3 log LP_SigCurv[a] − log Variability_Index[a]
ModSigCurv	0.176	3 log LP_SigCurv[a] − 2 log Signif_Avg[a]
LP_beta[a]	0.128	
LP_SigCurv[a]	0.109	
K24	0.079	$\frac{2F(1.0\text{–}3.0\,\mathrm{GeV}) - F(0.3\text{–}1.0\,\mathrm{GeV}) - F(3\text{–}30\,\mathrm{GeV})}{2F(1.0\text{–}3.0\,\mathrm{GeV}) + F(0.3\text{–}1.0\,\mathrm{GeV}) + F(3\text{–}30\,\mathrm{GeV})}$
Frac_Variability[a]	0.051	
HR34	0.038	$\frac{F(3\text{–}30\,\mathrm{GeV}) - F(1.0\text{–}3.0\,\mathrm{GeV})}{F(3\text{–}30\,\mathrm{GeV}) + F(1.0\text{–}3.0\,\mathrm{GeV})}$
SymLat	0.033	Symmetric Galactic latitude, i.e., $\lvert b \rvert$
EFluxErr	0.032	log Unc_Energy_Flux100[a] − 0.4 log Energy_Flux100[a]
Variability_Index[a]	0.031	
HR45	0.024	$\frac{F(30\text{–}1000\,\mathrm{GeV}) - F(3\text{–}30\,\mathrm{GeV})}{F(30\text{–}1000\,\mathrm{GeV}) + F(3\text{–}30\,\mathrm{GeV})}$
PL_Index[a]	0.021	

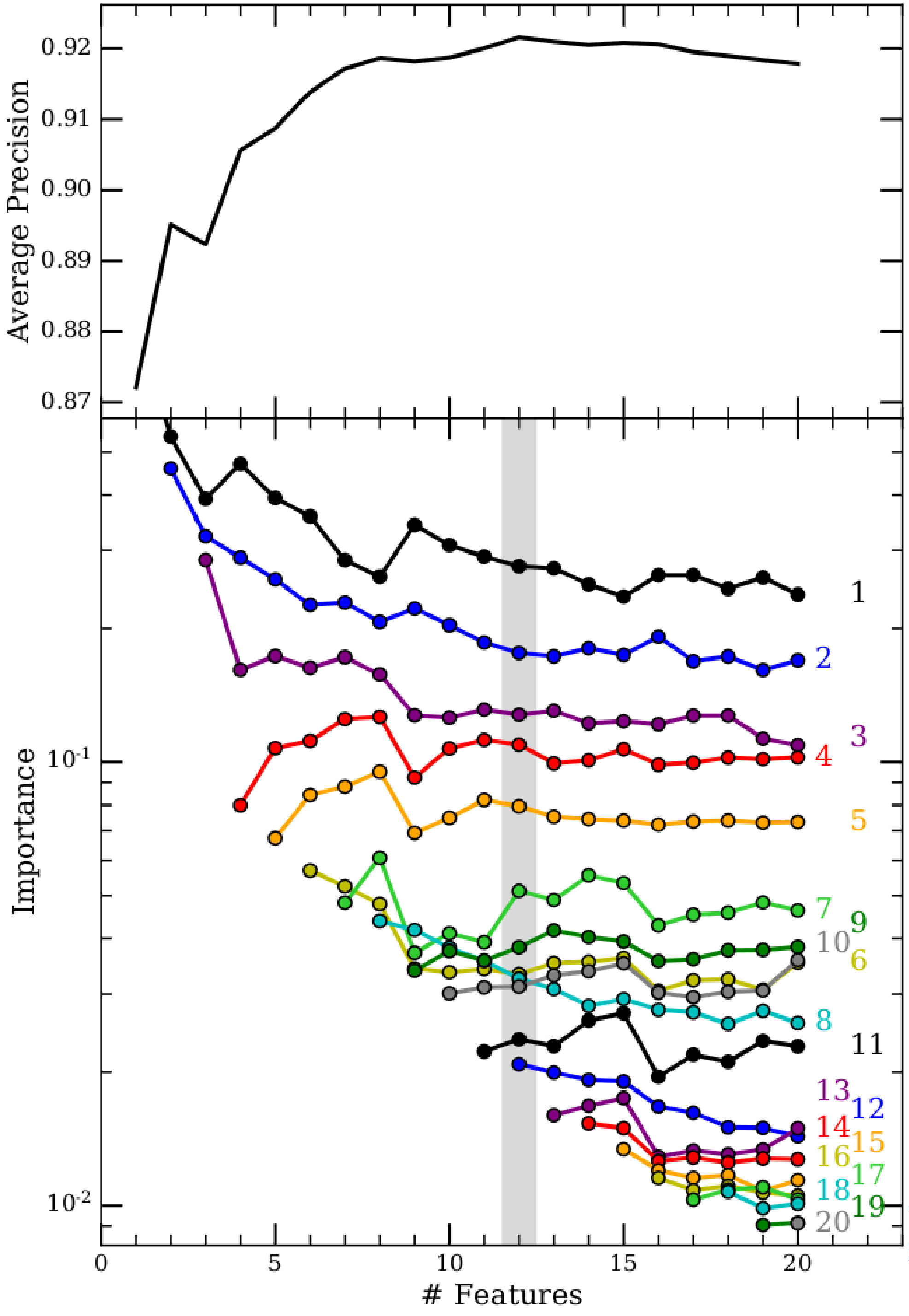

Search Strategy: Multiwavelength Fluxes

Mayer & Becker 2024

- Improve on pure positional cross-match using basic X-ray & gamma-ray source properties:

  - Constrain expected X-ray flux based on observed flux distribution of pulsars (young and millisecond) and blazars

  ➢ Implies many pulsar counterparts below X-ray detection limit

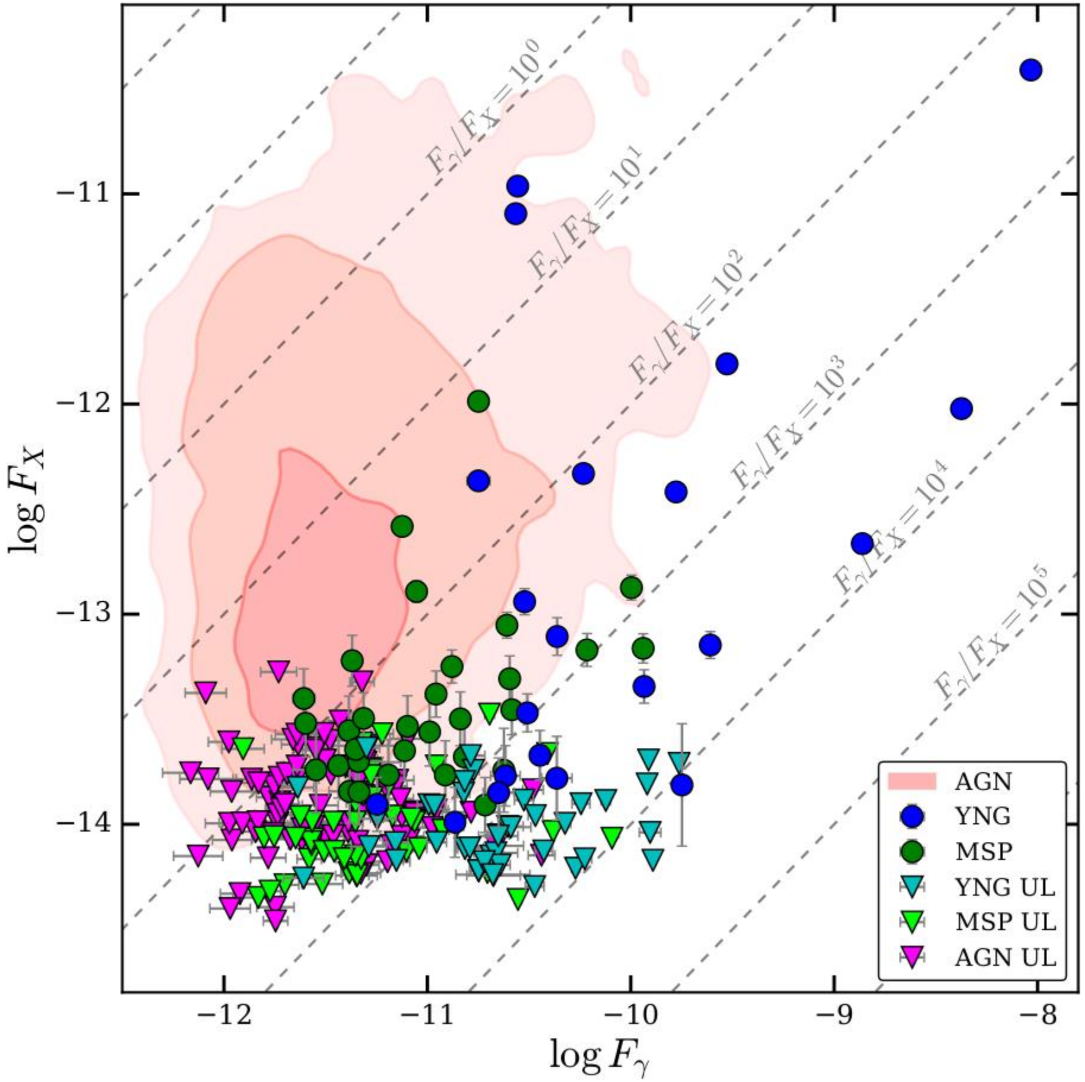

Search Strategy: Multiwavelength Fluxes

- Improve on pure positional cross-match using basic X-ray & gamma-ray source properties:

  - Constrain expected X-ray flux based on observed flux distribution of pulsars (young and millisecond) and blazars

  ➢ Implies many pulsar counterparts below X-ray detection limit

Mayer & Becker 2024

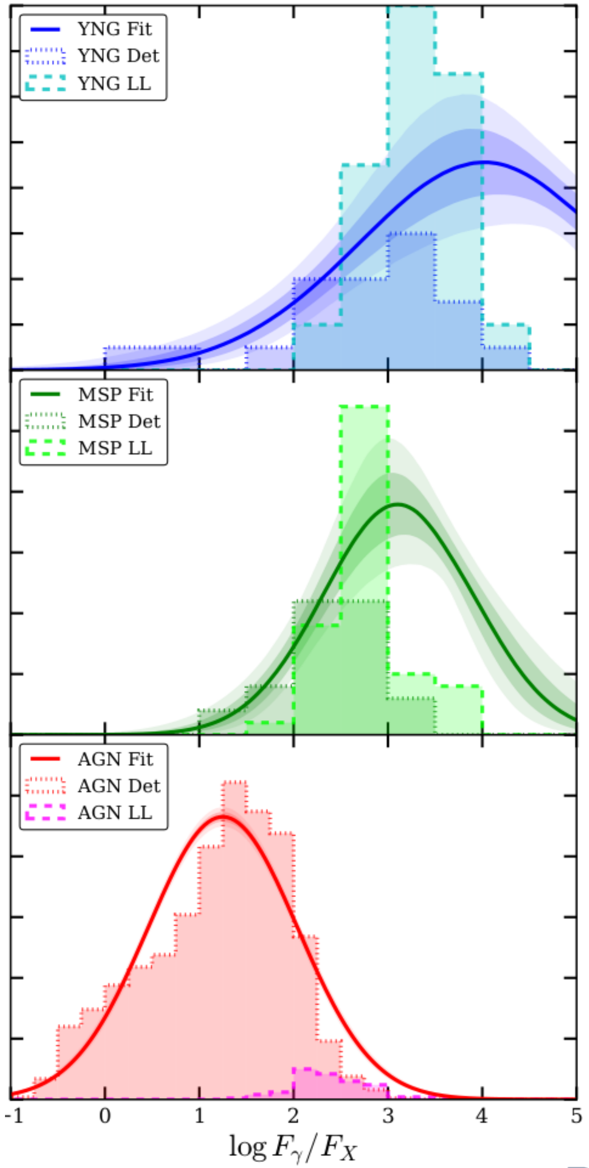

Visual Inspection

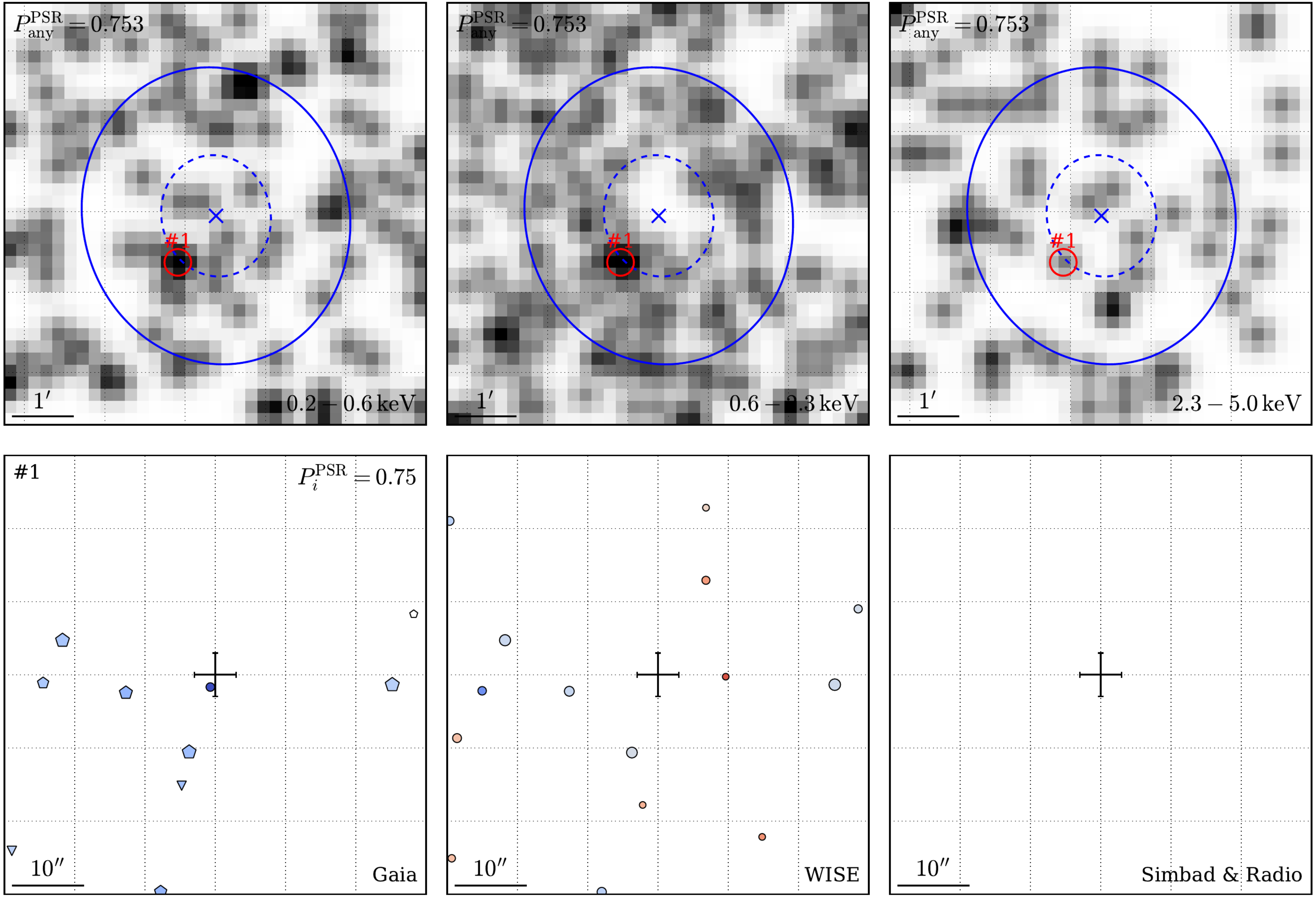

Visual Inspection

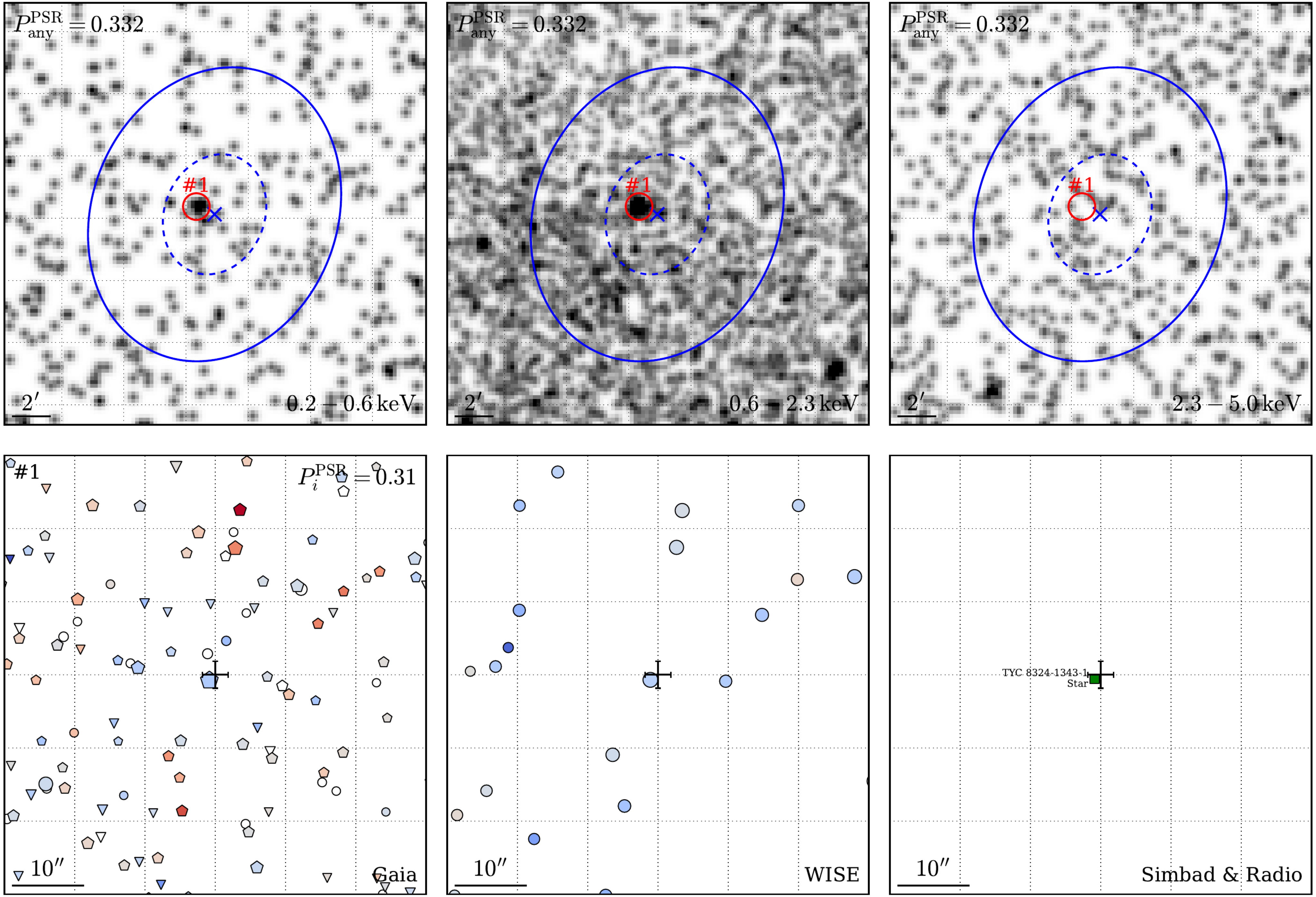

Verification of Probabilities

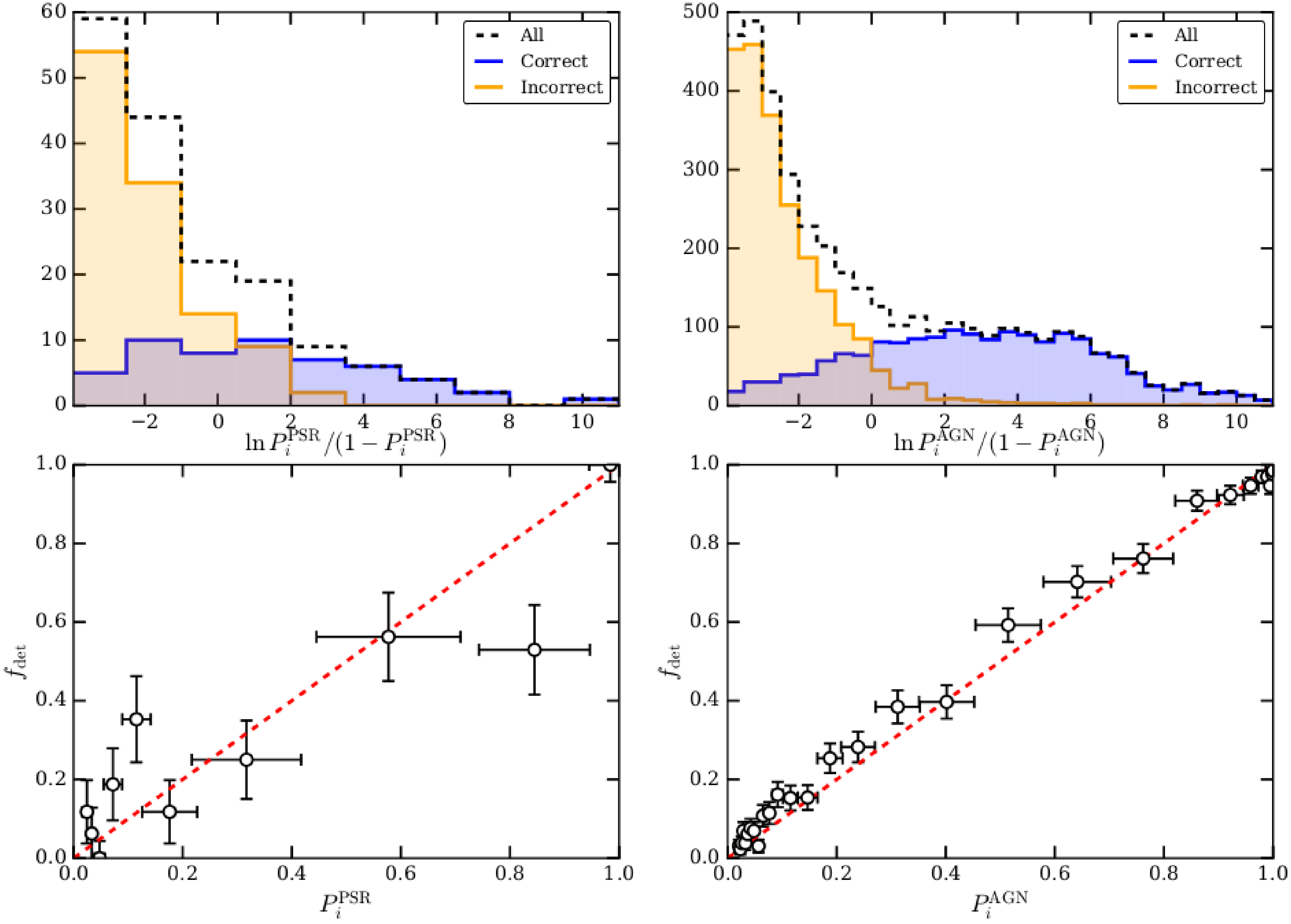

Prediction of expected detections

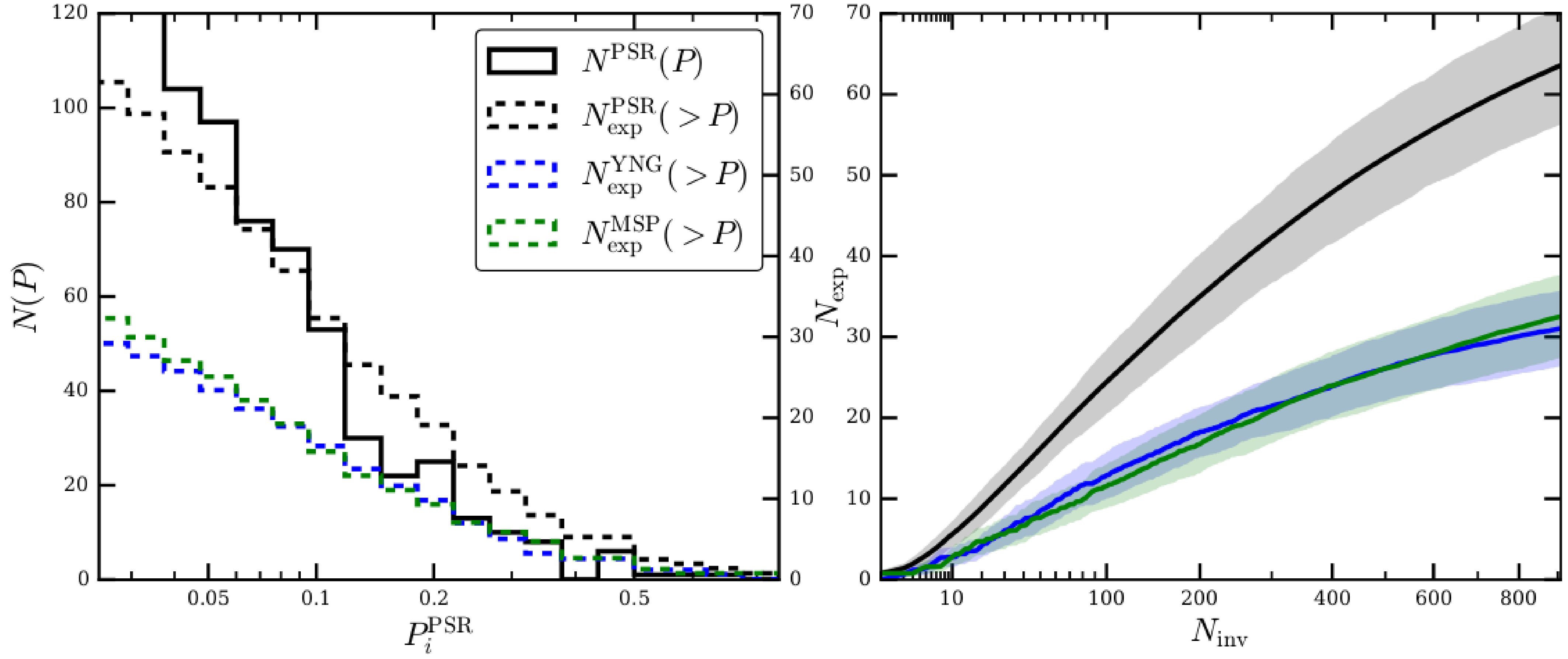

Followup example: PSR J1803–6707 in eRASS1

Clark et al. 2023

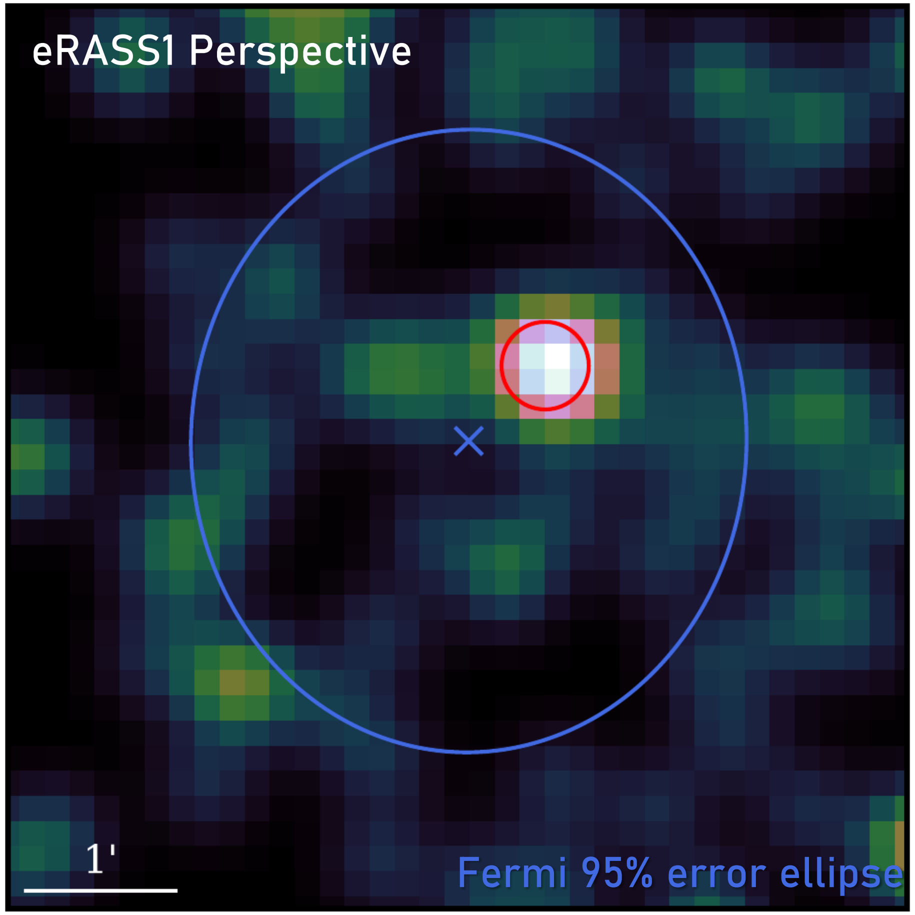

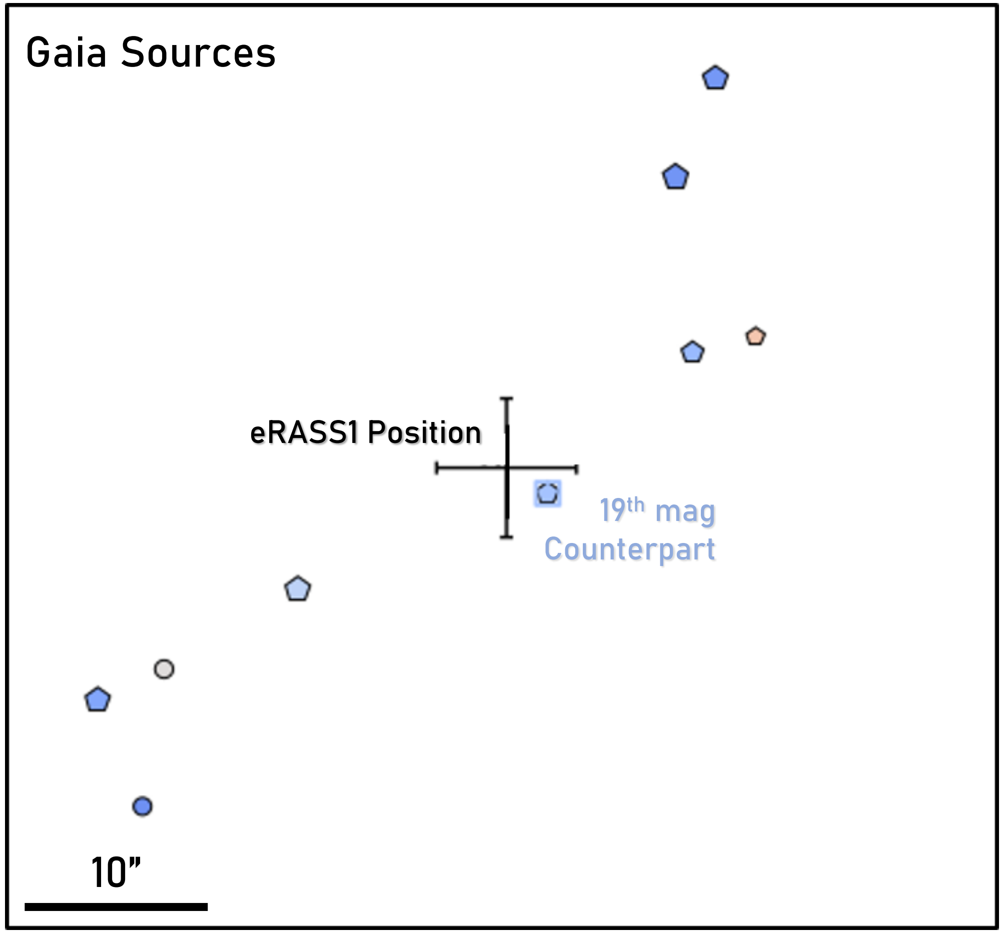

Followup example: PSR J1803–6707 in eRASS1

Clark et al. 2023

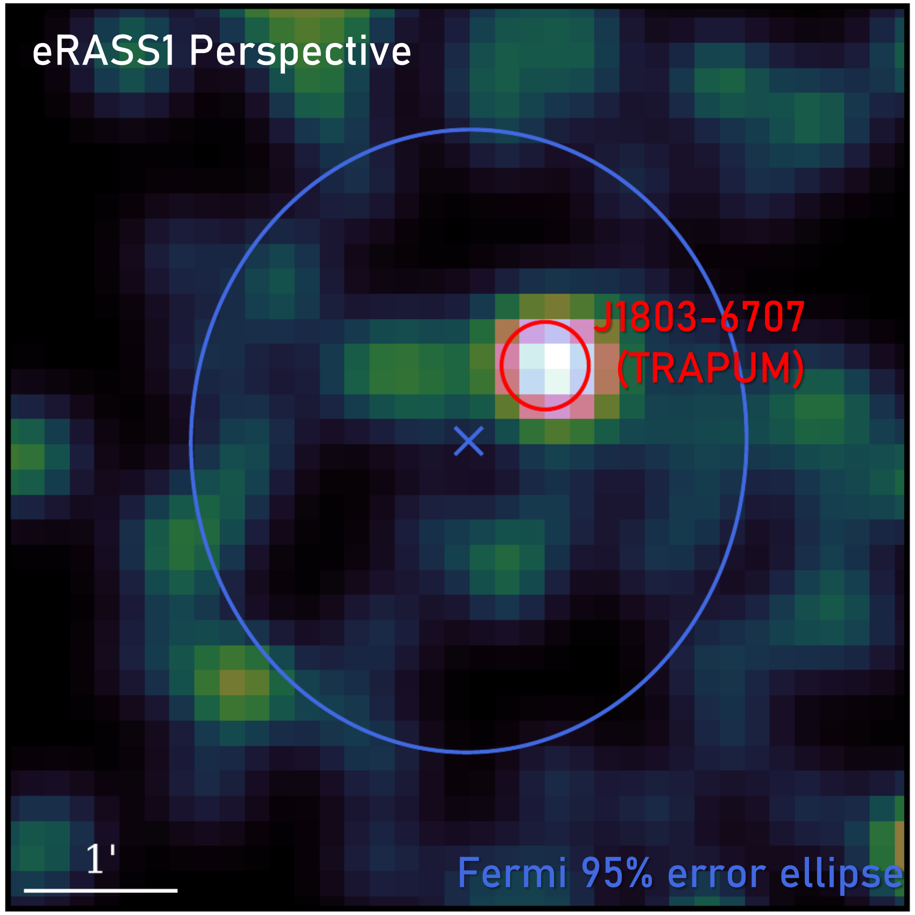

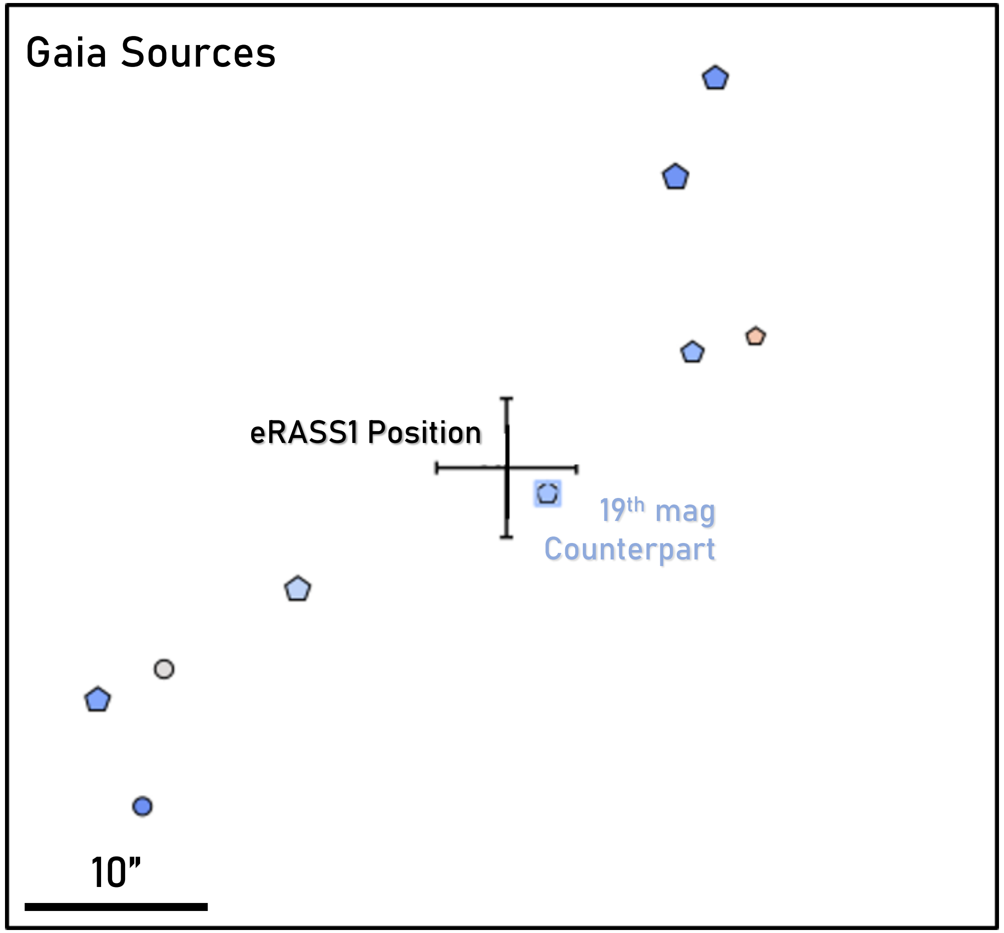

Followup example: Multiwavelength view of PSR J1803–6707

Redback binary pulsar (Clark et al. 2023)

- 2.1 ms spin period
- 9.1 h orbital period
- $M_{Companion} > 0.26\ M_\odot$

Followup example: Multiwavelength view of PSR J1803–6707

Redback binary pulsar (Clark et al. 2023)

- 2.1 ms spin period
- 9.1 h orbital period
- $M_{Companion} > 0.26\ M_{\odot}$

➢ γ-ray & radio pulsations from pulsar

Radio pulsations (Clark et al. 2023)

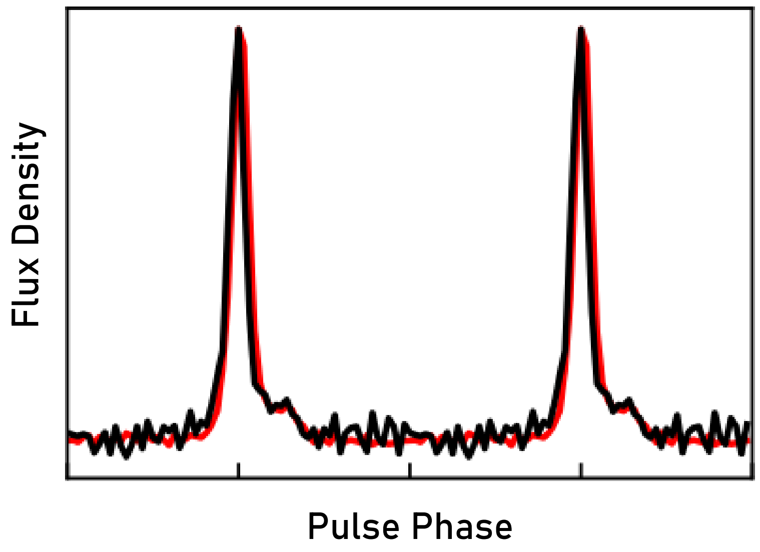

Followup example: Multiwavelength view of PSR J1803–6707

Redback binary pulsar (Clark et al. 2023)

- 2.1 ms spin period
- 9.1 h orbital period
- $M_{Companion} > 0.26\ M_{\odot}$

➢ γ-ray & radio pulsations from pulsar

γ-pulsations (Clark et al. 2023)

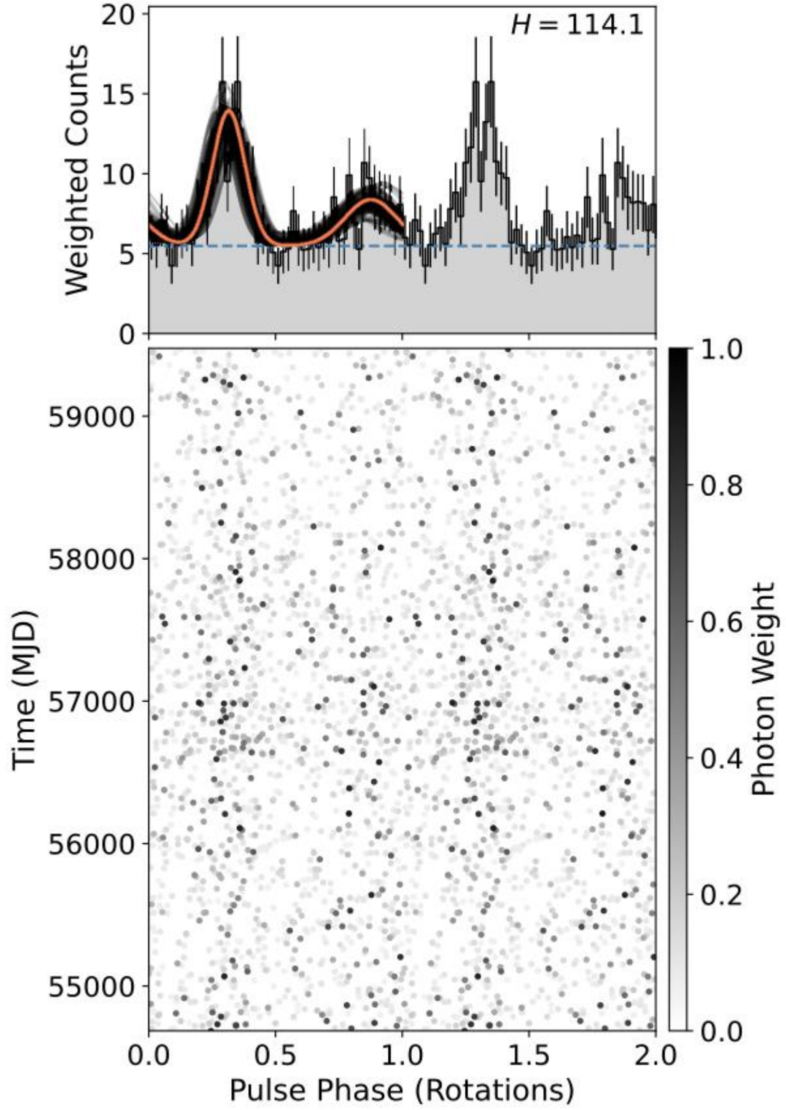

Radio pulsations (Clark et al. 2023)

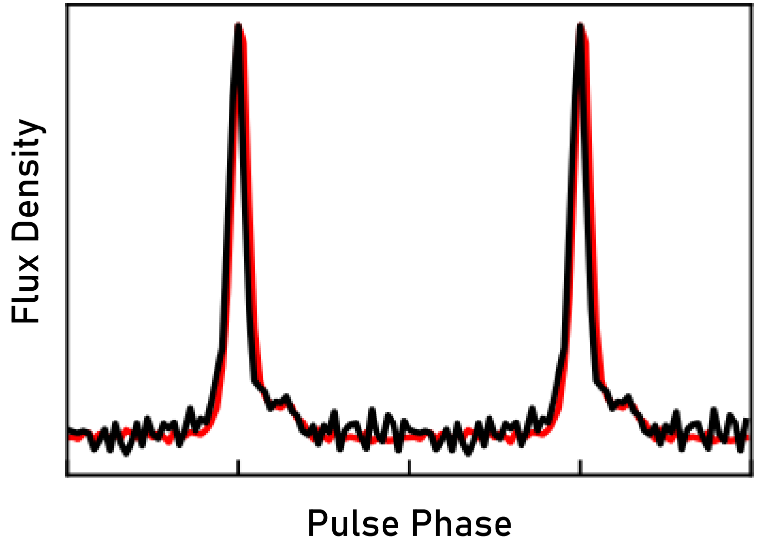

Followup example: Multiwavelength view of PSR J1803–6707

Redback binary pulsar (Clark et al. 2023)

- 2.1 ms spin period
- 9.1 h orbital period
- $M_{Companion} > 0.26\ M_{\odot}$

➢γ-ray & radio pulsations from pulsar

➢Orbital modulation in the optical

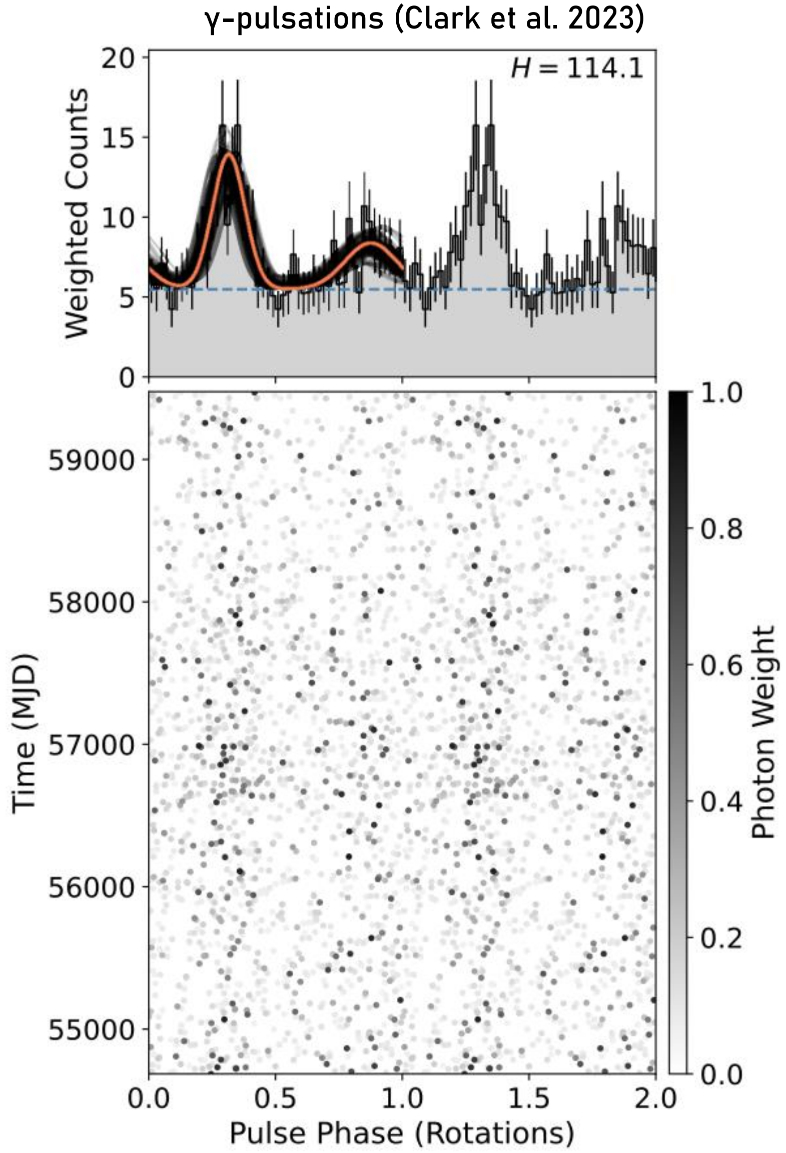

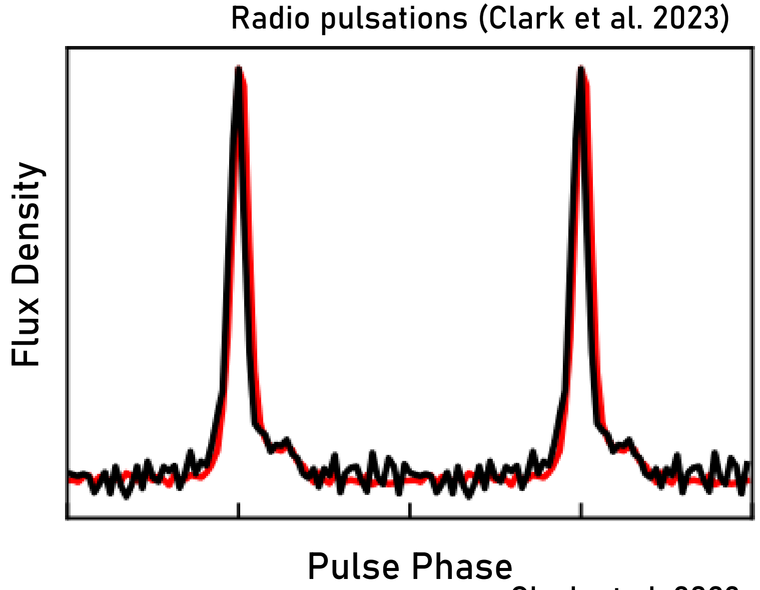

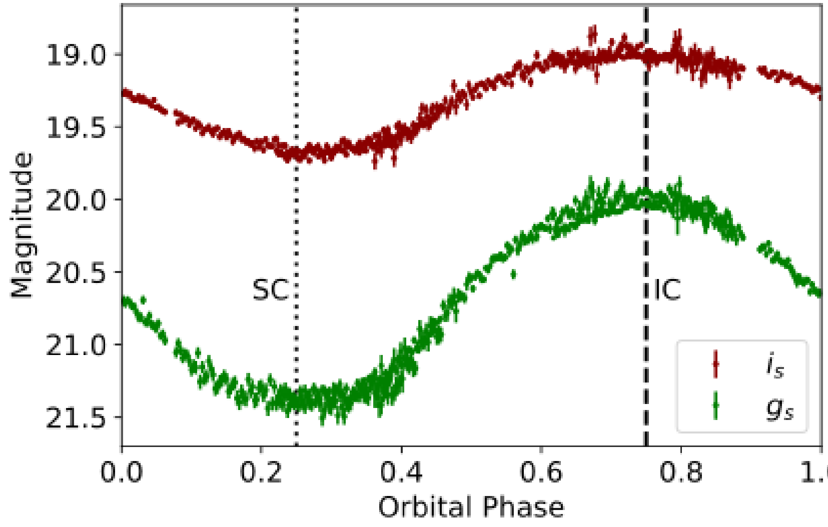

Followup example: Multiwavelength view of PSR J1803–6707

Redback binary pulsar (Clark et al. 2023)

- 2.1 ms spin period
- 9.1 h orbital period
- $M_{Companion} > 0.26\ M_{\odot}$

➢ γ-ray & radio pulsations from pulsar

➢ Orbital modulation in the optical

➢ (No X-ray pulsations yet)

γ-pulsations (Clark et al. 2023)

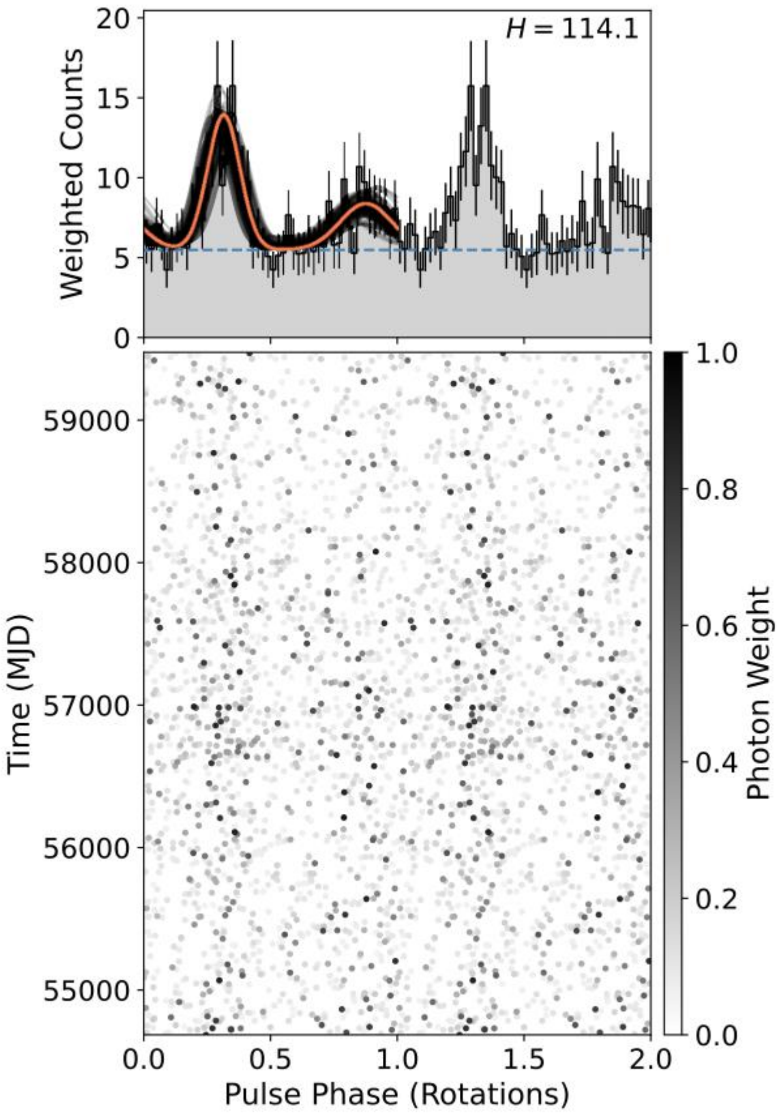

Radio pulsations (Clark et al. 2023)

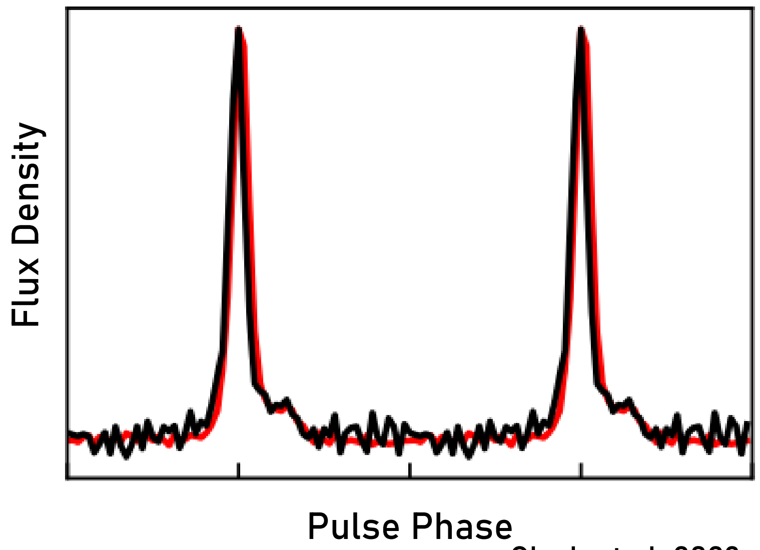

Clark et al. 2023

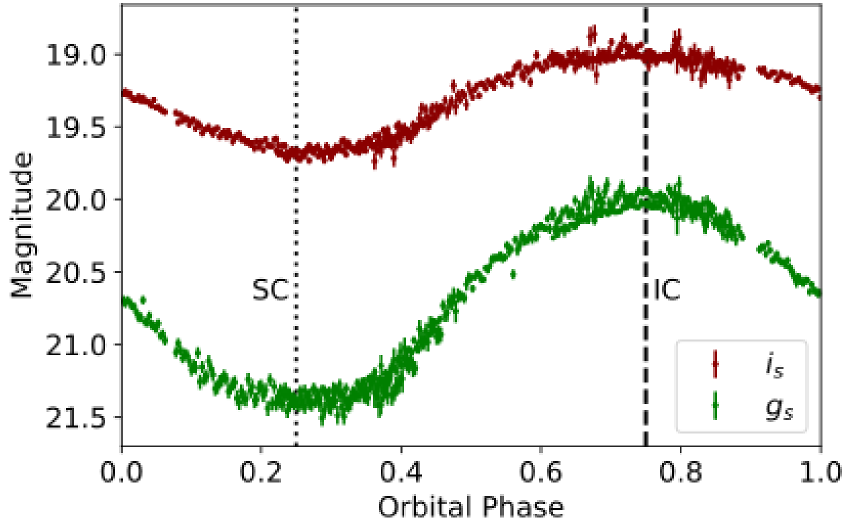

Math

- Probabilistic matching similar to NWAY (Salvato et al. 2018), and using Bayesian approach of Budavari & Szalay (2008)

$$
\begin{aligned}
P_i^t &= \frac{\rho_i^t}{\bar{c} + \sum_i \sum_t \rho_i^t}, \text{ with} \\
\rho_i^t &= P_\gamma^t \frac{\phi_t(\log F_X \mid \log F_\gamma)}{\phi_{\mathrm{B}}(\log F_X)} \frac{\exp\left(-\frac{1}{2}\boldsymbol{\psi}^\top \boldsymbol{\Sigma}^{-1} \boldsymbol{\psi}\right)}{2\pi\nu(\mathbf{x})\sqrt{|\boldsymbol{\Sigma}|}} \\
\bar{c} &= 1 - \sum_t P_\gamma^t \int \phi_t(\log F_X \mid \log F_\gamma)\, \mathrm{d}\log F_X,
\end{aligned}
$$

Math

- Probabilistic matching similar to NWAY (Salvato et al. 2018), and using Bayesian approach of Budavari & Szalay (2008)

Normalized probability

$$P_i^t = \frac{\rho_i^t}{\bar{c} + \sum_i \sum_t \rho_i^t}, \text{ with}$$

Spatial separation

Positional errors

Gamma-ray prior

$$\rho_i^t = P_\gamma^t \frac{\phi_t(\log F_X \mid \log F_\gamma)}{\phi_B(\log F_X)} \frac{\exp\left(-\frac{1}{2}\psi^\top \Sigma^{-1} \psi\right)}{2\pi\nu(\mathbf{x})\sqrt{|\Sigma|}}$$

Flux distributions

Local source density

$$\bar{c} = 1 - \sum_t P_\gamma^t \int \phi_t(\log F_X \mid \log F_\gamma) \, \mathrm{d}\log F_X,$$

Prior incompleteness

Math

- Probabilistic matching similar to NWAY (Salvato et al. 2018), and using Bayesian approach of Budavari & Szalay (2008)

Normalized probability

$$P_i^t = \frac{\rho_i^t}{\bar{c} + \sum_i \sum_t \rho_i^t}, \text{ with}$$

Gamma-ray prior · Flux distributions · Spatial separation · Positional errors · Local source density

$$\rho_i^t = P_\gamma^t \frac{\phi_t(\log F_X \mid \log F_\gamma)}{\phi_\mathrm{B}(\log F_X)} \frac{\exp\left(-\frac{1}{2}\psi^\top \Sigma^{-1} \psi\right)}{2\pi\nu(\mathbf{x})\sqrt{|\Sigma|}}$$

$$\bar{c} = 1 - \sum_t P_\gamma^t \int \phi_t(\log F_X \mid \log F_\gamma)\, \mathrm{d}\log F_X,$$

Prior incompleteness

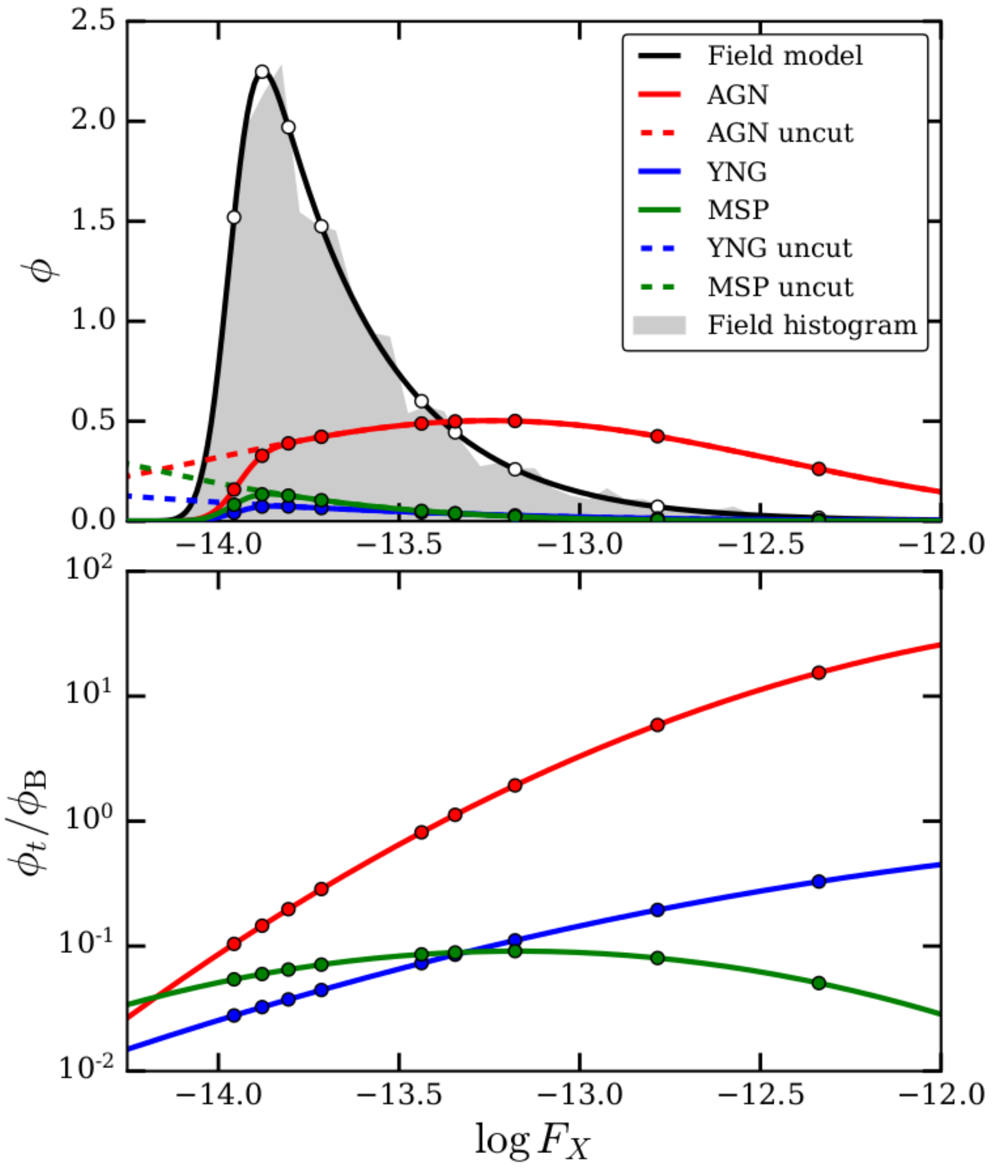

Extra Slides Vela X

Analysis: Imaging & Morphology

- Complex energy-dependent morphology with multiple components
  - Soft band: Diffuse shell & thick tangential filaments
  - Medium band: Thin radial fingers & clumps
  - Hard band: Nonthermal emission from Vela X & Vela Jr.

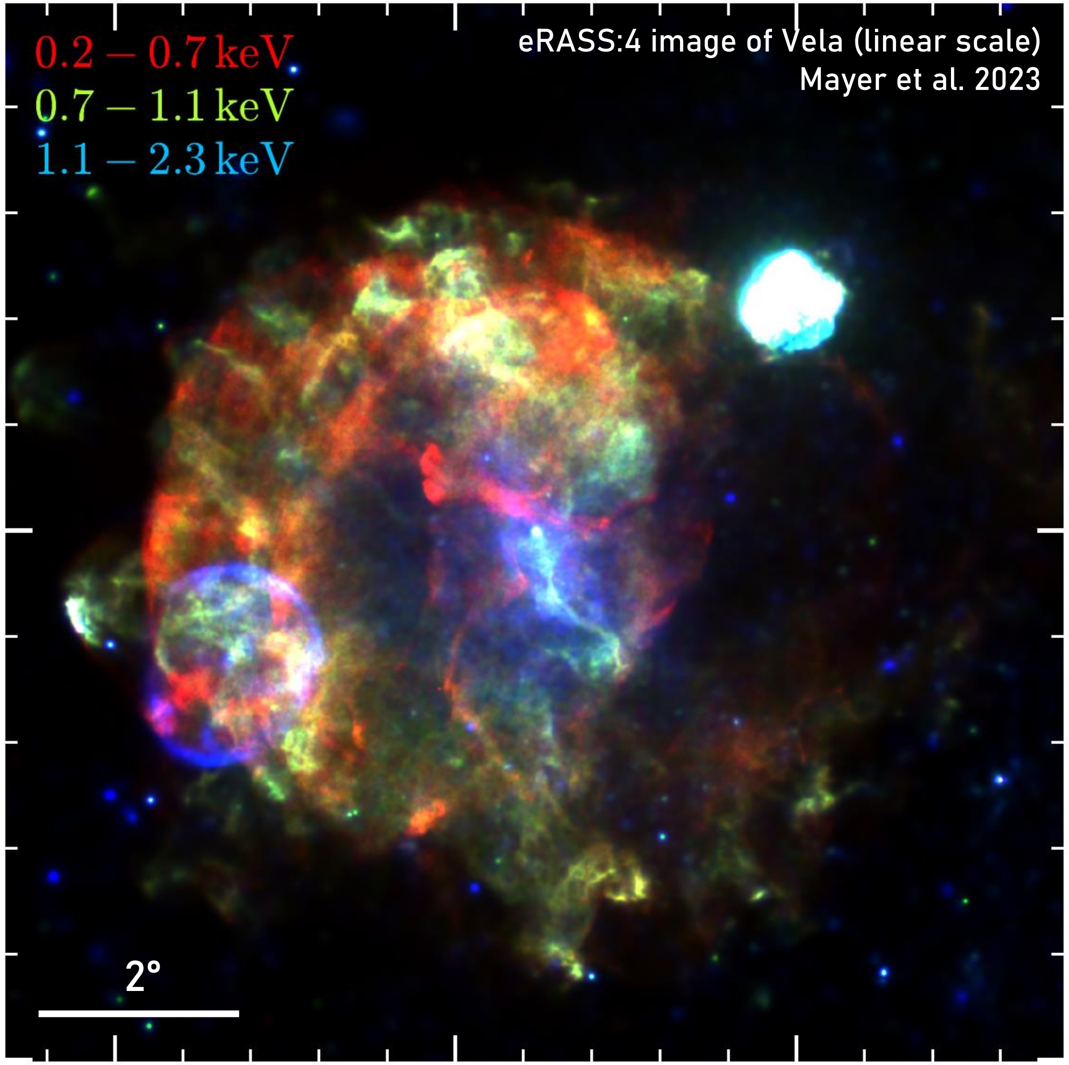

Analysis: Imaging & Morphology

- Complex energy-dependent morphology with multiple components
  - Soft band: Diffuse shell & thick tangential filaments
  - Medium band: Thin radial fingers & clumps
  - Hard band: Nonthermal emission from Vela X & Vela Jr.

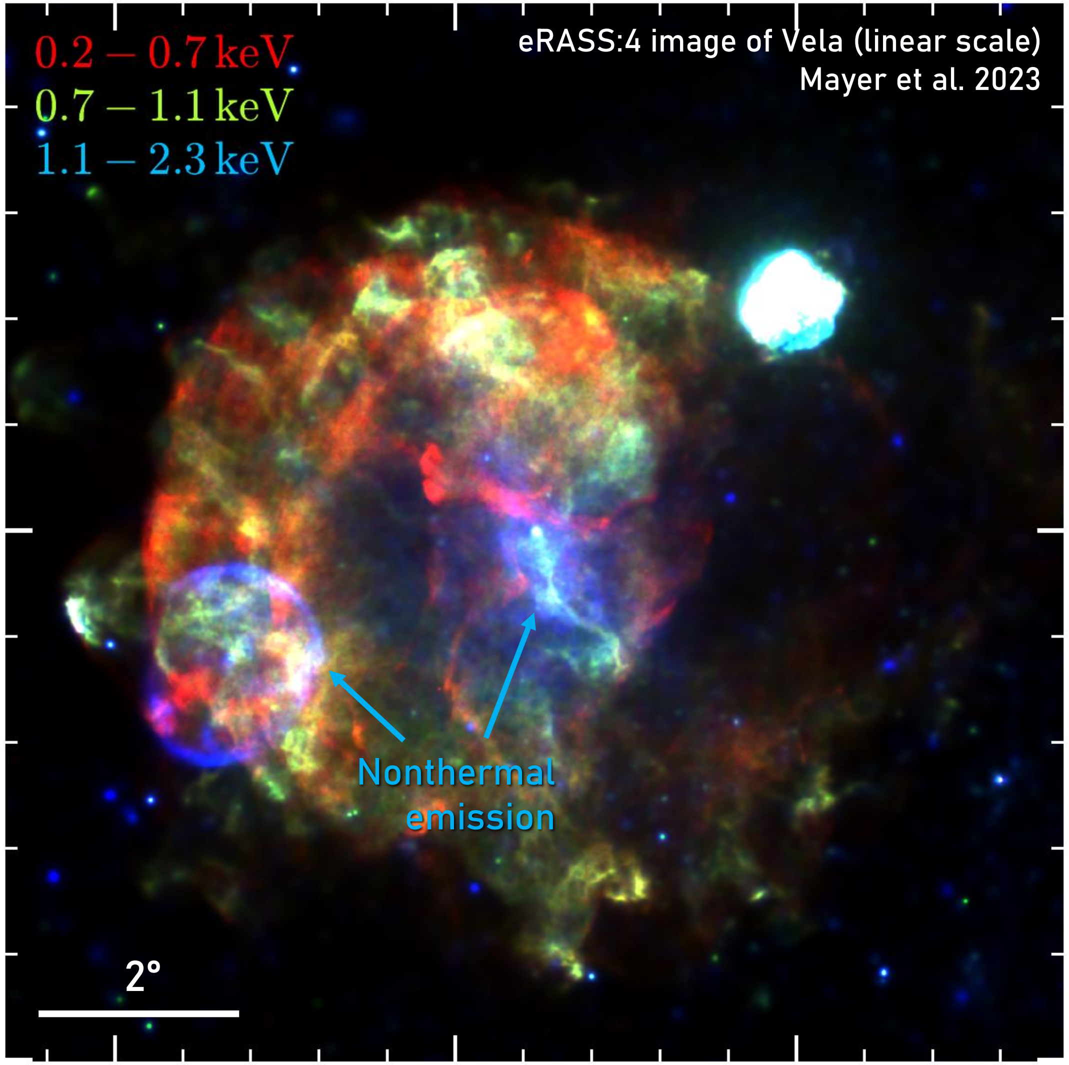

Imaging & Morphology

- Complex energy-dependent morphology with multiple components
  - Soft band: Diffuse shell & thick tangential filaments
  - Medium band: Thin radial fingers & clumps
  - Hard band: Nonthermal emission from Vela X & Vela Jr.

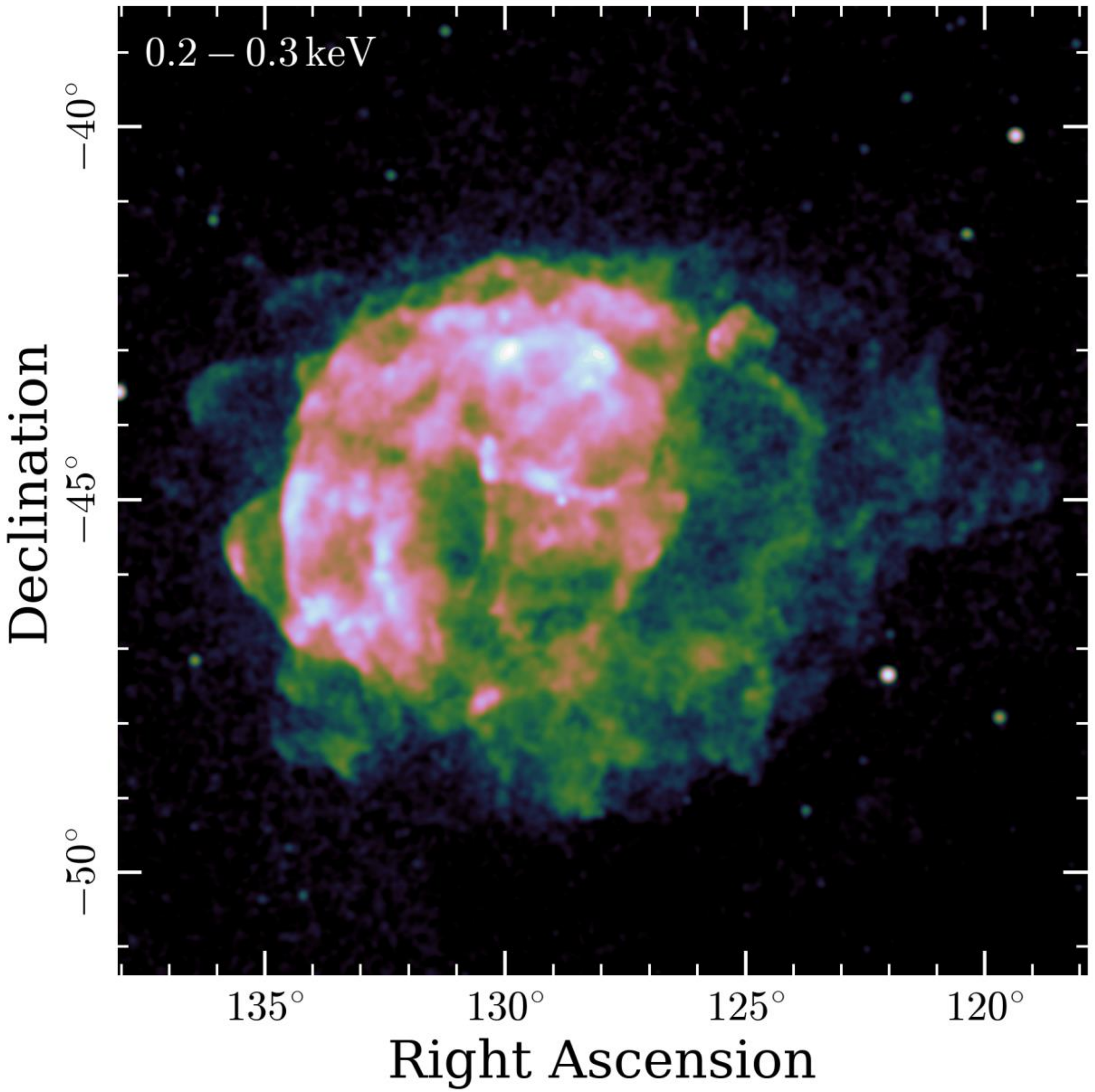

Spectral model

Absorbed plasma in NEI + nonthermal component

TBabs*(vpshock+powerlaw) + backgrund

- ➢Photon index in region 2 too steep ($\Gamma = 4$)
- ➢Hard to constrain kT, τ individually

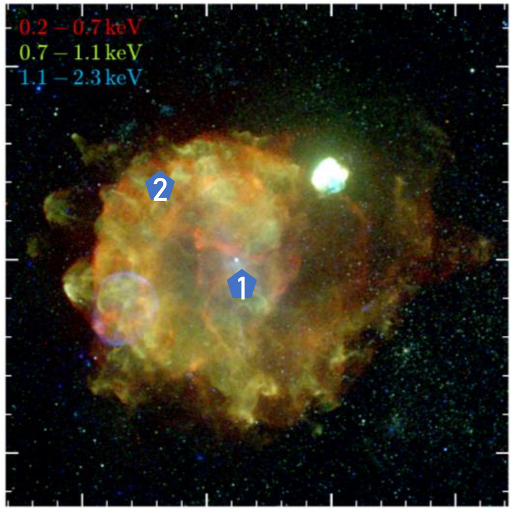

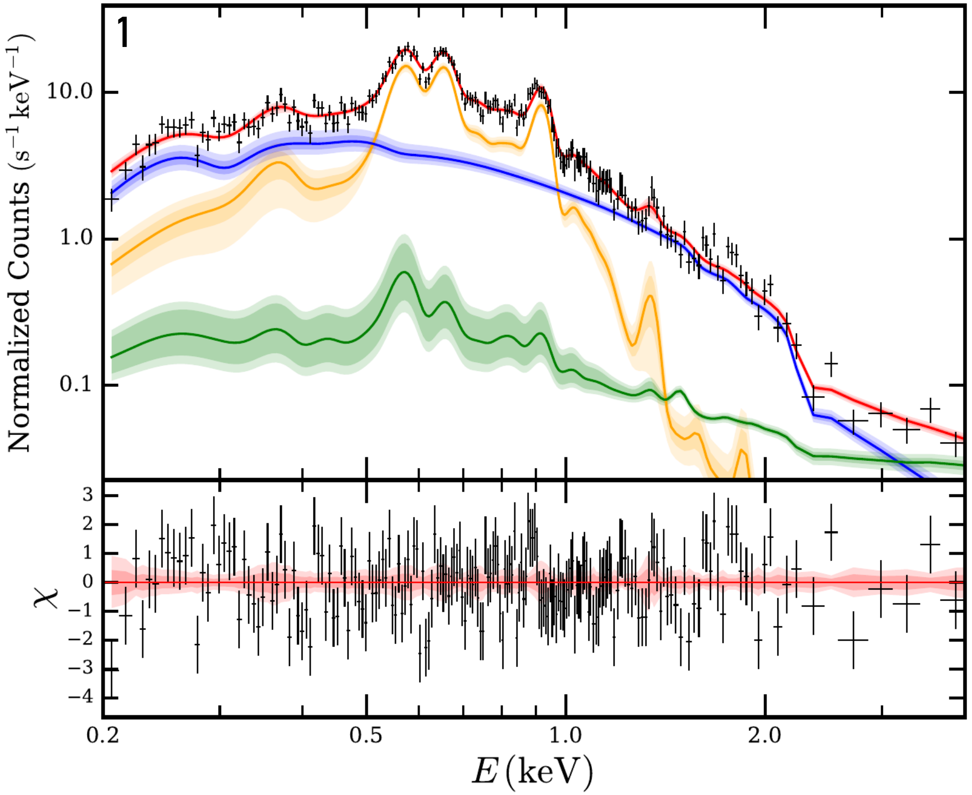

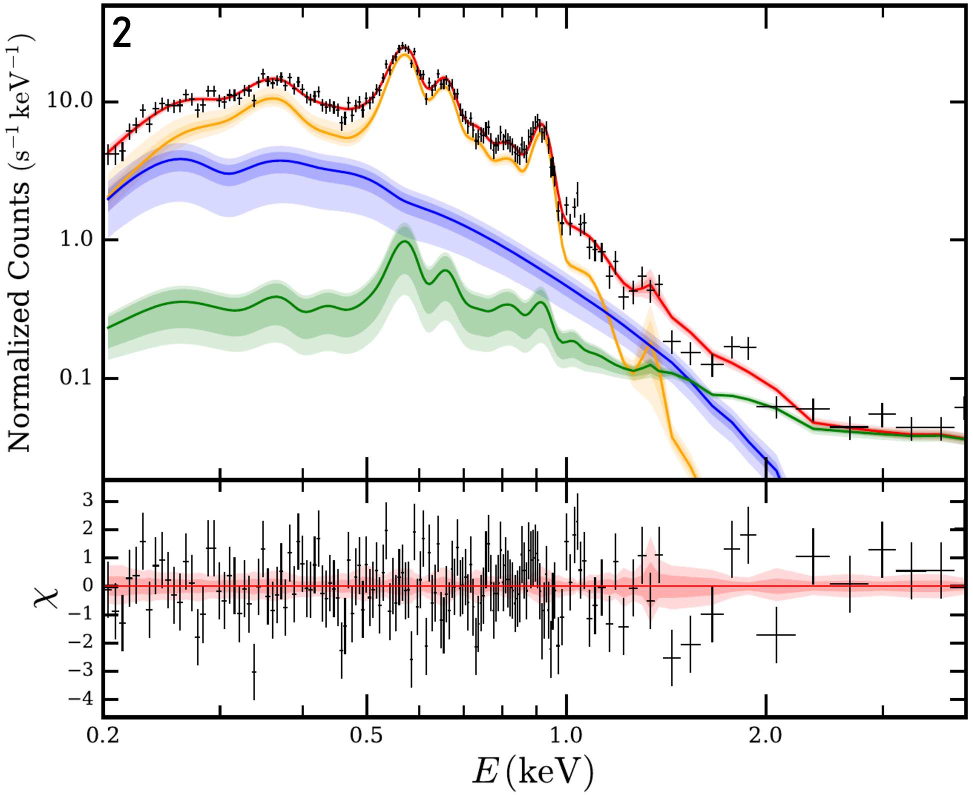

Spectral model

Two absorber plasmas + nonthermal component

TBabs*(vapec+vapec+powerlaw) + background

- ➢Mean plasma temperature more well-defined

•

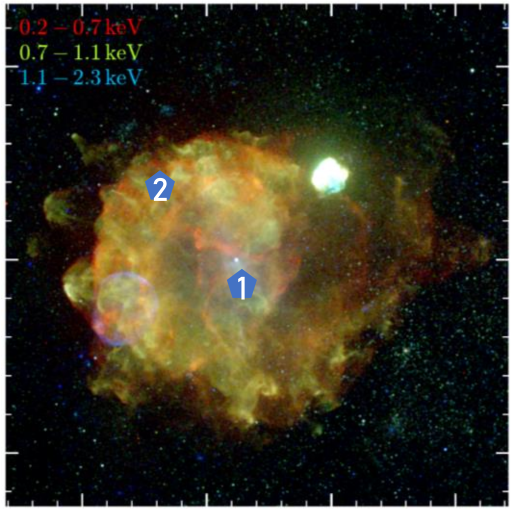

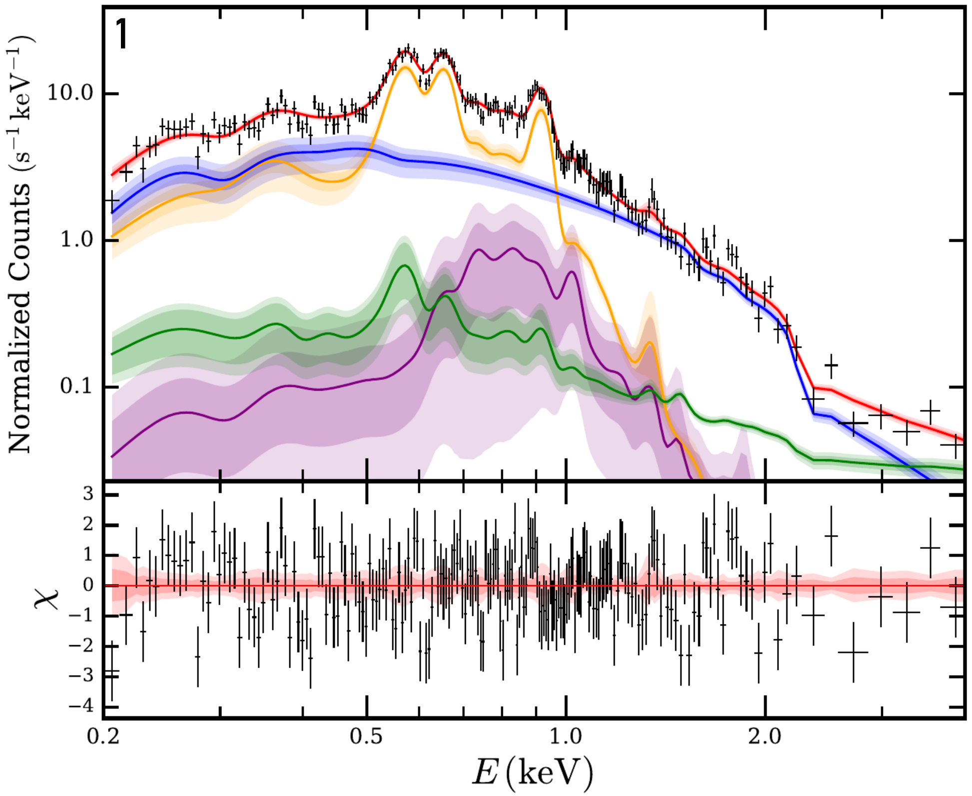

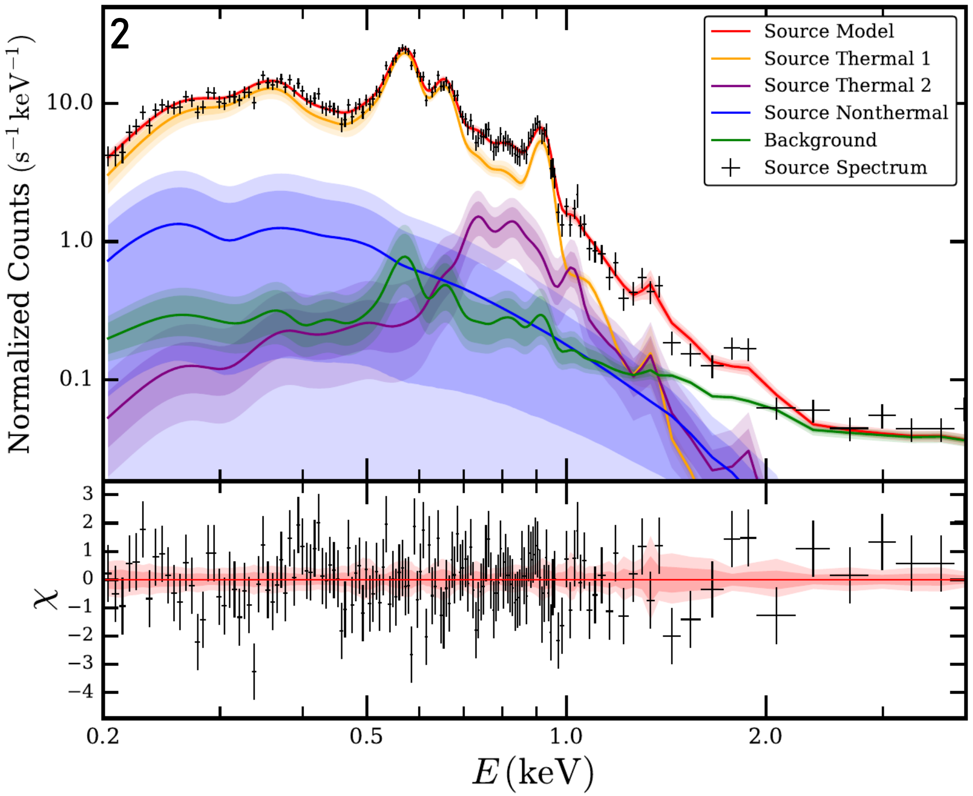

Fits with NEI Plasma

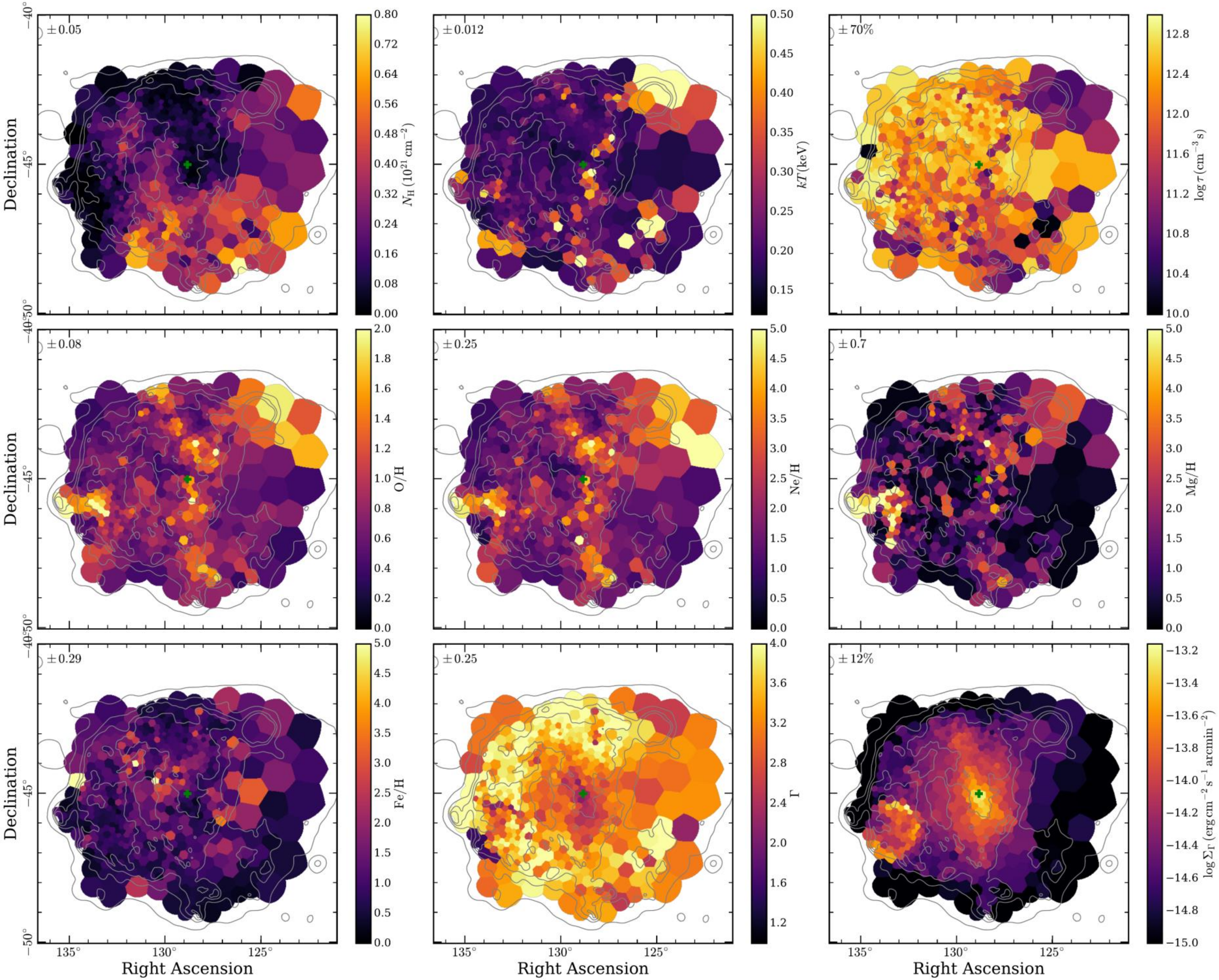

Results: Absorption & Plasma Temperature

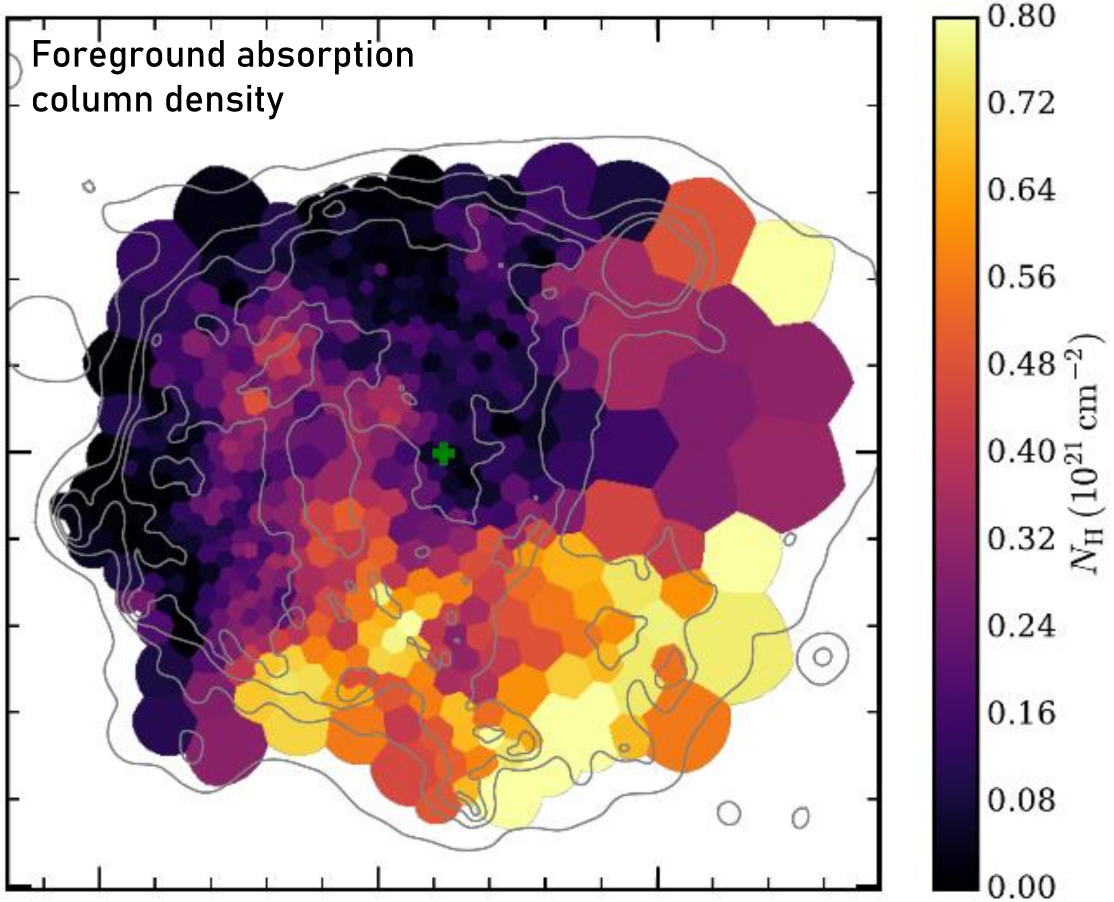

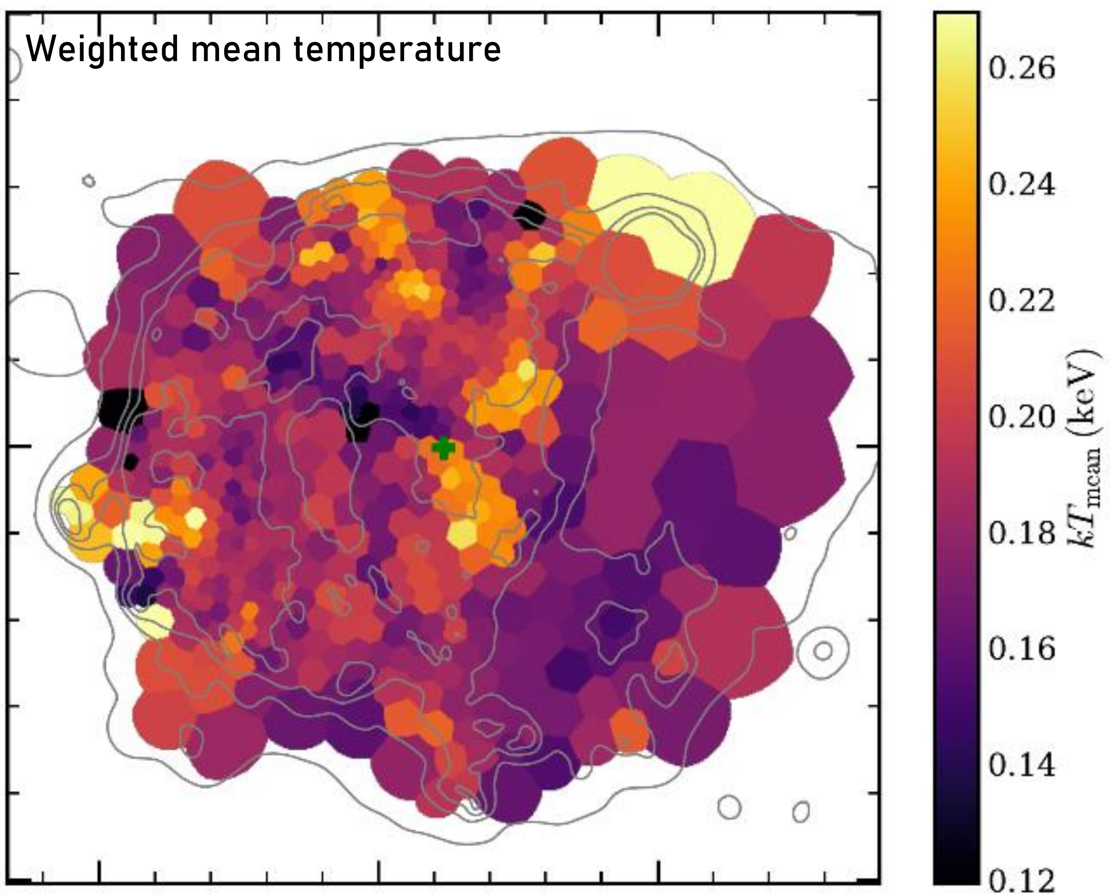

Results: Absorption & Plasma Temperature

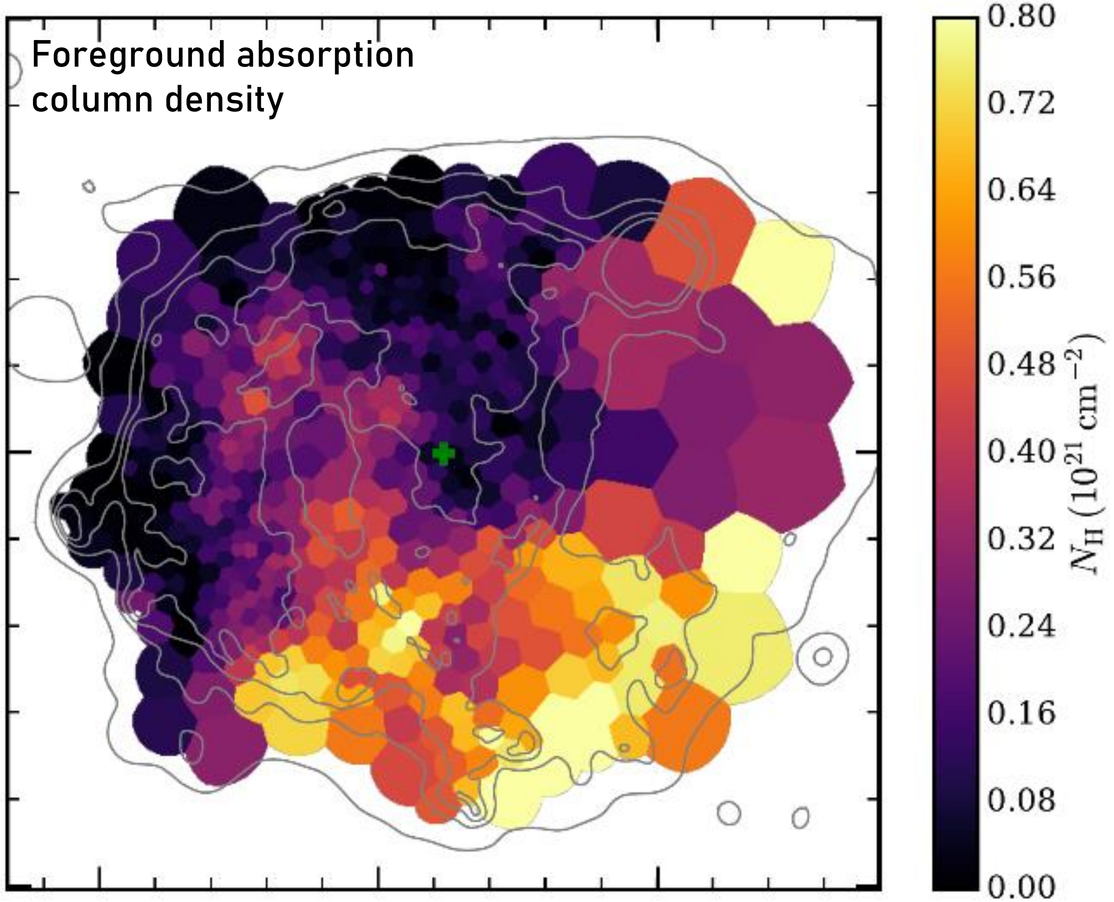

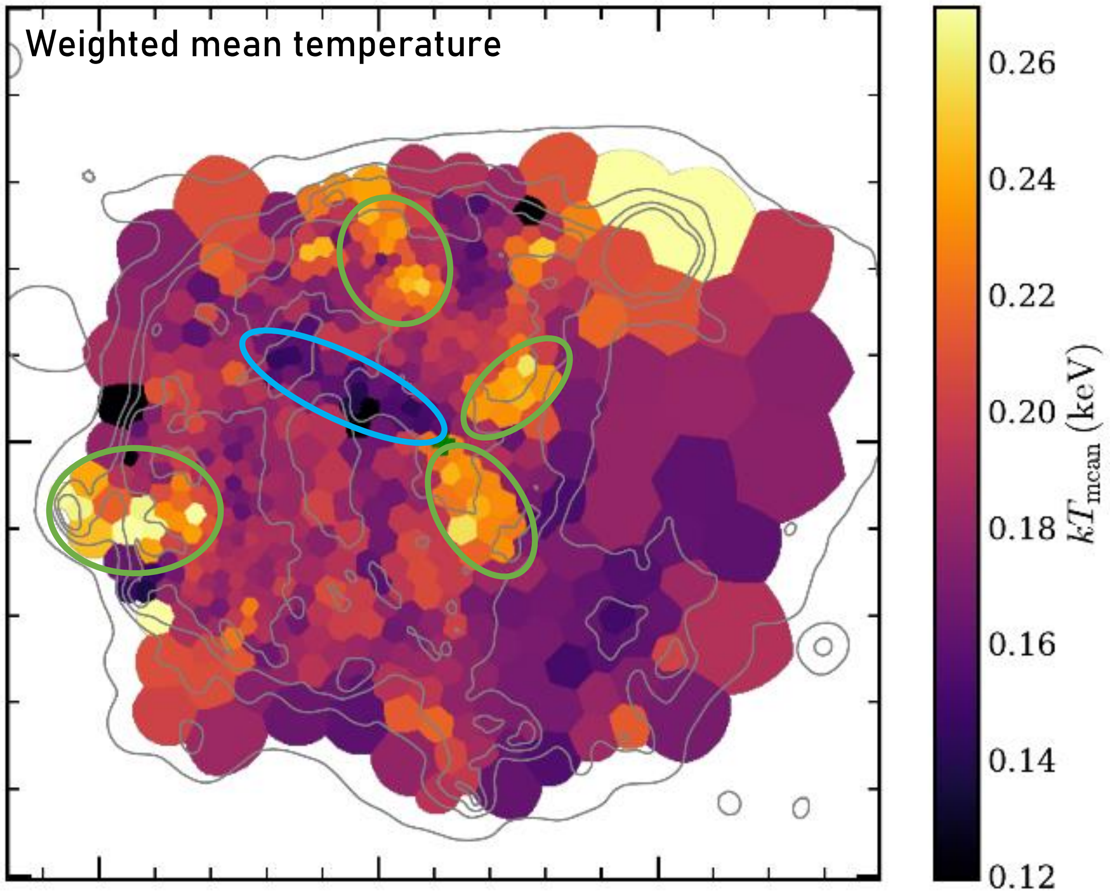

Results: Intervening ISM

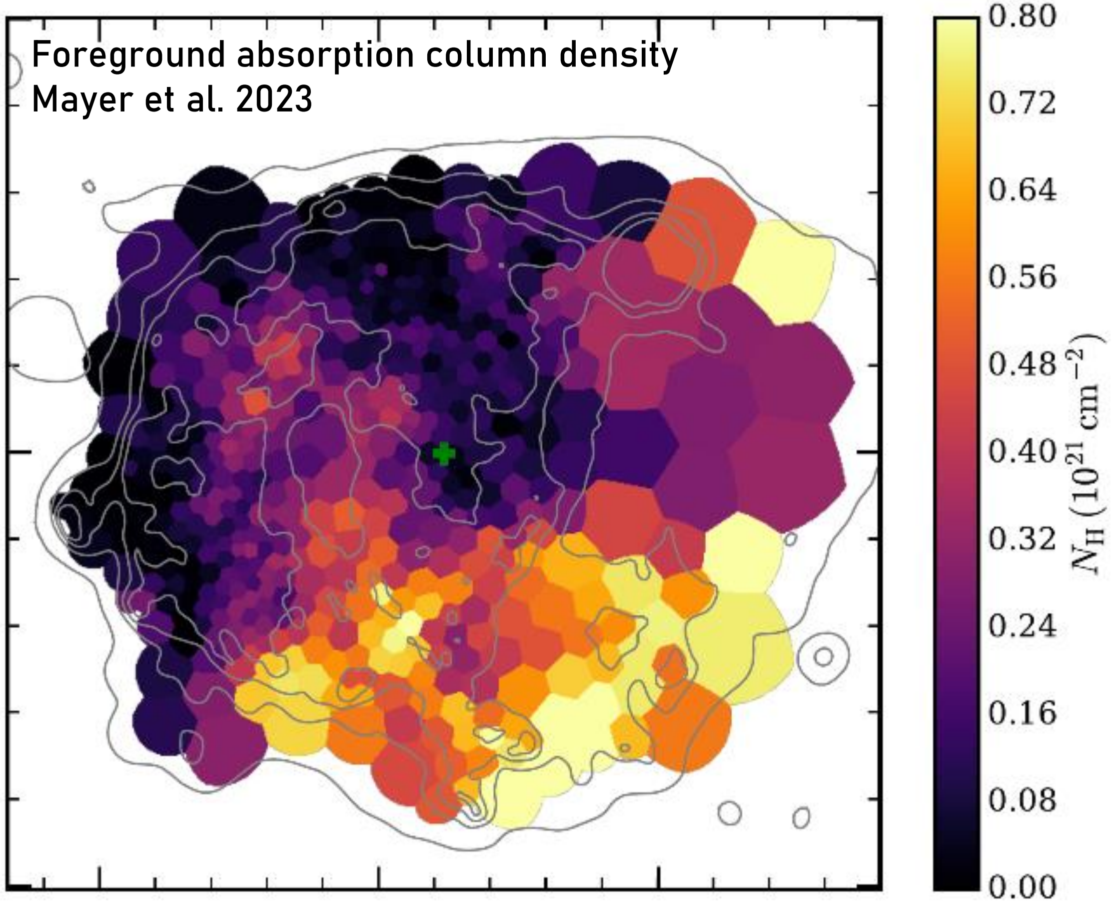

Results: Intervening ISM

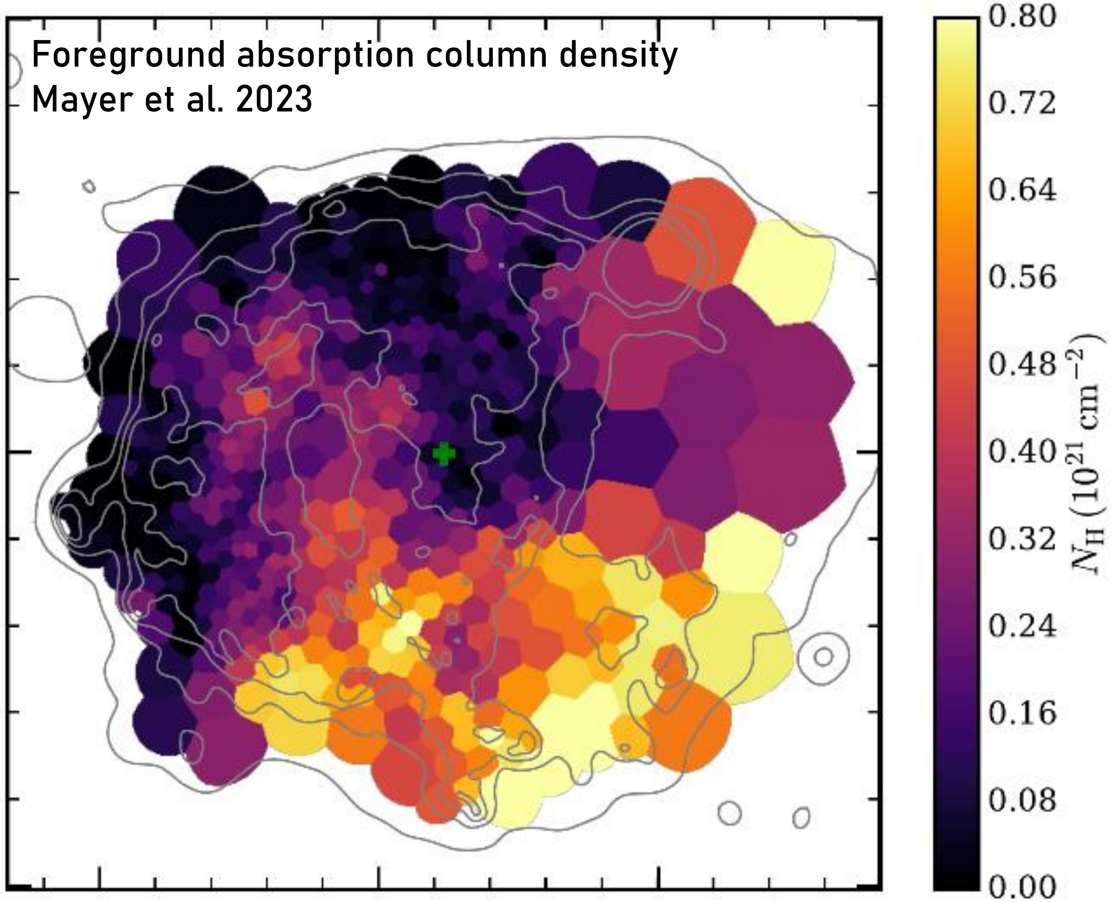

Optical Extinction towards Vela
(StarHorse, *Anders+22*)

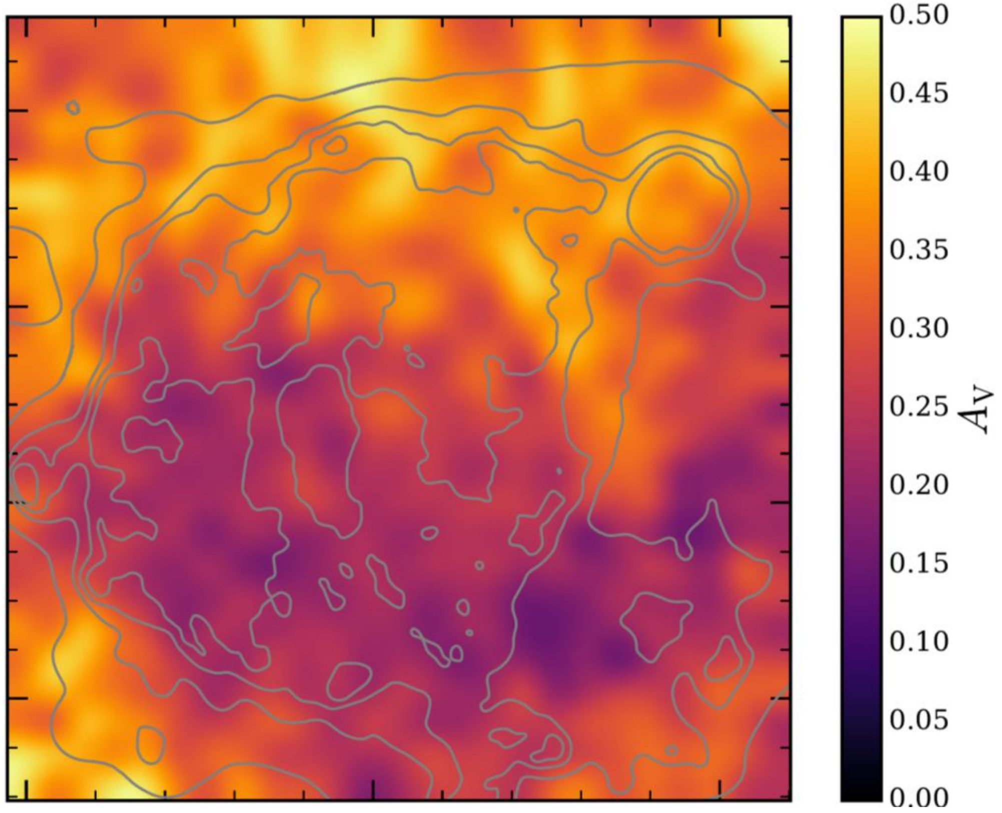

Results: Intervening ISM

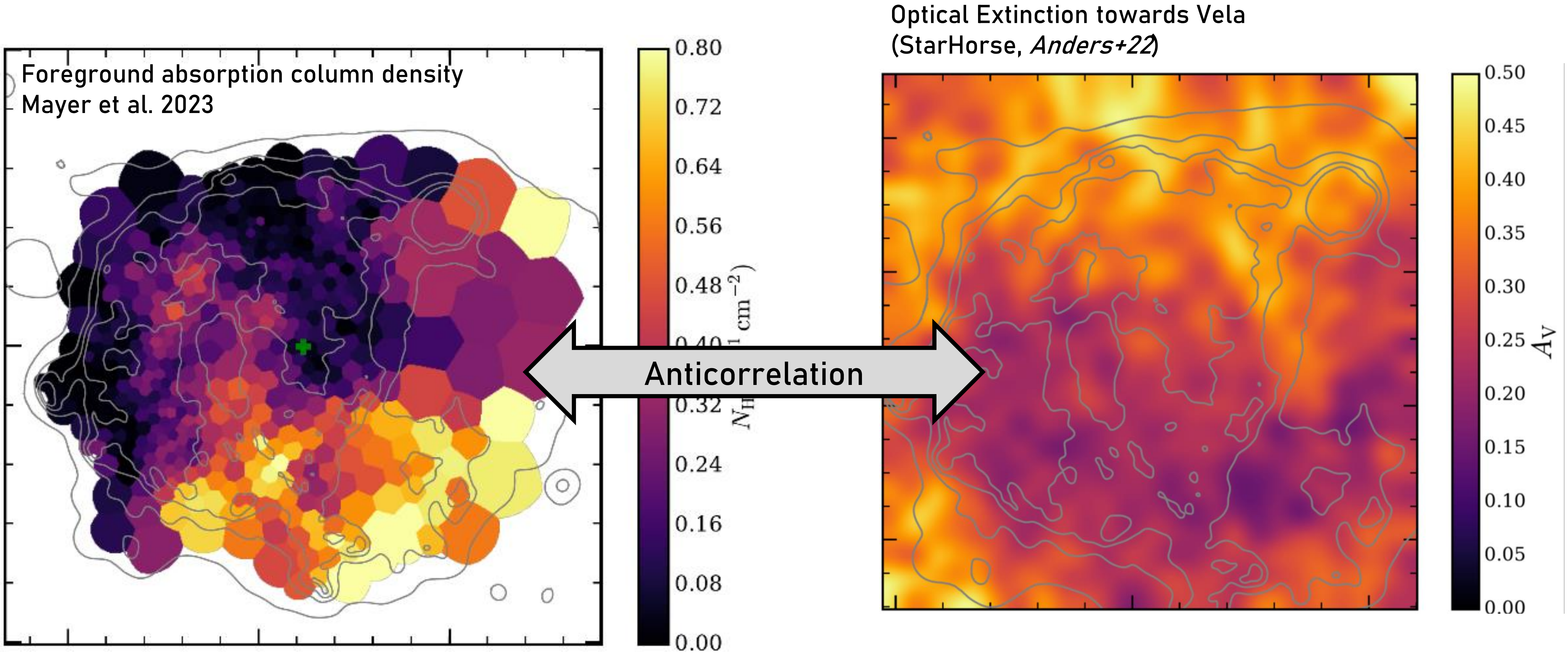

Results: Foreground Absorption

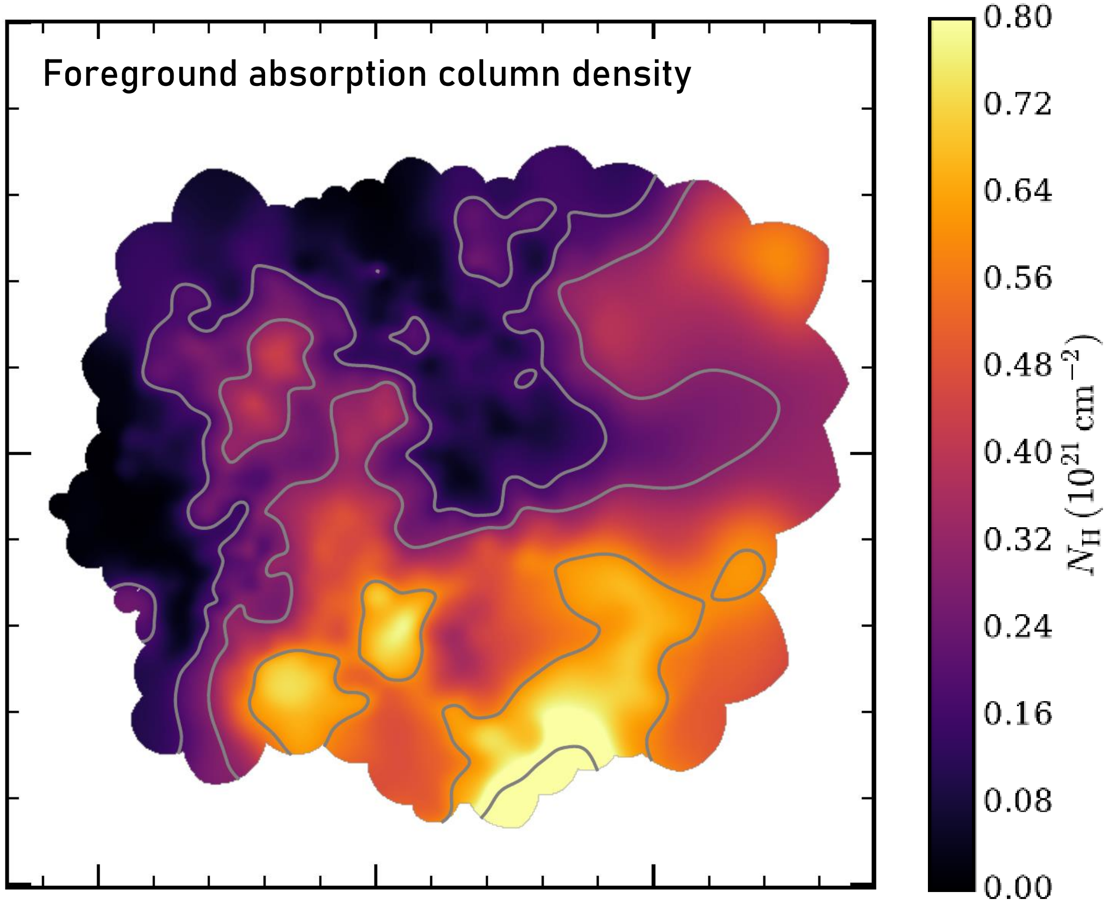

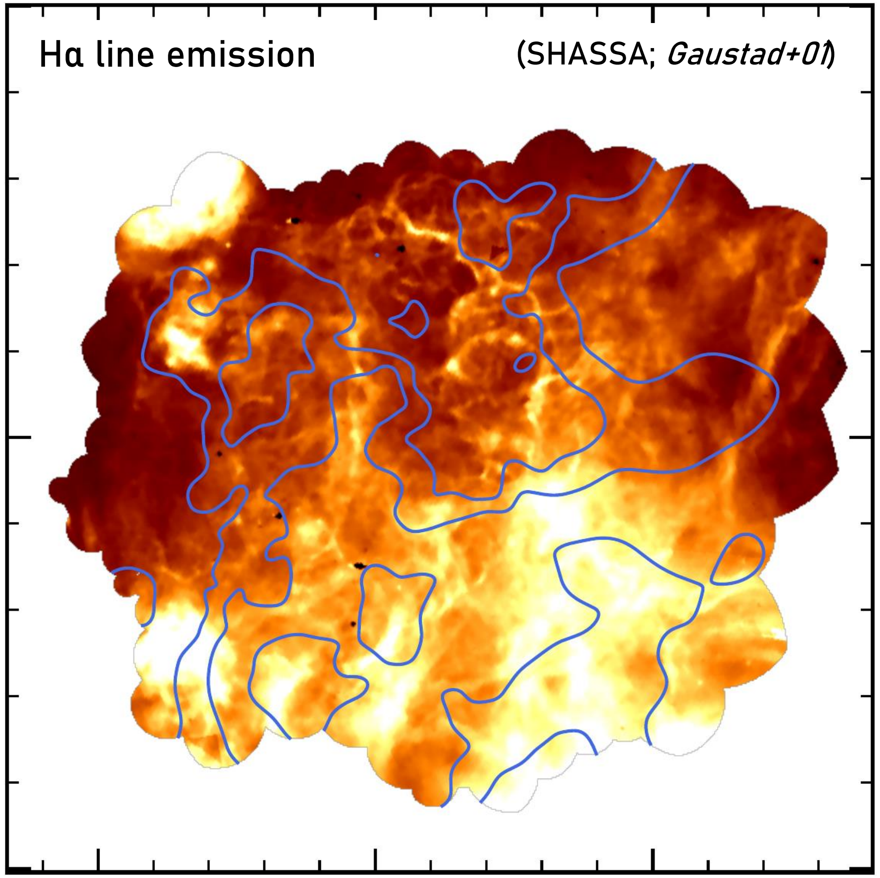

Results: Foreground Absorption

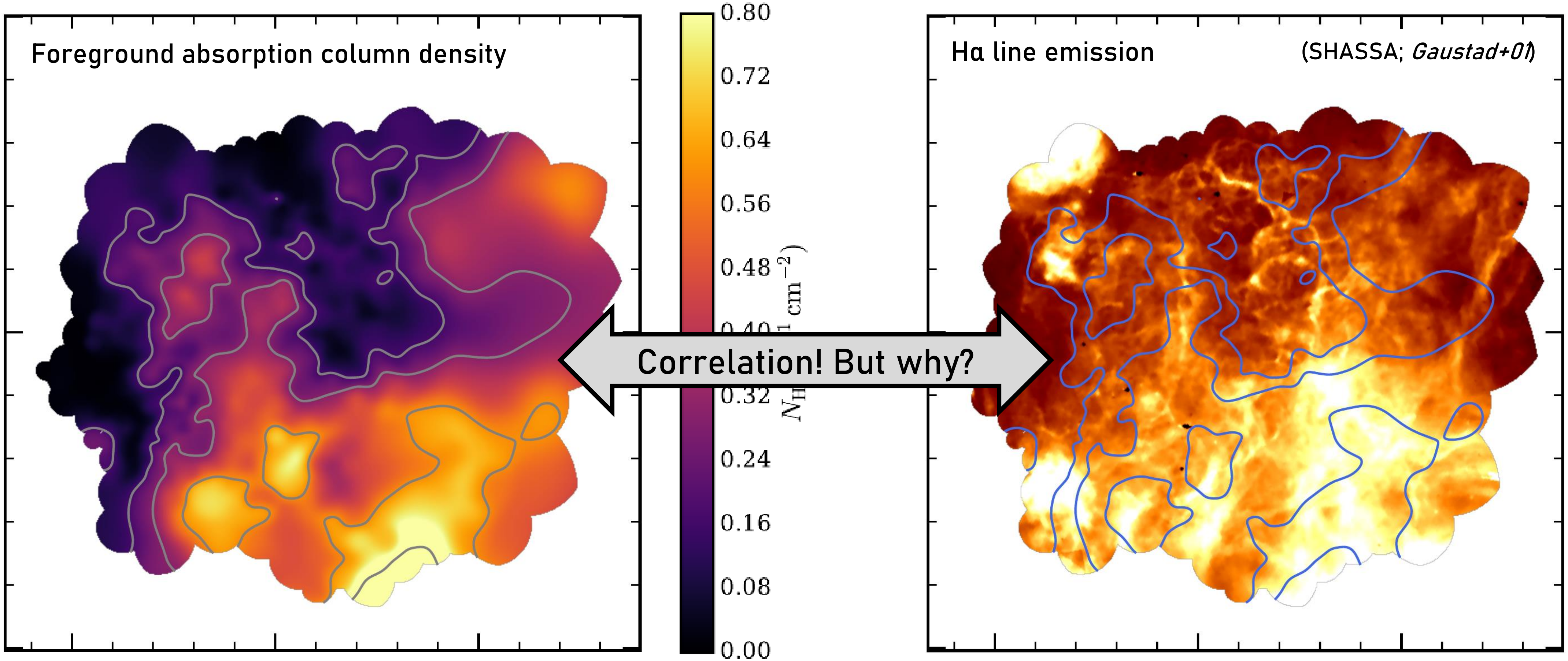

Results: ISM & Ejecta

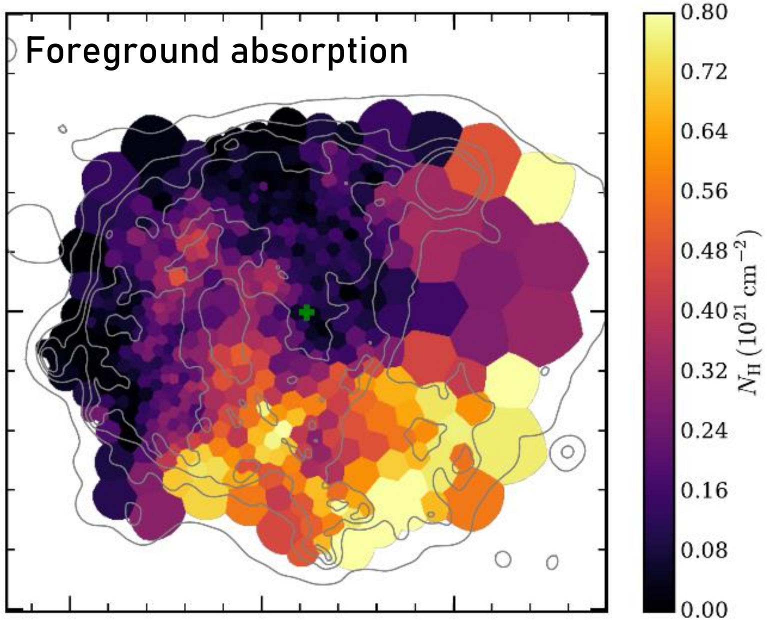

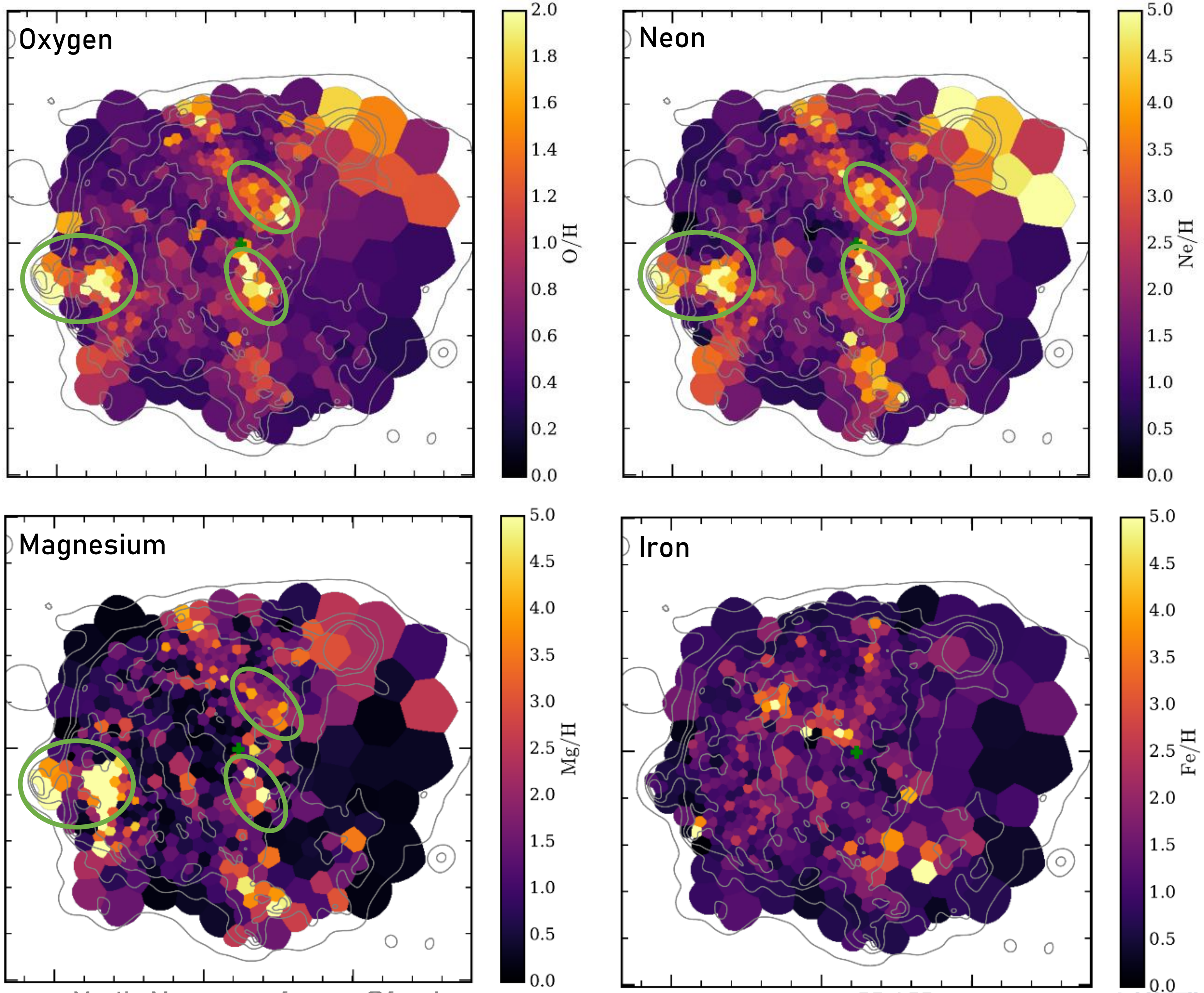

Results: Ejecta

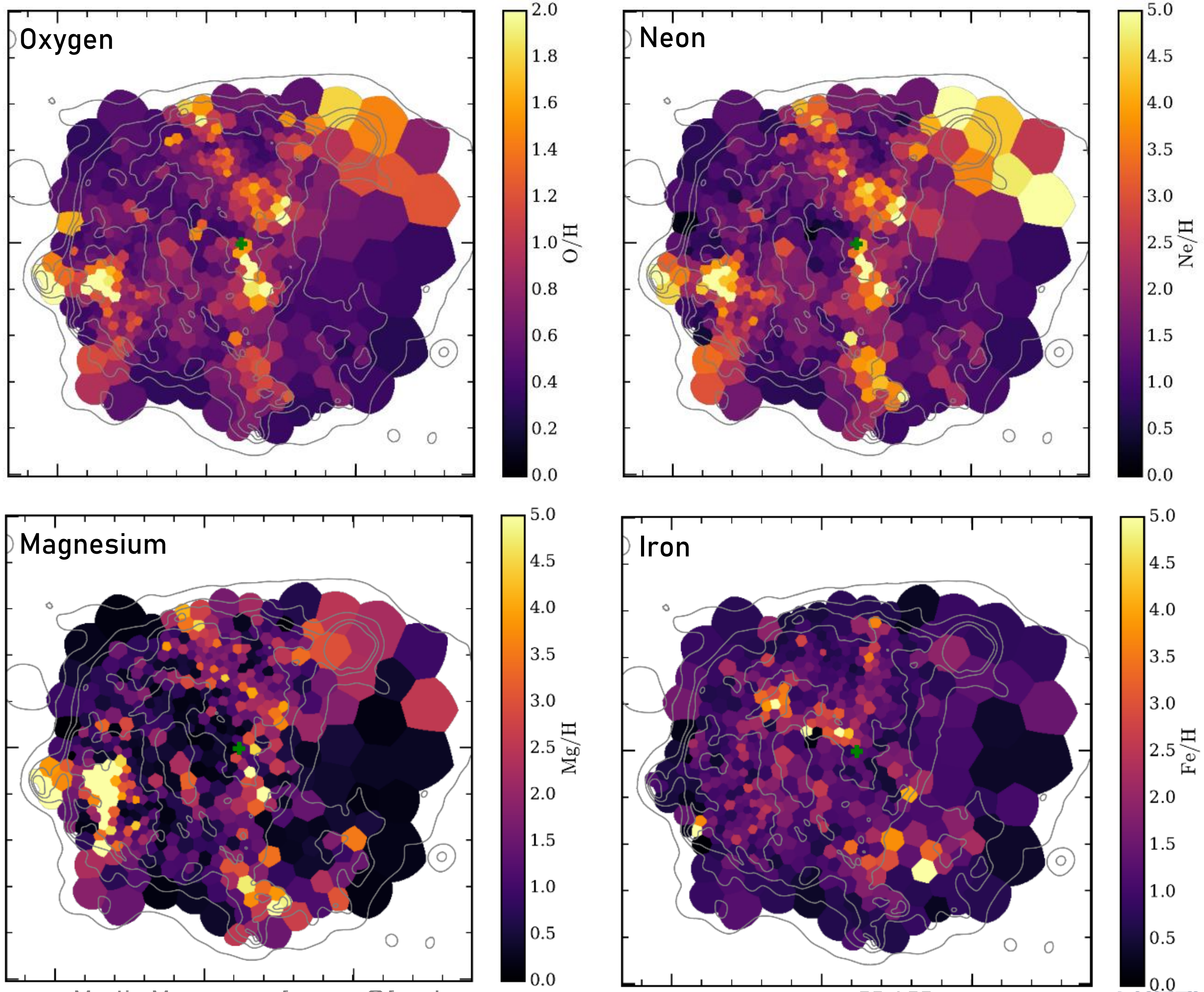

Results: Ejecta

- Correlated abundance peaks of oxygen, neon, magnesium

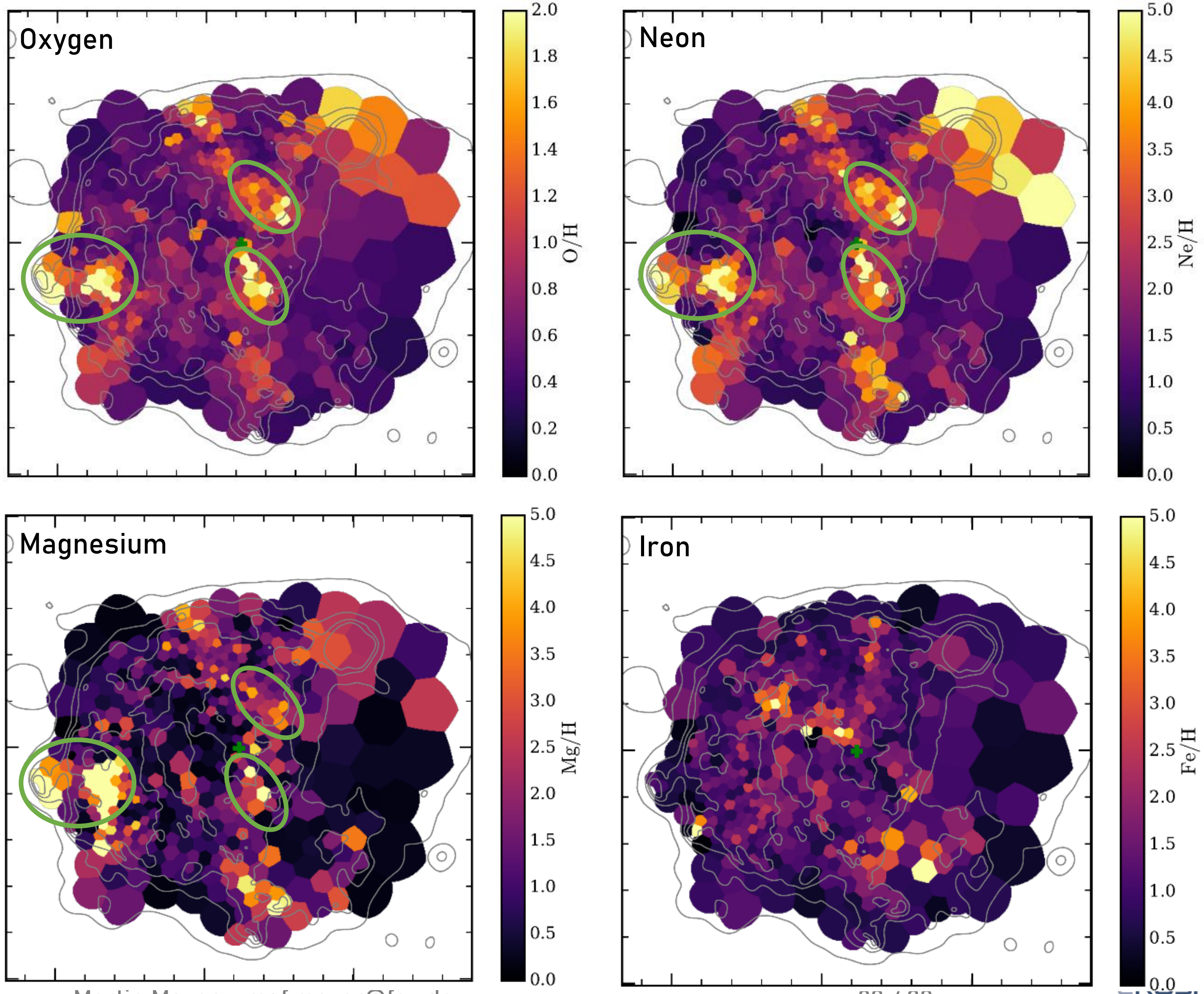

Results: Ejecta

- Correlated abundance peaks of oxygen, neon, magnesium
    - ➢Iron distribution independent from lighter elements

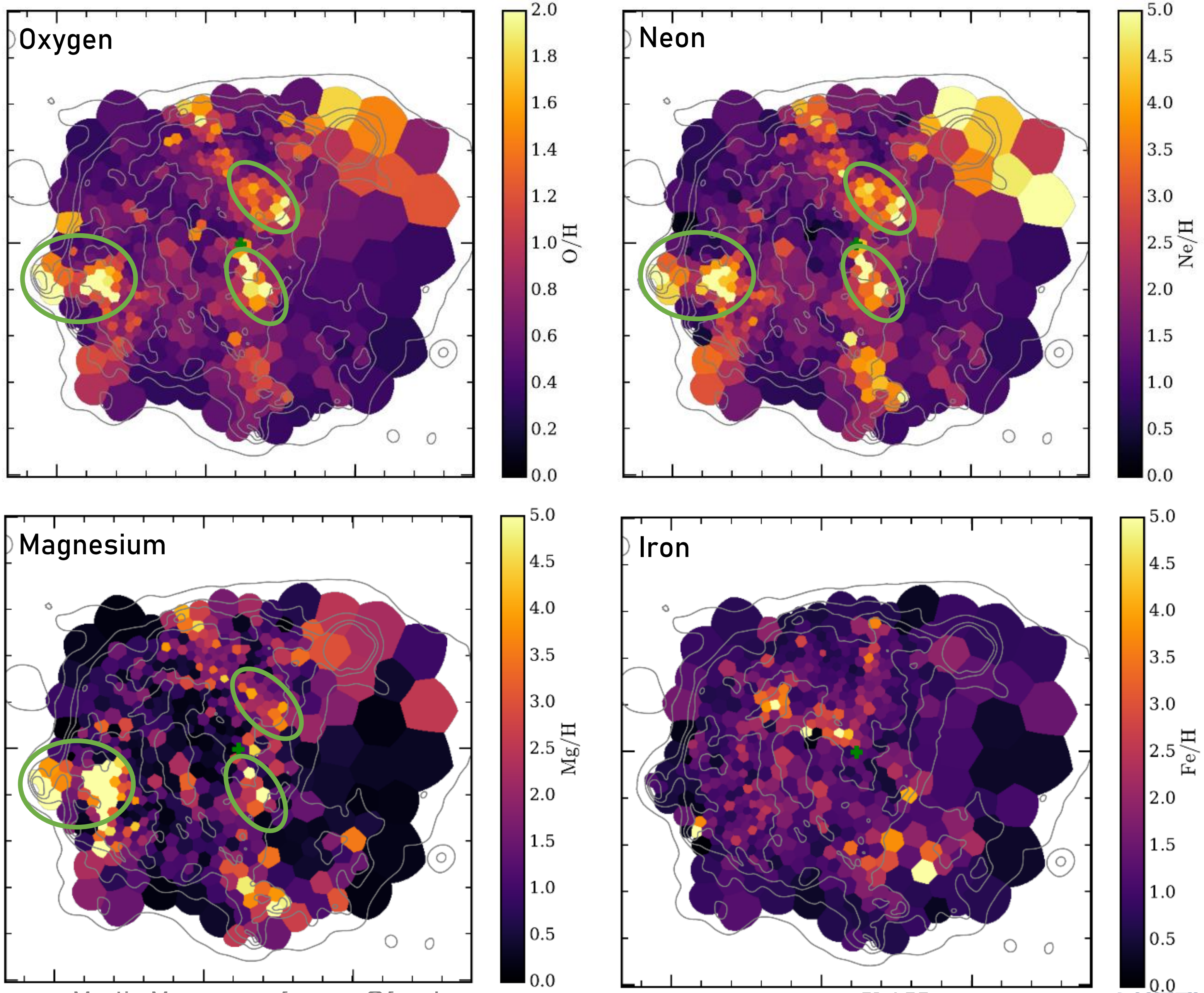

Results: Ejecta

- Correlated abundance peaks of oxygen, neon, magnesium
  - Iron distribution independent from lighter elements
  - General pattern: Ne/O, Mg/O supersolar
  - Not reproduced in nucleosynthesis models (*Sukhbold+16*)

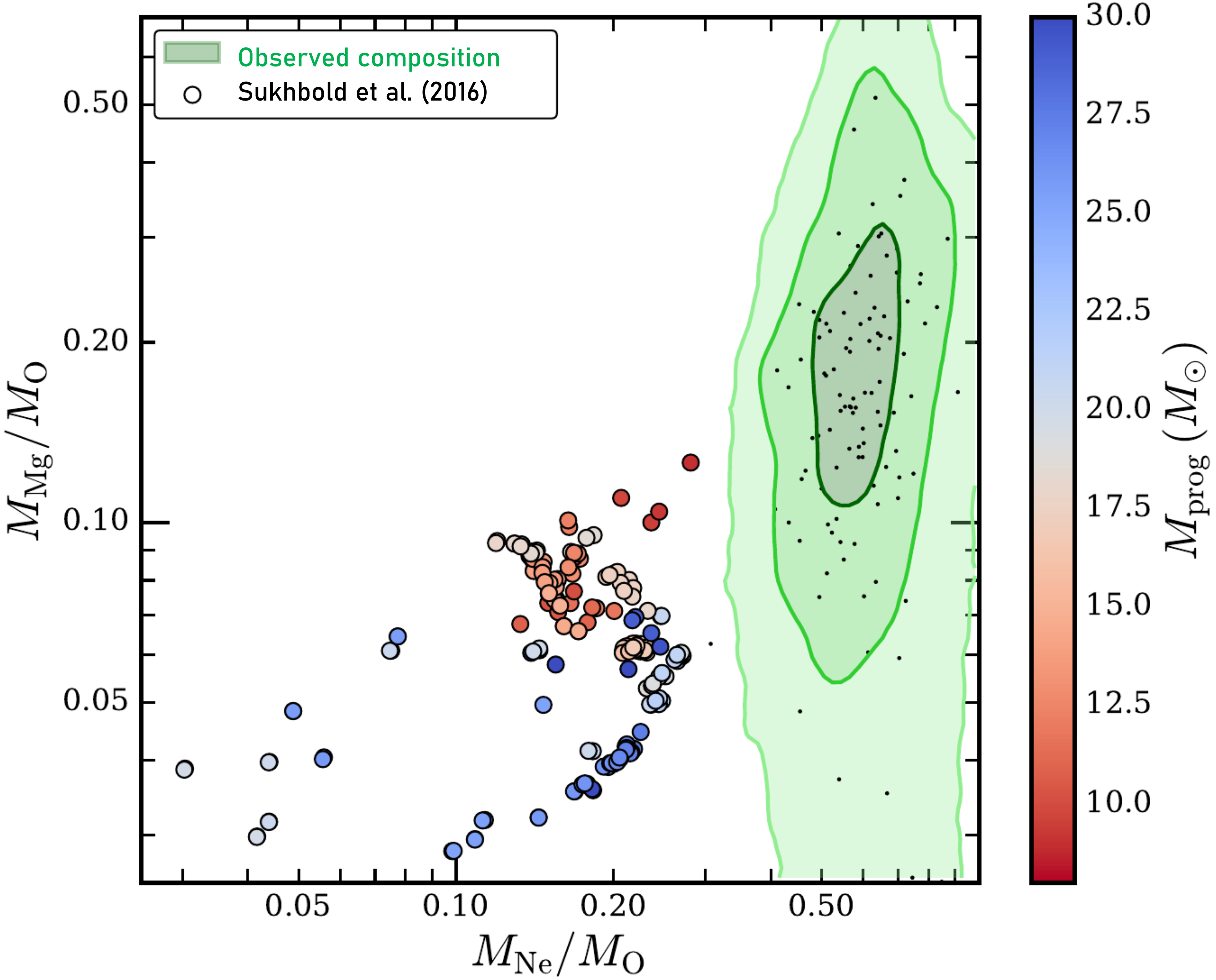

Results: Ejecta

Results: Ejecta

- Correlated abundance peaks of oxygen, neon, magnesium

Results: Ejecta

- Correlated abundance peaks of oxygen, neon, magnesium
  - ➢Iron distribution independent from lighter elements

Results: Ejecta

- Correlated abundance peaks of oxygen, neon, magnesium
  - ➢Iron distribution independent from lighter elements
  - ➢General pattern: Ne/O, Mg/O supersolar
  - ➢Reproducable in low-metallicity model? *(Nomoto+06)*

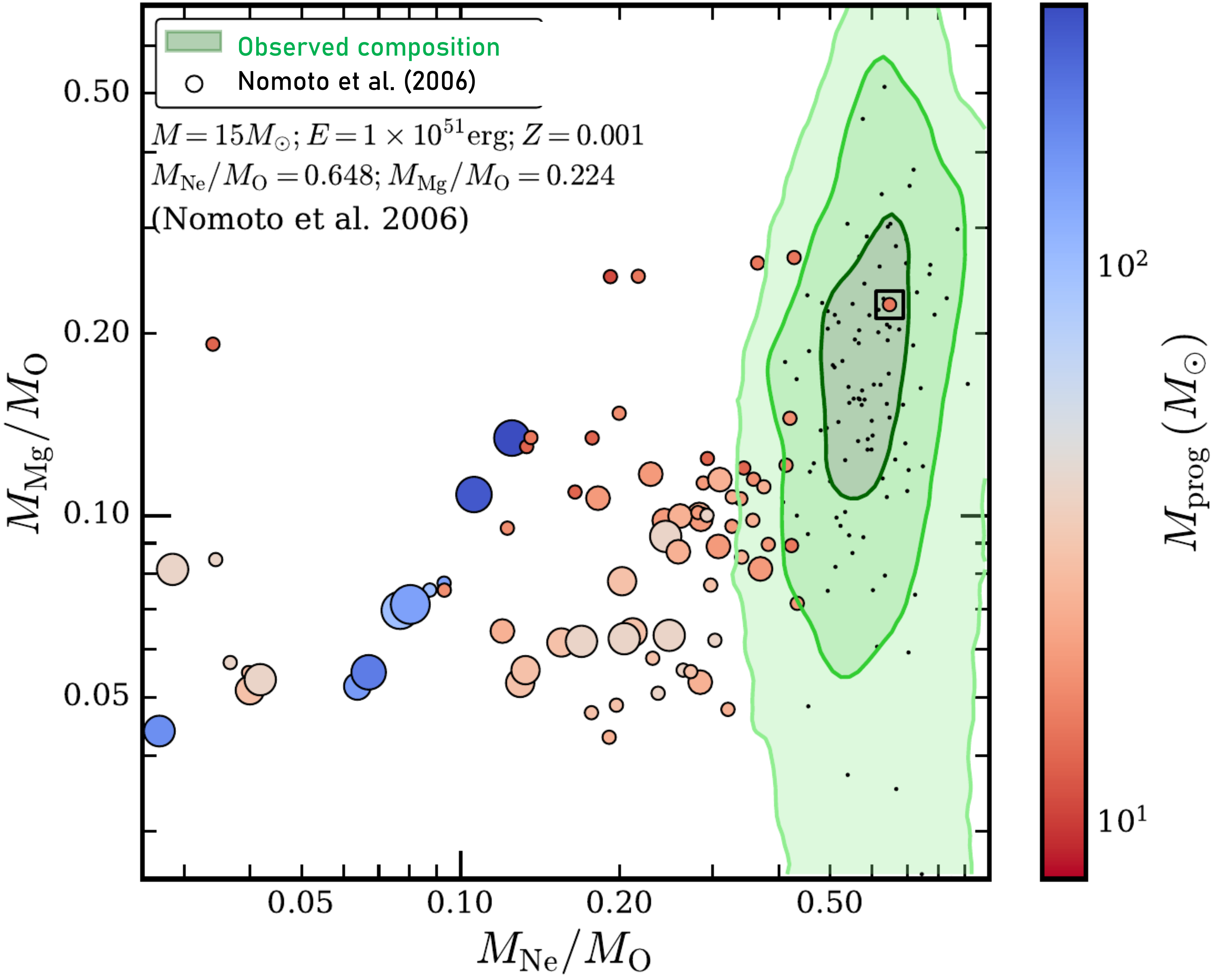

Results: Shrapnels A, B, C

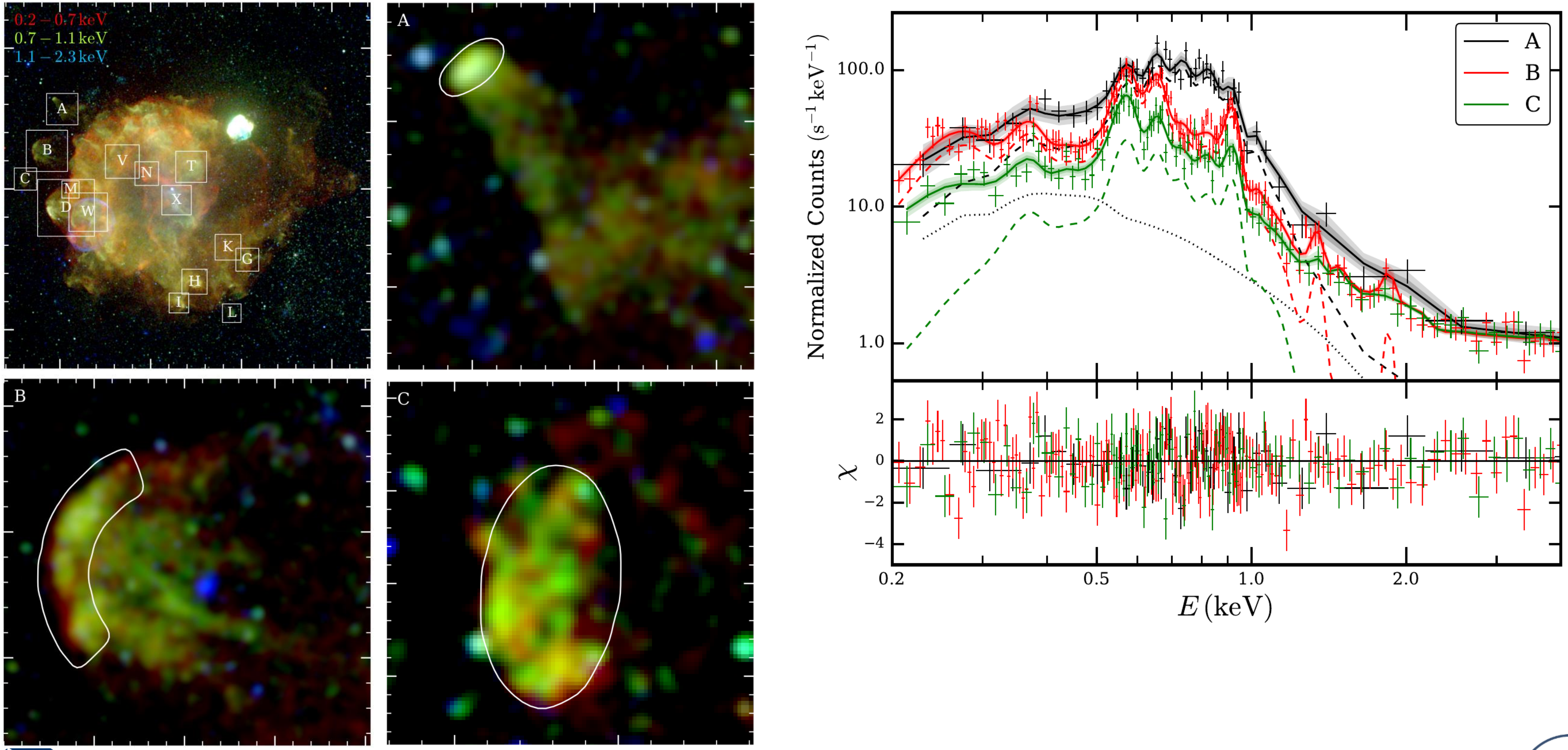

Results: Shrapnels A, B, C

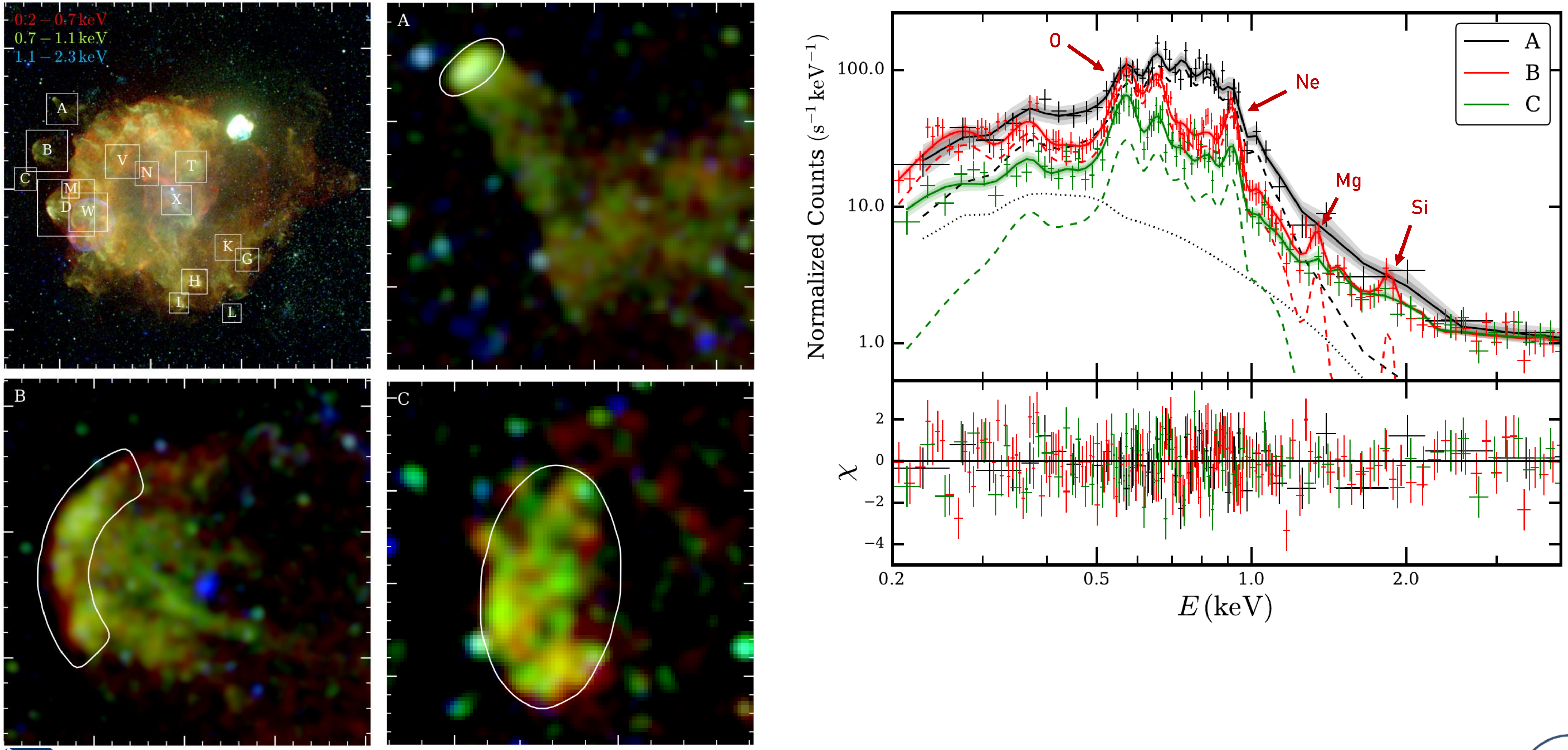

Results: Shrapnels A, B, C

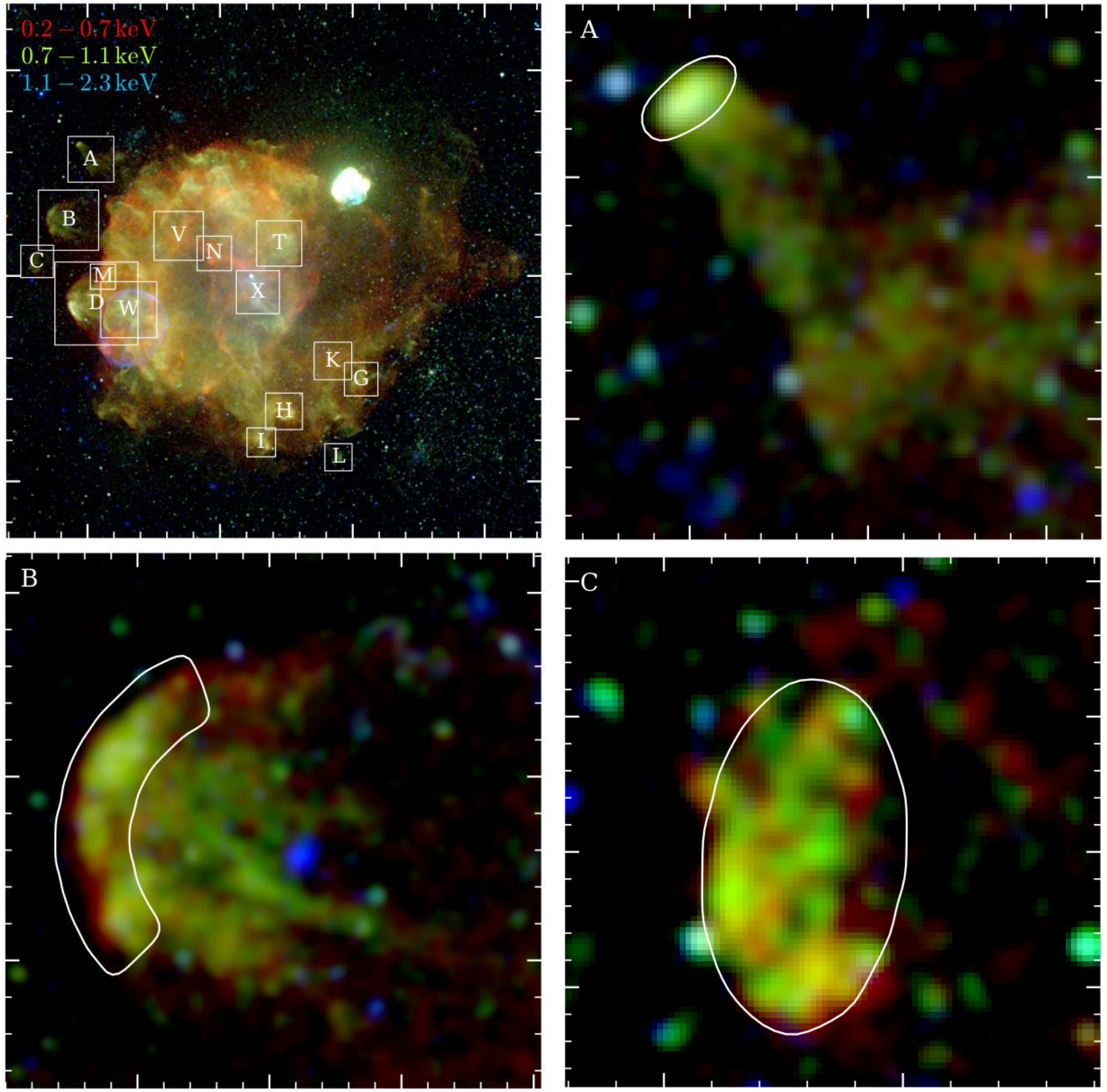

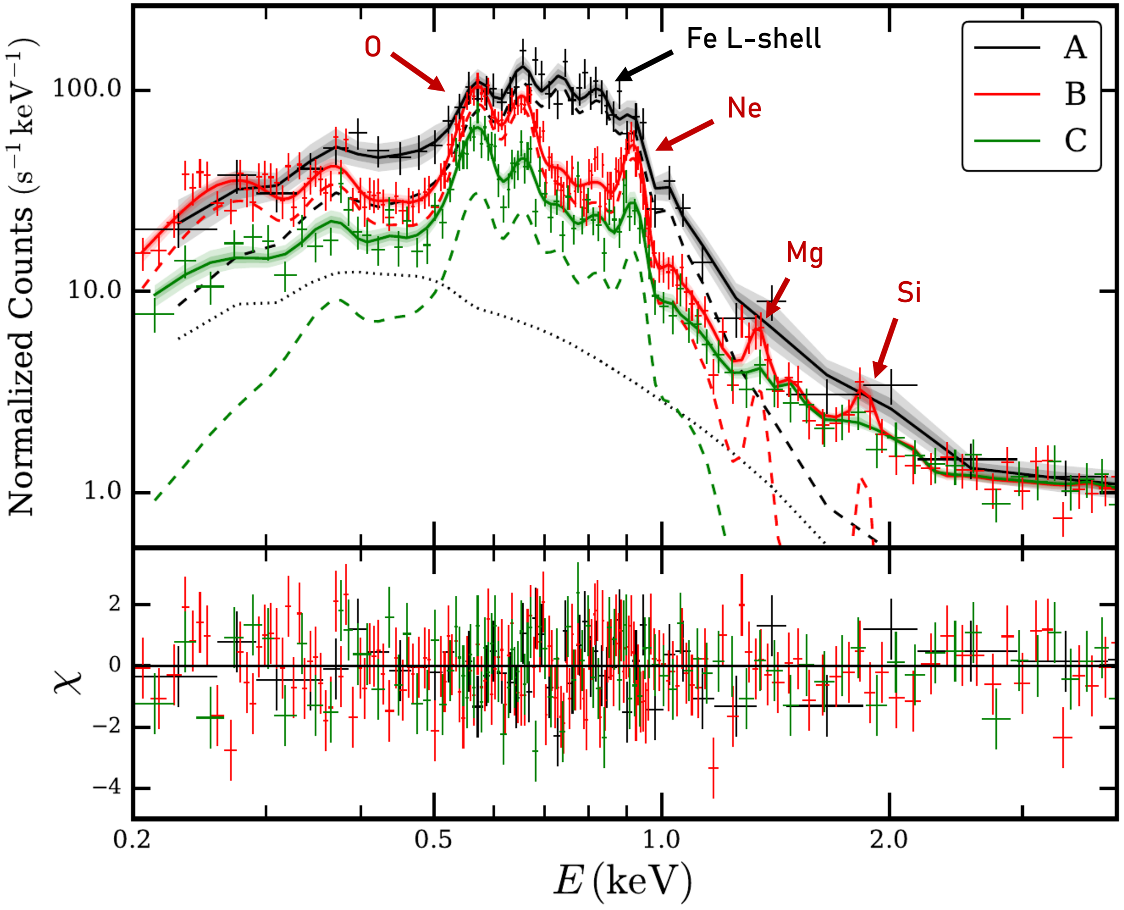

Results: Shrapnels A, B, C

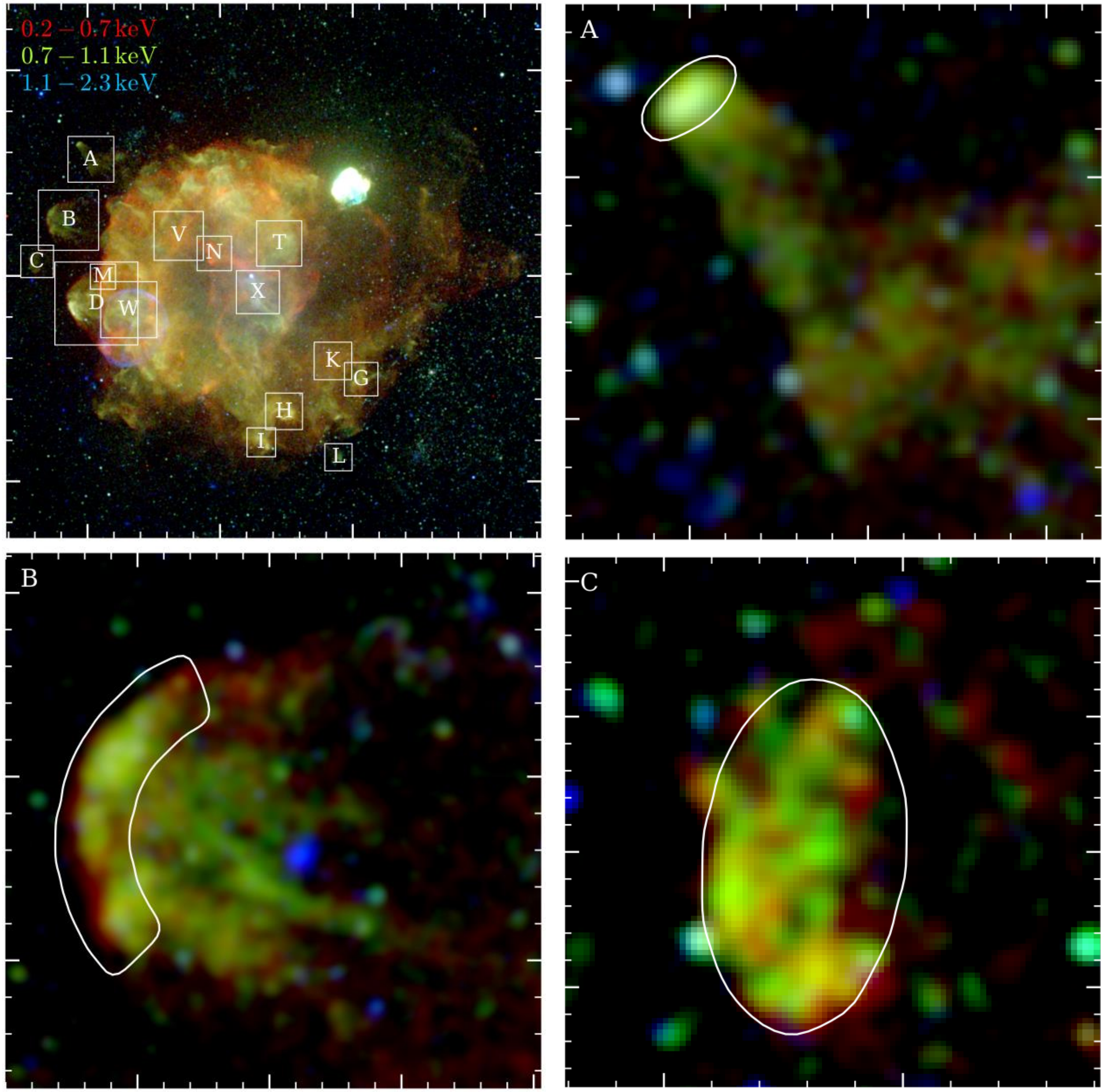

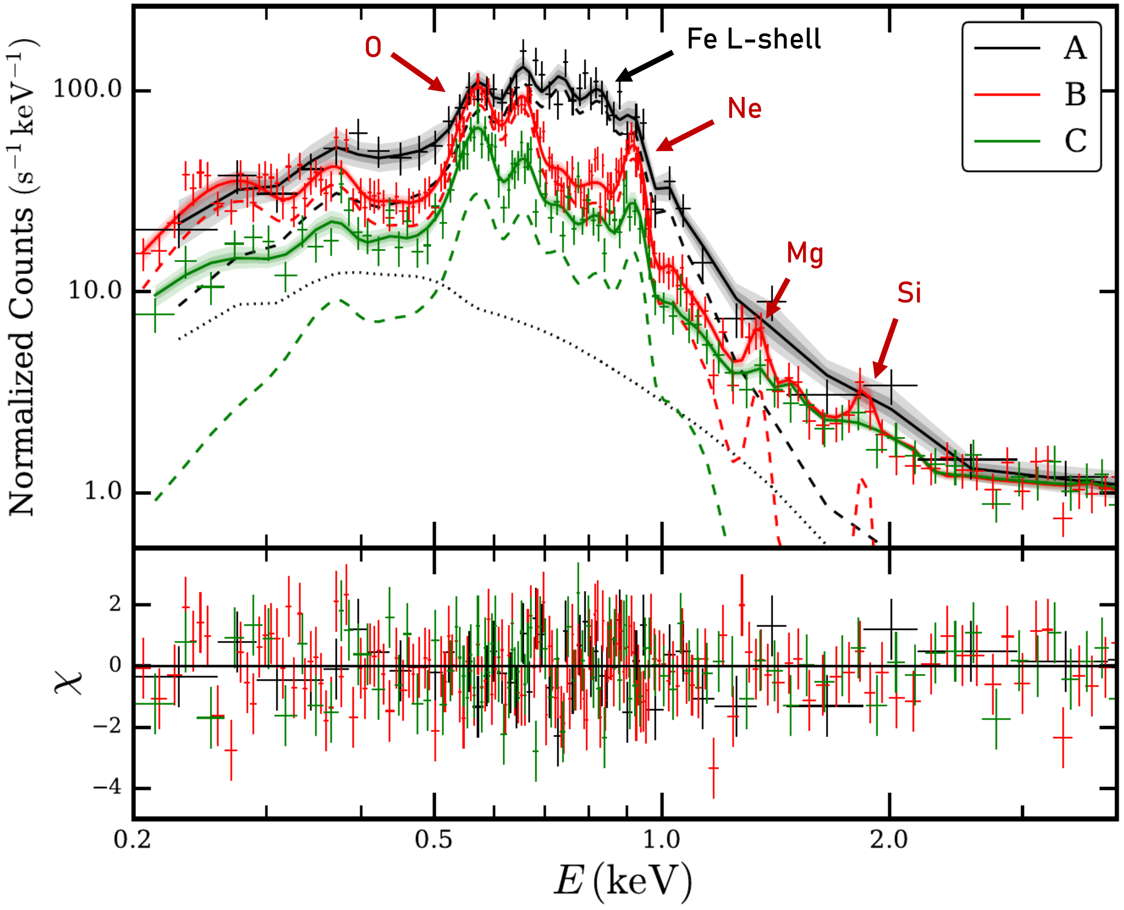

- Iron ejecta present in silicon-rich (*Katsuda+06*), fast shrapnel A?

Results: Ejecta in Shrapnel D

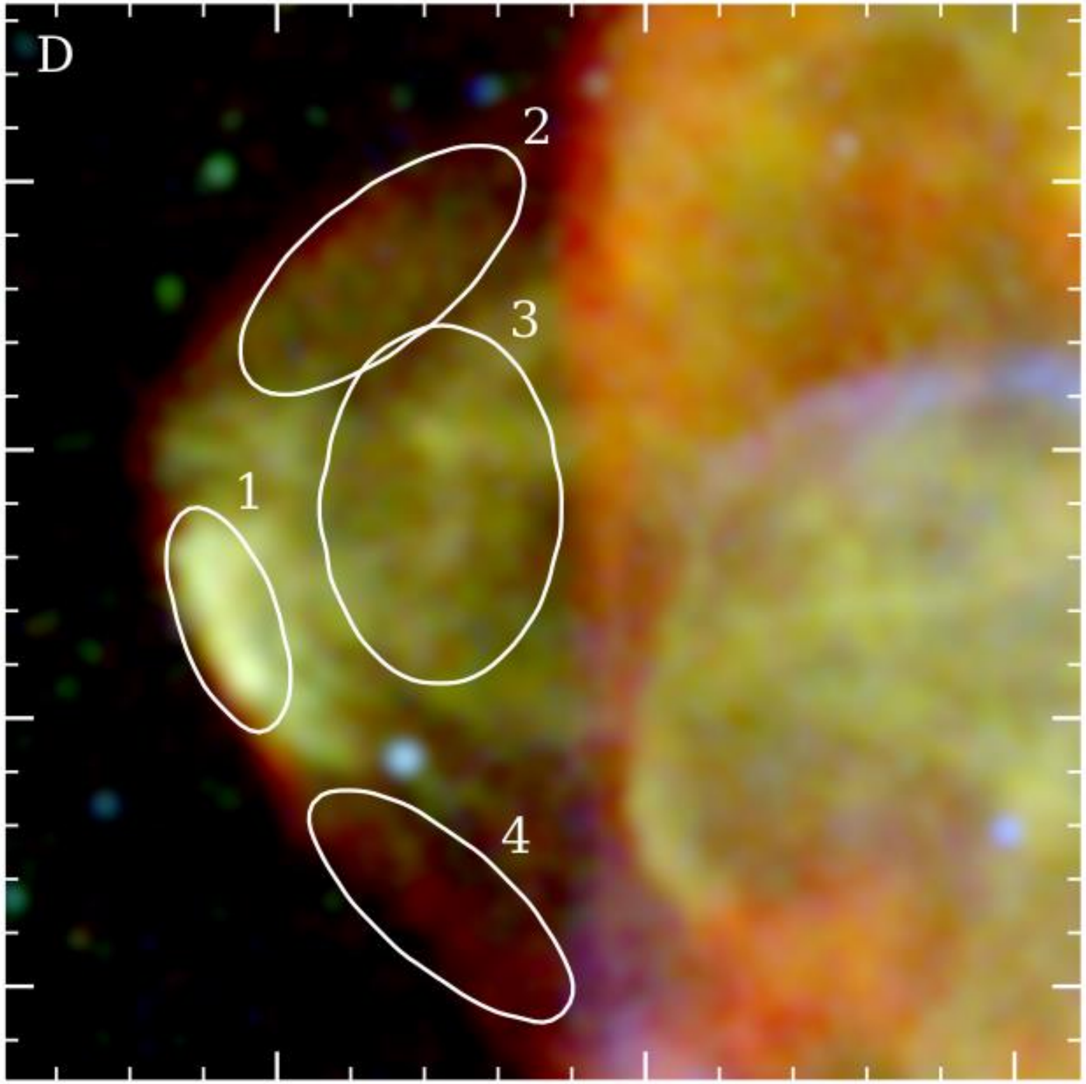

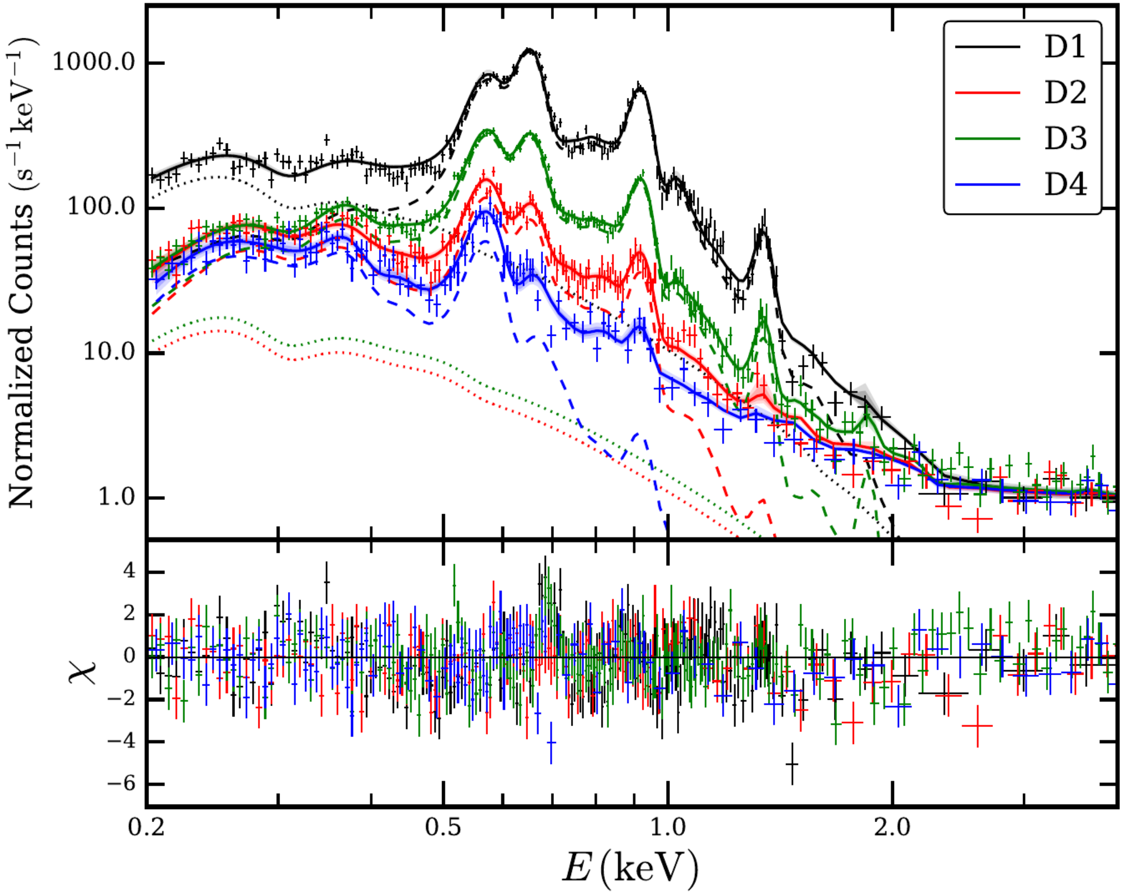

Results: Ejecta in Shrapnel D

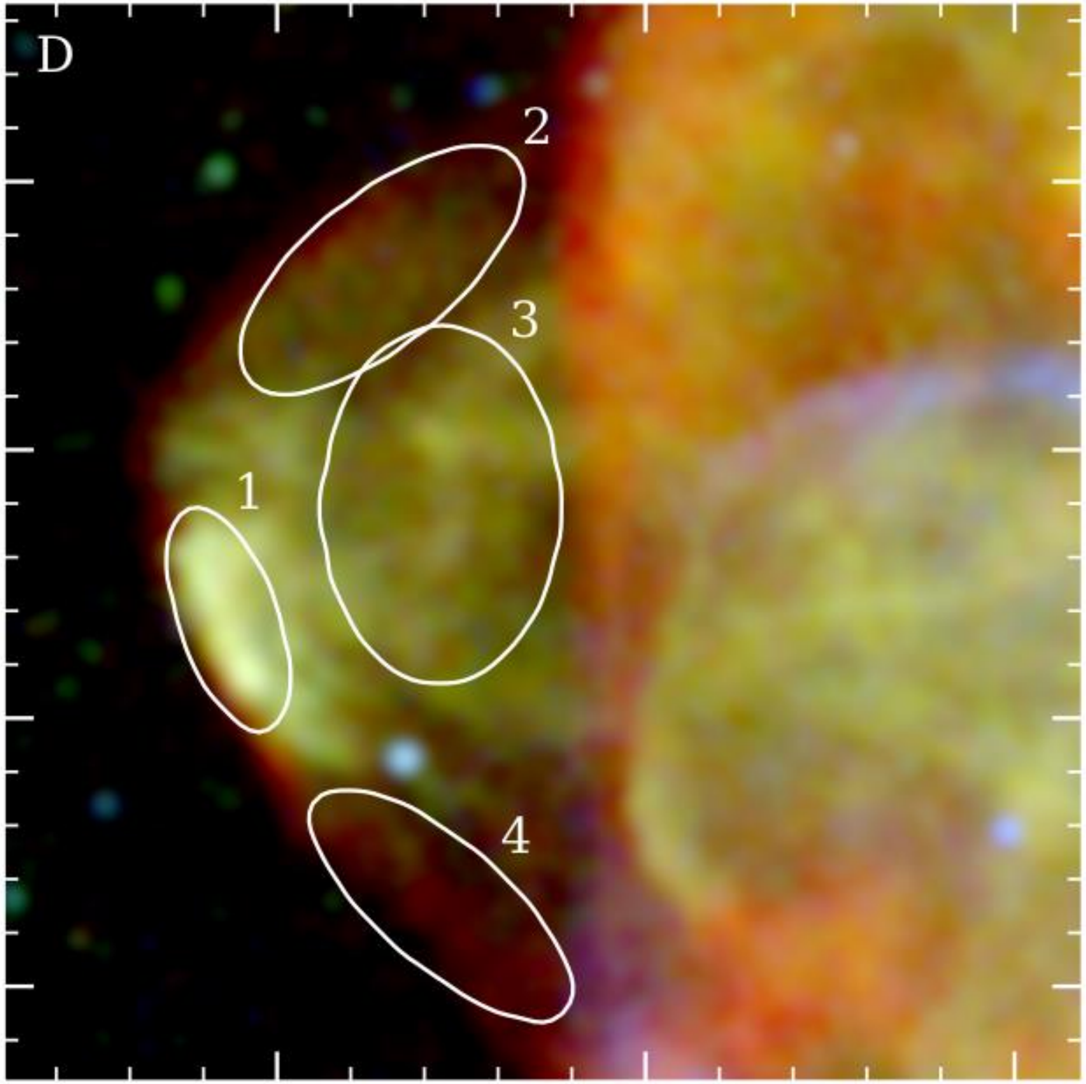

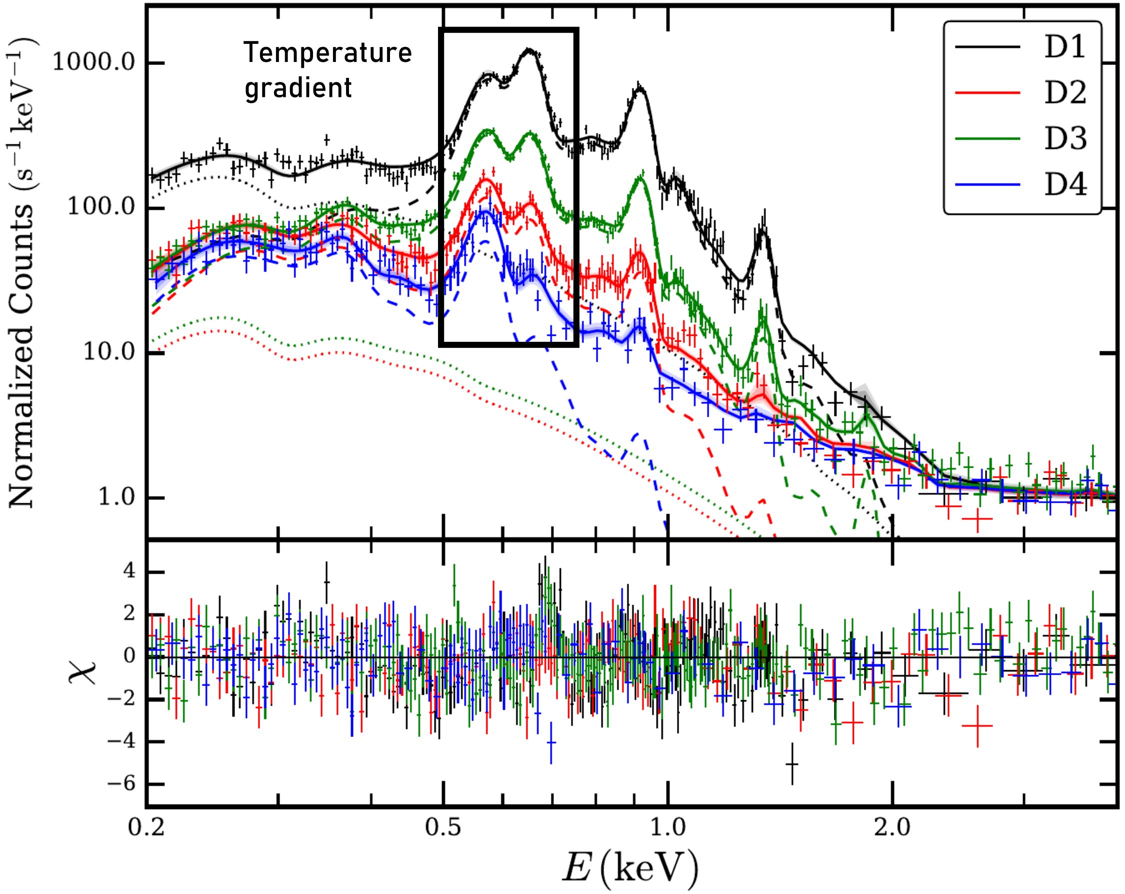

Results: Ejecta in Shrapnel D

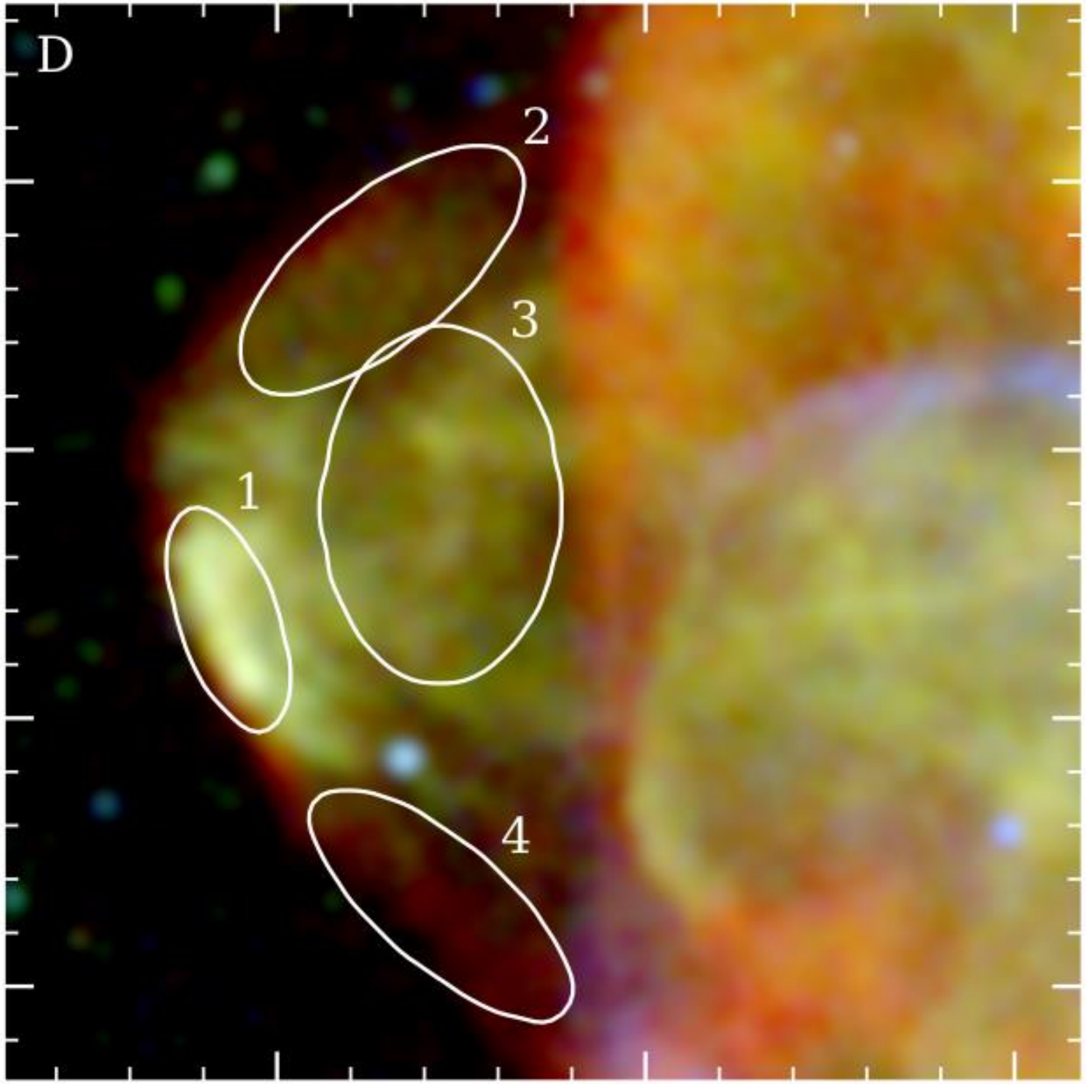

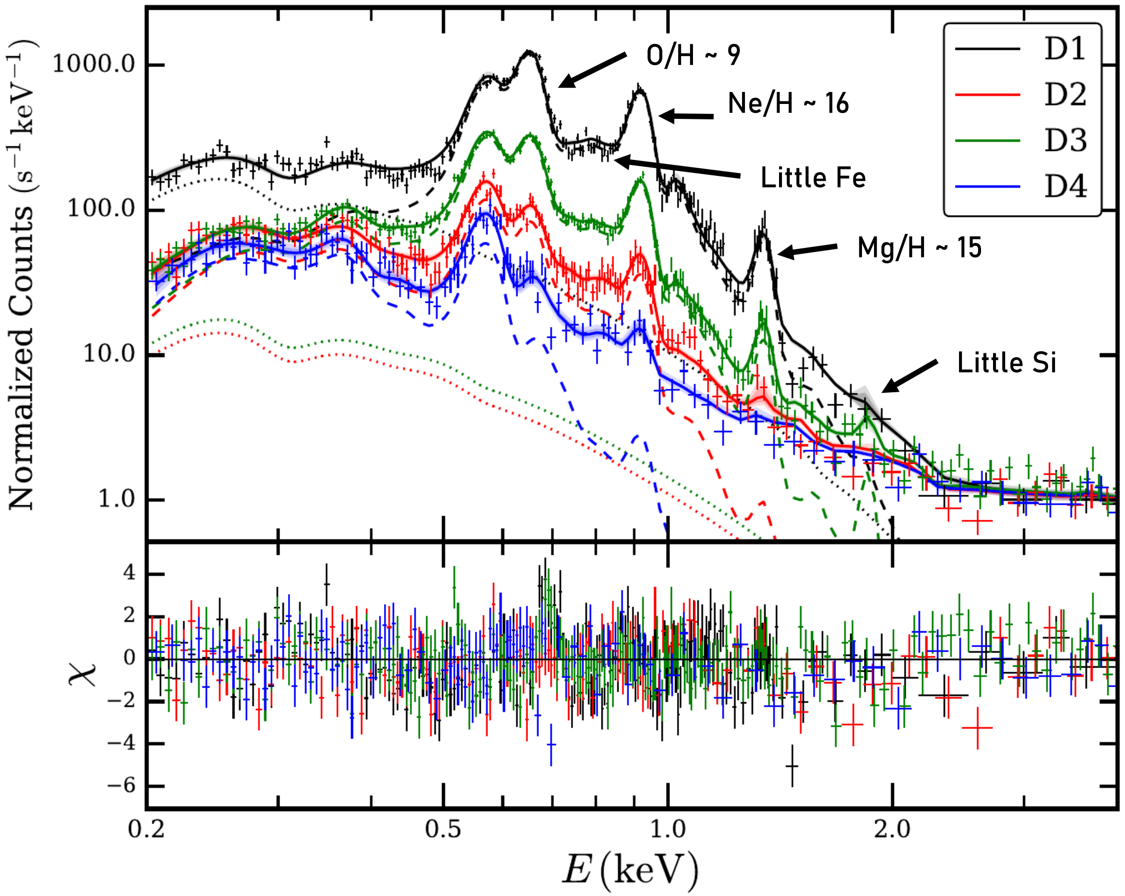

Results: Ejecta in Shrapnel D

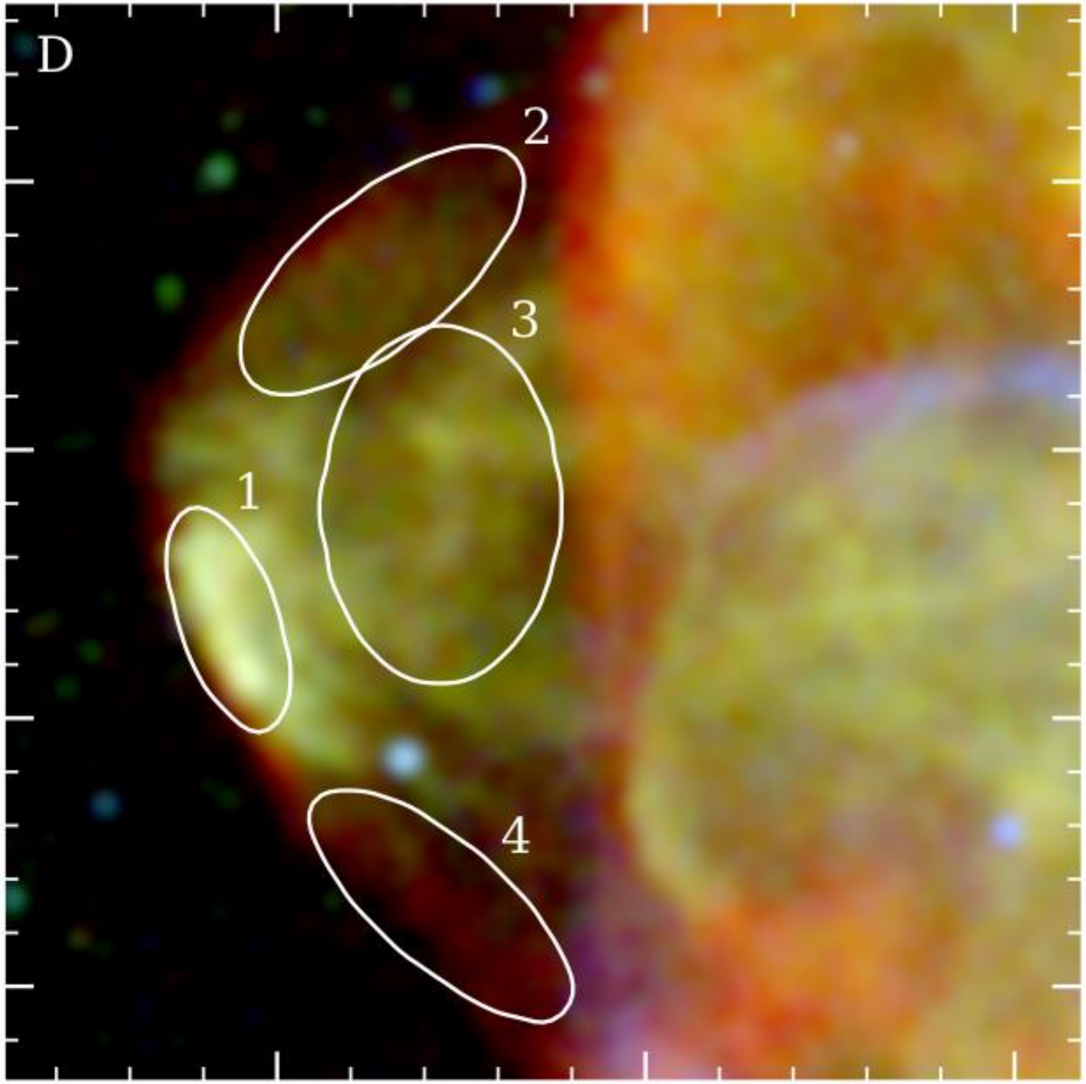

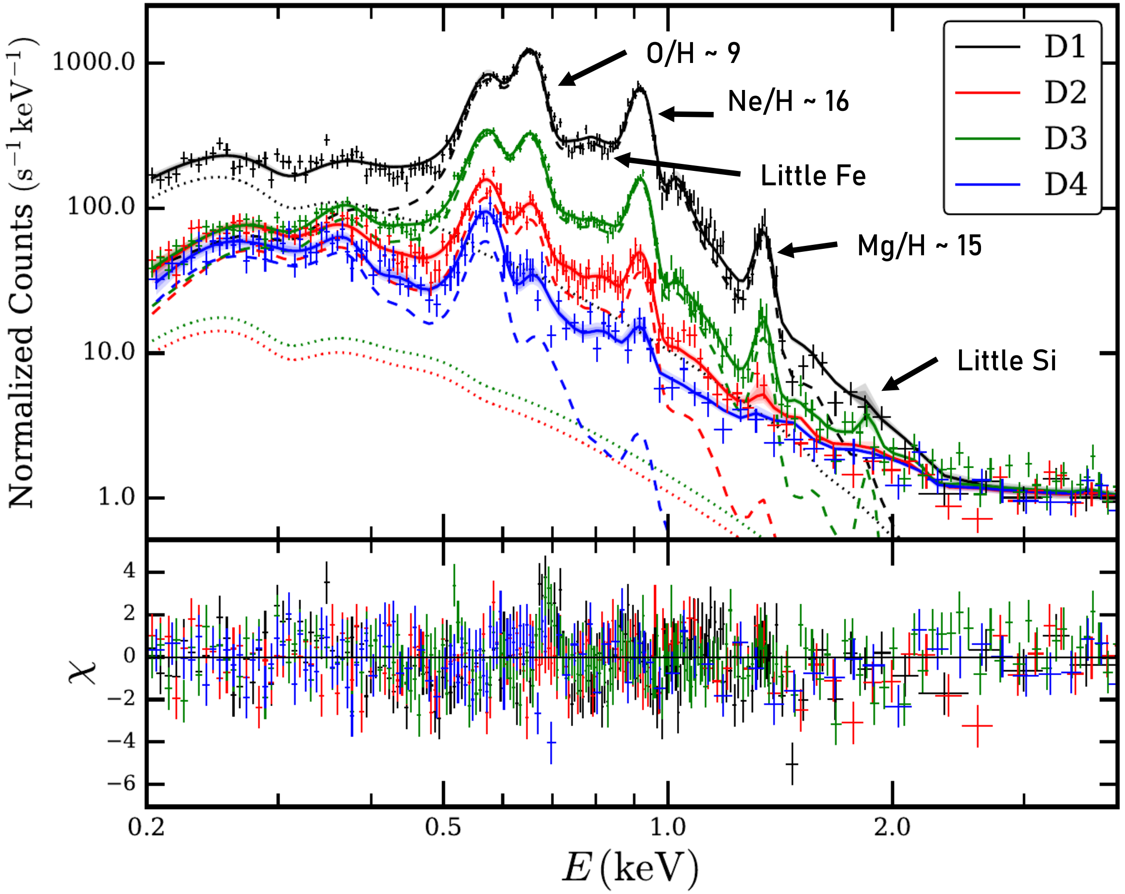

- ➢Hot light-element ejecta at the apex; cooler shocked ISM along the sides

Shrapnel D: Simulations (Miceli et al. 2013)

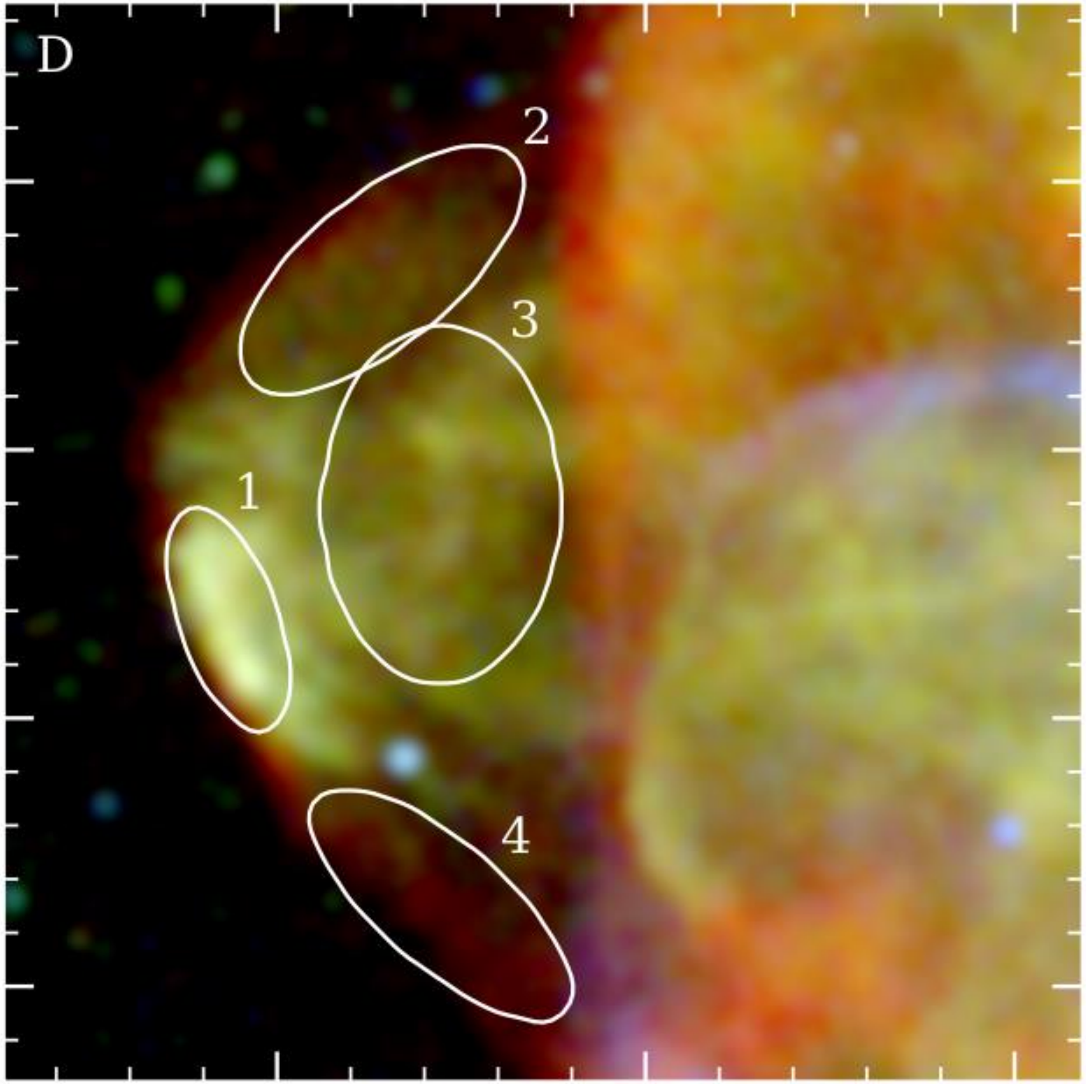

Miceli+13: Simulation of an ejecta clump protruding into the unshocked ISM

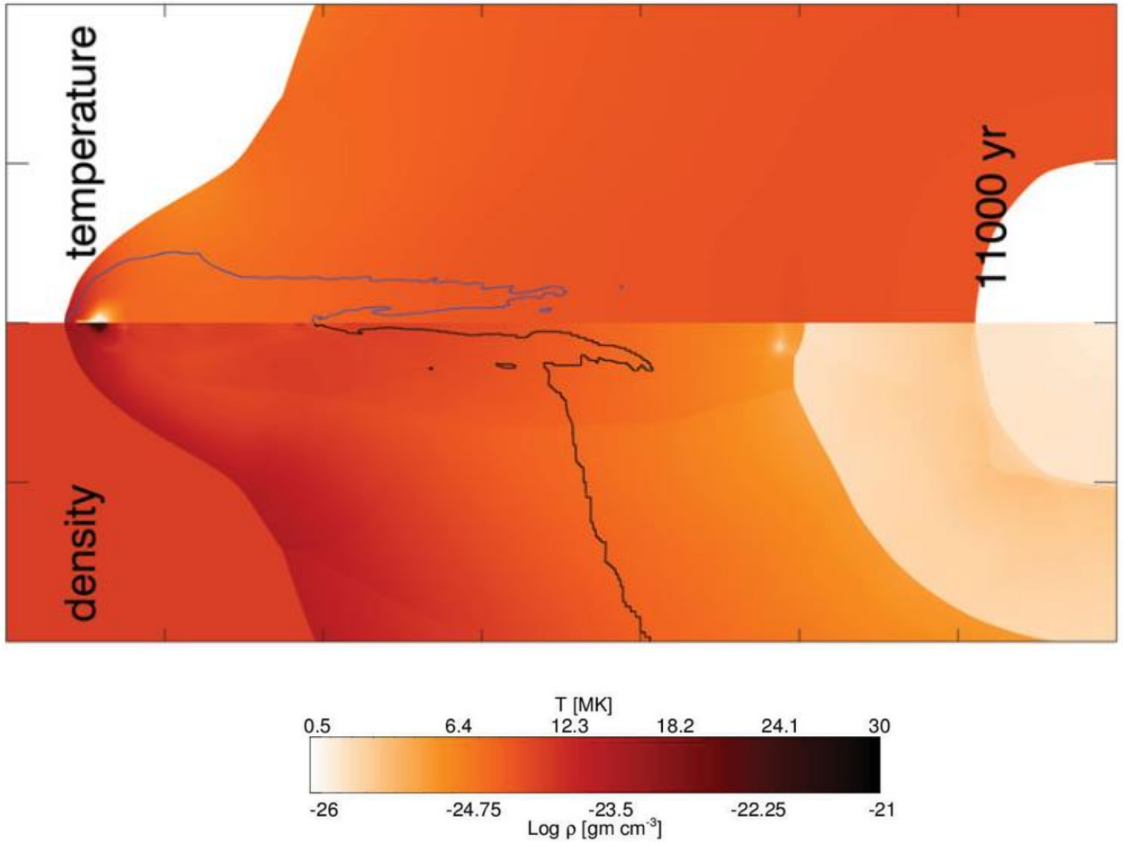

➢Unexpected temperature structure?

Comparison with ROSAT (Lu & Aschenbach, 2000)

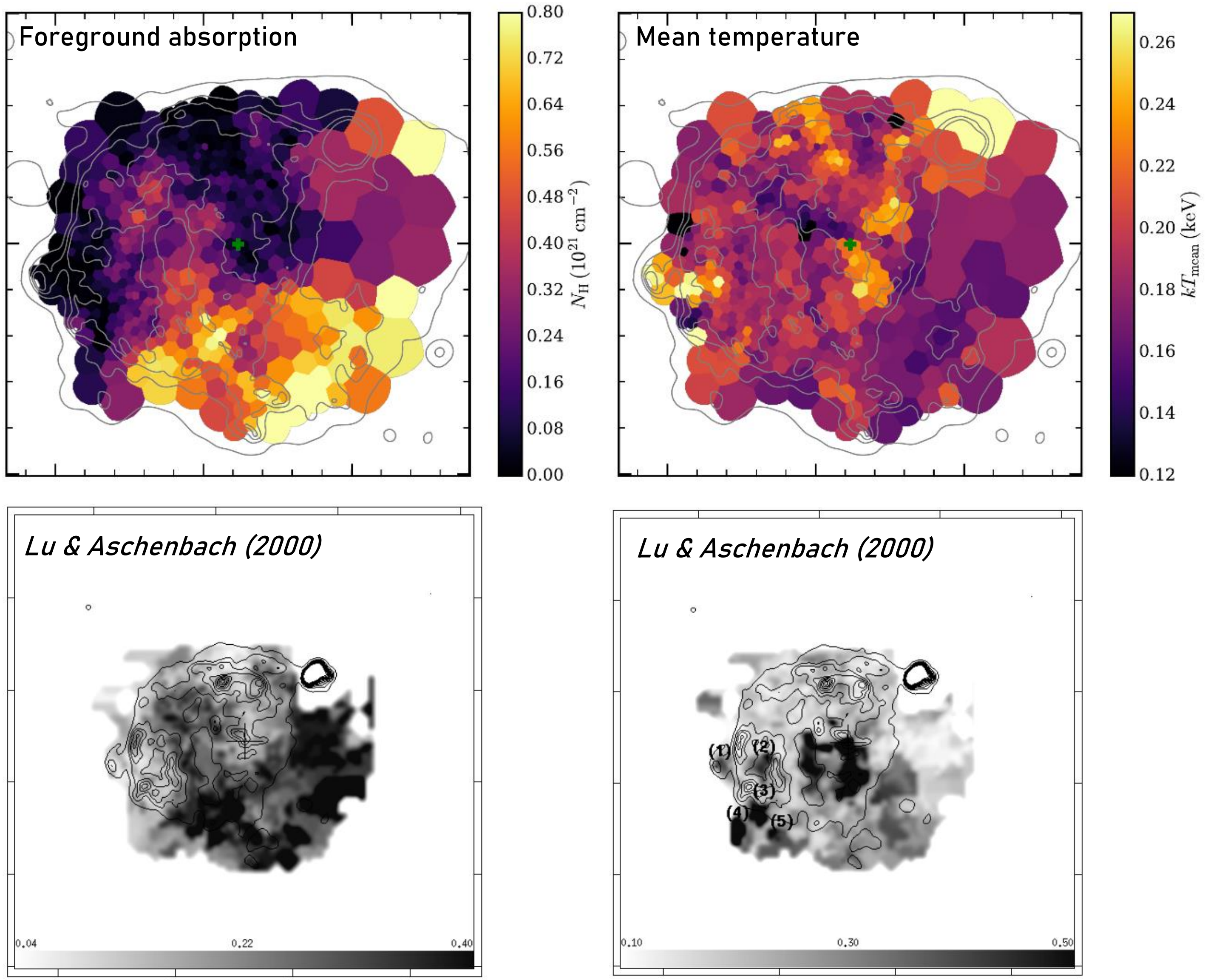

N_H & Hα

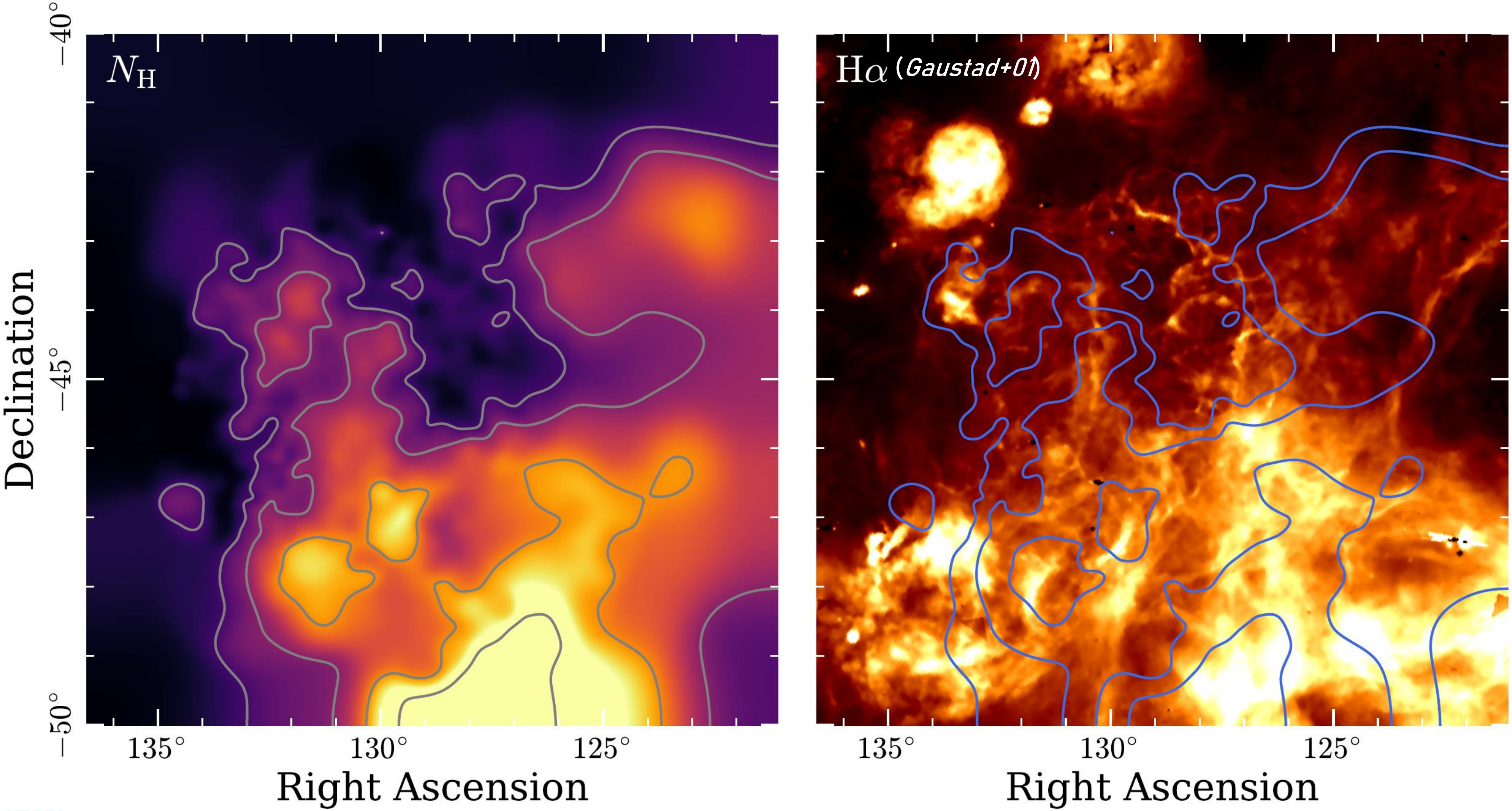

N_H
Hα (Gaustad+01)
Declination
−40°
−45°
−50°
135°
130°
125°
Right Ascension
135°
130°
125°
Right Ascension

More Ejecta Clumps

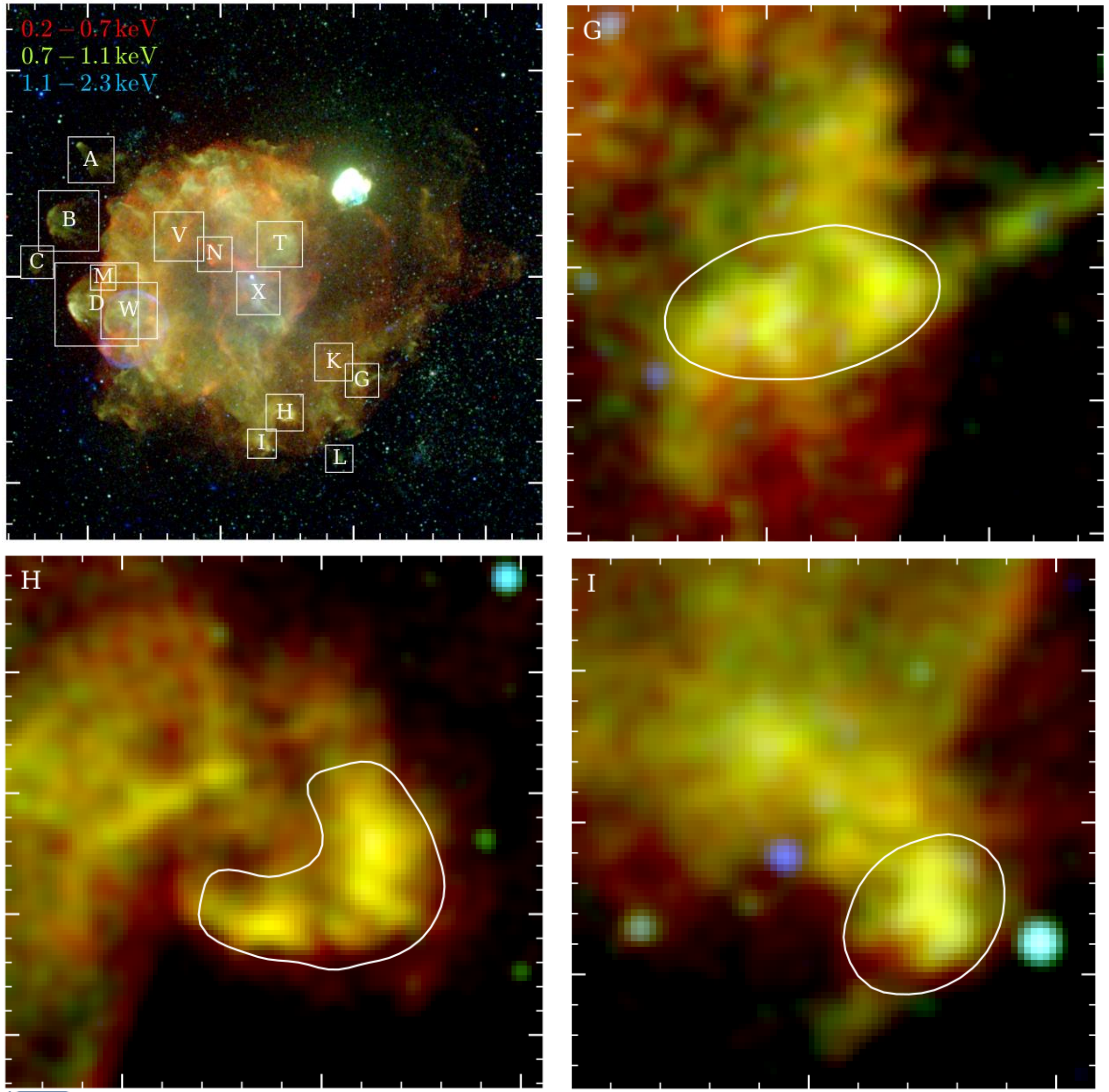

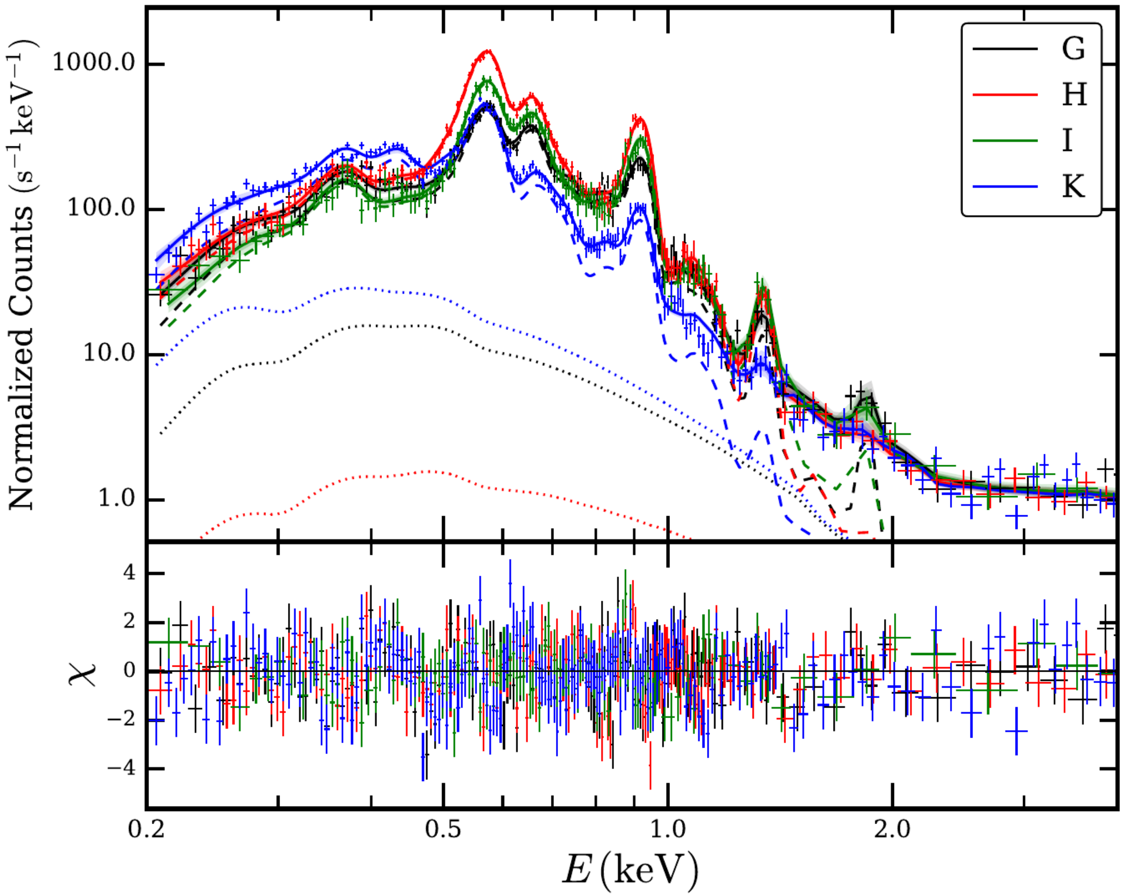

More Ejecta Clumps

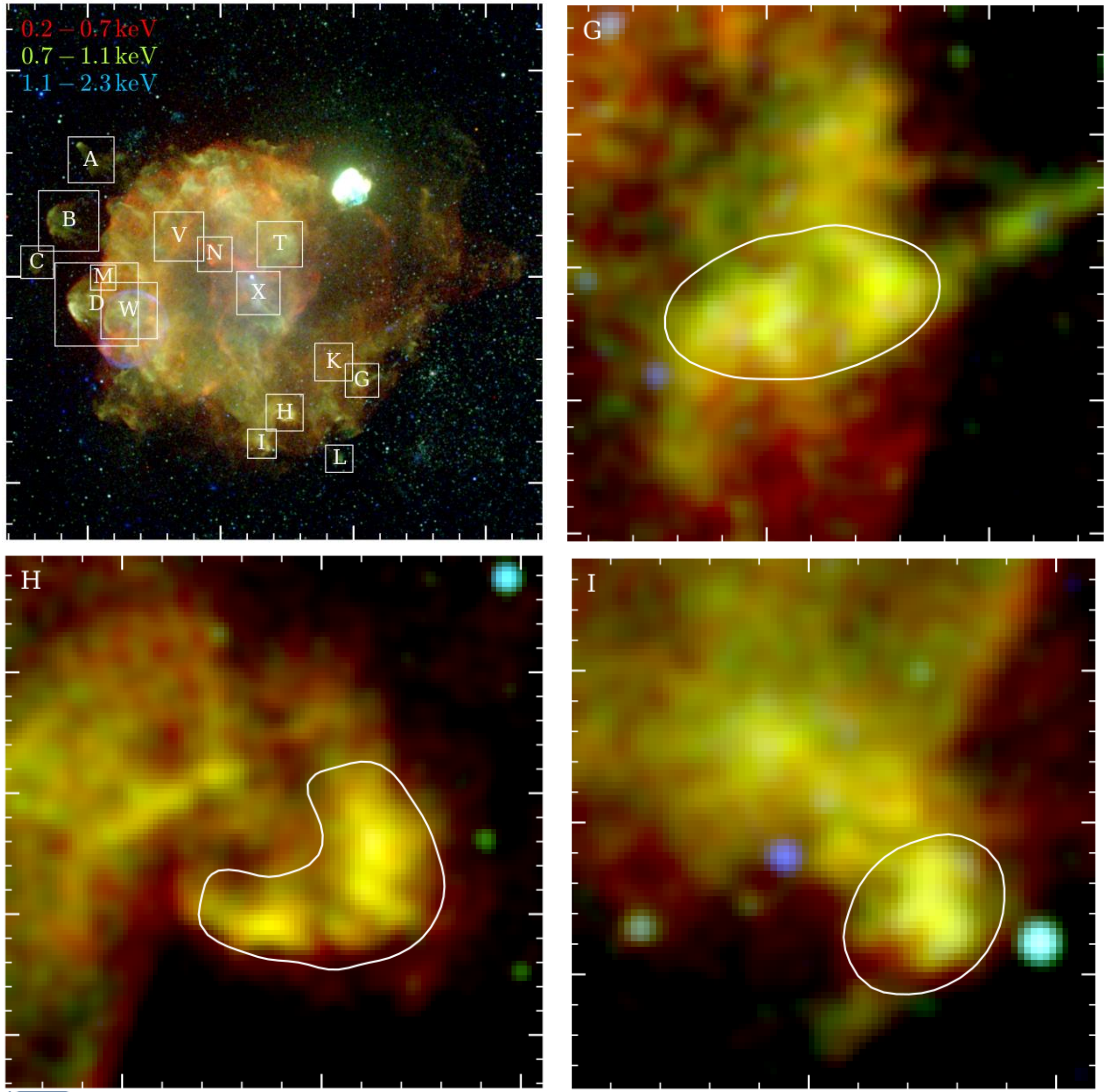

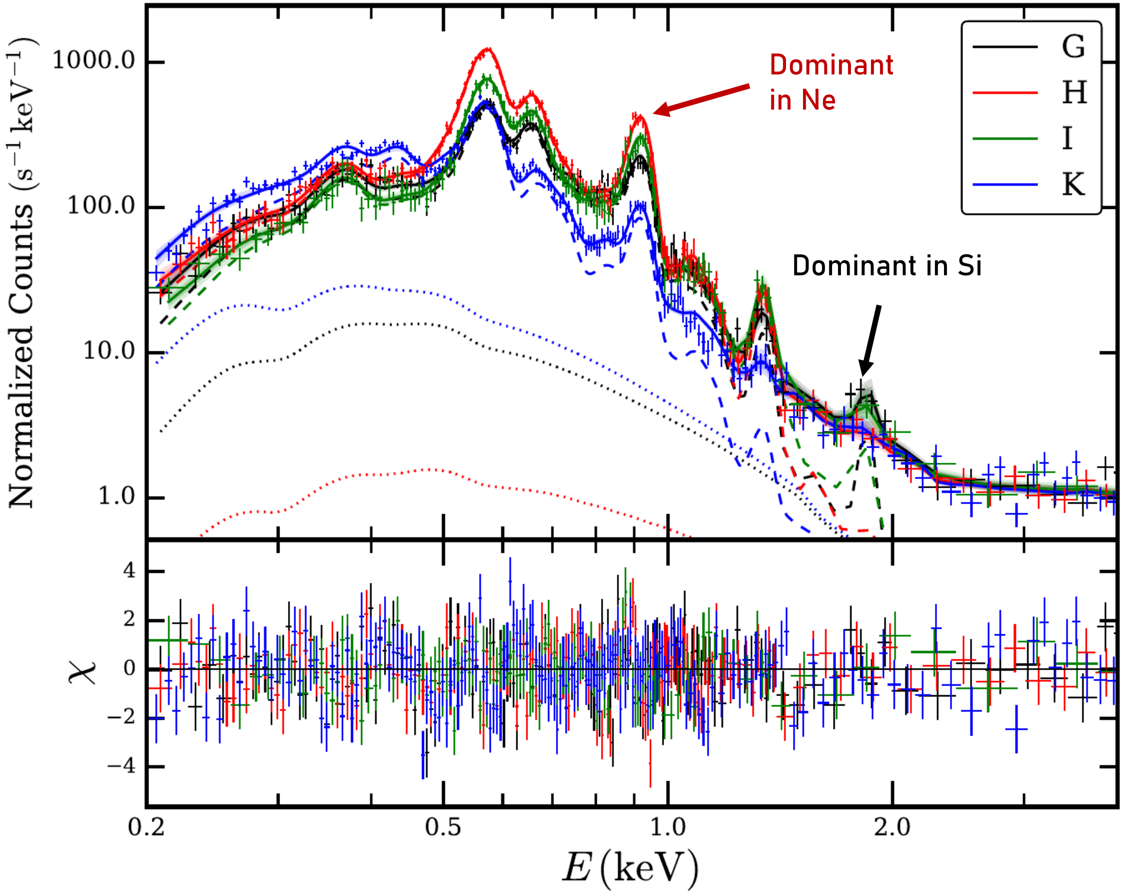

More Ejecta Clumps

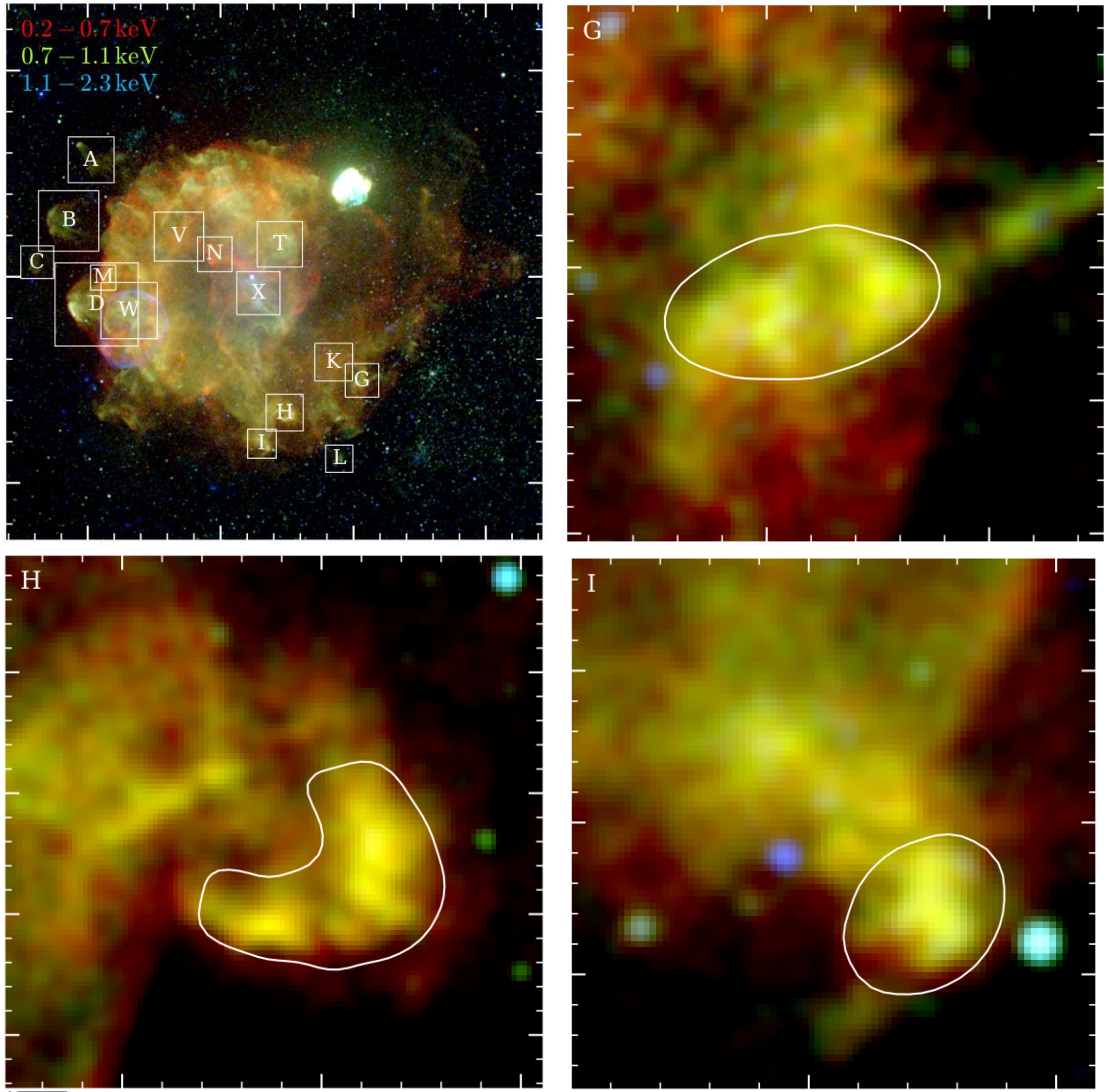

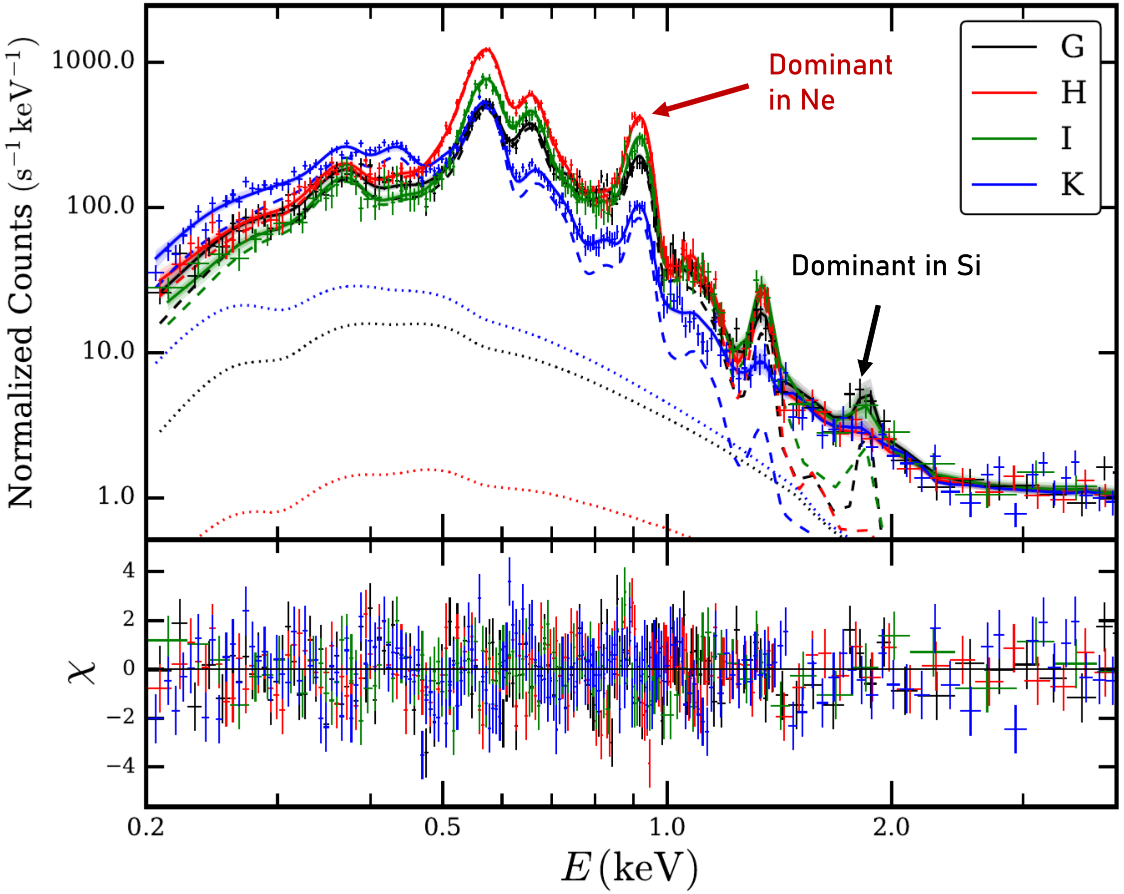

➢Silicon abundance varies between individual clumps

Spectrum at the shock front

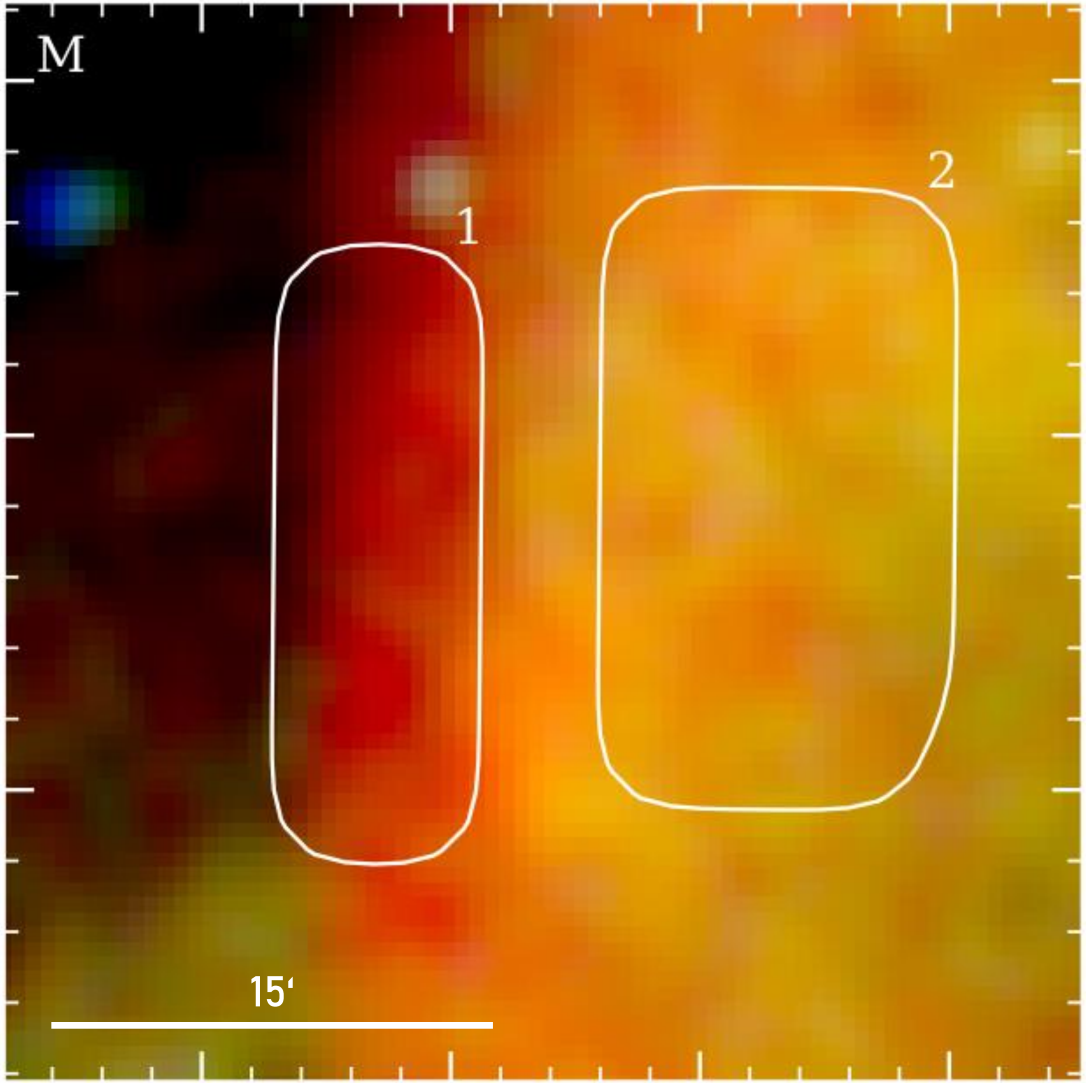

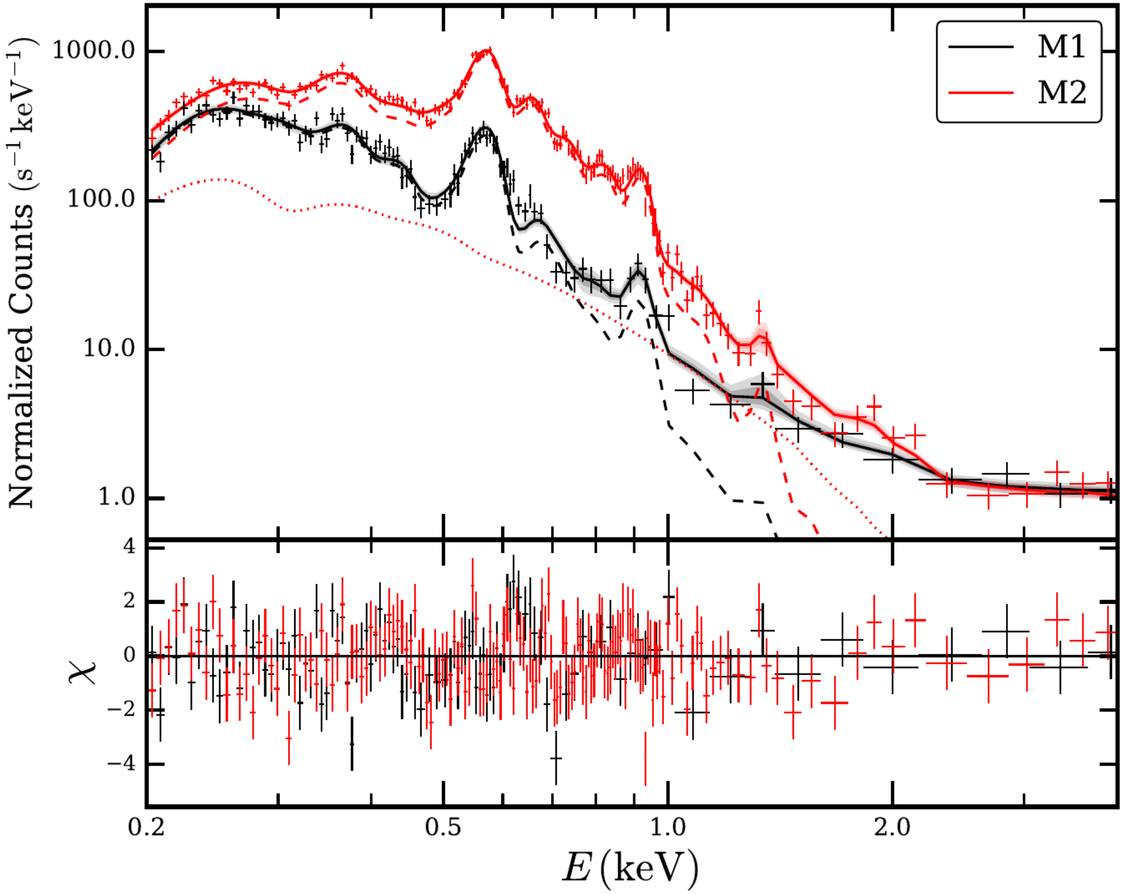

Spectrum at the shock front

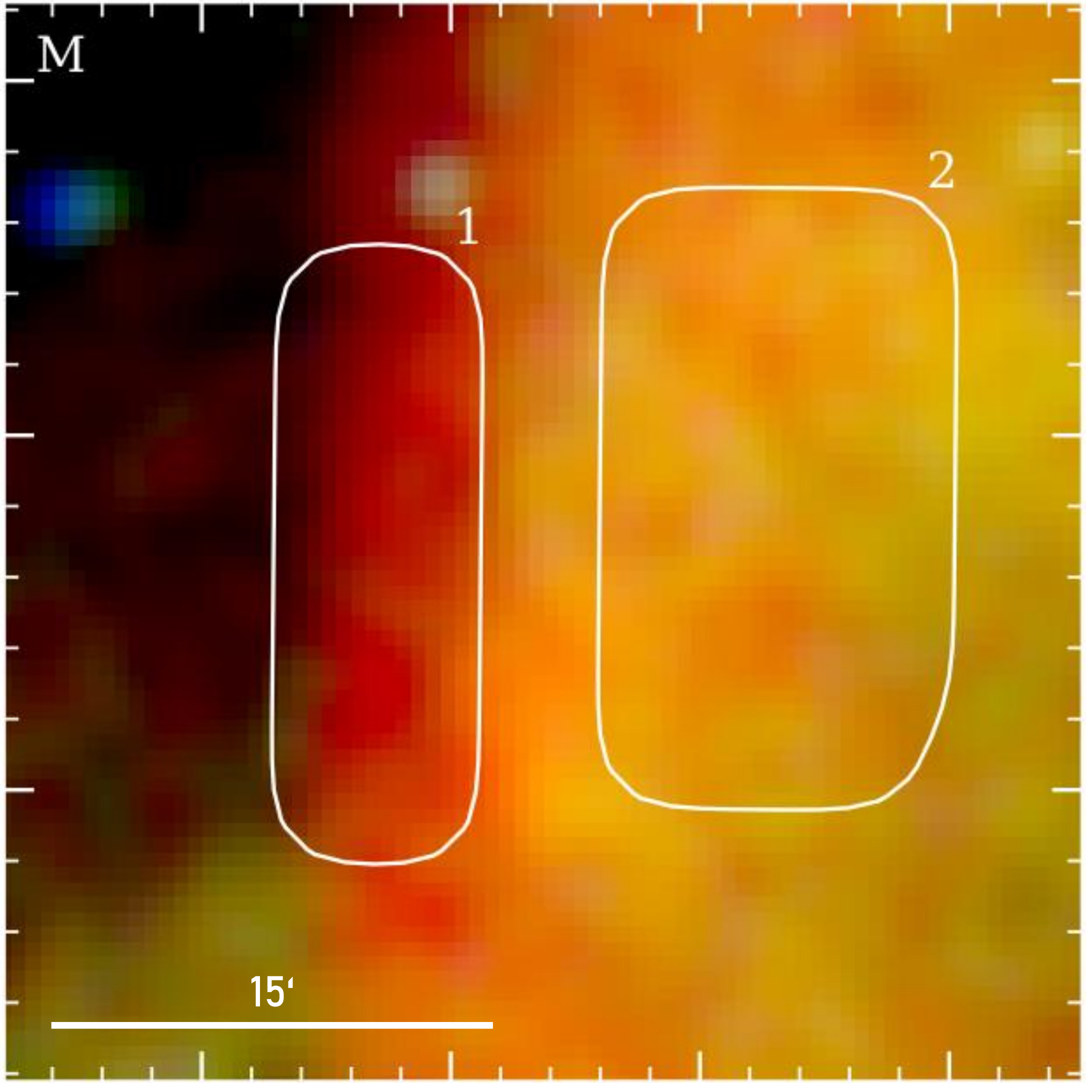

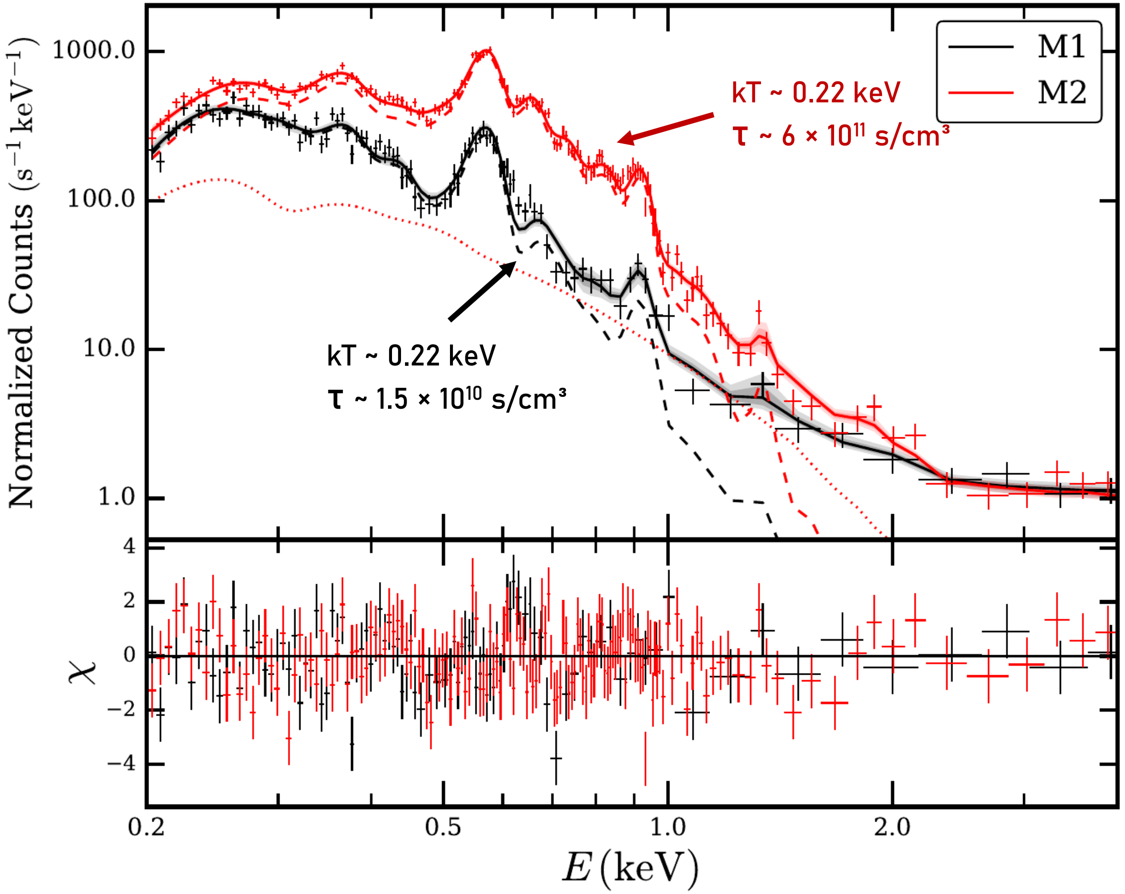

Spectrum at the shock front

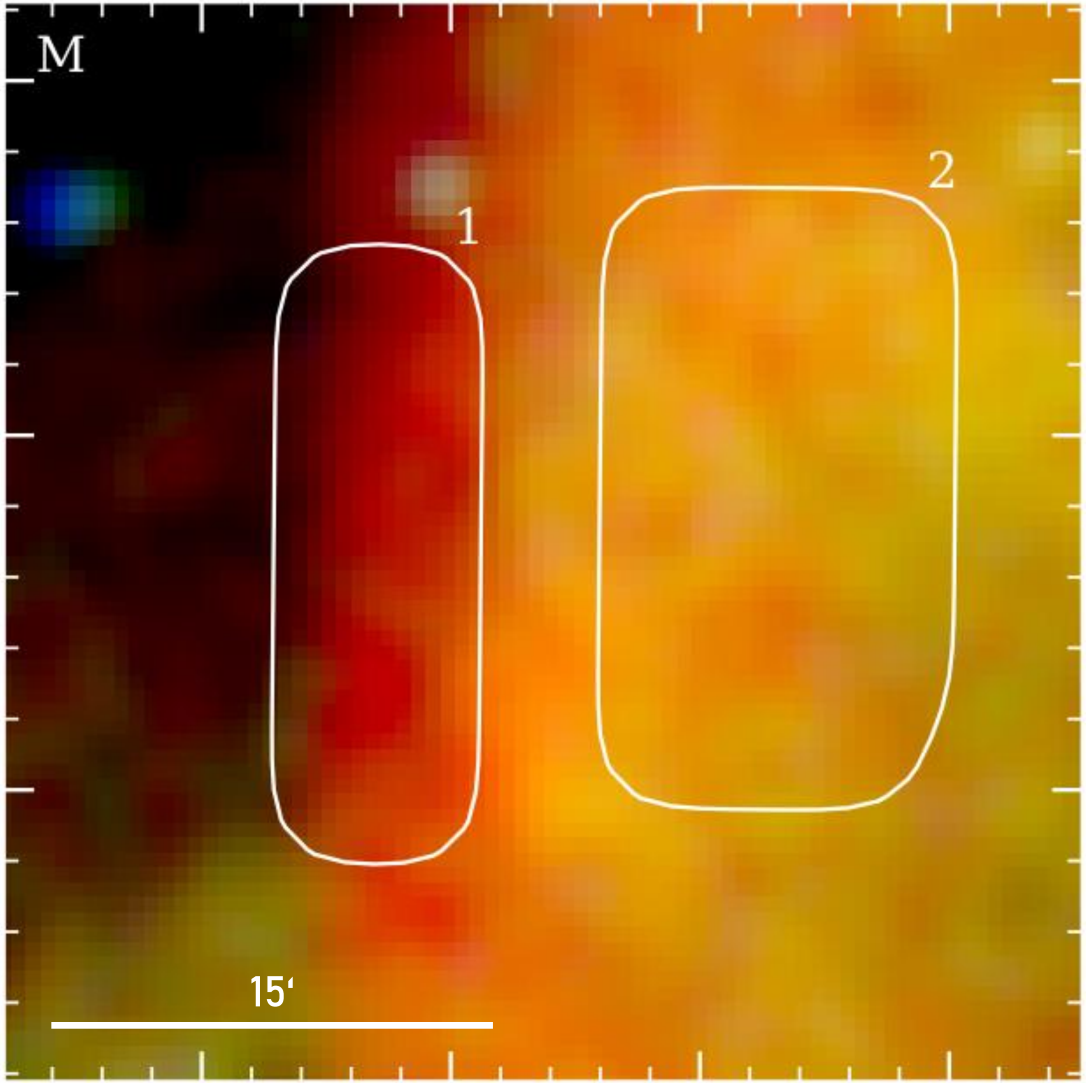

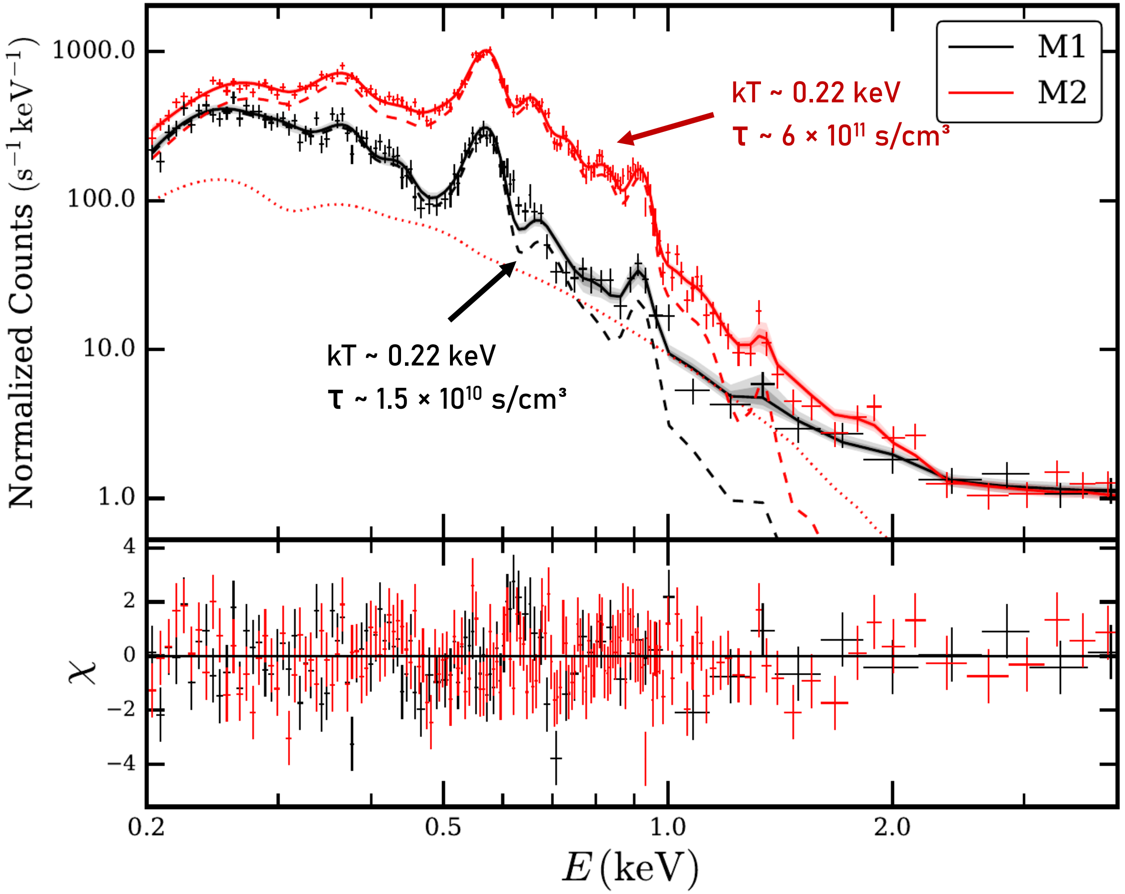

- Spectral differences mostly due to different shock ages!

Nonthermal Photon Index & Surface Brightness

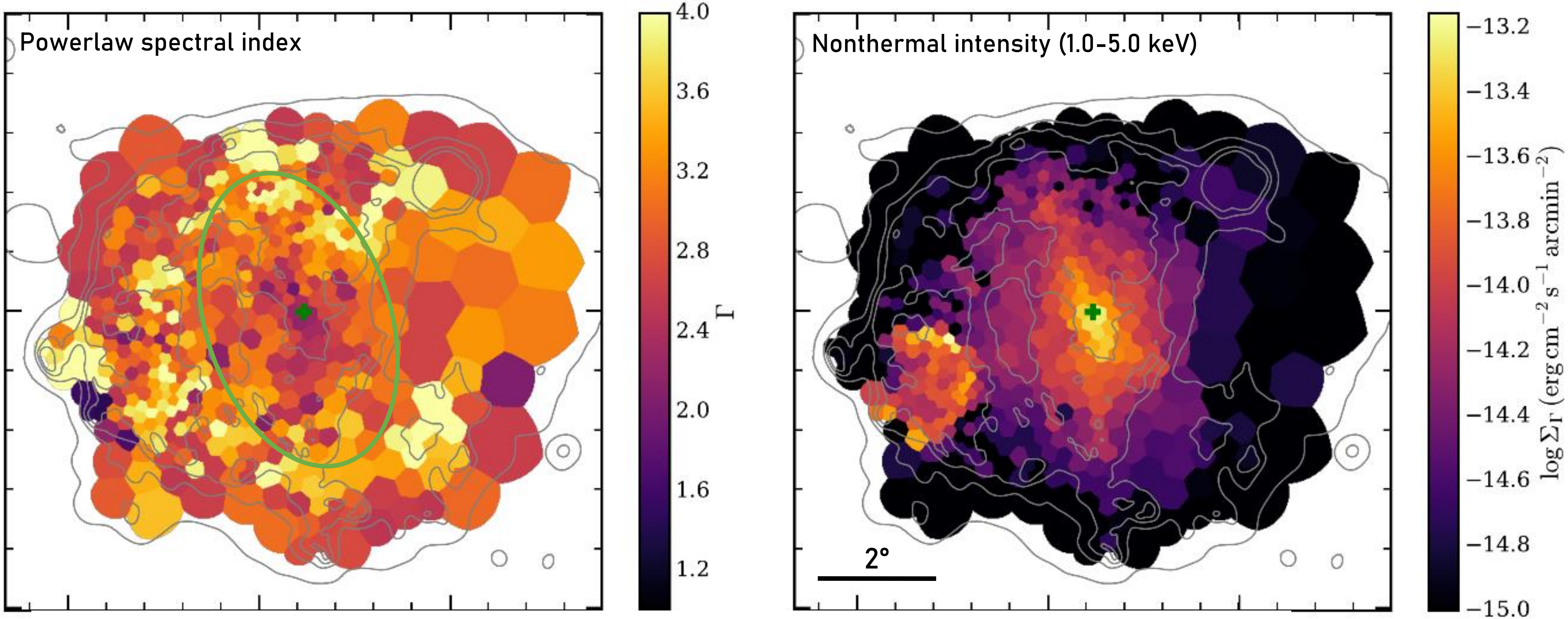

Nonthermal Emission in radial projection

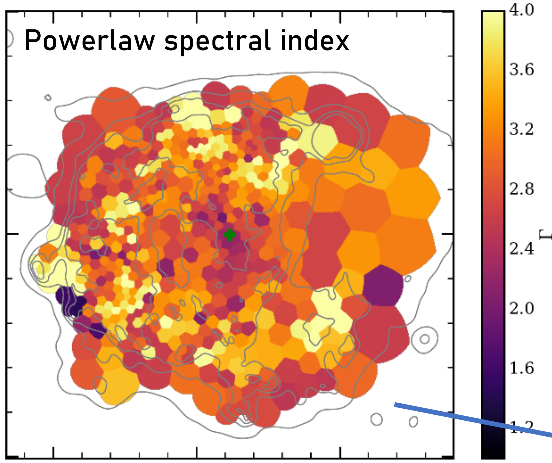

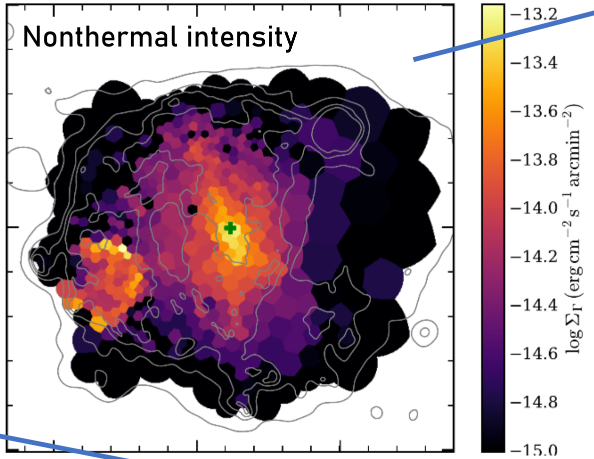

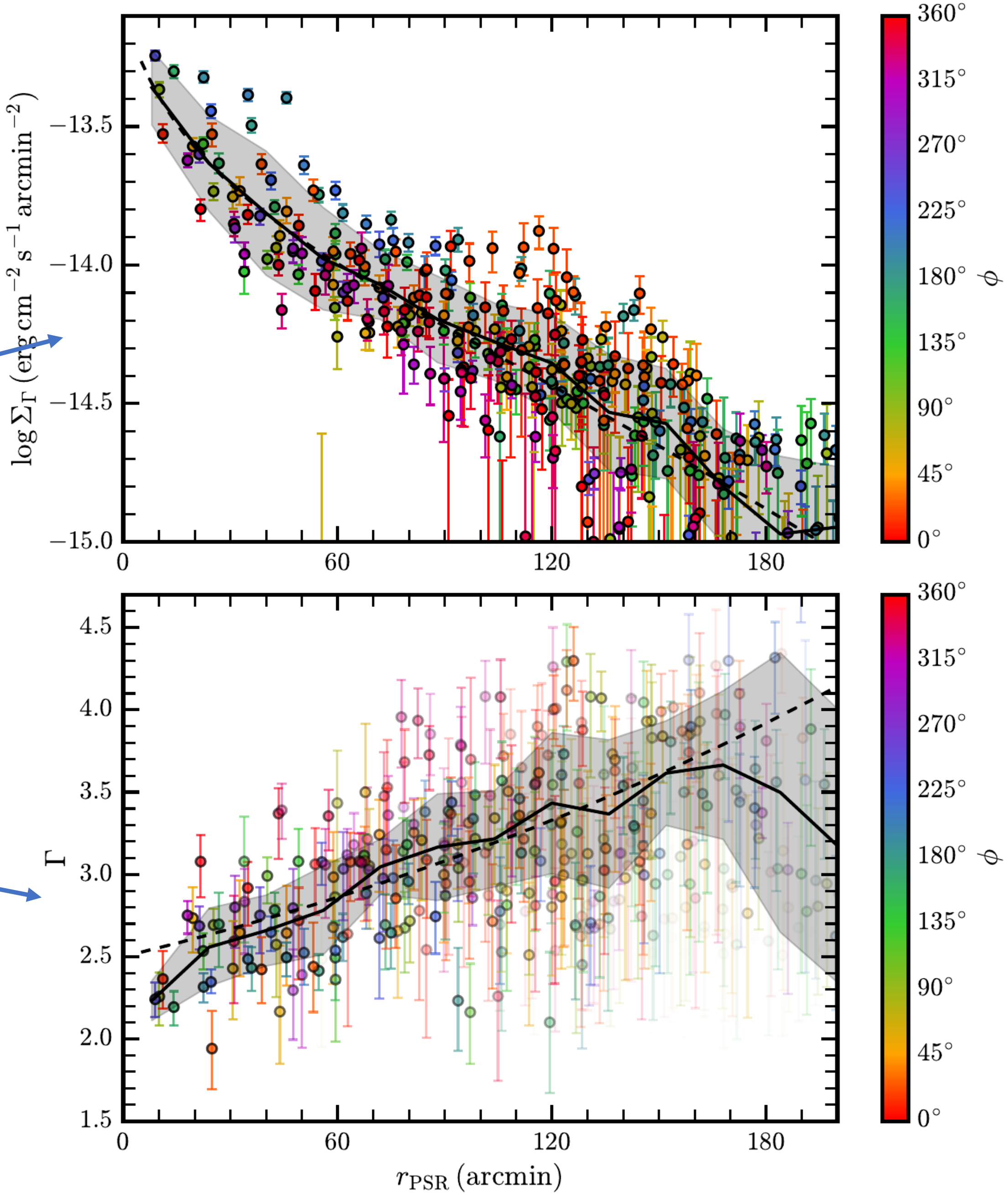

Nonthermal Emission in radial projection II

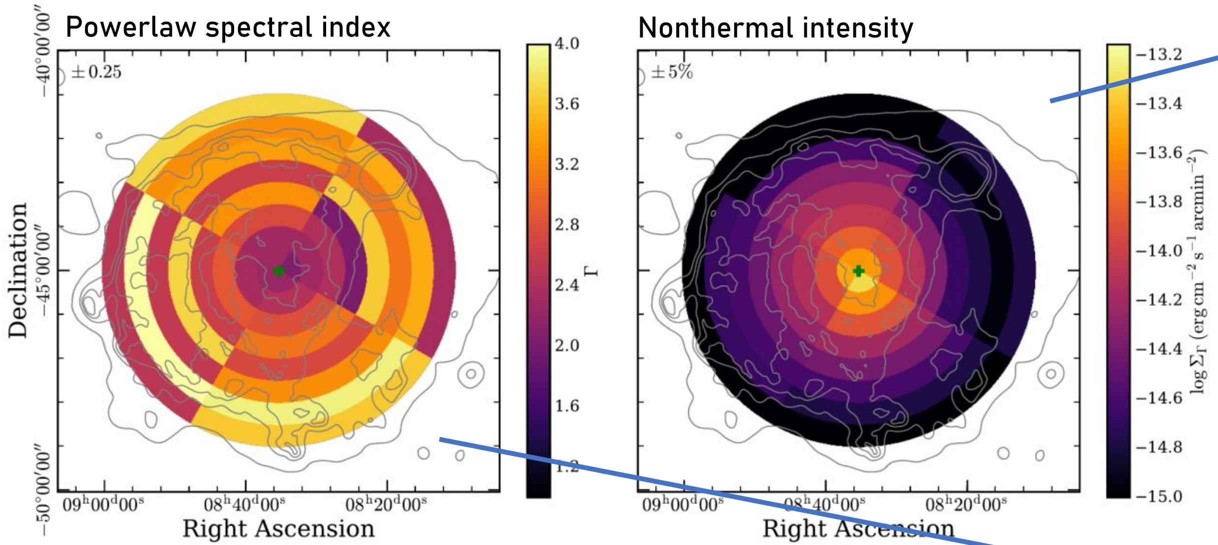

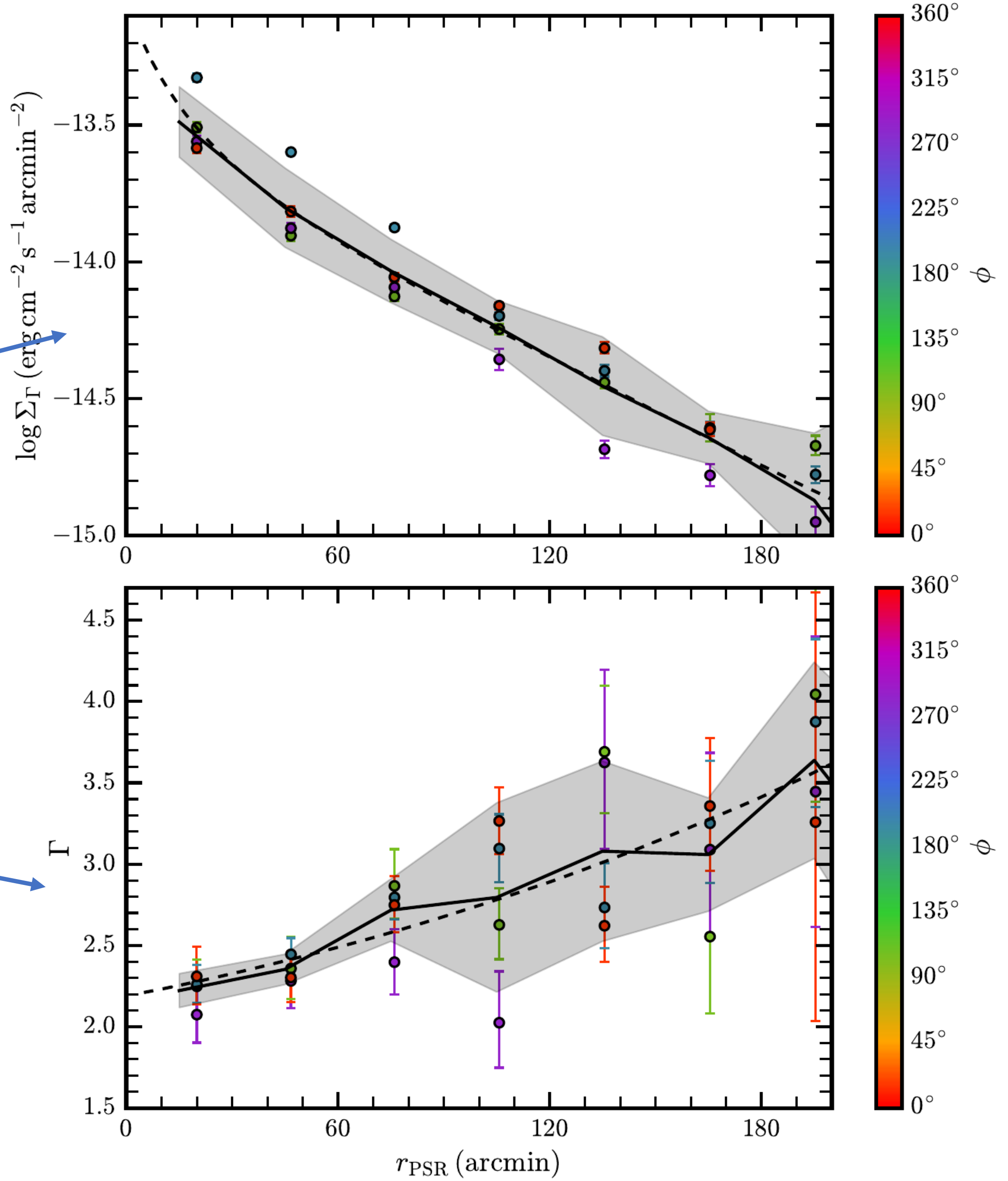

Bayesian Evidence in Favor of Nonthermal Emission